

Enhancing reliability-based assessments of quay walls

Roubos, Alfred

DOI

[10.4233/uuid:40632b7a-970e-433d-9b4e-ff2d2249b156](https://doi.org/10.4233/uuid:40632b7a-970e-433d-9b4e-ff2d2249b156)

Publication date

2019

Document Version

Final published version

Citation (APA)

Roubos, A. (2019). *Enhancing reliability-based assessments of quay walls*. [Dissertation (TU Delft), Delft University of Technology]. <https://doi.org/10.4233/uuid:40632b7a-970e-433d-9b4e-ff2d2249b156>

Important note

To cite this publication, please use the final published version (if applicable).
Please check the document version above.

Copyright

Other than for strictly personal use, it is not permitted to download, forward or distribute the text or part of it, without the consent of the author(s) and/or copyright holder(s), unless the work is under an open content license such as Creative Commons.

Takedown policy

Please contact us and provide details if you believe this document breaches copyrights.
We will remove access to the work immediately and investigate your claim.



ENHANCING RELIABILITY-BASED ASSESSMENTS OF QUAY WALLS

A.A. ROUBOS

ENHANCING RELIABILITY-BASED ASSESSMENTS OF QUAY WALLS

A.A. ROUBOS



Ontwerp en vormgeving omslag: Cees van Iem en Elisa Calamita, persoonlijkproefschrift.nl

Foto omslag: Freek van Arkel

Layout: Elisa Calamita, persoonlijkproefschrift.nl

Print: Ridderprint | www.ridderprint.nl

ISBN 978-94-6375-534-4

Copyright © A.A. Roubos, 2019

An electronic version of this dissertation is available at

<http://repository.tudelft.nl/>.

ENHANCING RELIABILITY-BASED ASSESSMENTS OF QUAY WALLS

Proefschrift

ter verkrijging van de graad van doctor
aan de Technische Universiteit Delft,
op gezag van de Rector Magnificus prof.dr.ir T.H.J.J. van der Hagen;
voorzitter van het College voor Promoties,
in het openbaar te verdedigen
op woensdag 16 oktober 2019 om 15:00 uur

door

Arie Alfred ROUBOS

Civiel Ingenieur, Technische Universiteit Delft, Nederland
geboren te Zwijndrecht, Nederland

Dit proefschrift is goedgekeurd door de promotoren:

Prof.dr.ir. S.N. Jonkman

Prof.dr.ir. R.D.J.M. Steenbergen

Samenstelling promotiecommissie:

Rector Magnificus

Voorzitter

Prof.dr.ir. S.N. Jonkman

Technische Universiteit Delft, promotor

Prof.dr.ir. R.D.J.M. Steenbergen

Universiteit Gent, promotor

Onafhankelijke leden:

Prof. C. Bauduin

Katholieke Universiteit Leuven

Prof.dr.ir. P.H.A.J.M. van Gelder

Technische Universiteit Delft

Dr.ir. J.G. de Gijt

Technische Universiteit Delft

Prof.dr.ir. M. van Koningsveld

Technische Universiteit Delft

Prof.dr. R.E. Melchers

The University of Newcastle, Australia

ABSTRACT

In the coming years, thousands of quay walls will approach the end of their intended fifty-year design lifetime and become part of lifetime extension programmes throughout the world. It is presently unclear how reliable these structures are and whether they are still capable of bearing ship and crane loads. An appropriate assessment of a quay wall's reliability is essential to safely and responsibly determining its remaining service life. This thesis demonstrates how quay wall reliability can be evaluated and what aspects should be taken into consideration.

In this study, reliability targets were derived from various risk-acceptance criteria, such as the individual risk, group risk, economic optimisation and human safety. For the commercial quay walls considered in this study, the economic risk-acceptance criterion prevails when deriving reliability targets, provided that the requirements concerning human safety have been met. The lifetime reliability targets obtained for a reference period of fifty years were in the range of the acceptable reliability levels recommended in literature. Furthermore, it was found that the failure rate of quay walls evolves over time, whereas the design codes currently in use implicitly assume that rate to be constant. As a result, the annual reliability targets obtained are lower than in the Eurocode or ISO 2394. This finding is quite relevant, since using a reference period of one year enables us to evaluate quay-wall reliability, while taking into account the effects of past performance and degradation. Moreover, within a one-year reference period, the effects of past performance and degradation can be taken into account in an appropriate manner. These findings can play an important role in the evaluation of the reliability of an existing quay wall, since then its remaining service life and the associated reference period are generally unknown a priori. Hence, using annual target reliability indices is preferred.

In addition, the quay wall's actual reliability level was estimated by performing finite element-based reliability analyses. Despite a fairly complex soil-structure interaction (e.g. due to inclined retaining walls, relieving platforms and non-linear soil behaviour) and a large number of random design variables, this thesis shows that the reliability level of a quay wall can be estimated successfully by performing finite element-based reliability assessments using the Abdo-Rackwitz' algorithm. The resulting reliability indices for critical failure modes are in the range of the recommended lifetime reliability targets from the Eurocode. Moreover, it was found that time-independent variables, such as material properties of soil, steel and grout, as well as model uncertainty, significantly influence the reliability of a quay wall.

By performing fully time-dependent reliability analyses, taking into account both past service performance and degradation, this thesis demonstrates that the presence of dominant time-independent variables is crucial when assessing the reliability of existing quay walls. It was found that the (epistemic) uncertainty in time-independent variables, such

as the strength of sand, is likely to decrease over time for structures with successful service histories. As a result, in the absence of degradation, the quay wall's failure rate decreases over time. Consequently, not only is the quay wall's actual reliability higher than in its early service period, but the net present value of the residual risk will also decrease, and hence reliability targets derived from an economic perspective will decrease accordingly. Due to corrosion, however, the reliability of a quay wall decreases over time, while our confidence in a service-proven structure increases. Both aspects therefore affect the reliability of existing quay walls. Since the maximum stresses close to the harbour bottom prevail, and corrosion rates are quite low there, it is expected that the lifetime of many existing quay walls can be extended safely, despite some degradation.

Furthermore, German and Dutch ports provided this research with new field measurements of berthing manoeuvres, which were used to reduce uncertainty in berthing impact loads acting on quay walls. The field measurements were statistically examined to establish design values for berthing velocity – the speed at which a ship approaches the quay wall – since the uncertainty in berthing velocity dominates the uncertainty in the associated berthing impact load. No significant correlation was found between berthing velocity and ship dimensions, whereas well-established design guidelines for marine structures, such as PIANC, suggest a fairly strong negative correlation. By contrast, the berthing velocity depends on the berthing policy (e.g. type of landing, experience of pilots and the use tug assistance or of berthing aid systems). It is therefore recommended that these design guidelines be revised.

In summary, the applicability of finite element-based reliability assessments in quay-wall engineering has increased considerably. The methods developed for evaluating quay-wall reliability can be used to determine the remaining service life, to make better use of existing structures and to improve the design of new quay walls. The findings of this thesis can play a crucial role in the assessment of existing quay walls, and presumably all other service-proven geotechnical structures subject to degradation.

¹ Gradient-based first order reliability method.

SAMENVATTING

In de komende periode naderen duizenden kademuren het einde van hun beoogde ontwerplevensduur van 50 jaar, waardoor wereldwijd rehabilitatieprogramma's zullen worden opgestart. Op dit moment is het onduidelijk hoe betrouwbaar kadeconstructies zijn en of ze de belastingen door schepen en kranen nog aankunnen. Het op een juiste wijze beoordelen van de betrouwbaarheid is essentieel om de resterende levensduur van deze kades veilig en verantwoord vast te kunnen stellen. In dit proefschrift wordt nader ingegaan op welke wijze de betrouwbaarheid van kademuren kan worden beoordeeld en met welke aspecten hierbij rekening moet worden gehouden.

In dit onderzoek is allereerst bepaald hoe betrouwbaar een kade moet zijn door streefwaardes af te leiden op basis van verschillende risicoacceptatiecriteria, zoals het individuele risico, het groepsrisico, economische optimalisatie en menselijke veiligheid. Voor de commerciële kademuren die beschouwd zijn in deze studie is gevonden dat het economische acceptatiecriterium maatgevend is, mits rekening gehouden wordt met sociaaleconomische gevolgschade. De afgeleide streefwaarden voor een referentieperiode van vijftig jaar komen overeen met de aanbevolen betrouwbaarheidsniveaus in de literatuur. Daarnaast bleek dat de jaarlijkse faalkans van een kademuur aanzienlijk verandert in de tijd. Dit in tegenstelling tot de huidige ontwerpcodes, die impliciet veronderstellen dat deze faalkans constant is. Hierdoor zijn de streefwaarden voor een referentieperiode van één jaar lager dan de aanbevolen waarden uit de Eurocode en ISO 2394. Daarnaast kunnen binnen een referentieperiode van één jaar de effecten van bewezen sterkte en degradatie goed meegenomen worden. Deze bevindingen kunnen een belangrijke rol gaan spelen bij het toetsten van bestaande kademuren, omdat de resterende levensduur en de daarmee samenhangende referentieperiode vooraf meestal niet bekend zijn. Om die reden geniet het toepassen van jaarlijkse streefwaarden de voorkeur.

Vervolgens is een betrouwbaarheidsanalyse uitgevoerd met als doel de werkelijke betrouwbaarheid te schatten, waarbij de kade gemodelleerd is in een eindige elementen omgeving. Ondanks de relatief complexe grondconstructie interactie (veroorzaakt door een hellende voorwand, een ontlastvloer of sterk niet-lineair grondgedrag) en het grote aantal stochastische variabelen kan de betrouwbaarheid van een kademuur worden berekend middels een op eindige elementen gebaseerde betrouwbaarheidsanalyse met het Abdo-Rackwitz' algoritme. De gevonden betrouwbaarheid komt voor de maatgevende faalmechanismes goed overeen met de aanbevolen streefwaarden uit de Eurocode. De resultaten laten ook zien dat tijdsafhankelijke stochastische variabelen (zoals materiaaleigenschappen van grond, staal en grout) en modelonzekerheid een grote invloed hebben op de betrouwbaarheid van een kademuur.

Door het uitvoeren van volledig tijdsafhankelijke betrouwbaarheidsanalyses, waarbij rekening is gehouden met zowel bewezen sterkte als degradatie, is in dit onderzoek aangetoond dat de aanwezigheid van dominante tijdsafhankelijke variabelen cruciaal is bij het beoordelen van bestaande kademuren. De resultaten laten zien dat de (epistemische) onzekerheid in tijdsafhankelijke variabelen (zoals de sterkte van zand) in de loop van de tijd zal afnemen als de kadeconstructie goed functioneert. Hierdoor daalt, in afwezigheid van degradatie, de faalkans en is niet alleen de berekende betrouwbaarheid hoger in vergelijking met het oorspronkelijke ontwerp, maar zal ook de netto contante waarde van het restrisiko afnemen, waardoor de daarmee samenhangende streefwaarde voor betrouwbaarheid vanuit een economisch perspectief eveneens zal afnemen. Als gevolg van corrosie neemt de betrouwbaarheid van een kade na verloop van tijd echter af, terwijl ons vertrouwen in een goed functionerende kade daarentegen met de tijd toeneemt. Beide aspecten hebben daarmee invloed op de betrouwbaarheid van bestaande kademuren. Aangezien de maximale spanningen optreden net boven of onder de havenbodem en de corrosiesnelheid hier relatief laag is, is de verwachting dat de levensduur van veel bestaande kademuren, ondanks enige degradatie, veilig kan worden verlengd.

Daarnaast hebben Duitse en Nederlandse havens nieuwe veldmetingen van afmeer manoeuvres ter beschikking gesteld, welke zijn gebruikt om de onzekerheid in de afmeerbelasting op kademuren te reduceren. De veldmetingen zijn – om te bepalen met welke snelheid een schip mag afmeren – statistisch geanalyseerd, omdat de onzekerheid in de afmeersnelheid een belangrijke rol speelt bij de daarmee samenhangende afmeerkracht en zodoende invloed heeft op de betrouwbaarheid van een kademuur. In dit onderzoek is geen noemenswaardige correlatie gevonden tussen de afmeersnelheid en de grootte van een schip, terwijl veel gebruikte ontwerprichtlijnen voor maritieme constructies, als PIANC, dit tot op heden wel veronderstellen. De afmeersnelheid is daarentegen afhankelijk van het gevoerde afmeerbeleid (bijvoorbeeld de uitgevoerde manoeuvre, de ervaring van de loods en het gebruik van sleepboten of andere dockingsystemen). Het wordt dan ook aanbevolen om de huidige ontwerpaanbevelingen op dit vlak te herzien.

Kortom, de toepasbaarheid van op eindige elementen gebaseerde betrouwbaarheidsanalyses bij het beoordelen van kademuren is aanzienlijk toegenomen. De ontwikkelde methodes voor het beoordelen van de betrouwbaarheid van kademuren kunnen worden gebruikt om de resterende levensduur te bepalen, om de bestaande constructies beter te benutten en het ontwerp van nieuwe kademuren te optimaliseren. De bevindingen uit dit proefschrift kunnen een belangrijke rol spelen bij het toetsen van kademuren en vermoedelijk ook voor andere goed functionerende geotechnische constructies die onderhevig zijn aan degradatie.

¹ Een op gradiënten gebaseerde eerste orde betrouwbaarheidsmethode.

CONTENTS

ABSTRACT	VI
SAMENVATTING	VIII
1 INTRODUCTION	15
1.1 Motivation and societal relevance	16
1.2 Knowledge gaps	17
1.3 Research aim and questions	20
1.4 Scope and outline	21
1.5 Limitations	22
2 TARGET RELIABILITY INDICES FOR QUAY WALLS	25
Abstract	26
2.1 Introduction	27
2.2 Target reliability indices in literature	29
2.2.1 Principles of target reliability	29
2.2.2 Reliability differentiation in literature	30
2.3 Method for deriving target reliability indices for quay walls	35
2.3.1 Introduction	35
2.3.2 System decomposition and relevant failure modes	35
2.3.3 Modelling time-variant reliability	37
2.3.4 Marginal construction costs	40
2.3.5 Consequences of failure	41
2.3.6 Risk-based optimisation of structural components	43
2.4 Risk-acceptance criteria	45
2.4.1 Individual risk criterion	46
2.4.2 Societal risk criterion	47
2.4.3 Life quality index criterion	47
2.4.4 <i>SERI</i> criterion	48
2.5 Reliability targets for failure modes of quay walls	48
2.5.1 Reliability optimum β^* on the basis of cost minimisation	48
2.5.2 Sensitivity analysis of reliability optimum β^*	49
2.5.3 Reliability minimum β_{acc} on the basis of human safety criteria	51
2.5.4 Sensitivity analysis of reliability minimum β_{acc}	52
2.6 Discussion of reliability targets	53
2.6.1 Target reliability indices for commercial quay walls	53
2.6.2 Assessment criteria for classification	54

2.6.3	Compliance with codes and standards and proposal for classification	57
2.7	Conclusion and recommendations	59
3	FINITE ELEMENT-BASED RELIABILITY ASSESSMENT OF QUAY WALLS	63
	Abstract	64
3.1	Introduction	65
3.2	Basic principles of reliability-based assessments	65
3.3	Method for finite element-based reliability assessment of quay walls	67
3.3.1	Introduction	67
3.3.2	Main failure modes and limit state functions	69
3.3.3	Distribution functions and correlations	72
3.3.4	Derivation of sensitivity and partial factors in the event of correlations	77
3.4	Results of reliability-based assessments of quay walls	80
3.4.1	Evaluation of Abdo-Rackwitz algorithm outcomes	80
3.4.2	Results of finite element-based reliability assessments	80
3.4.3	Sensitivity analysis	83
3.4.4	Results: partial factors of safety	85
3.5	Discussion on parameters that influence reliability and partial factors	87
3.5.1	Evaluation of results	87
3.5.2	Evaluation and derivation of partial factors of safety	89
3.5.3	Reflection on results from a practical perspective	94
3.6	Conclusion and recommendations	95
4	THE EFFECT OF CORROSION ON THE RELIABILITY OF SERVICE-PROVEN QUAY WALLS	99
	Abstract	100
4.1	Introduction	101
4.2	Allowable stress-based method to assess corroded combi-walls	103
4.3	Reliability-based method to assess corrosion-induced degradation	107
4.3.1	Introduction	107
4.3.2	Limit state functions of combi-walls subject to corrosion	108
4.3.3	Distribution functions and correlations	110
4.3.4	Numerical approach to time-dependent reliability	114
4.3.5	Finite-element-based calibration of Blum's method	117

4.4	Results of reliability analysis of corroded combi-walls	119
4.4.1	Comparison of Blum-based and FEM-based reliability assessment	119
4.4.2	Influence of corrosion on the FoS and the reliability index β	120
4.4.3	Sensitivity analysis	122
4.5	Discussion	124
4.5.1	Influence of corrosion on FoS and β of reference quay wall	124
4.5.2	Influence of remaining service life on probability of failure of service-proven quay walls	125
4.5.3	Evaluation of allowable stress-based method to assess corroded combi-walls	126
4.6	Conclusion and recommendations	128
5	REDUCING UNCERTAINTY BY ANALYSING BERTHING RECORDS	131
	Abstract	132
5.1	Introduction	133
5.2	Berthing velocity in literature	135
5.2.1	General principles of berthing energy and impact	135
5.2.2	Return periods of berthing velocity curves	137
5.2.3	Abnormal berthing and load factors	138
5.3	Methods to examine berthing velocity	140
5.3.1	Data collection	140
5.3.2	Partial factors of safety	141
5.3.3	Data analysis	143
5.3.4	Characteristic and design berthing velocities	147
5.4	Design values for berthing velocity and partial factors	149
5.4.1	Extreme berthing velocities	149
5.4.2	Characteristic berthing velocities	153
5.4.3	Partial factors of safety for berthing velocity γ_v	154
5.5	Discussion on how to determine design values for berthing velocity	155
5.5.1	How to use berthing velocity records and partial factors in the design	155
5.5.2	Evaluation of partial factors of safety	160
5.5.3	Influence of berthing frequency	161
5.6	Conclusions and recommendations	162
6	CONCLUSION AND RECOMMENDATIONS	165
6.1	Main findings	166
6.2	Detailed findings	168

6.2.1	Risk-based reliability targets for quay walls	168
6.2.2	Finite element-based reliability assessment of quay walls	168
6.2.3	The effect of corrosion on the reliability of service-proven quay walls	169
6.2.4	Customised design values for berthing velocity to enhance quay wall reliability	170
6.3	Recommendations	171
6.3.1	Reliability targets and failure consequences	171
6.3.2	Reducing uncertainty in strength	172
6.3.3	Reducing uncertainty in loads	174
6.4	Relevance and implications	175
REFERENCES		178
APPENDICES		191
Appendix A1. Derivation of analytical formulas		192
Appendix A2. Probability distribution functions		198
Appendix B1. Additional information on reference quay walls		199
Appendix B2. Abdo-Rackwitz <i>FORM</i> algorithm		200
Appendix B3. Comparison of Blum & Prob2B with Plaxis & OpenTURNS		205
Appendix C1. Comparison of reliability methods		206
Appendix C2. Comparison with and without truncation		207
Appendix D1. Berthing velocity of large seagoing vessels in Rotterdam		208
D.1.1	Berthing records and data analysis	210
D.1.2	Results of data analysis of Rotterdam berthing records	217
D.1.3	Discussion of berthing records at the port of Rotterdam	228
D.1.4	Conclusions on berthing velocities of large seagoing vessels in Rotterdam	234
Appendix D2. Typical distribution functions for berthing velocity		235
CURRICULUM VITAE		236
LIST OF PUBLICATIONS		237
ACKNOWLEDGEMENTS		239

1





INTRODUCTION

"Information is the resolution of uncertainty"

Claude Shannon

Numerous marine structures such as quay walls, jetties and flexible dolphins have been constructed all over the world to accommodate ships' berthing, mooring and loading operations. The reliability of these structures has played an essential role in the global transshipment of goods and is the cornerstone of a well-functioning port. New quay walls are equipped with modern sensors, such as fibre-optic strain sensors installed on soil-retaining walls or anchor systems, and can therefore become potentially more intelligent and reliable (Fig. 1.1). Global digitisation has already created smart port infrastructure using 'internet of things' technologies. However, the biggest challenge is neither to collect data nor to facilitate connections, but to translate the available data into useful information and to identify which data is lacking in order to resolve uncertainty. The main theme of this thesis is the reliability of quay walls, with the present chapter providing an overview of the general background and motivation (Section 1.1), the knowledge gaps (Section 1.2), the research aim and questions (Section 1.3), the thesis outline (Section 1.4) and limitations (Section 1.5).

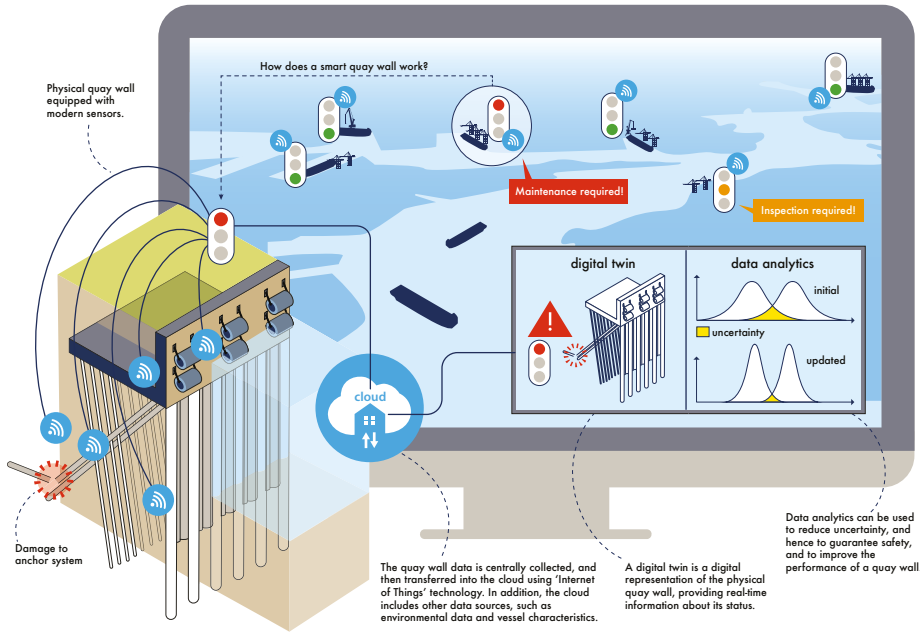


Fig. 1.1. Risk-based and data-driven decisions using real-time quay-wall data

1.1 MOTIVATION AND SOCIETAL RELEVANCE

In port engineering, many uncertainties must be taken into consideration in order to ensure the effective, safe and efficient handling of ships during their service life. Port authorities and terminals have to guarantee quay-wall functionality in accordance with service-level agreements with their clients. Quay walls are generally designed in such a way that they are likely to fulfil the functional and technical requirements for at least 50 years (De Gijt & Broeken, 2013), whereas the duration of these service-level agreements is normally 25 years. As a result, adjustments may be necessary to improve functionality – for instance, by increasing water depths or enhancing terminal loads, since ships are evolving constantly.

New port infrastructure will still be developed, although the focus is shifting towards the maintenance, repair, rehabilitation and adaptation of existing structures in fully up-and-running terminals (Roubos & Grotegoed, 2014). In the coming years, thousands of quay walls will have to be reassessed as part of lifetime extension programmes throughout the world. Numerous existing marine structures, including half of the 85 kilometres of quay walls in the port of Rotterdam (Fig. 1.2), which represent a value of approximately 2 billion euros, will approach the end of their design lifetime in the next few decades. However, the end of their design lifetime does not automatically align with the end of their service life, because most of the quay walls are still in good condition.

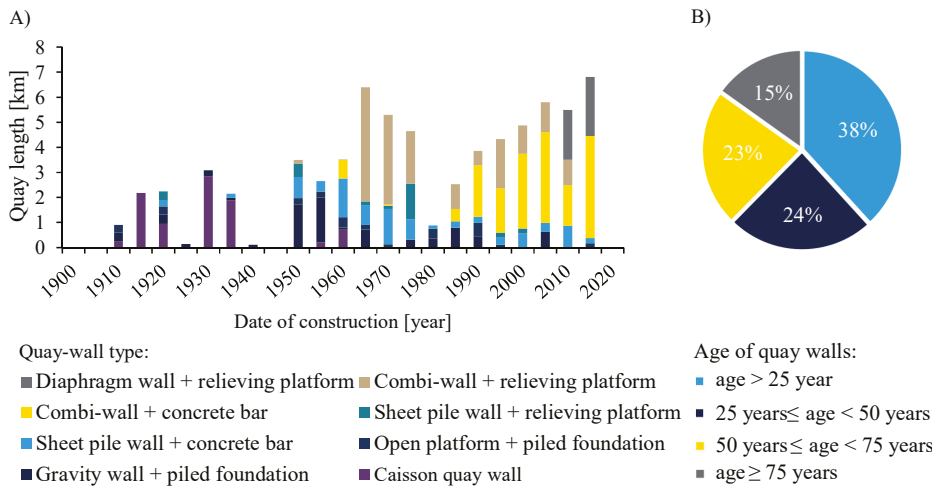


Fig. 1.2. Overview of the type (A) and age (B) of quay walls in the port of Rotterdam

Nonetheless, these structures may have undergone alteration, deterioration, misuse and other changes during their service life. Consequently, port authorities and terminals frequently perform inspections and have to maintain their assets to guarantee safety. The Port of Rotterdam Authority has already addressed an urgent need to focus on asset management. They equip their new quay walls with modern sensors and have developed a quay-wall monitoring system for their existing assets (Voogt et al., 2015). This system objectively supports the decision-making process, focusing on budgeting and prioritising the maintenance of quay walls. Over the years, the Port of Rotterdam Authority has collected a great deal of data, which has been used predominantly for asset-management purposes.

1.2 KNOWLEDGE GAPS

Although some quay walls have been equipped with sensors, and as a result new and additional data is being collected, the actual reliability level of most of these structures is still unknown; this is mainly because the practical applicability of reliability-based assessments in quay-wall engineering is rather low and a probabilistic framework that suits their specific risk profile is lacking. In the coming period, the demand for such advanced analyses is likely to increase, since many quay walls have to be reassessed and the required computation effort will further decrease. This section summarises the main knowledge gaps in relation to the evaluation of the reliability of quay walls.

Unlike reliability-based assessments, conventional structural and geotechnical assessments use generalised safety factors to deal with uncertainties. As a result, the reliability requirements of existing quay walls are frequently not satisfied even though the existing structure itself is performing quite well. One reason is that the target reliability indices presently in use were developed mainly for buildings (Vrouwenvelder, 2001; Vrouwenvelder & Siemens, 1987) and bridges (Steenbergen & Vrouwenvelder, 2010), assuming a constant annual failure rate (Holický, 2011; Leonardo da Vinci Pilot Project, 2005). In reality, a quay wall will be subject to both time-dependent and time-independent sources of uncertainty, such as inherent natural variability in strength and loads (aleatory uncertainty), as well as lack of knowledge or insufficient information (epistemic uncertainty) (ISO 2394, 2015). Consequently, it is unclear whether the reliability indices derived for buildings are applicable to the specific risk profile of quay walls. Since important assumptions in geotechnical engineering, such as characteristic strength properties of soil, are fraught with uncertainties (Fenton et al., 2016), it is expected that the annual failure rate (the frequency with which a structure fails, expressed in failures per year) of a service-proven and non-deteriorating quay wall will decrease during its early years of service and over time approach an almost constant value, since after a period of successful service only the uncertainty in time-dependent design variables, such as live loads, remains (Fig. 1.3-A).

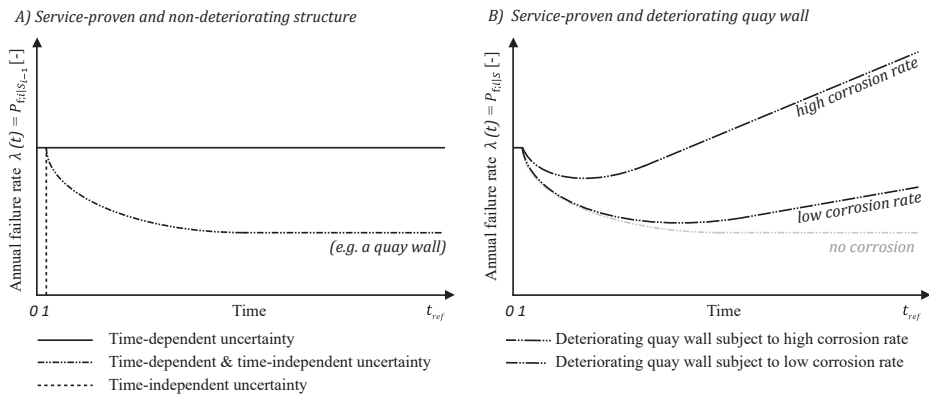


Fig. 1.3. Failure rate of service-proven and non-deteriorating structures (A) and the effect of service-proven deteriorating quay walls (B).

Since quay walls frequently have a complex soil-structure interaction (e.g. due to inclined retaining walls or relieving platforms, see Fig. 1.1), structural and geotechnical assessments are usually performed semi-probabilistically while modelling the quay wall on the basis of finite elements. A more systematic way to account for uncertainties is to perform a reliability-based assessment (Phoon & Retief, 2016). While reliability methods

have already been widely adopted in civil engineering and for flood-risk evaluation (Jonkman & Schweckendiek, 2015), the efficiency and robustness of finite element-based reliability assessments of quay walls are still fairly low. In particular, it remains quite a challenge to achieve a robust coupling between probabilistic methods and finite element models, e.g. due to the highly complex and non-linear character of soil behaviour. Although a few studies (Rippi & Teixeira, 2016; Schweckendiek et al., 2012; Teixeira et al., 2016; Wolters et al., 2012) show promising results for quay walls and other soil-retaining structures, most use simplified models, a limited number of stochastic variables, neglect correlations and they generally do not consider structures that have actually been built. As a result, it is unknown to port authorities and terminals to what extent design variables influence quay walls' reliability, what data is relevant and what data or information is lacking.

Two recent studies (Boero et al., 2012; Teixeira et al., 2016) show that the uncertainty in material loss due to corrosion significantly influences the reliability level of soil-retaining walls. However, clear guidance on how to assess service-proven quay walls subject to corrosion-induced degradation is lacking. The Port of Rotterdam Authority therefore collected millions of wall-thickness measurements and developed an allowable stress-based method using specific corrosion curves to predict the end of the service life of its assets (Jongbloed, 2019). It is unclear, however, if this method adequately covers the actual reliability level of a quay wall that has successfully been in service for a certain period of time, since in the absence of degradation it has become more likely that this structure will remain satisfactory and safe (Melchers & Beck, 2018). In the event of corrosion-induced degradation, the failure rate of a quay wall is expected to increase over time (Fig. 1.3-B). The extent of this effect will depend on the corrosion rate. Only a few other studies have investigated the influence of corrosion on the reliability of steel soil-retaining walls (Houyoux et al., 2007; Osório et al., 2010; Schweckendiek et al., 2007), mainly using the first-order reliability method (*FORM*). None of these studies took successful past performance into account, however, and so they most likely overestimate the probability of failure of service-proven soil-retaining walls. This is because not all effects of the passage of time and service on structural reliability are negative (Hall, 1988). These beneficial effects can partly offset negative ones induced by degradation (Fig. 1.3-B).

In addition to uncertainties in strength, uncertainties related to loads must be taken into consideration. During this research, new datasets of berthing records were provided by the port authorities of Bremerhaven, Rotterdam and Wilhelmshaven. Meanwhile, it became clear that berthing velocity curves developed during the 1970s are still embedded in the design of marine structures throughout the world. Since vessel dimensions have evolved, collecting and studying the available berthing records will directly enhance quay wall reliability. The datasets obtained have provided a unique opportunity to develop new design guidance

for berthing energy. This will be beneficial for assessing structural reliability and for lifetime extension of quay walls and other marine structures.

Experts in the field of marine structures expect that hidden capacities must be present in the failure modes of quay walls, but they are not yet able to explicitly identify and activate these. One solution to this situation is to evaluate the failure modes of critical structural members by performing reliability-based assessments (Phoon & Retief, 2016).

1.3 RESEARCH AIM AND QUESTIONS

This research aims to evaluate the reliability of quay walls and to show which aspects need to be considered. The associated research objectives are fourfold: (i) to develop methods to allocate reliability targets that suit the risk-profile of quay walls over time; (ii) to enable finite element-based reliability assessments of quay walls in realistic design conditions; (iii) to analyse the effect of corrosion-induced degradation and past service performance on the reliability and failure rate of quay walls; and (iv) to provide guidance on the use of field observations and derivation of partial factors of safety for loads acting on quay walls. The central research question of this thesis is therefore defined as follows.

“How can quay wall reliability be evaluated, and what aspects should be considered?”

The central research question is answered by considering the following key questions.

- i. How can reliability targets for commercial quay walls be derived using different risk acceptance criteria? (Chapter 2)*
- ii. How can we perform a finite element-based reliability assessment in quay-wall engineering? (Chapter 3)*
- iii. What is the effect of corrosion-induced degradation on the reliability of service-proven quay walls? (Chapter 4)*
- iv. How can berthing records be used to improve the reliability of existing quay walls? (Chapter 5)*

The key questions comply with the requirements and critical success factors of this thesis. Ideally, this thesis should provide new target reliability levels and increase the applicability of reliability-based analyses in quay-wall engineering, in order to evaluate quay walls' reliability. In addition, the results must be reproducible and should be verified in practice. To be successful, the research output should bridge the gap between theory and practice and should benefit port authorities or terminals – for example, by identifying

hidden capacities or new business opportunities. It should also provide port authorities or terminals with more insight into their quay walls' reliability, allowing them to safely and responsibly evaluate their remaining service life and/or make better use of their assets. Furthermore, port authorities need to know what data should be collected and whether this data is available. To improve the study's applicability, the insights acquired should be shared with the industry, e.g. code developers, authorities, clients and practising engineers. A more technical success factor of this study is enhancing the practical application by coupling Plaxis – one of the most advanced finite-element models presently used in quay-wall engineering – to probabilistic tools, using the as-built information and the data available from real ports.

1.4 SCOPE AND OUTLINE

This thesis demonstrates how quay-wall reliability can be evaluated and what aspects should be taken into consideration when doing so. Performing reliability-based assessments involves allocating reliability targets, estimating the actual probability of failure and taking into account variable loads, degradation and past-service performance. In line with these aspects and the research questions, this thesis covers four research components (Fig. 1.3). It is therefore structured as follows.

- The first research component (Chapter 2) provides suggestions for quantifying reliability targets and enables the allocation of appropriate ones on the basis of the specific risk profile of commercial quay walls. In addition, it includes a framework based on the consequences of failure to differentiate the reliability targets of various quay wall types. The target reliability indices were derived from various risk-acceptance criteria, such as economic optimisation, individual risk, societal risk and human safety. This chapter presents a new method to determine reliability targets, which takes into account the influence of both time-dependent and time-independent model parameters.
- The second research component (Chapter 3) features the finite element-based reliability interface named ProbAna® (Laera & Brinkgreve, 2017), developed to calculate a quay wall's actual reliability level – which is directly related to the probability of failure – in respect of critical failure modes. This interface is used to estimate the actual failure probability of two real quay walls, taking into account a large number of stochastic variables. Since using these advanced tools can become a 'black box', the second part of this research evaluates the outcomes using alternative reliability tools and fairly simple methods. Furthermore, it also reflects upon the partial factors presently in used in quay-wall engineering.

- The third research component (Chapter 4) investigates the effect over time of corrosion-induced degradation on the reliability of quay walls by performing a fully time-dependent reliability analysis, taking into account both past service performance and degradation. The development of the annual failure rate of service-proven quay walls is of particular interest, having been modelled by performing approximately 7.5 billion limit state evaluations.
- The final research component (Chapter 5) translates the available field observations provided by Dutch and German ports into information by statistically examining berthing records of large seagoing vessels. Various types of vessel and various navigation conditions were examined. The main focus was on berthing velocity, because this is the dominant design variable in assessing the berthing impact loads acting on quay walls and other types of berthing facility (Ueda et al., 2010). This research component evaluates some historically embedded hypotheses within the industry, such as the assumption that berthing velocities correlate strongly with vessel size, and presents new design values and partial factors of safety. The results of this component should help make better use of existing quay walls, e.g. by allowing larger vessels to berth and to extend the service life of berthing facilities.

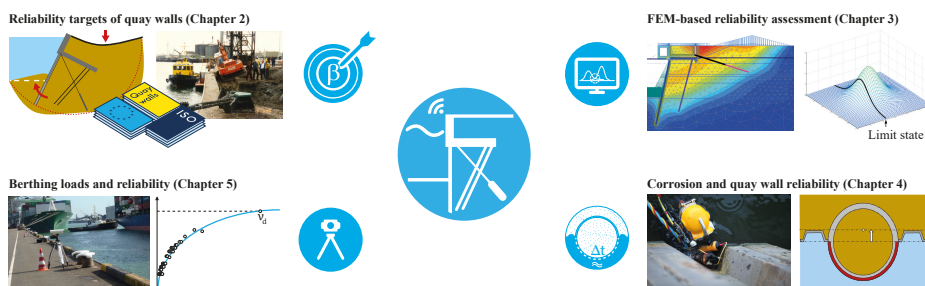


Fig. 1.4. Structure of this thesis.

1.5 LIMITATIONS

Since the primary aim of this thesis is to demonstrate how quay wall-reliability can be evaluated and what aspects should be taken into consideration when doing so, some assumptions and limitations have been imposed on its scope.

- The evaluation of quay-wall reliability involves information about social and economic impacts – such as damage to the image and reputation of a port – which is both relatively complex to quantify and influenced by local conditions. More measurable

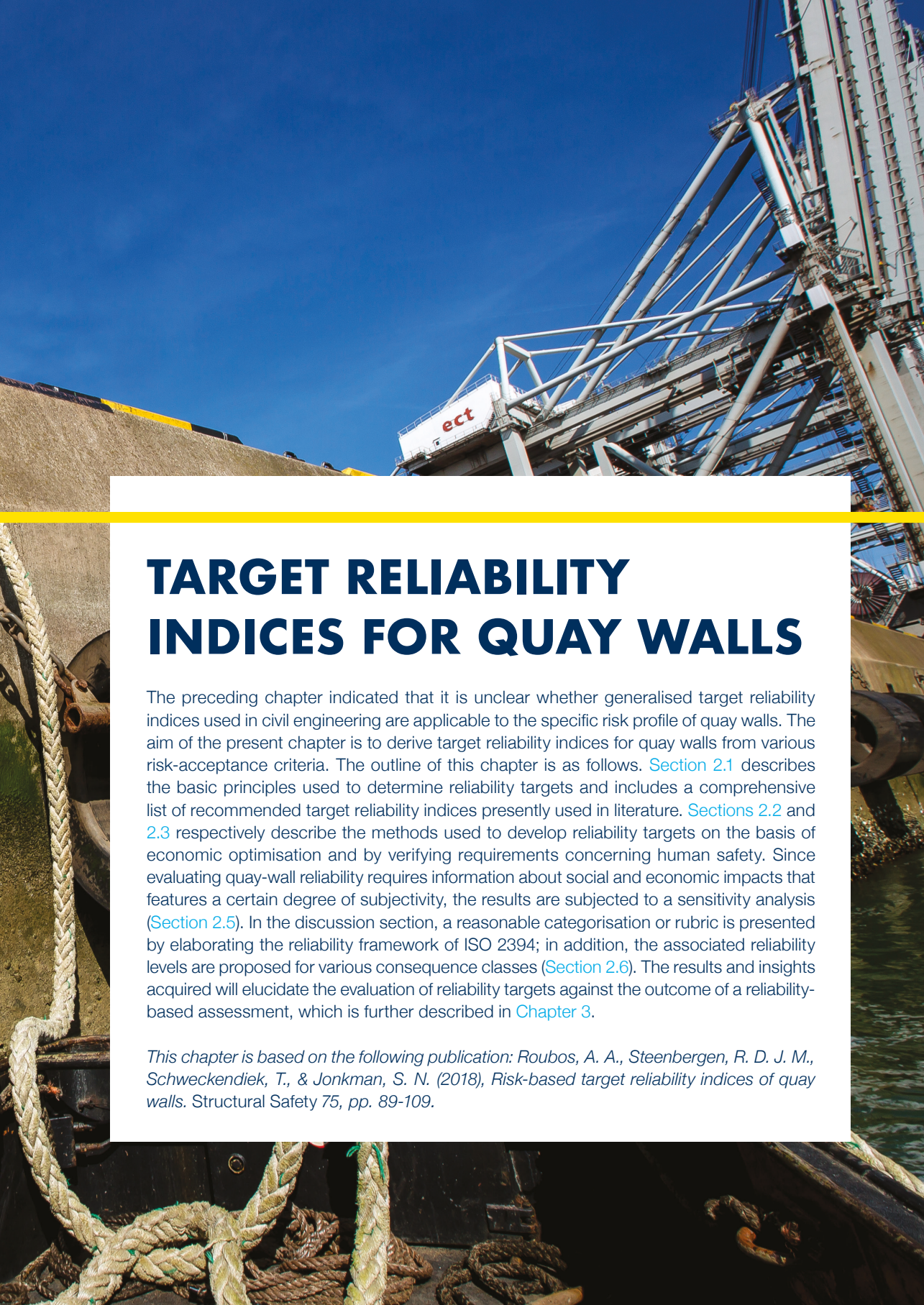
parameters, such as the discount rate, also contain a certain degree of subjectivity. A sensitivity analysis was thus performed to illuminate the impact of the input parameters considered.

- The type of marine structure as well as the local situation, such as soil properties and environmental and/or navigation conditions, may differ per site. The methods used have predominantly been verified in the port of Rotterdam, mainly because the research was largely funded by Smartport, the collaborative arrangement between the Port of Rotterdam Authority, industry representative body Deltalinqs, the City of Rotterdam, Erasmus University Rotterdam, TNO, Deltares and Delft University of Technology. Although local conditions differ, the type of quay walls considered in this study are also found in many other ports throughout the world.
- In quay-wall design, many failure modes need to be evaluated and these may depend on geographical location – for example, those associated with earthquake-induced failure. The reliability-based assessments performed in this study are limited to relevant structural and geotechnical failure modes. Others, such as ‘liquefaction’, ‘excessive settlement’, ‘crack width’ and ‘insufficient bearing capacity’, are not taken into consideration.
- This study shows that past performance can have a positive effect on quay-wall reliability. In this study, however, soil properties were assumed to be time-independent, which is not always true. In some circumstances, the strength of the soil can further increase over time, whereas in other circumstances (such as fatigue, overconsolidated soil, creep or high groundwater flow velocities) the strength of materials can decrease with time. In the latter, the passing of time will negatively influence quay-wall reliability. Furthermore, failure modes driven by extreme events, such as earthquakes, scour, liquefaction, typhoons or tsunamis were not taken into consideration. When quay walls are subject to such dominant time-dependent loads the positive effects of past performance are likely to be fairly low.

Other limitations and assumptions concerning more detailed aspects of the research are discussed in the relevant chapters.

2





TARGET RELIABILITY INDICES FOR QUAY WALLS

The preceding chapter indicated that it is unclear whether generalised target reliability indices used in civil engineering are applicable to the specific risk profile of quay walls. The aim of the present chapter is to derive target reliability indices for quay walls from various risk-acceptance criteria. The outline of this chapter is as follows. [Section 2.1](#) describes the basic principles used to determine reliability targets and includes a comprehensive list of recommended target reliability indices presently used in literature. [Sections 2.2](#) and [2.3](#) respectively describe the methods used to develop reliability targets on the basis of economic optimisation and by verifying requirements concerning human safety. Since evaluating quay-wall reliability requires information about social and economic impacts that features a certain degree of subjectivity, the results are subjected to a sensitivity analysis ([Section 2.5](#)). In the discussion section, a reasonable categorisation or rubric is presented by elaborating the reliability framework of ISO 2394; in addition, the associated reliability levels are proposed for various consequence classes ([Section 2.6](#)). The results and insights acquired will elucidate the evaluation of reliability targets against the outcome of a reliability-based assessment, which is further described in [Chapter 3](#).

This chapter is based on the following publication: Roubos, A. A., Steenbergen, R. D. J. M., Schweckendiek, T., & Jonkman, S. N. (2018), Risk-based target reliability indices of quay walls. Structural Safety 75, pp. 89-109.

ABSTRACT

Design codes and standards rely on generalised target reliability indices. It is unclear, however, whether these indices are applicable to the specific risk profile of marine structures. In this chapter, target reliability indices for quay walls are derived from various risk acceptance criteria, such as economic optimisation, individual risk (*IR*), societal risk (*SR*), the life quality index (*LQI*) and the social and environmental repercussion index (*SERI*). Important stochastic design variables in quay-wall design, such as retaining height, soil strength and material properties, are largely time-independent, whereas other design variables are time-dependent. The extent to which a reliability problem is time-variant affects the present value of future failure costs and the associated reliability optimum. A method was therefore developed to determine the influence of time-independent variables on the development of failure probability over time. This method can also be used to evaluate target reliability indices of other civil and geotechnical structures. The target reliability indices obtained for quay walls depend on failure consequences and marginal costs of safety investments. The results have been used to elaborate the reliability framework of ISO 2394, and associated reliability levels are proposed for various consequence classes. The insights acquired are used to evaluate the acceptable probability of failure for different types of quay walls.

2.1 INTRODUCTION

There are thousands of kilometres of quay wall along inland waterways, in city centres, in commercial port areas and even in flood-defence systems throughout the world. The reliability level of quay walls is generally determined in accordance with a certain design code or standard, such as the Eurocode standard EN 1990 (2011). Table 2.1 shows an example of reliability differentiation for buildings by employing a risk-based approach that directly relates the target probability of failure and the associated target reliability index to the consequences of failure. The consequences of failure can take many different forms, such as loss of human life and social, environmental and economic repercussions (Diamantidis, 2017). It should be noted, too, that target reliability indices were developed mainly for buildings (Vrouwenvelder, 2001; Vrouwenvelder & Siemens, 1987) and bridges (Steenbergen & Vrouwenvelder, 2010), assuming fully time-variant reliability problems (Holický, 2011; Leonardo da Vinci Pilot Project, 2005). However, the source of aleatory and epistemic uncertainty (Kubler, 2006) as well as the consequences of failure could be very different for quay walls in port areas (Ligtvoet & Van der Lei, 2012).

2

Table 2.1. Consequence and reliability classes for civil engineering works in EN 1990.

Consequence/ reliability Class	Description	Examples of buildings and civil engineering works	Reliability index	
			$\beta_{t_1}^1$	$\beta_{t_{50}}^1$
CC3/ RC3	High consequences for loss of human life <u>or</u> economic, social or environmental consequences very great .	Grandstands, public buildings where the consequences of failure are high (e.g. a concert hall).	5.2	4.2
CC2/ RC2	Medium consequence for loss of human life; economic, social or environmental consequences considerable .	Residential and office buildings, public buildings where the consequences of failure are medium (e.g. an office building).	4.7	3.8 ²
CC1/ RC1	Low consequence for loss of human life <u>and</u> economic, social or environmental consequences small or negligible .	Agricultural buildings where people do not normally enter (e.g. storage buildings and greenhouses).	4.2	3.3

¹) The annual (β_{t_1}) and lifetime reliability ($\beta_{t_{50}}$) indices only represent the same reliability level if limit state functions are time-dependent.

²) This value is equal to the mean value derived by calibrating building codes (Vrouwenvelder & Siemens, 1987).

In the Netherlands, the design handbooks for quay walls (De Gijt & Broeken, 2013) and sheet pile walls (Janssen, 2012) further elaborate the recommendations of the Eurocode standard, because examples of soil-retaining walls are lacking (Table 2.1).

Table 2.2. Reliability classes for quay walls in accordance with Quay Walls handbook (De Gijt & Broeken, 2013).

Consequence/ reliability Class	Description consequences of failure	Examples of quay walls	Reliability index β_{-50}
CC3/ RC3	Risk danger to life high Risk of economic damage high	Quay wall in flood defence/LNG plant or nuclear plant (hazardous goods)	4.2
CC2/ RC2	Risk danger to life negligible Risk of economic damage high	Conventional quay wall for barges and seagoing vessels. Retaining height > 5 m	3.8
CC1/ RC1	Risk danger to life negligible Risk of economic damage low	Simple sheet pile structure/quay wall for small barges. Retaining height < 5 m	3.3

Table 2.2 suggests that reliability differentiation is influenced to a certain extent by the retaining height of a quay wall. Although the retaining height is an important design variable, it is not necessarily an assessment criterion for reliability. In port areas, ‘danger to life’ is fairly low (OCDI, 2009) because few people are present and quay walls are ideally designed in such a way that adequate warning is mostly given by visible signs, such as large deformations (Gaba et al., 2017; De Gijt & Broeken, 2013). In reality, however, the factors influencing reliability differ per failure mode (Allaix et al., 2017; JCSS, 2001). Fig. 2.1 gives an impression of the types of quay walls built in the Port of Rotterdam.

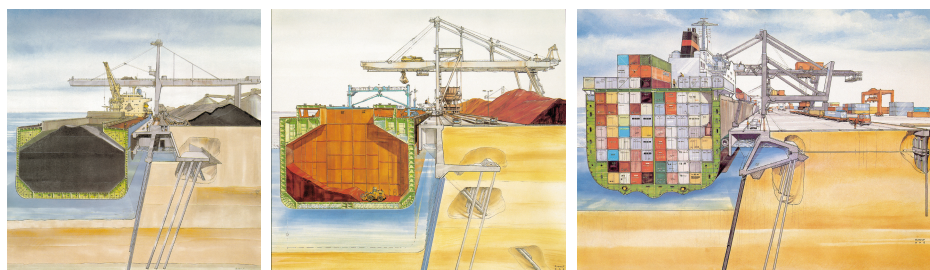


Fig. 2.1. Typical quay walls equipped with a relieving platform in the Port of Rotterdam (De Gijt & Broeken, 2013). Used by permission of the Port of Rotterdam Authority.

The primary aim of this chapter is to provide code developers with material to establish target reliability indices for quay walls and similar structures in a substantiated manner. In addition, its secondary aim is that quay walls can be categorised into existing reliability classes by authorities, clients and/or practising engineers. The first part of the chapter

is devoted to examining the reliability optimum by economic optimisation on the basis of cost minimisation. In quay-wall design, the dominant stochastic design variables, such as retaining height, soil strength and material properties, which influence the risk profile and hence willingness to invest in safety measures are largely time-independent (Schweckendiek et al., 2007; Wolters et al., 2012). In this chapter, a method is developed to determine capitalised risk and the associated reliability optimum. The second part of this chapter focuses on assessing minimum requirements concerning human safety. A sensitivity analysis is performed in order to obtain an insight into those parameters which influence the reliability index, such as discount rates, time horizons, marginal costs of safety investments and degree of damage in terms of monetary units or number of fatalities. The results have been used to elaborate the reliability framework of ISO 2394 (2015), in order both to be consistent with most of the codes and standards currently used in quay-wall design and to improve guidance on reliability differentiation.

2.2 TARGET RELIABILITY INDICES IN LITERATURE

2.2.1 PRINCIPLES OF TARGET RELIABILITY

Basic performance measures are frequently expressed as an allowable probability of failure on the basis of a limit state function (Gulvanessian & Holický, 2005). International bodies, such as the International Organisation for Standardisation (ISO) and the Joint Committee on Structural Safety (JCSS), support reliability-based design and assessments of structures. ISO has provided an international standard, ISO 2394 (2015), in order to develop a more uniform and harmonised design approach regarding resistance, serviceability and durability. ISO 2394 has formed the foundation for many design codes and standards, such as all the guidelines compliant with the Eurocodes (BS 6349-1, 2016; BS 6349-2, 2010; Gaba et al., 2017; De Gijt & Broeken, 2013; Grabe, 2012; NTC, 2008; ROM 0.0, 2002) and technical standards and commentaries for port and harbour facilities in Japan (OCDI, 2009). Modern design codes define the probability of failure $P_f = P(Z \leq 0)$ by a limit state function (JCSS, 2001). The target reliability index and target probability of failure are then related as follows:

$$\beta_t = \Phi^{-1}(P_{f,t}) \quad (1)$$

Where:

β_t	Target reliability index [-]
$P_{f,t}$	Target probability of failure [-]
Φ^{-1}	Inverse of the standard normal cumulative distribution function [-]

Chapter 2

Target reliability indices are always related to a reference period of, for example, one year or fifty years, as presented in Table 2.1. Eq. (2) is often used to transform annual into lifetime probabilities of failure (Leonardo da Vinci Pilot Project, 2005). However, this equation is valid only if reliability problems are largely time-variant (Sýkora et al., 2017) and hence should be used carefully (Vrouwenvelder, 2001) in the case of dominant time-independent stochastic design variables of quay walls.

$$P_{f;t_{ref}} = 1 - (1 - P_{f;t_1})^{n_{ref}} \approx P_{f;t_1} \cdot n_{ref} \quad (2)$$

Where:

$P_{f;t_{ref}}$	Probability of failure in the interval $[0, t_{ref}]$ [-]
$P_{f;t_1}$	Probability of failure over the interval $[0, t_1]$ [-]
$n_{t_{ref}}$	Number of years in reference period t_{ref} [-]
t_1	Reference period of one year [year]

2.2.2 RELIABILITY DIFFERENTIATION IN LITERATURE

This section presents an overview of reliability differentiation and associated target reliabilities in literature for civil-engineering works. In practice, reliability indices are often derived by calibrating against previous design methods in order to maintain an existing reliability level (Bhattacharya et al., 2001; Böckmann & Grünberg, 2009). However, target reliability indices can also be derived on the basis of economic optimisation by minimising costs. The associated reliability optimum is strongly influenced by marginal costs of safety measures, distribution type and the coefficient of variation of stochastic design variables (Leonardo da Vinci Pilot Project, 2005; Rackwitz, 2000).

Table 2.3. Marginal costs of safety measures and annual target reliability indices for structural components.

Marginal costs of safety measures	Consequences of failure		
	Insignificant	Normal	Large
High	2.3 ¹	3.1 ¹	3.7 ¹
Moderate	3.1 ¹	3.7 ¹	4.3 ¹
Low	3.7 ¹	4.3 ¹	4.7 ¹

¹) Target reliabilities were derived typically for bridges by cost minimisation assuming lognormal load and strength distributions and neglecting fatigue inspection, maintenance and failure costs upon reconstruction (Rackwitz, 2000).

The target reliabilities derived on the basis of assuming low costs of safety measures listed in [Table 2.3](#) correspond to the recommendations of Eurocode standard NEN-EN 1990 (2011) ([Table 1.1](#)). The *Implementation of Eurocodes* handbook (Leonardo da Vinci Pilot Project, 2005) and Rackwitz (2000) notes that optimum target reliability indices found by cost minimisation are largely influenced by distribution type and the coefficient of variation of stochastic design variables.

In civil engineering, the required reliability level is generally defined in terms of certain safety classes, such as occupancy, reliability or consequence classes. An overview of safety classes and the accompanying annual and lifetime target reliabilities in literature is presented in [Table 2.4](#) and [Table 2.5](#).

It should be noted that recommendations for the assessment of existing structures, such as ISO 13822 (2010) and NEN 8700 (2011), are not included.

The recommendations for reliability differentiation in literature initially seemed inconsistent and quite different (Bhattacharya et al., 2001; Sýkora et al., 2014). However, when all the assessment criteria and associated target indices were subsequently ordered in accordance with the framework of ISO 2394 (2015), reliability differentiation in literature appeared to be quite consistent and uniform. The classes A, B, C, D and E corresponding with ISO 2394 and the associated assessment criteria are further discussed in [Section 2.6.2](#).

The latest edition of ISO 2394 (2015) determines five consequence classes and associated annual target reliabilities for ultimate limit states. The National Building Code of Canada (NBCC) and the Canadian Highway Bridges Design Code (CHBDC) incorporate the consequence classes 'low', 'typical' and 'high' and reduce safety factors in the case of a detailed understanding of structural behaviour and a detailed site investigation (Fenton et al., 2016). For the assessment of existing structures, ISO 13822 (2010) and NEN-EN 8700 (2011) recommend specific target reliabilities for renewal and upgrade and minimum values for disapproval. The recommendations of NEN 8700 were adopted in the *Urban Quay Walls* handbook (Roubos & Grotegoed, 2014). The Italian structural code (NTC, 2008) does not explicitly recommend target reliability indices, but uses 'knowledge levels' and 'confidence factors'. When many people are at risk, safety requirements, often expressed as annual failure rates, will determine the acceptable reliability level (Vrouwenvelder & Scholten, 2010; Steenbergen et al., 2015). Detailed overviews of available methods for quantitative risk measures of loss of life and accompanying thresholds are given by Jonkman et al. (2003) and Bhattacharya et al. (2001). The minimum annual failure rates for ultimate limit states derived by Fischer et al. (2012) – namely 3.1, 3.7 and 4.2 for high, medium and low relative life-saving costs, respectively – are implemented in ISO 2394 (2015). Det Norske Veritas (DNV, 1992) differentiates the required reliability level of marine structures in terms of structural redundancy and warning signals. The American Society of Civil Engineers distinguishes four occupancy categories (ASCE 7-10, 2010), representing the number of lives

placed at risk by failure. The acceptable safety and the associated target reliability index are further differentiated for situations when failure is or is not sudden and does or does not lead to widespread progression of damage. In the Netherlands, hydraulic structures that are part of a flood-defence system are examined using risk-based methods (Jonkman & Schweckendiek, 2015). The maximum allowable risk is defined by frequency of inundation and socioeconomic damage. Reliability differentiation of failure modes of soil-retaining walls that are part of a flood-defence system is applied by distinguishing specific safety classes and associated lifetime target reliability indices (STOWA, 2011; TAW, 2003). The technical standards and commentaries for port and harbour facilities in Japan (OCDI, 2009) evolved into a performance-based design approach (Nagao et al., 2009) which implements the basic principles of ISO 2394. For seismic performance verification, high (*HR*), intermediate (*IR*) and normal seismic (*NR*) resistance classes were developed. International sea-container terminals and facilities with an important role in emergency recovery after earthquakes are classified as HR facilities. The Spanish recommendations for maritime structures, ROM 0.0 (2002), comply with NEN-EN 1990 and verify structural reliability, functionality and operability against failure and stoppage modes. The intrinsic nature of a maritime structure is expressed in terms of the social and environmental repercussion index (*SERI*) and the economic repercussion index (*ERI*) (Losada & Benedicto, 2005). Low and high/very high *SERI*-rated maritime works are assumed to correspond with RC1 and RC2 of EN 1990, respectively (ROM 0.5, 2008). ROM 0.5 notes that maritime works do not have an equivalent representation with RC3. *ERI* is used to determine the 'minimum useful' life. The German recommendations for the design of waterfront structures, EAU 2012 (Grabe, 2012), distinguish safety classes for resistance and typical loading cases, but do not explicitly recommend target reliability indices. Neither the British Standard (2016) nor CIRIA (the UK's Construction Industry Research and Information Association) (Cork & Chamberlain, 2015; Gaba et al., 2017) prescribe a specific target reliability index. However, EAU 2012 and BS 6349-2 (2010) are consistent with EN 1990 (2011). In the Netherlands, the reliability differentiation of EN 1990 is applied unaltered to the design of quay walls (De Gijt & Broeken, 2013), jetties (Broeken, 2018), dolphins (Roubos, 2018) and sheet pile walls (Janssen, 2012).

Table 2.4. Overview of annual target reliability indices in literature for the ultimate limit state (ULS).

Literature	Application	Consequence classes				
		A	B	C	D	E
		Low	Some	Considerable	High	Very high
ISO 2394 (2015) ¹	All	Class 1	Class 2	Class 3	Class 4	Class 5
			4.2	4.4	4.7	
JCSS (2001) ¹	All		Minor	Moderate	Large	
			4.2	4.4	4.7	
Structural concrete (2012) ¹	Concrete	Small	Some		Moderate	Great
		3.5	4.1		4.7	5.1
EN 1990 (2002)	All		RC1		RC2	RC3
			4.2		4.7	5.2
Rackwitz (2000) ¹	Bridges	Insignificant		Normal	Large	
		3.7		4.3	4.7	
DNV (1992)	Marine	Type I	Type I & II	Type II & III	Type III	
		3.09	3.71	4.26	4.75	
USACE (1997)	Geotechnical	Average	Good			High
		2.5/3.0	4.0			5.0

¹⁾ Reliability indices are derived by assuming low relative costs of safety measures

Table 2.5. Overview of lifetime target reliability indices in literature for the ultimate limit state (ULS).

Literature	Application	Consequence classes				
		A	B	C	D	E
		Low	Some	Considerable	High	Very high
ISO 2394 (1998) ¹	All	Small	Some		Moderate	Great
		2.3	3.1		3.8	4.3
ISO 23822 (2010) ¹	All	Small	Some		Moderate	Great
		2.3	3.1		3.8	4.3
EN 1990 (2002)	All		RC1		RC2	RC3
			3.3		3.8	4.3
SANS 10160 (2010)	All	RC1	RC2	RC3		RC4
		2.5	3.0	3.5		4.0

Chapter 2

Table 2.5. Continued.

Literature	Application	Consequence classes				
		A	B	C	D	E
		Low	Some	Considerable	High	Very high
NEN 6700 (2005)	All		Class 1	Class 2	Class 3	
			3.2	3.4	3.6	
ASCE (2010) ²	All	I ^a	II ^a , III ^a & I ^b	IV ^a , II ^b & 1 ^c	III ^b	IV ^b , II ^c , III ^c & IV ^c
		2.5	3.0/3.25/3.0	3.5/3.5/3.5	3.75	4.0/4.0/4.25/4.5
NBCC (2010)	Buildings		Low	Typical	High	
			3.1	3.5	3.7	
CDHBDC (2014)	Bridges		Low	Typical	High	
			3.1	3.5	3.7	
STOWA (2011)	Hydraulic	QC I	QC II, QC III	QC IV	QC V	
		2.3	2.7/3.1	3.4	3.7	
TAW (2003)	Hydraulic				River dike	Sea dike
					3.8	4.3
ROM 0.5-05 (2008)	Geotechnical	Minor	Low		High/very high	
		2.33	3.09		3.72	
CUR 166 (2012)	Sheet piles	Class I		Class II		Class II
		2.5		3.4		4.2
OCDI (2009)	Marine	NR ³	IR ³		HR ³	
		2.19/2.67	2.67		3.65	
CUR 211 (2003)	Quay walls		Class 1	Class 2	Class 3	
			3.2	3.4	3.6	
CUR 211 (2013)	Quay walls		RC1		RC2	RC3
			3.3		3.8	4.3

¹) Reliability indices are derived by assuming low relative costs of safety measures.

²) Not sudden, not widespread (a), sudden or widespread (b), sudden and widespread (c).

³) Normal, intermediate and high seismic performance verification.

2.3 METHOD FOR DERIVING TARGET RELIABILITY INDICES FOR QUAY WALLS

2.3.1 INTRODUCTION

This section briefly highlights the information required and methods used to establish target reliability indices. Fig. 2.2 shows that target reliability indices are influenced by the efficiency of safety investments (Section 2.3.4) and the consequences of failure (Section 2.3.5). The optimum reliability index β^* can be obtained by minimising the sum of investments in safety measures and the accompanying capitalised risk (Section 2.3.6). It is important to understand both the quay-wall system (Section 2.3.2) and the influence of time-dependent uncertainty (Section 2.3.2). The target reliability indices derived on the basis of economic optimisation might not be acceptable with regard to requirements concerning human safety (ISO 2394, 2015). These reliability indices are denoted as β_{acc} . The safety criteria are further explained in Section 2.4.

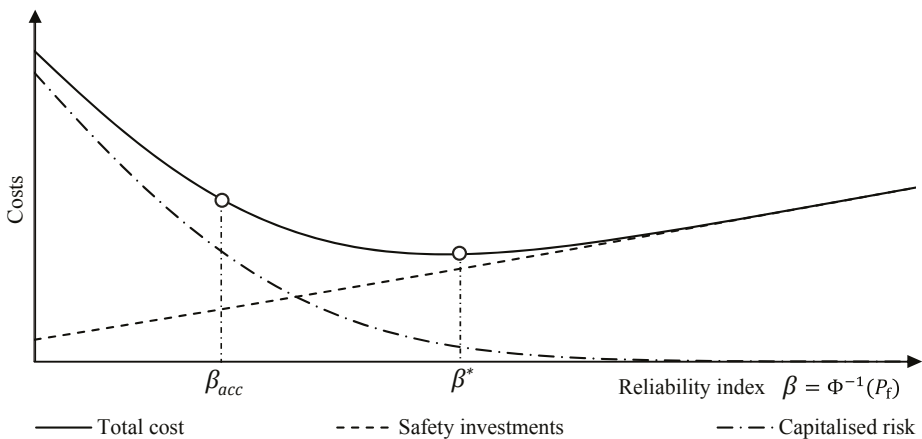


Fig. 2.2. Principles of cost minimisation, reliability optimum β^* and reliability minimum β_{acc} .

2.3.2 SYSTEM DECOMPOSITION AND RELEVANT FAILURE MODES

During the design of a quay wall, several failure modes have to be evaluated. Numerous design guidelines incorporate comprehensive fault trees including relevant failure modes (De Gijt & Broeken, 2013; Janssen, 2012) – for example, yielding of the retaining wall, failure of the anchor strut and geotechnical failure modes (Fig. 2.3). It should be noted that not all failure modes have been considered in this study. In literature, it is often not very clear whether target reliability indices of failure modes are assigned to the structure as a whole or to structural components (Leveson, 2004; Terwel, 2014). In this study, the reliability indices were ascribed to failure modes of structural components in accordance with modern design

Chapter 2

codes (Arangio, 2012; JCSS, 2001; Leonardo da Vinci Pilot Project, 2005; NEN-EN 1990, 2011), assuming that progressive damage is mitigated (Gaba, et al., 2017; De Gijt & Broeken, 2013; Janssen, 2012). Quay walls are generally designed in such a way that brittle failure is prevented and adequate warning is given by large deformations (Gaba, et al., 2017; De Gijt & Broeken, 2013). Consequently, the reliability level of a structural component is generally dominated by one specific failure mode. The following two simplified ultimate limit states were considered as a reasonable first approach (Fig. 2.3):

$$Z_{STR}(z) = f_y - \max\left(\frac{M_{wall}(z)}{W_{wall}} + \frac{N_{tube}(z)}{A_{tube}}\right) \quad (3)$$

$$Z_{GEO} = 1 - \Sigma Msf = 1 - \frac{c' + \sigma_n \tan(\varphi')}{c'_{reduced} + \sigma_n \tan(\varphi'_{reduced})} \quad (4)$$

Where:

Z_{STR}	Limit state representing structural failure [N/mm ²]
z	Depth [m]
f_y	Yield strength of retaining wall [N/mm ²]
M_{wall}	Bending moment in retaining wall [Nmm]
N_{tube}	Normal force in pile [N]
W_{wall}	Section modulus of retaining wall [mm ³]
A_{tube}	Section area of pile [mm ²]
Z_{GEO}	Limit state representing structural geotechnical failure [-]
ΣMsf	Global stability ratio related to φ - c reduction. The friction angle φ' and cohesion c' are successively decreased until geotechnical failure occurs [-]

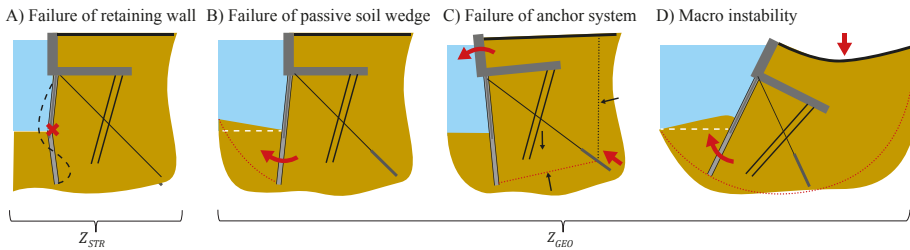


Fig. 2.3. Impression of some of the structural (Z_{STR}) and geotechnical failure modes (Z_{GEO}).

The ultimate limit state for structural failure represents the stresses in the outer fibre of the soil-retaining wall and largely influences safety investments, whereas the global stability ratio takes account of the mutual dependency of all geotechnical failure modes

simultaneously. Both limit states were evaluated by coupling the probabilistic package OpenTURNS (Andrianov et al., 2007) to the finite element hardening soil model from the firm Plaxis, in order to model the soil-structure interaction as realistically as possible. The correlation between soil properties was taken into consideration in order to preclude unrealistically high reliability indices. Typical coefficients of correlation between $E_{50,ref} - \phi'_{rep}$, $\gamma_{sat} - \phi'_{rep}$ and $E_{50,ref} - \gamma_{sat}$ are 0.25, 0.5 and 0.5, respectively (Teixeira et al., 2015; Wolters et al., 2012). The distribution types and coefficients of variation used are listed in Appendix A.2.

In this study, 2D-Plaxis calculations were performed to gain insight into the extent to which a reliability problem is time-variant (Section 2.3.3) and into the efficiency of safety measures (Section 2.3.4), but they represent only a certain distance along a quay wall due to spatial uncertainty concerning resistance and local loads (Calle & Spierenburg, 1991; Hannink, 2008). It is worth noting that it is theoretically impossible for a single metre of quay wall to fail. The length of a quay wall was therefore subdivided into equivalent sections for which failure events are assumed to be largely independent. In this study, the 'equivalent length' L_{eq} was assumed to be 40m (Allaix et al., 2018). This length is representative for the variability of the soil along a quay wall, but also corresponds with the section length of a quay wall that is on the one hand based on construction aspects and on the other hand provides sufficient flexural rigidity to redistribute local operational loads. Independent failure events are also observed in practice. An inventory of failure modes in Rotterdam, Spain and the United Kingdom (Allaix et al., 2017; Allaix et al., 2018) showed that the failure length of the limit states under consideration was approximately 25-50m. Consequently, the associated proportional change in marginal safety costs (Section 2.3.4) and failure consequences (Section 2.3.5) was taken into account for L_{eq} along a quay wall.

2.3.3 MODELLING TIME-VARIANT RELIABILITY

Introduction

The risk profile of a quay wall evolves over time and influences the capitalised risk, and hence the reliability optimum of a quay wall. This section discusses the method used to model the marginal increase in the probability of failure over time in order to determine the present value of future potential failure costs. The annual failure rate will generally decrease during the first period of a wall's service life if no failure has occurred in previous years (Fig. 2.4). Close to the end of the service life, failure due to deterioration is more likely and results in an increase in the annual failure rate. Fig. 2.4-A represents a limit state dominated by time-independent epistemic uncertainty (McCann & Paxson, 2016) in stochastic design variables – for example, a 'dam'. Many dam failures occur at the first filling of the reservoir because of unforeseen soil conditions. By contrast, the annual failure rate of buildings and bridges (Fig. 2.4-C) is often assumed to be constant because uncertainty is dominated by

time-dependent stochastic design variables and deterioration (Sýkora et al., 2017). In quay wall design, uncertainty is largely time-independent (Schweckendiek et al., 2007; Wolters et al., 2012). However, quay walls may show some degradation and are subjected to random loads, such as operational or ship loads and water head differences. The reliability of quay walls is influenced by both time-independent variables (mainly soil properties) and random loads, and will typically be in between Fig. 2.4-A and Fig. 2.4-C.

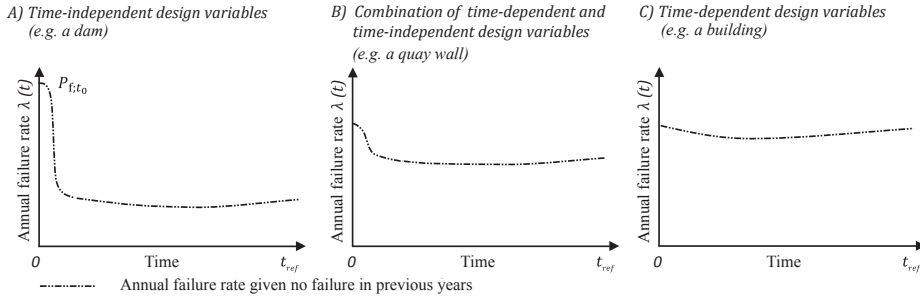


Fig. 2.4. Conceptual bathtub curves for time-independent (A), a combination of time-independent and time-dependent (B) and time-dependent (C) uncertainty in design variables.

Development probability of failure during the lifetime

The usual approach to time-variant reliability problems is based on the computation of the outcrossing rate of the limit state (Rackwitz, 2001; Sudret, 2008; Sudret, 2011). However, here the probability of failure $P_{f;t_n}$ in time interval $(t, t+\Delta t)$ was modelled assuming two blocks, with one block being largely time-independent $P_{f;0}$ and the other being fully time-dependent $\sum \Delta P_{f;t_n}$ (Fig. 2.5).

$$P_{f;t_n} = P_{f;0} + \sum \Delta P_{f;t_n} \tag{5}$$

$$P_{f;t_{ref}} = P_{f;0} + \sum_{n=1}^{n_{ref}} \Delta P_{f;t_n} \tag{6}$$

Where:

- $P_{f;t_n}$ Probability of failure in time interval $[0, n]$ [-]
- $P_{f;0}$ Time-independent probability of failure [-]
- $\Delta P_{f;t_n}$ Marginal change in probability of failure in time interval $(n-1, n)$ [-]
- $P_{f;t_{ref}}$ Probability of failure in the interval $[0, t_{ref})$ [-]
- n_{ref} Number of years during the reference period [year]
- t_{ref} Reference period [year]
- n Individual year of the reference period [-]
- t_n Period of n years in the reference period [year]

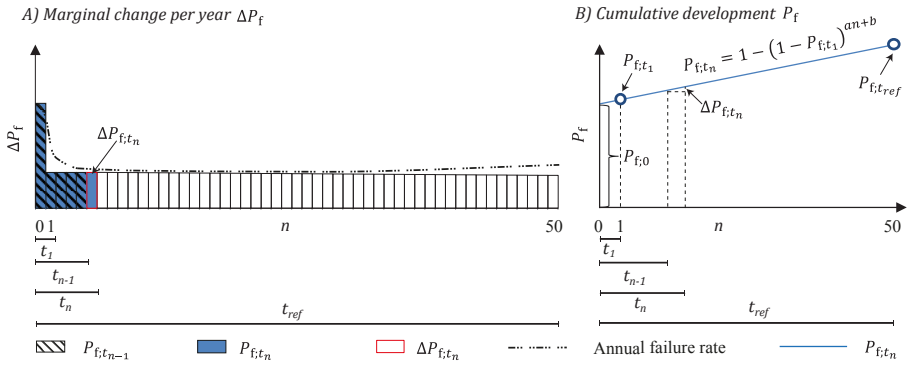


Fig. 2.5. Development of cumulative probability of failure (A) and the associated marginal increase per year (B) for a largely time-dependent limit state function.

In this study, it was assumed that risks related to human errors – such as design and construction errors – are taken into account by means of, for example, quality-control procedures and inspections (Melchers, 2007; ISO 2394, 2015; Vrouwenvelder et al., 2001). Deterioration was not taken into consideration, because new quay walls are equipped with a system of cathodic protection that prevents degradation (De Gijt & Broeken, 2013). Although soil conditions could be influenced by time – such as variability in soil pressure, liquefaction, settlements and compaction (Fenton et al., 2016) – the time effect on soil strength was assumed to be negligible (Section 1.5). The time-dependent part of the probability of failure was taken into consideration by modelling variable loads, such as water head differences and live loads, in accordance with extreme value theory.

Derivation of equivalent time period t_{eq}

Largely time-dependent limit state functions indicate that failure events are to some extent correlated. Sýkora et al. (2017) suggest using a ‘basic’ period in order to account for dependency of failure events, which in this study is denoted as t_{eq} ; in other words, the ‘equivalent’ period for which failure events are assumed to be independent in subsequent years. The cumulative lifetime probability of failure was determined by transforming Eq. (2) into the following equations, which formed the basis for the method used (see also Appendix A.1):

$$P_{f;t_{ref}} = 1 - (1 - P_{f;t_1})^{n_{eq}} \quad (7)$$

$$\beta_{t_{ref}} = \Phi^{-1}[\Phi(\beta_{t_1})^{n_{eq}}] \quad (8)$$

$$n_{eq} = \frac{t_{ref}}{t_{eq}} \quad (9)$$

Where:

$P_{f;t_{ref}}$	Probability of failure in the interval $[0, t_{ref})$ [-]
$P_{f;t_1}$	Probability of failure in the interval $[0, t_1)$ [-]
n_{eq}	Number of equivalent periods during the reference period [-]
$\beta_{t_{ref}}$	Reliability index of reference period t_{ref} [-]
β_{t_1}	Reliability index of a one-year reference period [-]
t_1	Reference period of one year [year]
t_{eq}	Equivalent period for which failure events are independent in subsequent years [year]

The equivalent period t_{eq} was determined using extreme value theory. Although other reference periods could have been considered, it appeared to be fairly practical to perform two probabilistic assessments using t_1 and t_{50} , representing the annual and lifetime probability of failure, respectively. The output of the probabilistic assessment was therefore twofold: a reliability index for a reference period of one year $\beta_{t_1} = \Phi^{-1}(P_{f;t_1})$ and one for a period of fifty years $\beta_{t_{ref}} = \beta_{t_{50}} = \Phi^{-1}(P_{f;t_{50}})$. The results of the probabilistic analysis were used to determine the equivalent period t_{eq} by transforming Eq. (8) into Eq. (10). Fig. 2.6 shows the application of equivalent period t_{eq} in a time-variant reliability problem. When dominant stochastic design variables of a limit state are time-independent $n_{eq} = 1$, but if dominant stochastic design variables are time-dependent $n_{eq} = n_{ref}$.

$$t_{eq} = \frac{t_{ref}}{\log\Phi(\beta_{t_1}) \left[\Phi(\beta_{t_{ref}}) \right]} = t_{ref} \log\Phi(\beta_{t_{ref}}) \left[\Phi(\beta_{t_1}) \right] \quad (10)$$

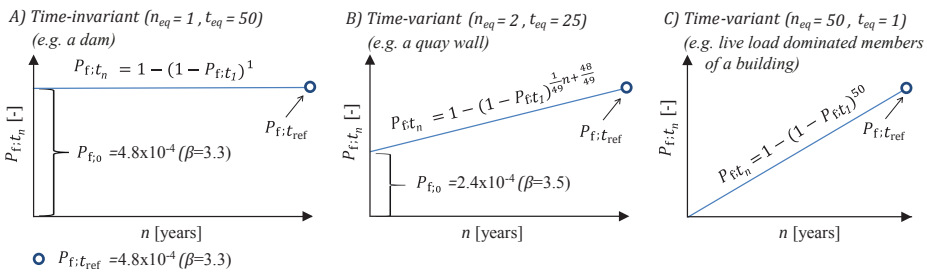


Fig. 2.6. Principal differences between development of failure probability for time-invariant (A), time-variant (B) and completely time-variant (C) reliability problems.

2.3.4 MARGINAL CONSTRUCTION COSTS

The uncertainty in design variables influences not only the extent to which a reliability problem is time-variant, but also the efficiency of safety investments (Rackwitz, 2000; Smit, 2014). As explained in Section 2.3.2, the length of a quay wall was subdivided into equivalent

sections for which failure events are independent. The associated proportional change in marginal safety investments (Fig. 2.2) was found by the following equation:

$$C_m(x) = L_{eq} \frac{\Delta C(x)}{\Delta \beta(x)} \quad (11)$$

Where:

C_m	Marginal costs of safety measures [€]
x	A vector representing changes in structural dimensions [.]
L_{eq}	Equivalent length along a quay wall for which failure events are independent [m]
ΔC	Change in construction costs [€/m]
$\Delta \beta$	Change in reliability index [-]

The costs $\Delta C(x)$ associated with a change in structural dimensions were derived in consultation with senior costs experts at the Port of Rotterdam Authority, and the associated change in reliability index $\Delta \beta$ was derived by performing four probabilistic assessments, two for each limit state. The changes in structural dimensions of the retaining wall, such as the section modulus $W_{wall}(D_{tube}, t_{tube})$ and the sectional area $A_{tube}(D_{tube}, t_{tube})$, were applied to the structural limit state function (Z_{STR}), and changes in length of the retaining wall L_{wall} and the grout body of the anchors L_{anchor} were applied to the geotechnical limit state function (Z_{GEO}). The fraction $\Delta C/\Delta \beta$ found was 5-10%, which is in accordance with the study by Schweckendiek et al. (2007). The marginal safety investments to prevent structural failure were assumed to be higher than those for geotechnically induced failure (Table 2.6).

Table 2.6. Initial construction costs C_0 being independent of β and marginal costs of safety measures C_m for a quay wall with $h_{retaining}=20m$, $L_{eq}=40 m$ and construction costs equal to €1m for $\beta=3.8$.

Failure modes	x	C_0	$C_m(x)$
All failure modes	All structural dimensions	€0.60m	€0.10m
Yielding of the combi-wall ($Z_{STR} < 0$)	$W_{wall}(D_{tube}, t_{tube}); A_{tube}(D_{tube}, t_{tube})$	€0.36m	€0.06m
Geotechnical failure ($Z_{GEO} < 0$)	$L_{wall}; L_{anchor}$	€0.12m	€0.02m

2.3.5 CONSEQUENCES OF FAILURE

As indicated, the consequences of failure can take various forms, and hence can be measured in monetary units C_f or number of fatalities N_{fl} (Chryssanthopoulos et al., 2011). Some information about failure costs C_f was found in the background documents of port authorities and terminals (Buijsingh, 2013; Ligtoet & Van der Lei, 2012), as well as in

some design guidelines (Cork & Chamberlain, 2015; STOWA, 2011). The little available information was extended by administering a questionnaire that asked experts to give both a qualitative and a quantitative estimate of the consequences of failure on the basis of the recommendations of ISO 2394 (2015) and JCSS (2001).

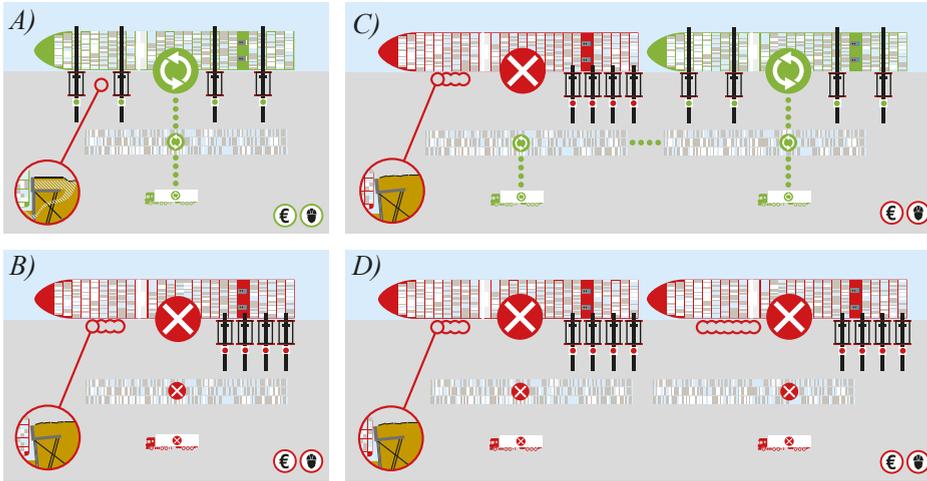


Fig. 2.7. Impression of failure consequences for commercial quay walls with (A & C) and without (B & D) functional redundancy.

Terminal and business managers largely agree that significant economic repercussions are not very likely in large ports, because it is often possible to mitigate damage within the overcapacity of a terminal or port cluster (Fig. 2.7-A and 2.7-C). Substantial economic damage is more likely for terminals without redundancy (Fig. 2.7-B and 2.7-D). The business managers also stated that it is important to prevent permanent damage to the image and reputation of a port. In reality, if a terminal has had some functional redundancy, the failure costs were estimated to be fairly close to the direct failure costs. The experts largely agreed that the failure costs associated with the equivalent length along a commercial quay wall are in the ranges €1-5m and €1-15m for structural failure (Z_{STR}) and geotechnical failure (Z_{GEO}), respectively. The influence of the failure costs on the optimum reliability index was taken into consideration in the sensitivity analysis presented in Section 2.5.2.

In this study, the expected number of fatalities was determined in accordance with Eq. (12). Little information is yet available about the number of people at risk due to their nearness to quay walls, and hence a fairly conservative estimate was made assuming $N_{PAR} = 5$ along 40 metres of quay wall. The successful escape of people largely depends on the type of failure, escape path, perception of danger and recognition of warning signals provided

(Lentz, 2007). The probability of a successful escape influences the conditional probability that an individual will die in the event of a failure. In Table 2.7, indicative estimates of $N_{F|f}$ are presented for the two failure modes under consideration.

$$N_{F|f} = N_{PAR}(1 - P_{Escape})P_{d|f} \quad (12)$$

Where:

$N_{F f}$	Expected number of fatalities in the event of failure [-]
N_{PAR}	Number of people at risk [-]
P_{Escape}	Probability of a successful escape [-]
$P_{d f}$	Conditional probability a random human being present will die in the event of failure [-]

2

Table 2.7. Expected number of fatalities for commercial quay walls.

Type of failure	N_{PAR}^1	P_{Escape}^2	$P_{d f}^3$	$N_{F f}^4$
Structural failure (Z_{STR})	5	0.70	0.10	0.15
Geotechnical failure (Z_{GEO})	5	0.30	0.20	0.70

¹⁾ Conservative estimate, derived by counting the number of people who are near to a quay wall. Catastrophic accidents and situations with lots of people near to a quay wall were not taken into consideration.

²⁾ Conservative value derived by administering a questionnaire.

³⁾ Values are based on a best estimate, and therefore a sensitivity analysis is included in Section 2.5.4.

⁴⁾ Values lower than 1 are only used in the *LQI* criterion.

The monetary value of a human life can be determined on the basis of societal willingness to pay (*SWTP*) (ISO 2394, 2015). However, assigning a monetary value to human life, on whatever basis, is a very controversial issue (Vrijling & Van Gelder, 2000). According to Rackwitz (2008), a monetary value of life does not exist: "...the value of human life is infinite and beyond measure ...". In this study, a monetary value of €3m, which is in line with the \$2-4m presented in ISO 2394 (2015), was used only in the evaluation of the marginal life-saving cost principle (Section 2.5.3).

2.3.6 RISK-BASED OPTIMISATION OF STRUCTURAL COMPONENTS

This section concerns the method used to determine target reliability indices using the principles of cost minimisation in accordance with the recommendations in literature (Rackwitz, 2000; Sykora & Holický, 2011; Sykora et al., 2017). The following objective function was considered:

$$f(\beta) = B - C_{Investments}(\beta) - C_{Maintenance} - C_{Obsolescence}(\beta) - C_{CapitalisedRisk}(\beta) \quad (13)$$

$$\max\{f(\beta)\} \rightarrow \frac{\partial f(\beta^*)}{\partial \beta} = 0 \quad (14)$$

Where:

f	Objective function [-]
B	Benefits related to the investments [€]
$C_{Investments}$	Investments in safety measures [€]
$C_{Maintenance}$	Cost of maintenance, repairs and inspections [€]
$C_{Obsolescence}$	Cost related to a structure becoming obsolete after some time because it is not able to fulfil its originally intended purpose [€]
$C_{CapitalisedRisk}$	Present value of future failure costs [€]
β	Decision parameter, reliability index [-]
β^*	Optimum reliability index [-]

It should be noted that the benefits and maintenance costs were considered to be independent of decision parameter β . The maintenance costs related to structural deterioration were not taken into account because corrosion is so aggressive that it is much more efficient to invest in a system of cathodic protection (De Gijt & Broeken, 2013). Costs of financing projects (e.g. interest rates) and costs related to obsolescence (lifetime buy versus design refresh) were not taken into account. Obsolescence costs are generally activated in the business case of a future design refresh. In this study, the failure costs were related to the design lifetime of the structure. If one assumes that the objective function is positive, the optimum reliability index β^* can be established by minimising the total costs and solving the associated derivative.

$$\min\{C_{Total}(\beta) = C_{Investments}(\beta) + C_{CapitalisedRisk}(\beta)\} \quad (15)$$

$$\frac{\partial C_{Total}(\beta^*)}{\partial \beta} = 0 \quad (16)$$

The investments in safety measures were divided into initial construction costs C_0 and marginal construction costs C_m (Section 2.3.4). The initial construction costs C_0 often dominate structural investments (De Gijt, 2010; De Gijt & Vinks, 2011), but unlike C_m do not influence the reliability optimum (Rackwitz, 2000).

$$C_{Investments}(\beta, x) = C_0 + C_m(x)\beta \quad (17)$$

Where:

C_0	Initial construction costs independent of the reliability index [€]
-------	---

C_m	Marginal construction cost dependent on the reliability index [€]
x	Vector representing the changes in design parameters, e.g. structural dimensions [-]

It should be noted that even if adequate safety measures are implemented, there will always be a residual capitalised risk. In this study, the method proposed by Holický (2011) was extended by distinguishing $P_{f,0}$ and $\sum \Delta P_{f,t_n}$ representing the blocks of the probability of failure over a certain time interval being time-independent and time-dependent, respectively (Section 2.3.3):

$$C_{\text{CapitalisedRisk}}(\beta) = C_f P_{f,0}(\beta) + C_f \cdot \sum_{n=1}^{n_{ref}} \frac{\Delta P_{f,t_n}(\beta)}{(1+r)^n} \quad \text{for } n \in (1, n_{ref}) \quad (18)$$

The capitalised risk represents the present value of future costs and was established by assuming a real discount rate r (nominal rate of interest after correction for inflation) (Sykora & Holický, 2011; Rackwitz, 2006). The minimum discount rate is equal to the time-averaged economic growth rate per capita (Rackwitz, 2008). Fischer et al. (2013) showed that different discount rates could be used for private and social decision-makers. The summation of direct and indirect economic consequences of failure was expressed by C_f (Section 2.3.5).

Eq. (20) presents an analytical formula of the objective function and was used to obtain an insight into the influencing factors of the reliability optimum. The reader is referred to Appendix A.1 for the full derivation and explanation of the total costs function and the associated derivative.

$$C_{\text{Total}}(\beta_{t_1}) = C_{\text{Investments}}(\beta_{t_1}) + C_{\text{CapitalisedRisk}}(\beta_{t_1}) \quad (19)$$

$$C_{\text{Total}}(\beta_{t_1}) = C_0 + C_m \beta_{t_1} + C_f (1 - \Phi_1^b) + C_f c (\Phi_1^b - \Phi_1) \frac{1 - (c \Phi_1^a)^{n_{ref}}}{1 - c \Phi_1^a} \quad (20)$$

$$c = 1/(1+r) \quad (21)$$

Where:

$$\Phi_1 = \Phi(\beta_{t_1}) = F(\beta_{t_1}) \quad \text{Cumulative distribution function } F(\beta) \text{ of normal distribution [-]}$$

2.4 RISK-ACCEPTANCE CRITERIA

The optimum reliability indices derived on the basis of cost minimisation have to be higher than the thresholds of acceptance. This section presents the evaluation of four risk-acceptance criteria, namely the individual risk (*IR*) criterion, the societal risk (*SR*) criterion, the life quality index (*LQI*) acceptance criterion and the social and environmental repercussion index (*SERI*).

2.4.1 INDIVIDUAL RISK CRITERION

The individual risk (*IR*) is often defined as the individual risk per annum (*IRPA*) or the localised individual risk per annum (*LIRA*) (Johansen, 2010; Paltrinieri & Khan, 2016). *IRPA* is generally used to assess work-related risks faced by particularly exposed individuals (NORSOK, 2001; Skjong et al., 2007) and is frequently used in decision-making processes, whereas *LIRA* represents the individual risk at a specific geographical location (Johansen, 2010). *LIRA* is mainly used in spatial planning and assessing external safety contours in the vicinity of hazardous installations or in the design of flood-defence systems (Jongejan et al., 2009; Jonkman et al., 2003; Vrijling, 2001; Vrijling et al., 1998). It should be noted that *LIRA* does not change even if no people are present, and hence the main difference between *IRPA* and *LIRA* is the probability that an individual is present:

$$IRPA = P_{f_{t_1}} P_{Present} (1 - P_{Escape}) P_{d|f} \quad (22)$$

$$LIRA = P_{f_{t_1}} (1 - P_{Escape}) P_{d|f} \quad (23)$$

Where:

<i>IRPA</i>	Annual probability that a specific individual or hypothetical group member will die due to exposure to hazardous events (Rausand, 2013) [-]
<i>LIRA</i>	Annual probability that an unprotected, permanently present individual will die due to an accident at a hazardous site (Jongejan, 2008) [-]
$P_{Present}$	Probability that a specific individual will be present [-]
P_{Escape}	Probability of a successful escape [-]
$P_{d f}$	Conditional probability that an individual being present will die in the event of failure [-]

The probability that a hypothetical crane driver is present was based on the following assumptions: cranes are used 60% of the time; the domain of a crane along a quay was assumed to correspond to three times L_{eq} ; a crane driver generally works on multiple types of cranes, eight hours a day, 220 days a year. If a crane driver works on three different cranes during a year, the probability that an individual driver is present at L_{eq} along a quay wall is approximately 1.5% of the time $(0.6/3/3*(220/365)/3=1.34\%)$.

According to various recommendations in literature, the risk level (*IRPA*) related to involuntary work activities corresponds to an annual risk level of 10^{-6} and is generally considered to be 'broadly acceptable' (Franks, 2017; Health and Safety Executive, 2001; ISO 2394, 1998). Individual risk levels higher than 10^{-4} corresponding to the annual probability of dying as a result of a traffic accident are defined as 'intolerable' in well-developed countries

(Steenbergen & Vrouwenvelder, 2010; TAW, 1985). An annual fatality rate of 10^{-6} representing *LIRA* is generally defined as ‘tolerable’ and was incorporated into the Dutch design code for flood-defence systems (Bötger & Linde, 2014; Jonkman et al., 2011; Terwel, 2014). The acceptable reliability index in accordance with *IRPA* and *LIRA* was derived using:

$$\beta_{acc;t_1} \geq -\Phi^{-1}(P_{f_{acc;t_1}}) = -\Phi^{-1}\left(\frac{IRPA}{P_{Present}(1 - P_{Escape})P_{dlf}}\right) \quad (24)$$

$$\beta_{acc;t_1} \geq -\Phi^{-1}(P_{f_{acc;t_1}}) = -\Phi^{-1}\left(\frac{LIRA}{(1 - P_{Escape})P_{dlf}}\right) \quad (25)$$

Where:

$$\begin{aligned} \beta_{acc;t_1} &= \text{Annual threshold of acceptance [-]} \\ P_{f_{acc;t_1}} &= \text{Acceptable annual probability of failure [-]} \end{aligned}$$

2.4.2 SOCIETAL RISK CRITERION

Although the number of people present near commercial quay walls is usually limited, the societal risk criterion was also evaluated (Vrouwenvelder et al., 2001) using the *F-N* curves. The influence of the expected number of fatalities in the event of failure was examined on the basis of the upper bound ($A=0.01$ and $k=2$) and lower bound ($A=0.1$ and $k=1$) of the *F-N* curves in Section 2.5.4.

$$P_{f_{acc;t_1}} = \Phi(-\beta_{acc;t_1}) \leq AN_{F|f}^{-k} \quad (26)$$

$$\beta_{acc;t_1} \geq -\Phi^{-1}(P_{f_{acc;t_1}}) = -\Phi^{-1}(AN_{F|f}^{-k}) \quad (27)$$

Where:

$$\begin{aligned} N_{F|f} &= \text{Expected number of fatalities [-]} \\ A &= \text{Acceptable risk for one fatality [-]} \\ k &= \text{Slope factor of the } F-N \text{ curve [-]} \end{aligned}$$

2.4.3 LIFE QUALITY INDEX CRITERION

ISO 2394 (2015) recommends employing the *LQI* acceptance criterion and provides information with regard to the social willingness to pay (*SWTP*), which corresponds to the amount of money that should be invested in saving one additional life (Rackwitz, 2006; Rackwitz, 2008). In a similar way, the willingness to prevent an injury could be taken into consideration. Studying the background documents of the *LQI* criterion (Fischer et al., 2012; Fischer & Faber, 2013) revealed that this criterion can be evaluated by applying the principles of cost minimisation if the capitalised ‘societal’ risk is taken into consideration. The corresponding present value of societal losses, denoted by $C_{f,Societal}$, then depends on

the *SWTP* and the expected number of fatalities $N_{F|f}$. The associated annual threshold of acceptance $\beta_{acc;t_1}$ was found by solving the derivative of the societal costs function:

$$\min_{f(\beta)>0} \{C_{Societal}(\beta) = C_{Investments}(\beta) + C_{CapitalisedRisk}(\beta)\} \quad (28)$$

$$C_{CapitalisedRisk}(\beta) = C_{f,Societal}P_{f,0}(\beta) + C_{f,Societal}C_{f,Societal} \cdot \sum_{n=1}^{t_{ref}} \frac{\Delta P_{f,t_n}(\beta)}{(1 + \gamma_s)^n} \quad (29)$$

$$C_{f,Societal} = N_{F|f}SWTP \quad (30)$$

$$\frac{\partial C_{Societal}(\beta_{acc;t_1})}{\partial \beta} \geq 0 \quad (31)$$

where

$$C_{Societal} = \text{Total societal costs [€]}$$

$$C_{f,Societal} = \text{Societal failure cost [€]}$$

2.4.4 SERI CRITERION

The social and environmental repercussion index (*SERI*) of the Spanish ROM represents the loss of human lives, damage to the environment and to historical and cultural heritage and the degree of social disruption. The social repercussion index was derived by examining Eq. (32) on the basis of the guidance in ROM 0.0 (2002) and the accompanying lifetime target reliability index (Table 2.5) was established in accordance with ROM 0.5 (2008).

$$SERI = \sum_{i=1}^3 SERI_i \quad (32)$$

2.5 RELIABILITY TARGETS FOR FAILURE MODES OF QUAY WALLS

2.5.1 RELIABILITY OPTIMUM β^* ON THE BASIS OF COST MINIMISATION

This section presents the reliability indices obtained by economic optimisation of the structural and geotechnical limit states described in Section 2.3.2. The optimum annual and lifetime reliability indices for structural failure found were approximately 2.8 and 2.5 (Fig. 2.8-A), whereas for geotechnical failure 3.5 and 3.3 (Fig. 2.8-B) were found, respectively. The steepness of the left side of the total costs function was strongly influenced by the absolute value of the capitalised risk and explains the different shapes of the graphs. The steepness of the right side was fairly modest due to the quite low absolute value of marginal safety

investments C_m . The influencing parameters of the reliability optimum are further examined by performing a sensitivity analysis in the following section.

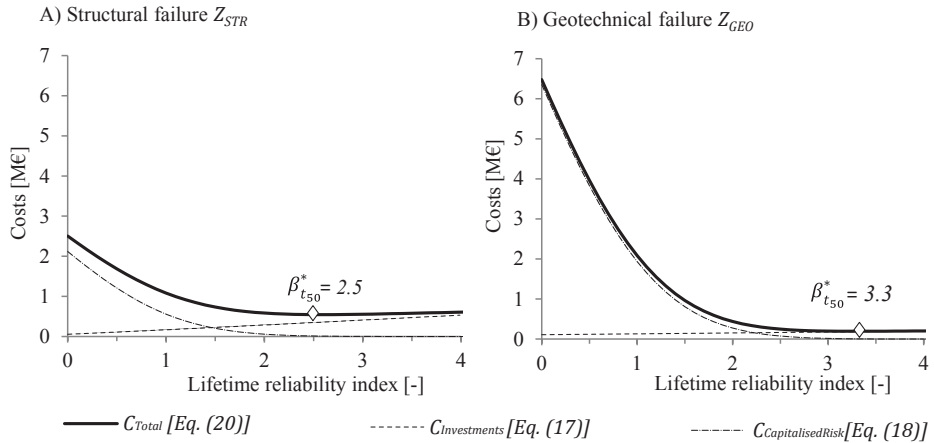


Fig. 2.8. (A) Optimum lifetime reliability indices for structural failure $t_{eq}=20$, $r=0.03$, $t_{ref}=50$, $L_{eq}=40$, $C_0=€0.36m$, $C_m=€0.06m$ and $C_f=€5m$; (B) optimum lifetime reliability indices for geotechnical failure $t_{eq}=30$, $r=0.03$, $t_{ref}=50$, $L_{eq}=40$, $C_0=€0.12m$, $C_m=€0.02m$ and $C_f=€15m$.

2.5.2 SENSITIVITY ANALYSIS OF RELIABILITY OPTIMUM β^*

The aim of the sensitivity analysis was to gain an insight into the influence of the extent to which reliability problems are time-variant, expressed by t_{eq} . The effect of discount rates, the marginal costs of safety measures, failure costs and reference period were taken into consideration. Fig. 9 shows the optimum target reliability indices for a reference period of one year (left) and for the lifetime (right). It should be noted that the optimum annual and lifetime reliability indices for $t_{eq}=50$ or t_{ref} (solid black lines) are identical because the limit state function was assumed to be time-independent.

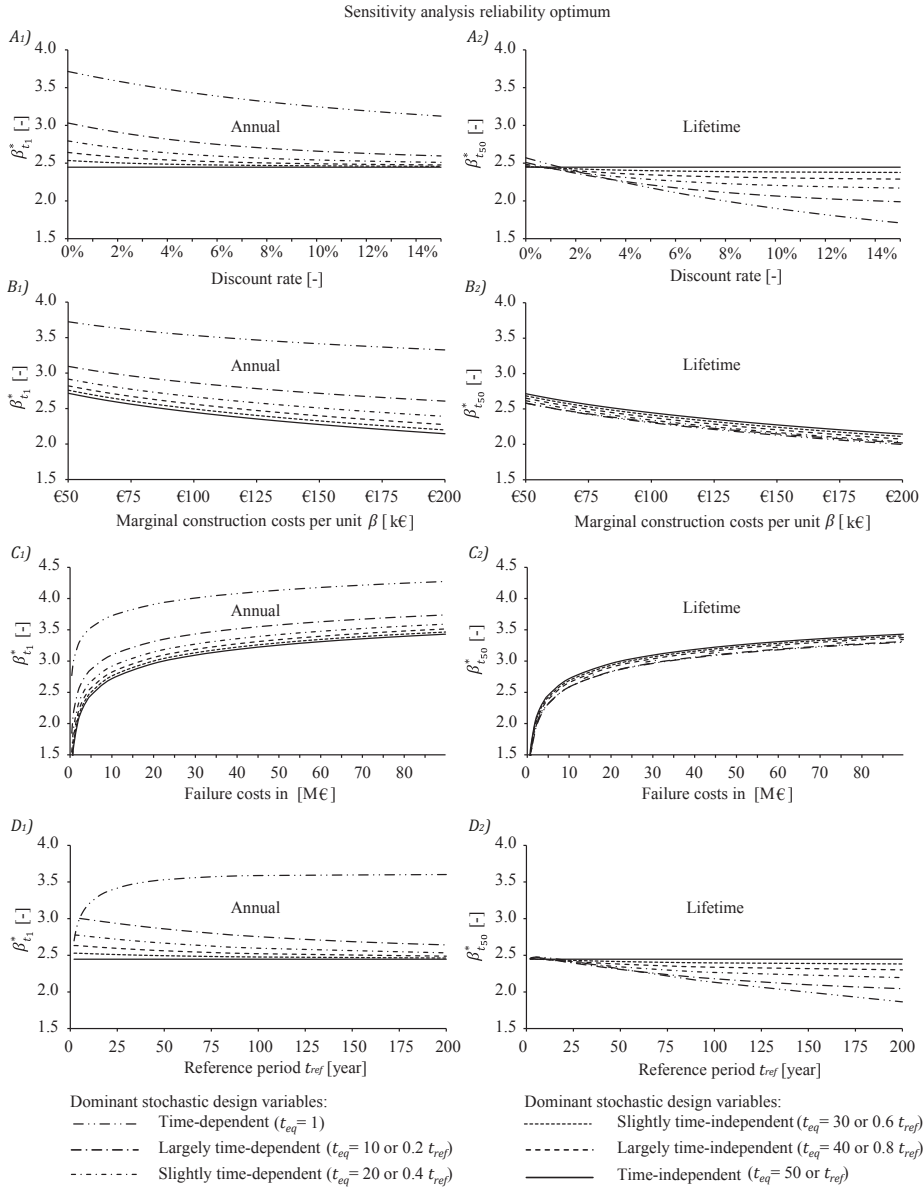


Fig. 2.9. Influence of discount rate (A), marginal safety investments (B), failure costs (C) and reference period (D) on the annual (left) and lifetime (right) reliability optimum for $t_{ref}=50$, $L_{eq}=40$, $C_0=€0.6m$, $C_m=€0.1m$ and $C_i=€5m$.

Time-dependent limit state functions show relatively high annual reliability indices, but the associated lifetime reliability indices are fairly low compared with largely time-independent limit state functions. In the case of a high risk profile, expressed in terms of high

discount rates, there is less willingness to invest in initial safety measures and hence a lower reliability optimum was found (Fig. 9-A). As expected, the effect of discount rates is stronger for time-dependent limit state functions. The variance in optimum lifetime reliability indices caused by t_{eq} was much lower than that in annual reliability indices given changes in C_m and C_f . This was explained by analysing the effect of discounting future costs. However, the absolute value of both C_m and C_f significantly influence the reliability optimum (Fig. 9-B and 9-C). Low failure costs ($C_f \leq \text{€}10\text{m}$) result in an exponential decrease in the reliability optimum. A longer reference period will generally result in less variability in the optimum annual reliability indices and seem to approach an asymptote. A longer reference period resulted in an enhancement of the cumulative probability of failure, and hence in a lower lifetime reliability optimum (Fig. 9-D). An important finding is that if time-independent stochastic design variables dominate uncertainty, the difference between annual and lifetime target reliability indices becomes quite low.

2.5.3 RELIABILITY MINIMUM β_{acc} ON THE BASIS OF HUMAN SAFETY CRITERIA

The minimum requirements concerning human safety were examined on the basis of the individual risk (*IR*) and the societal risk (*SR*) criterion, the life quality index (*LQI*) and the social and environmental repercussion index (*SERI*) criteria. Table 2.5 presents the results of all safety criteria. The reader is referred to Section 2.3.6 for further background information with regard to the input variables used.

Table 2.8. Reliability minimum β_{acc} in accordance with the IR criterion, SR criterion, LQI criterion and SERI criteria.

Type of failure	Input			Annual reliability β_{t_1}				Lifetime reliability $\beta_{t_{50}}$			
	t_{eq}	N_{Fif}	SWTP	$\sum SERI$	IRPA= 10^{-6}	LIRA= 10^{-6}	LIRA= 10^{-5}	SR	LQI_{t_1}	$LQI_{t_{50}}^2$	$SERI^2$
Z_{STR}	20	0.15	€3m	3	2.8	4.0	3.4	<2.3 ¹	1.8	1.4	2.3
Z_{GEO}	30	0.70	€3m	15	3.3	4.3	3.8	<2.3 ¹	2.8	2.7	3.0

¹⁾ The expected value of the number of fatalities was assumed to be equal to 1.

²⁾ It should be noted that requirements concerning human safety are generally related to the annual and not the lifetime reliability index.

Table 2.8 shows that the *SR* criterion is not relevant for failure modes of commercial quay walls, because the number of people at risk is fairly low. The reliability minimum β_{acc} derived using the *LQI* criterion led to lower reliability indices compared with the reliability optimum found by economic optimisation in Section 2.5.1. It was also found that the optimum reliability indices are quite similar to the results obtained by examining the *IRPA* criterion. However, *LIRA*

within risk contours 10^{-5} and 10^{-6} resulted in higher reliability indices. The influence of the input variables on the reliability minimum β_{acc} is further discussed in the following section.

2.5.4 SENSITIVITY ANALYSIS OF RELIABILITY MINIMUM β_{acc}

Similar to the sensitivity analysis performed for economic optimisation, the differentiating factors related to the requirements concerning human safety were evaluated. Fig. 2.10 shows that the *IR* criterion was largely influenced by the product of the conditional probability that an individual will die in the event of the failure of a quay wall and the probability of not being able to escape in time. When this product becomes fairly low (< 0.05), a significant decrease in the acceptable annual reliability index was found. Fig. 2.10-A shows that the probability that a hypothetical person, such as a crane driver, is present influences the development of the *IRPA*. Fig. 2.11 shows that the *SR* criterion and the *LQI* criterion were largely influenced by the expected number of fatalities in the event of the failure of a quay wall. It is worth noting that the upper boundary of the *SR* criterion will become relevant when the expected number of fatalities is quite large. Similar to the insights derived by economic optimisation, the *LQI* criterion is influenced by the absolute value of marginal safety investments, social failure costs and the extent to which the reliability of failure modes are time-variant. The results of the sensitivity analysis are further discussed in Section 2.6.

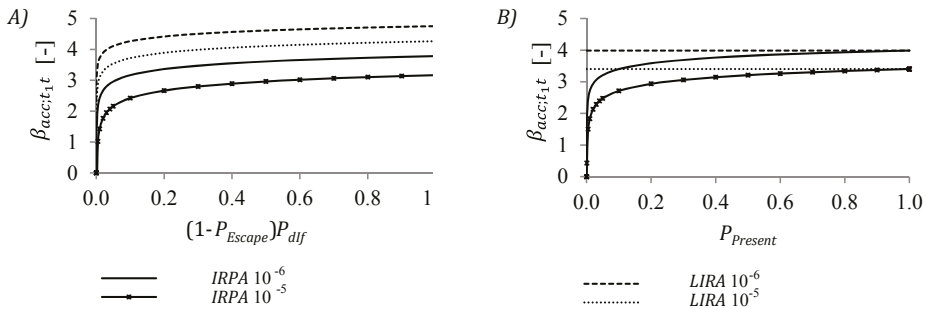


Fig. 2.10. Sensitivity analysis of IR criterion: influence of conditional probability of failure (A); influence that a specific individual will be present (B).

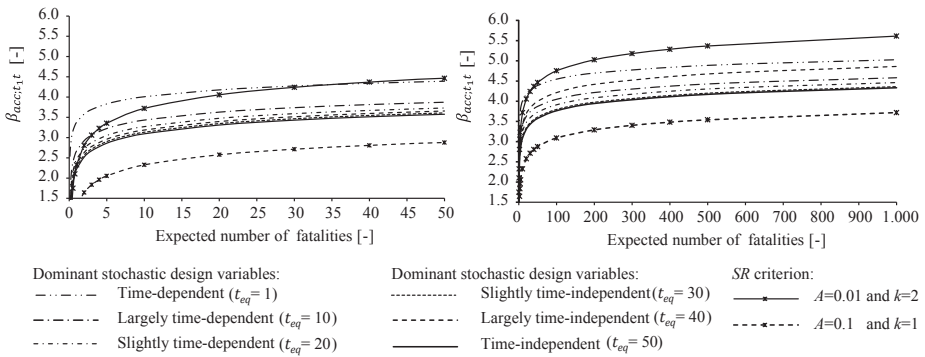


Fig. 2.11. Sensitivity analysis of SR and LQI criterion with $t_{ref}=50, L_{eq}=40, C_0=€0.6m, C_m=€0.1m$ and $SWTP=€3m$.

2.6 DISCUSSION OF RELIABILITY TARGETS

2.6.1 TARGET RELIABILITY INDICES FOR COMMERCIAL QUAY WALLS

The results in this chapter show that target reliability indices for commercial quay walls can be determined by economic optimisation on the basis of cost minimisation. The annual and lifetime target reliability indices ascribed to limit states of structural components and geotechnical failure modes of quay walls with a retaining height of 20m are in the ranges 2.8-3.5 and 2.5-3.3, respectively. The acceptable annual reliability index in accordance with the individual risk criterion ($IRPA=10^{-6}$) led to fairly similar reliability indices. Table 2.9 gives an overview of the reliability indices for economic optimisation (β^*) and acceptability regarding human safety (β_{acc}). It should be noted that quay walls with a fairly small retaining height and fairly high variable loads could lead to higher differences between annual and lifetime target reliability indices ($t_{eq} < 20$).

Table 2.9. Overview of risk-based optimum and acceptable reliability indices for commercial quay walls.

Risk-acceptance criteria	Type of criterion	$Z_{STR}(t_{eq} \approx 20)$		$Z_{GEO}(t_{eq} \approx 30)$	
		β_{1-year}	$\beta_{50-years}$	β_{1-year}	$\beta_{50-years}$
Economic optimisation β^*	Cost minimisation	2.8	2.5	3.5	3.3
Human safety β_{acc}	Individual risk ($IRPA=10^{-6}$)	2.8	-	3.3	-
	Societal risk (SR)	<2.3	-	<2.3	-
	Life quality index (LQI)	1.8	1.4	2.8	2.7
	Social and economic repercussion index (SERI)	-	2.3	-	3.0

It should be noted that the localised individual risk per annum (*LIRA*) criterion is assumed to be inactive because the failure of a quay wall will generally not induce the failure of hazardous installations, such as chemical plants. However, if the *LIRA* criterion is active the acceptable annual reliability indices are in the range 4.0-4.3. The societal risk (*SR*) criterion is mostly not so relevant for assessing human safety in relation to commercial quay walls, but should be taken into account if a large number of people are at risk – for example, when quay walls are part of a cruise terminal or a flood-defence system. It is always recommended that the *LQI* criterion be accounted for in order to verify whether the marginal life-saving costs principle is sufficiently covered. The *SERI* criterion is fairly straightforward and seems to be quite efficient for selecting a consequence class in accordance with the reliability framework proposed in the following section.

2.6.2 ASSESSMENT CRITERIA FOR CLASSIFICATION

In Table 2.10, an assessment framework for reliability differentiation is proposed which complies with the qualitative descriptions embedded in many codes and standards in order to make reliability differentiation for quay walls more accessible and interpretable. The reliability framework of ISO 2394 (2015) provided a solid foundation, and hence was further elaborated by implementing the recommendations from ASCE 7-10 (2010) and DNV (1992) for structural redundancy and progression of failure. The social and environmental repercussion index (*SERI*) (ROM 0.0, 2002) and the ratio between the direct costs of failure and construction costs (JCSS, 2001) were also incorporated. In reality, quay-wall failure can have a significant effect on accessibility as well as on the image and reputation of a port. The service values of the Port of Rotterdam Authority, which are in line with those of other multinationals (Ligtvoet & Van der Lei, 2012), were therefore embedded in the new assessment framework. An upper limit to the allowable degree of economic damage was defined for each consequence class using the results of the sensitivity analysis and assuming the equivalent length L_{eq} along a quay wall, for which failure events are independent, to be in the range 25-50 m. It is worth noting that the row in Table 2.10 which shows the most onerous failure consequence determines the required consequence class.

Table 2.10. Assessment criteria for each consequence class for the structure as a whole N_{PAR} .

Description	Consequence class				
	A	B	C	D	E
Qualitative	Negligible/low	Some	Considerable	High	Very high
Human safety					
- Number of fatalities (ISO 2394, 2015)	$N \leq 1$	$N \leq 5$	$N \leq 50$	$N \leq 500$	$N > 500$
- Number of people at risk (ASCE 7-10, 2010)	$N_{PAR} < 5$	$N_{PAR} < 50$	$N_{PAR} < 500$	$N_{PAR} < 1500$	$N_{PAR} > 1500$
- Degree of warning (ASCE 7-10, 2010; DNV, 1992)	Progression of failure is not possible and people at risk are able to escape in time.	Redundant structural response and progression of failure is mitigated and failure is not sudden providing adequate warning signals.	Progression of failure is mitigated, but failure is sudden without providing warning signals.	Widespread progression of damage is likely to occur and failure is sudden without providing warning signals.	Widespread progression, induced by unexpected and sudden environmental disasters, is possible.
- Social and environmental repercussion index (ROM 0.0, 2002)	$SERI \leq 5$	$SERI \leq 15$	$SERI \leq 25$	$SERI \leq 30$	$SERI > 30$
Economic					
- Description (ISO 2394, 2015)	Predominantly insignificant material damages.	Material damages and functionality losses of significance for owners and operators and low or no social impact.	Material losses and functionality losses of societal significance, causing regional disruptions and delays in important societal services over several weeks.	Disastrous events causing severe losses of societal services and disruptions and delays at national scale over periods in the order of months.	Catastrophic events causing losses of societal services and disruptions and delays beyond national scale over periods in the order of years.
- Accessibility (Ligthvoet & Van der Lei, 2012)	Very little hindrance to shipping, railway transport, pipeline systems. (Very short period: less than one day.)	Minor consequences for availability of navigation channels, railways, roads or pipeline corridors. (Obstruction for a period of one day.)	Short period of obstruction with regard to navigation channels, railways, roads or pipeline corridors. (Availability is lower for a period of one week.)	Damage to navigation channels, railways, roads or pipeline corridors. (Availability is lower for a period of weeks.)	Loss of main navigation channels, railways, roads or pipeline corridors. (Main transport routes are unavailable for a period of months.)

Table 2.10. Continued.

Description	Consequence class				
	A	B	C	D	E
-Ratio between direct failure costs and costs of safety investments $\rho = C_{\text{direct}} / C_{\text{investments}}$ (JCSS, 2001). -Failure costs C_f corresponding to a failure length of 40 m	$\rho \leq 1$	$\rho \leq 2$	$\rho \leq 5$	$\rho \leq 10$	$\rho > 10$
Environmental (ISO 2394, 2015)	$C_f < €8\text{m}$	$C_f < €50\text{m}$	$C_f < €200\text{m}$	$C_f < €1500\text{m}$	$C_f > €1500\text{m}$
	Damage to the quality of the environment of an order which can be restored completely in a matter of days.	Damage to the quality of the environment of an order which can be restored completely in a matter of weeks.	Damage to the quality of the environment limited to the surroundings of the failure event and which can be restored in a matter of weeks.	Significant damage to the quality of the environment contained at national level but spreading significantly beyond the surroundings of the failure event and which can be only partly restored in a matter of months.	Significant damages to the quality of the environment spreading significantly beyond the national level and which can be only partly restored in a matter of years to decades
Reputation (Ligtvoet & Van der Lei, 2012)	No negative attention in media and no damage to the image of the port.	Very short period of negative attention in local, regional and national media (>1 day). Serious concerns among people living in the vicinity, local government, national government or external clients. Damage to image of a few stakeholders.	Short and limited period of negative attention in local, regional and national media (>2 days). Serious concerns among people living in the vicinity, local government, national government or external clients. Damage to image of the port for some time.	Period of negative attention in local, regional and national media (>week). Serious concerns among people living in the vicinity, local government, national government or external clients. Damage to image of the port for some time.	Long period of negative attention in local, regional and national media (>month). Very serious concerns among people living in the vicinity, local government, national government or external clients. Permanent damage to image of the port.

2.6.3 COMPLIANCE WITH CODES AND STANDARDS AND PROPOSAL FOR CLASSIFICATION

In engineering, reliability problems are often assumed to be fully time-variant (Section 2.2.2). The results of this chapter, however, show that limit state functions of quay walls are to a certain extent time-independent. Fairly dangerous geotechnical failure modes, in particular, seem to be dominated by uncertainty in time-independent variables, indicating that the associated failure rate is higher during the first years of service (Chapter 4). This theory is supported by the fact that quay-wall failures not induced by environmental disasters are mostly identified directly upon construction or in the first year after completion. In addition, no fatalities of end users due to quay failure have been identified at the Port of Rotterdam. The decrease in the failure rate during the useful life may explain the relatively low failure frequency of geotechnical structures compared with other civil-engineering works (Terwel, 2014).

The target reliability indices derived in this chapter were determined from three risk-acceptance criteria: economic optimisation, the individual risk (*IRPA*) criterion and the life quality index (*LQI*) criterion. The results were used to determine target reliability indices in accordance with the assessment criteria for structural robustness described in Table 2.10. It should be noted that the description of the failure consequences is related to the system as whole rather than to individual structural components (ISO 2394, 2015). The recommended target reliability indices in Table 2.11 are ascribed to the limit state functions of structural components and geotechnical failure modes, because the efficiency of safety measures as well as failure consequences differ per limit state. It should be noted that the recommended target reliability indices are only valid if progressive failure is mitigated (Janssen, 2012; Gaba et al., 2017; De Gijt & Broeken, 2013). The sensitivity analysis showed that differences in annual target reliability indices are fairly small for time-independent limit state functions. It is therefore recommended that annual target reliabilities be evaluated, rather than lifetime reliability indices, and that annual reliability indices be implemented in design codes in accordance with the recommendations of ISO 2394 (2015) and Rackwitz (2000). Economic optimisation was found to be the governing risk criterion. However, the societal costs will become fairly dominant in the case of class D. The *LIRA* and *SR* criteria are only relevant for failures with consequences that reach far beyond the quay-wall site itself – for instance, if installations with hazardous materials are affected. They are therefore not included in the recommended values, but should be considered separately when applicable. Table 2.11 also shows that the recommended annual target reliability indices are within the range of the guidance in ISO 2394 (2015).

Table 2.11. Annual target reliability indices for consequence classes of largely time-independent limit state functions of quay walls.

Criterion	Type	Consequence class				
		A	B	C	D	E
		Low	Some	Considerable	High	Very high
ISO 2394 (2015)	Large ¹	-	3.1	3.3	3.7	-
	Medium ¹	-	3.7	4.2	4.4	-
	Small ¹	-	4.2	4.4	4.7	-
Economic optimisation ^{2,3}		2.8	3.4	3.8	4.2	excl. ⁵
<i>LQI</i> criterion ^{2,3}		2.5	3.0	3.7	4.2	excl. ⁵
<i>IR</i> criterion	<i>IRPA</i> =10 ⁻⁶	2.8	3.3	3.7	n/a	n/a
	<i>IRPA</i> =10 ⁻⁵	1.9	2.5	3.1	n/a	n/a
	<i>LIRA</i> =10 ⁻⁶	n/a	n/a	n/a	4.3 ⁴	excl. ⁵
	<i>LIRA</i> =10 ⁻⁵	n/a	n/a	n/a	3.4 ⁴	excl. ⁵
<i>SR</i> criterion	<i>A</i> =0.01; <i>k</i> =2	n/a	3.4	4.5	5.4	excl. ⁵
	<i>A</i> =0.1; <i>k</i> =1	n/a	2.1	2.9	3.5	excl. ⁵
Recommendation for design codes	($n_{eq} \ll n_{ref}$ or $t_{eq} \geq 20$)	2.8	3.4	3.8⁶	4.2⁶	excl.⁵

¹) Relative costs of safety measures.

²) Dominant design variables are considered to be time-independent ($n_{eq} \ll n_{ref}$ or $t_{eq} \geq 20$) (Section 2.3.3).

³) Input variables $t_{ref}=50$, $L_{eq}=40$, $C_0=€0.6m$, $C_m=€0.1m$ and $SWTP=€3m$.

⁴) This criterion is only active at a hazardous site/project location (Section 2.4).

⁵) It is not possible to provide general recommendations. A project-specific study is recommended (Section 2.4).

⁶) Verify whether *LIRA* or *SR* criteria are active.

The failure consequences of quay walls in port areas (Fig. 2.12) with and without functional redundancy differ (Section 2.3.5) and have been classified as class A and class B, representing ‘low’ and ‘some’ damage respectively. The required reliability level of a commercial quay wall also depends on the image and reputation of a port as a safe environment for investments and work (Section 2.3.5). Another aspect that needs to be considered is the impact of failure on the availability and accessibility of major sailing routes. After an earthquake in Japan, numerous quay walls failed simultaneously (Iai et al., 1996) and hence multiple berths were unavailable for recovery, leading to much more serious economic repercussions (OCDI, 2009). When quay-wall failure could lead to an explosion in, for instance, a chemical plant (Fig. 2.12-V) or to the breaking loose of a cruise ship induced by the failure of bollards, many more people are at risk. In these circumstances, a higher consequence class must be considered. The design of soil-retaining walls that are part of another system, such as a preliminary flood-defence system, should take account of the length effect and hence higher reliability indices need to be taken into consideration (Calle & Spierenburg, 1991;

Janssen, 2012; Roubos & Grotegoed, 2014; STOWA, 2011; TAW, 2003). Although undoubtedly not all types of quay walls are covered, the examples listed in Table 2.12 will serve as a useful reference for categorising quay-wall types for each consequence class.

Table 2.12. Examples of quay-wall types for the consequence classes described in Table 2.10 if (and only if) progressive failure is mitigated.

Examples of quay wall types				
A	B	C	D	E
Negligible or low	Some	Considerable	High	Very high
Soil-retaining walls where the risk of fatalities is negligible or very low; quay walls that are part of a terminal or port with functional redundancy.	Quay walls that are part of a terminal or port without functional redundancy.	Quay walls in urban areas.	Quay walls for which failure will lead to the failure of other structures, such as chemical or power plants; soil-retaining walls that are part of secondary flood-defence systems or dams; quay walls needed for recovery after earthquake damage or tsunamis; quay walls that facilitate cruise ships.	Soil-retaining walls that are part of a primary flood defence system, major dam or important sailing route.

2

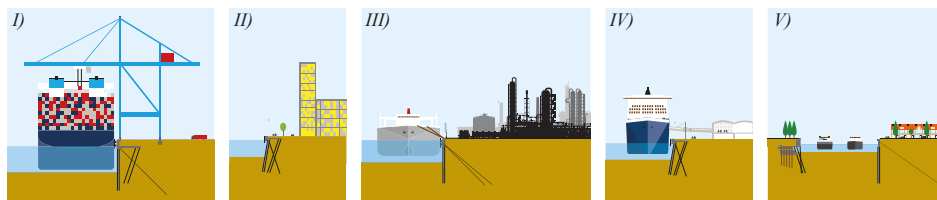


Fig. 2.12. Impression of different quay-wall types: (I) commercial quay wall; (II) quay wall in urban area; (III) quay wall that is part of a dangerous plant; (IV) quay wall that facilitates cruise ships; (V) quay walls that facilitate main sailing routes.

2.7 CONCLUSION AND RECOMMENDATIONS

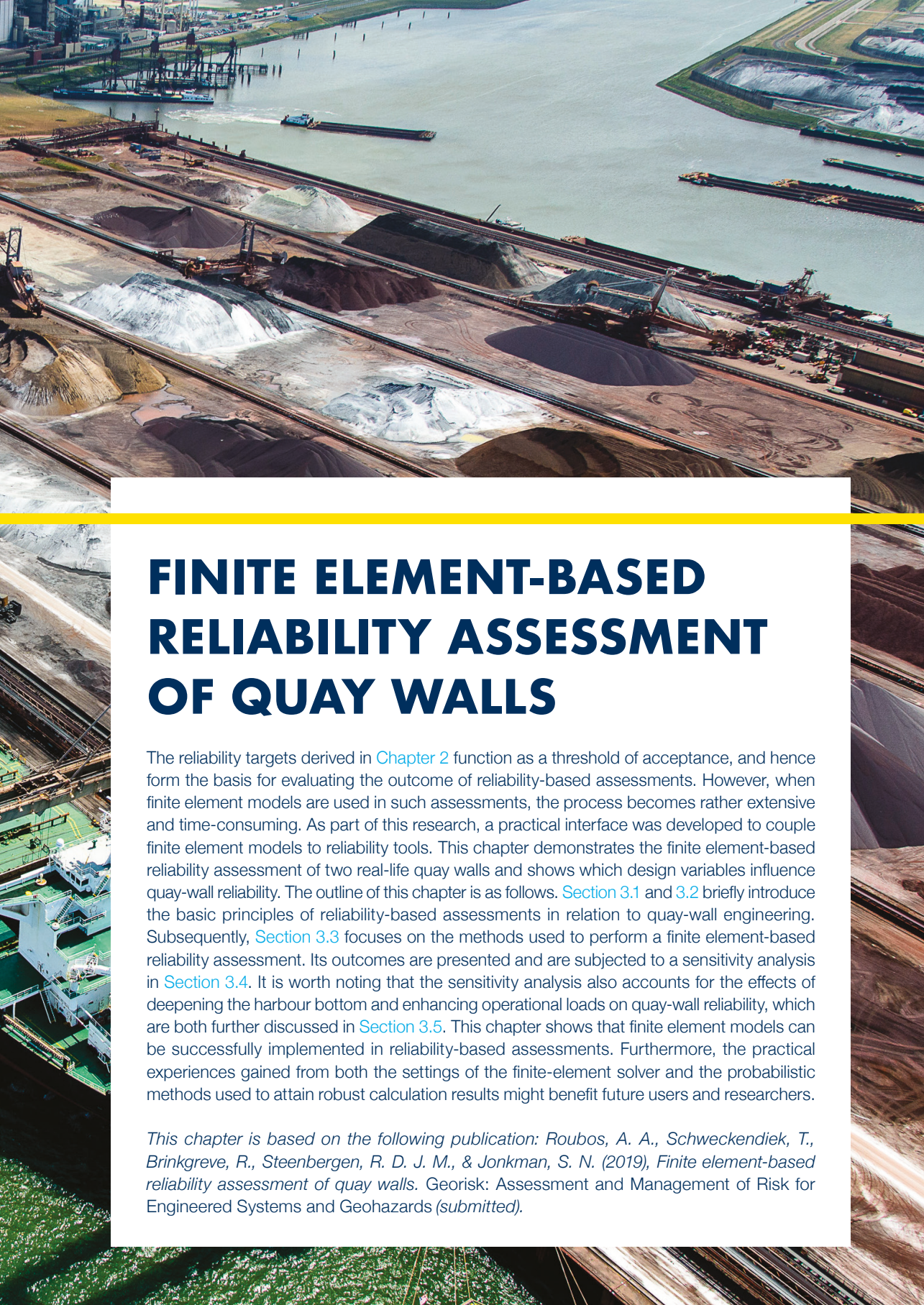
The results of this chapter provide guidance on reliability differentiation for commercial quay walls, but have also been used to evaluate reliability indices for other types of quay and soil-retaining walls. The most important findings of this chapter are as follows.

- In quay-wall design, it is highly likely that dominant stochastic design variables are largely time-independent. This influences both the efficiency of safety measures and the present value of future failure costs, and hence optimum annual and lifetime target reliability indices.
- The extent to which limit state functions of quay walls are time-dependent differs between failure modes.
- Target reliability indices can be derived on the basis of economic optimisation in combination with the marginal life-saving cost principle. The annual and lifetime target reliability indices for failure modes of commercial quay walls found were in the ranges 2.8-3.5 and 2.5-3.3, respectively.
- The recommendations for reliability differentiation in literature become more consistent and interpretable if the assessment framework ISO 2394 (2015) is extended with detailed information about type of failure, warning signals and the consequences of failure.

When defining target reliability indices for quay walls and other geotechnical structures, one should be very careful using the general guidance developed for buildings and bridges, because the degree and source of aleatory and epistemic uncertainty differ, as do the consequences of failure. It is strongly recommended that damage to the reputation of a terminal or port be taken into account, because marginal safety costs appeared to be quite low compared to the total construction costs and expected benefits. During this research it was noticed that many experts find it difficult to make a quantitative estimate of the costs associated with failure and that little information is available with regard to the conditional probability of death in the event of a quay-wall failure. Both aspects require further research. A detailed study with regard to the influence of time-independent design variables, failure costs and the efficiency of safety measures for each failure mode is highly recommended if we are to improve quay-wall design in respect of reliability and safety. The failure rates of fairly dangerous geotechnical failure modes seem to be much higher in the first period of service, indicating that if a quay wall has already survived a certain period these failure modes are less likely to occur (Kunz, 2015). It is therefore highly recommended that specific guidance for assessing the reliability and safety of existing quay walls be drawn up, which would involve adopting a new and different approach incorporating development of the probability of failure over time. It is expected that insight into the actual reliability level of soil-retaining walls will increase significantly if the uncertainty in the soil-structure interaction is reduced by advanced monitoring – for instance, during the capital dredging works of the construction stage. The suggestions for quantifying reliability levels developed in this chapter also enable the determination of project-specific target reliability indices.

3





FINITE ELEMENT-BASED RELIABILITY ASSESSMENT OF QUAY WALLS

The reliability targets derived in [Chapter 2](#) function as a threshold of acceptance, and hence form the basis for evaluating the outcome of reliability-based assessments. However, when finite element models are used in such assessments, the process becomes rather extensive and time-consuming. As part of this research, a practical interface was developed to couple finite element models to reliability tools. This chapter demonstrates the finite element-based reliability assessment of two real-life quay walls and shows which design variables influence quay-wall reliability. The outline of this chapter is as follows. [Section 3.1](#) and [3.2](#) briefly introduce the basic principles of reliability-based assessments in relation to quay-wall engineering. Subsequently, [Section 3.3](#) focuses on the methods used to perform a finite element-based reliability assessment. Its outcomes are presented and are subjected to a sensitivity analysis in [Section 3.4](#). It is worth noting that the sensitivity analysis also accounts for the effects of deepening the harbour bottom and enhancing operational loads on quay-wall reliability, which are both further discussed in [Section 3.5](#). This chapter shows that finite element models can be successfully implemented in reliability-based assessments. Furthermore, the practical experiences gained from both the settings of the finite-element solver and the probabilistic methods used to attain robust calculation results might benefit future users and researchers.

This chapter is based on the following publication: Roubos, A. A., Schweckendiek, T., Brinkgreve, R., Steenbergen, R. D. J. M., & Jonkman, S. N. (2019), Finite element-based reliability assessment of quay walls. Georisk: Assessment and Management of Risk for Engineered Systems and Geohazards (submitted).

ABSTRACT

While reliability methods have already been widely adopted in civil engineering, the efficiency and robustness of finite element-based reliability assessments of quay walls are still fairly low. In this chapter, the reliability indices of structural and geotechnical failure modes of two real-life quay walls are determined by coupling probabilistic methods with finite element models, taking into account a large number of stochastic variables. The reliability indices found are within the range of the targets suggested in the design codes presently in use. Nevertheless, neglecting model uncertainty and correlations between stochastic variables leads to an underestimation of the probability of failure. In addition, low sensitivity factors are found for time-independent variables, such as material properties and model uncertainty. Furthermore, the results are used to reflect on the partial factors used in the original design. Important variables, such as the angle of internal friction, are subjected to a sensitivity analysis in order to illuminate their influence on the reliability index. Port authorities and terminal operators might be able to use the findings of this chapter to derive more insight into the reliability of their marine structures and to optimise their service life and functionality, for example by deepening berths or increasing operational loads.

3.1 INTRODUCTION

Quay walls are marine structures that ensure safe and efficient handling of ships (Fig. 2.1). Since they frequently have a complex soil-structure interaction (e.g. due to inclined retaining walls or relieving platforms), structural and geotechnical assessments are usually performed semi-probabilistically while modelling the quay wall on the basis of finite elements. A more systematic way to account for uncertainties is to perform a reliability-based assessment (Phoon & Retief, 2016). However, the efficiency and robustness of finite element-based reliability assessments in quay-wall engineering are rather low. In particular, it is still quite a challenge to achieve a robust coupling between probabilistic methods and finite element models, e.g. due to the highly complex and non-linear character of soil behaviour. Although a few studies (Rippi & Texeira, 2016; Schweckendiek et al., 2012; Teixeira et al., 2016; Wolters et al., 2012) show promising results for quay walls and other soil-retaining structures, most use simplified models and they generally do not consider structures that have actually been built.

The aim of this chapter is threefold: (i) to develop a method to enable finite element-based reliability assessments of quay walls in realistic design conditions; (ii) to evaluate partial factors of safety; and (iii) to provide port authorities with information on the relevant parameters to measure and monitor. The following approach was adopted. First, a reliability interface named ProbAna[®] (Laera & Brinkgreve, 2017) was developed to couple Plaxis – an advanced finite element software package presently used in quay-wall engineering and geotechnical engineering in general – with the open source probabilistic toolbox OpenTURNS ('Open source initiative for the treatment of uncertainties, risks and statistics'). Since using these advanced tools can become a 'black box', the outcome was evaluated by performing reliability-based assessments using an alternative reliability tool, Prob2B (Courage & Steenbergen, 2007) while analytically modelling the quay wall using Blum's method (Blum, 1931). The results of the reliability-based assessment were subjected to a sensitivity analysis in order to illustrate the impact of relevant design variables on the quay walls' reliability level. Unlike in previous studies, two reference quay walls that have actually been built in the port of Rotterdam and comply with the Eurocode standard (NEN-9997-1, 2016), were selected. Consequently, it has been possible to use the results of this chapter to reflect on the safety factors used in the original design.

3.2 BASIC PRINCIPLES OF RELIABILITY-BASED ASSESSMENTS

Basic performance measures of reliability-based assessments are typically expressed as a probability of failure P_f on the basis of the limit state function (LSF) $Z=g(x)=0$ (JCSS, 2001). The

Chapter 3

failure probability P_f is defined as outcrossing $g(\dot{x})=0$ (Eq. 34), and is generally directly related to the reliability index β (Eq. 35) (Cornell, 1969; Hasofer & Lind, 1974). This reliability index can be compared with the required or 'target' reliability indices stated in codes and standards (Table 3.1) and derived in Chapter 2. A limit state function can be defined for all sorts of failure, such as local or global collapse and exceeding serviceability limits (Vrouwenvelder, 2017). Section 3.4.2 describes the main failure modes of quay walls and the associated limit state functions.

$$Z = g(X) \quad (33)$$

$$P_f = P(g(X) \leq 0) = \int_{g(X) \leq 0} f_X(x) dx \quad (34)$$

$$P_f = \Phi(-\beta) \quad (35)$$

Where:

Z	Limit state function
$g(X)$	State function of variable X
X	Vector of stochastic variables
P_f	Probability of failure [-]
$f_X(x)$	Joint probability density function of variable X [-]
β	Reliability index [-]
Φ	Standard normal cumulative distribution function [-]

Table 3.1. Overview of lifetime target reliability indices in literature for the ultimate limit state (Chapter 2).

Literature	Application	Failure consequences				
		Low	Some	Considerable	High	Very high
ISO 2394 (2015) ¹	All	Small 2.3	Some 3.1		Moderate 3.8	Great 4.3
EN 1990 (2011)	All		RC1 3.3		RC2 3.8	RC3 4.3
ROM 0.5-05 (2008)	Geotechnical	Minor 2.33	Low 3.09		High/very high 3.72	
CUR 166 (2012)	Sheet piles	Class I 2.5		Class II 3.4		Class II 4.2
OCDI (2009)	Marine	NR^2 2.19/2.67	IR^2 2.67		HR^2 3.65	
CUR 211 (2013)	Quay walls		RC1 3.3		RC2 3.8	RC3 4.3

¹) Reliability indices are derived by assuming low relative costs of safety measures.

²) Normal, intermediate and high seismic performance verification.

Currently, several reliability methods are available. These include the first-order reliability method (*FORM*), the second-order reliability method (*SORM*), directional sampling (*DS*), directional adaptive response surface sampling (*DARS*), and crude Monte Carlo (*MC*), all of which have advantages and disadvantages (Jonkman et al., 2015). The methods used in this chapter are described in the next section. For further details with regard to probabilistic assessments, the reader is referred to ISO 2394 (2015) or the Probabilistic Model Code (JCSS, 2001).

3.3 METHOD FOR FINITE ELEMENT-BASED RELIABILITY ASSESSMENT OF QUAY WALLS

3.3.1 INTRODUCTION

This section briefly introduces the information and methods used to perform finite element-based reliability assessments of a quay wall without (Fig. 3.1-A) and with a relieving platform (Fig. 3.1-B). Further structural information can be found in Appendix B.1. The failure modes were evaluated on the basis of limit state functions, which are described in Section 3.3.2.

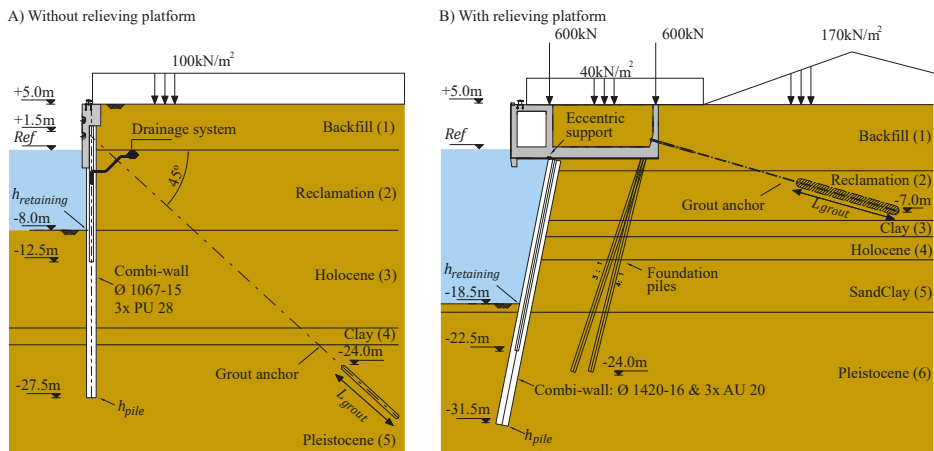


Fig. 3.1. Cross-section of the reference quay walls without (A) and with (B) a relieving platform, located in the port of Rotterdam.

Both of these structures have been built in practice and were modelled with the finite element software Plaxis using the hardening soil constitutive model to represent the soils' stress-strain behaviour, which takes into account the stress dependency of soil stiffness. In addition, recently developed modelling options were implemented, such as embedded beam rows to model foundation piles (Sluis, 2012), and realistically take into account the

soil pressure acting on the combi-wall. Although monitoring data, ‘as-built’ documents and detailed soil investigation were used to minimise model uncertainty, its influence was explicitly taken into consideration as a stochastic variable. This is because, as in any non-linear analysis, the numerical solution is an approximation since we do not exactly know the real solution. The stochastic variables considered are described in Section 3.3.3.

As part of this research, a new reliability interface was developed. It couples the finite element model with the probabilistic toolbox (Andrianov et al., 2007; Laera & Brinkgreve, 2017) (Fig. 3.2). In this study, a research version of the reliability interface was used, including additional options and features such as the possibility to account for uncertainty in water levels and geometry. Moreover, this interface enables the use of customised limit state functions. It controls both the input and the output for the finite element model via ‘remote scripting’ and the settings of the selected reliability method.

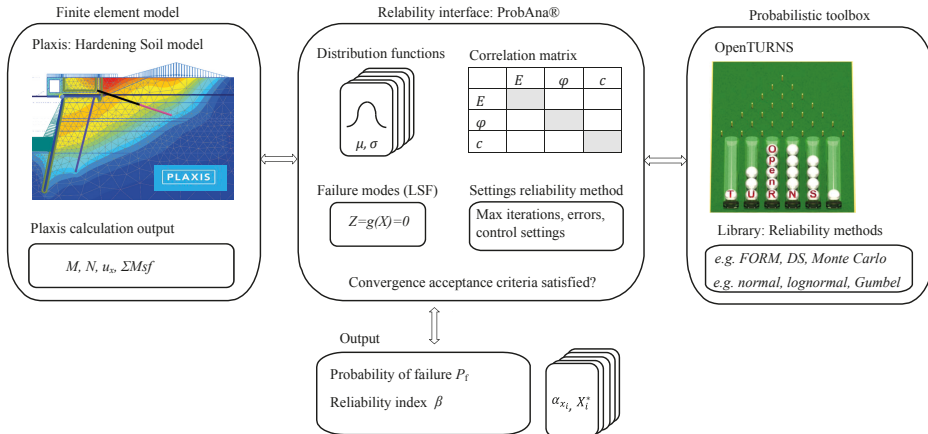


Fig. 3.2. Reliability interface coupling the finite element software Plaxis with the probabilistic toolbox OpenTURNS.

In this study, the Abdo-Rackwitz *FORM* algorithm was used to solve the reliability problem. This algorithm and the settings used are further described in Appendix B.2. Since coupling a finite element model with a reliability method can easily become a ‘black box’, the outcomes were evaluated. This was done by performing reliability-based assessments using an alternative reliability tool while analytically modelling the quay wall using Blum’s method (Blum, 1931), which was commonly used until the end of the twentieth century to design all quay walls in Rotterdam. The Blum-based probabilistic analysis was performed on the basis of the Rackwitz-Fiessler *FORM* algorithm (Rackwitz & Fiessler, 1997), and a more computational extensive crude Monte Carlo analysis (Section 3.4.1 and Chapter 4). One advantage of *FORM* is that it provides the design point X^* and sensitivity factors α_i ,

for each stochastic variable i . Since some variables are correlated, their input sequence significantly influences the sensitivity factors obtained. Section 3.4.3 therefore presents the method used to determine partial factors of safety for correlated stochastic variables.

3.3.2 MAIN FAILURE MODES AND LIMIT STATE FUNCTIONS

Failures of quay walls can be categorised into different failure modes, and hence multiple limit states have to be evaluated. This study evaluates the most relevant limit state functions of the failure modes in terms of reliability (Fig. 3.3); it does not extend to evaluation of the entire system of failure modes, but rather focuses on the reliability index of individual structural components or failure modes in accordance with the Eurocode approach (NEN-EN 1990, 2011). For a detailed fault tree, the reader is referred to design guidelines for soil-retaining walls (Calle & Spierenburg, 1991; De Gijt, 2003; De Gijt & Broeken, 2013; Janssen, 2012).

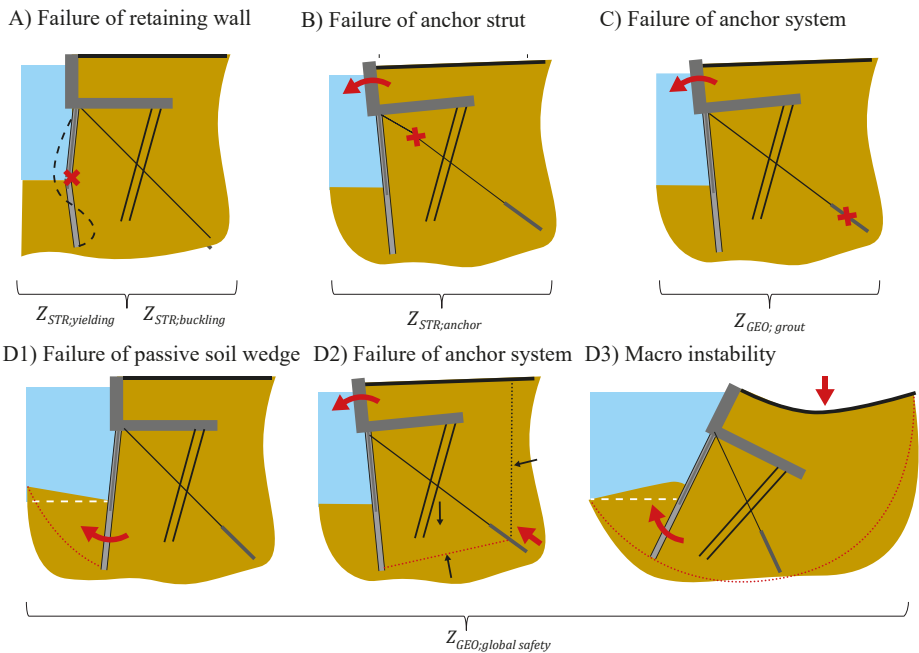


Fig. 3.3. Failure modes of quay walls considered in this study.

The limit states for yielding and local buckling in the outer fibres (Fig. 3.3-A) were evaluated using Eq. (36) and Eq. (37), respectively, to assess the reliability of the combi-wall. The formula to evaluate local buckling was developed on the basis of recent experiments, including an empirical formula for the buckling factor f_b , which represents the ratio between

the actual and the theoretical bending moment capacity (Peters et al., 2017). The risk of local buckling is stress and strain-level dependent, and hence the parameter $D_{tube}/t_{tube}\varepsilon^2$ is generally used instead of D_{tube}/t_{tube} . The tubes' diameter and wall thickness represent the actual dimensions, while the yield strength was based on tensile tests. Particularly because f_B was determined on the basis of experiments, an additional stochastic factor θ_B was added in this study to account for model uncertainty. In addition, the calculation output of the finite element model – such as bending moments, axial forces, anchor forces and ΣMsf – was also subjected to model uncertainty by introducing $\theta_{M'}$, $\theta_{N'}$, $\theta_{f'}$ and θ_{Msf} respectively.

$$Z_{STR,yield}(z) = f_y - \max\left(\frac{\theta_M M_{wall}(z)}{W_{wall}} + \frac{\theta_N N_{tube}(z)}{A_{tube}}\right) \quad (36)$$

$$Z_{STR,buckling}(z) = M_{Rd} - M_{Ed} \\ = \min\left(\theta_B f_B f_y W_{tube} \left(1 - \left(\frac{\theta_N N_{tube}(z) L_s}{N_{Rd}}\right)^{1.7}\right) - \theta_M M_{wall}(z) L_s\right) \quad (37)$$

$$f_B = 1.573e^{\frac{-0.0021D_{tube}}{t_{tube}\varepsilon^2}} \quad (38)$$

Where:

$Z_{STR,yield}$	State function of maximum stress in the combi-wall [kN/m ²]
$Z_{STR,buckling}$	State function of local buckling of the tube of the combi-wall [kNm/m ¹]
f_y	Yield strength [kN/m ²]
$f_{y,ref}$	Reference yield strength, equal to 235 N/mm ² [kN/m ²]
M_{wall}	Bending moment in combi-wall [kNm/m ¹]
N_{tube}	Axial force in combi-wall [kNm/m ¹]
W_{wall}	Section modulus, combi-wall [m ³ /m ¹]
W_{tube}	Section modulus, combi-wall [m ³ /m ¹]
A_{tube}	Sectional area of tube [m ² /m ¹]
M_{Ed}	Maximum bending moment [kNm/pile]
M_{Rd}	Reduced resisting bending moment [kNm/pile]
N_{Rd}	Maximum resistance for axial compressive force [kN/pile]
L_s	Centre-to-centre distance of combi-wall system [m]
f_B	Empirical formula representing mean value experiments, with variation θ_B [-]
ε	Ratio of reference to nominal yield strengths, which equals $\sqrt{f_{y,ref}/f_y}$ [-]
z	Depth across height of combi-wall [m]
θ_B	Factor to account for model uncertainty related to buckling experiments [-]

θ_M	Factor to account for model uncertainty for bending moments [-]
θ_N	Factor to account for model uncertainty for axial forces [-]

The structural (Fig. 3.3-B) and the geotechnical limit states (Fig. 3.3-C) of the anchors were evaluated using Eq. (39) and Eq. (40), respectively. The strength of the grout body depends largely on the factor α_t , which represents the shear capacity along the grout body.

$$Z_{STR;anchor} = f_y - \frac{\theta_F F_{anchor}}{A_{anchor}} \quad (39)$$

$$Z_{GEO;grout} = \alpha_t O_A L_A q_c - \theta_F F_{anchor} \quad (40)$$

Where:

$Z_{STR;anchor}$	State function of maximum stress in cross-section anchor strut [kN/m ²]
$Z_{GEO;grout}$	State function of capacity of grout body anchor system [kN]
F_{anchor}	Anchor force [kN]
A_{anchor}	Sectional area of anchor strut [m ²]
α_t	Tension capacity factor of grout body [-]
O_A	Circumference of grout body [m]
q_c	Cone penetration resistance [MPa]
L_A	Length of grout body [m]
θ_N	Factor to account for model uncertainty for axial forces [-]
θ_F	Factor to account for model uncertainty for anchor forces [-]

Furthermore, the limit state function $Z_{GEO;global}$ covers all geotechnical failure modes (Fig. 3.3-D) simultaneously (Roubos et al., 2018) and is defined as:

$$Z_{GEO;global} = 1.0 - \theta_{Msf} \Sigma Msf = 1 - \theta_{Msf} \frac{c' + \sigma_n \tan(\varphi')}{c'_{reduced} + \sigma_n \tan(\varphi'_{reduced})} \quad (41)$$

Where:

$Z_{GEO;global}$	State function of global safety factor, geotechnical failure modes [-]
ΣMsf	Global stability ratio related to φ - c reduction. The friction angle φ' and cohesion c' are successively decreased until geotechnical failure occurs [-]
θ_{Msf}	Factor to account for model uncertainty for global stability ratio [-]

3.3.3 DISTRIBUTION FUNCTIONS AND CORRELATIONS

This section presents the type of probability distribution function and the variation coefficients for each stochastic variable used in this study (Table 3.2), which can significantly affect the outcome of reliability-based assessments (Rackwitz, 2000). The marginals of the distribution functions are based on the values used in the original design (Eijk, 2011; Timmermans, 2017). By contrast, the type of distribution function was determined in accordance with recommendations found in literature, but predominantly on the basis of the Probabilistic Model Code (JCSS, 2001).

Material properties X_i

The background documents for NEN-EN 9997 (2016) show that the low characteristic value of soil strength φ or c and soil stiffness E_{50} commonly represents a 5% fractile of the layer average, while the recommendations for weight density γ_{sat} typically represent the expected value. Since previous studies have shown that the variability in soil strength is a dominant source of uncertainty and that the variation coefficient in the literature varies widely (Calle & Spierenburg, 1991; Cherubini, 1999; Das & Das, 2010; ISO 2394, 2015; Rippi & Teixeira, 2016; Schweckendiek et al., 2012; Teixeira et al., 2016; Wolters et al., 2012) its influence was investigated by performing a sensitivity analysis (Section 3.4.3). Furthermore, the angle of internal friction depends on the strain rate. In this study, the reference calculation was based on $V_{\varphi} = 0.1$, considered at 5% strain rate (Lindenberg, 2008), which is in accordance with the original design.

Loads F_i

The variable loads represent the lifetime maxima for a reference period of 50 years, and are determined using the Gumbel extreme value distribution function. The characteristic value of terminal loads is generally determined by an operational limit, whereas characteristic wind-induced crane loads typically represent a return period, e.g. $T_R = 50$ years. In accordance with the design report, the characteristic value of the outer water level equals the mean value of the ‘low low water’ spring tide level, which seems acceptable because waterhead differences are not the dominant load. Furthermore, the corresponding groundwater table is largely influenced by the presence of the drainage system. Analogous with NEN-EN 9997 (2016), the outer water and groundwater levels were considered to be a geometric variable.

Geometric variable a_i

The variation coefficients of structural dimensions such as t_{tube} and D_{tube} were determined taking into account execution tolerances and project-specific acceptance criteria, which in Rotterdam are slightly stricter than the recommendations in the Probabilistic Model Code (JCSS, 2001) and NEN-EN 10029 (2010). In this study, geometrical variations such

as variation in retaining height, installation depth and the length of the grout body (Fig. 3.1) were taken into account. Initially, geological variations in soil deposition were distinguished. Their geometrical standard deviations were initially set at $\Delta_a=0.35$ m in order to investigate whether geological variations in soil-layer thickness are relevant. This appeared not to be the case, and consequently the standard deviations were not investigated further.

Model uncertainty θ_i

Although the measured deformations and anchor forces align with the predictions using the finite element model (Berg et al., 2018), a stochastic model factor was applied to the calculation output (Section 3.3.2). A variation coefficient of 0.1 was used, which seems a reasonable value. Since experiments are lacking, the influence of model uncertainty on the reliability index was investigated by performing a sensitivity analysis (Section 3.4.3).

Table 3.2. Stochastic model variables and the associated marginals of their distribution function for the reference quay wall, without and with a relieving platform.

Random variables X_i	SI	Characteristic value	Without relieving platform	With relieving platform	Type of distribution function	Coefficient of variation V or geometrical standard deviation Δa
Materials						
$E_{50\text{-Backfill}}$	MPa	$X_{i,k}$ μ_x	$X_{i,k}$ 50	μ_x 35	Lognormal	V_x 0.20 (NEN-EN 9997, 2016; Wolters et al., 2012)
$E_{50\text{-Reclamation}}$	30	75
$E_{50\text{-Clay}}$	5	8
$E_{50\text{-Hobocene}}$	30	22
$E_{50\text{-SandClay}}$	n/a	10
$E_{50\text{-Pleistocene}}$	50	60
$\varphi_{\text{Backfill}}^4$	o	$X_{i,5\%}$	38.9	32.5	Normal	0.10 (NEN-EN 9997, 2016)
$\varphi_{\text{Reclamation}}^4$	35.9	41.8
φ_{Clay}^4	26.9	22.5
$\varphi_{\text{Hobocene}}^4$	35.9	38.9
$\varphi_{\text{SandClay}}^4$	n/a	32.3
$\varphi_{\text{Pleistocene}}^4$	38.9	41.8
$\gamma_{\text{sat, Backfill}}$	kN/m ³	H_x	20	18	Normal	0.05 (NEN-EN 9997, 2016; Wolters et al., 2012)
$\gamma_{\text{sat, Reclamation}}$	20	20
$\gamma_{\text{sat, Clay}}$	17	17.1
$\gamma_{\text{sat, Hobocene}}$	20	20
$\gamma_{\text{sat, SandClay}}$	n/a	19

Table 3.2. Continued.

Random variables	SI	Characteristic value	Without relieving platform	With relieving platform	Type of distribution function	Coefficient of variation V or geometrical standard deviation Δa
$\gamma_{\text{sat, Pleistocene}}$	20	21
c_{clay}	kPa	$X_{i,5\%}$	6.9	13.9	Lognormal	0.20 (NEN-EN 9997, 2016; Wolters et al., 2012)
c_{sandClay}	n/a	13.9
$f_{\text{y,tube}}^1$	N/mm ²	$X_{i,5\%}$	517	483	..	0.04 ⁷
$f_{\text{y,anchor}}^1$	539	641
α_t	-	$X_{i,5\%}$	0.018	0.015	Normal ⁷	0.10 ⁷
q_c	MPa	μ_x	15	10	..	0.10 ⁸
Loads F_i	-	$F_{i,k}$	μ_F	μ_F	-	V_F
$Q_{\text{surchARGE}}^2$	kN/m ²	Nominal ⁶	104.8	41.9	Gumbel	0.10 ² (Grave, 2002; Huijzer, 1996)
Q_{bulk}^2	n/a	178.2
F_{crane}^2	kN	$F_{i,TR=50}$	n/a	628.7
F_{bollard}^2	..	SWL^5	35.9	104.8
Geometry a_i	-	$a_{i,k}$	μ_a	μ_a	-	Δa
h_{OWL}	m	$LLWS^5$	-0.96	-0.96	Gumbel	0.20m
h_{GWL}	..	$h_{\text{drainage}}+0.3m$	-0.40	-0.40	..	0.25m
$h_{\text{retaining}}$	m to MSL^5	μ_a	-27.5	-31.5	..	0.35m ⁹
h_{pile}^1	m	..	-8	-18.5	..	0.35m ⁷
$D_{\text{scilla,layer}}^1$	varies	varies

Table 3.2. Continued.

Random variables	SI	Characteristic value	Without relieving platform	With relieving platform	Type of distribution function	Coefficient of variation V or geometrical standard deviation Δa
D_{tube}^1	1.067	1.067	Normal	$V_a=0.05'$ (JCSS, 2001)
t_{tube}^1	0.015	0.016
L_{grout}^1	8.5	12	..	$V_a=0.04'$
O_{grout}^1	1.31	1.06
Model uncertainty	-	θ_{ijk}	μ_{θ}	μ_{θ}	-	V_{θ}
θ_i	-	μ_{θ}	1	n/a	Normal(Peters et al., 2017)	0.10 (Peters et al., 2017)
θ_M	1	n/a	Lognormal	0.10
$\theta_N; \theta_F$	1	n/a	..	0.10 (Berg et al., 2018; JCSS, 2001; Roubos et al., 2016)
θ_{MSF}	1	n/a	..	0.10

¹⁾ Based on production and execution tolerances as well as project-specific acceptance criteria in the port of Rotterdam.

²⁾ Extreme value distribution for a reference period of 50 years.

³⁾ Based on expert judgement. This also considers small morphological changes, erosion and sedimentation. The effect of large scour holes and deepening the harbour bottom were not taken into consideration.

⁴⁾ Analogous with Table 2.1b, NEN-EN 9997 (2016), considered at 5% strain rate and represent the layer average.

⁵⁾ LLWWS = low low water at spring tide; SWL = safe working load; MSL = mean sea level.

⁶⁾ The characteristic value is based on an operational limit.

⁷⁾ Little information is available in the literature. In this study, a normal distribution was assumed. The values are based on full-scale field tests (Well, 2018).

⁸⁾ Based on soil investigation used in the design of the quay wall.

⁹⁾ Mean values were derived on the basis of empirical correlations with the cone resistance (Berg et al., 2018; Eijk, 2011).

¹⁰⁾ Based on maximum allowable cone resistance (cut-off), in accordance with design guidance (Janssen, 2012).

Correlation matrix

The dependency between stochastic variables was taken into account to accurately estimate the probability of failure. Correlations between soil parameters were determined statistically by analysing a relatively large database, including the data from site investigations of several projects adjacent to the reference quay walls (Wolters et al., 20012), which align with other literature (Teixeira et al., 2016). Table 3.3 presents the correlation matrix used in this study. The unsaturated (γ_{dr}) and saturated soil-weight densities (γ_{sat}) were assumed to be fully dependent; likewise, the elastic unloading (E_{ur}) and reloading moduli (E_{oed}) were considered to be fully dependent on the soil stiffness E_{50} . These correlations were implemented implicitly in the model by applying a constant deterministic difference or ratio between the variables in order to reduce the number of stochastic variables and hence minimise the calculation effort. The same approach was undertaken to correlate the two vertical crane loads (F_{crane}).

Table 3.3. Simplified correlation matrix.

	E_{50}	φ	γ_{sat}	c'	h_{OWL}	h_{GWL}
E_{50}	-	0.25 ¹	0.50 ¹	0.12 ¹	-	-
φ	0.25 ¹	-	0.50 ¹	-0.65 ¹	-	-
γ_{sat}	0.50 ¹	0.50 ¹	-	-0.09 ¹	-	-
c'	0.12 ¹	-0.65 ¹	-0.09 ¹	-	-	-
h_{OWL}	-	-	-	-	-	0.75 ²
h_{GWL}	-	-	-	-	0.75 ²	-

¹) Based on a statistical analysis of a large dataset in Rotterdam (Wolters et al., 20012).

²) Approximated on the basis of statistical examination of the waterhead difference of a quay wall equipped with sensors in the port of Rotterdam (Berg at al., 2018; Well, 2018). This correlation is only valid when waterhead differences are non-dominant loads.

3.3.4 DERIVATION OF SENSITIVITY AND PARTIAL FACTORS IN THE EVENT OF CORRELATIONS

This section describes the derivation of the sensitivity factors and the partial factors of safety, taking into account correlations between some dominant stochastic variables. The factor α_p , obtained by performing a FORM-based reliability assessment, commonly describes the sensitivity to variations in random variables with regard to the reliability index β found for a specific limit state. In the event that input variables are uncorrelated, the sensitivity factors in the normalised physical space (U -space), denoted as $\alpha_{u,i}$, can be used in analytical formulae to determine the partial material factors γ_m or load factors γ_f (Table 3.4).

Table 3.4. Typical fractiles for characteristic (X_k, F_k) and design values (X_d, F_d), and the associated partial factors of safety (γ_m, γ_f) for friction angle φ and live load Q (Leonardo da Vinci Pilot Project, 2005).

Material property X	Action F
Normal distribution	Gumbel distribution
$X_{k;\varphi} = \mu_\varphi(1 - 1.645V_\varphi)$	$F_{k;Q} = \mu_Q - \frac{1}{c} \ln(-\ln(0.98))$
$X_{d;\varphi} = \mu_\varphi(1 - \alpha_\varphi\beta_tV_\varphi)$	$F_{d;Q} = \mu_Q - \frac{1}{c} \ln(-\ln(\Phi(-\alpha_Q\beta_t)))$
$\gamma_{m;\varphi} = \frac{X_{k;\varphi}}{X_{d;\varphi}}$	$\gamma_{f;Q} = \frac{F_{d;Q}}{F_{k;Q}}$

In the event of correlations between variables, however, the direct use of these formulae will lead to an incorrect physical design point X^* . The input sequence of correlated random variables in a *FORM* approximation can significantly influence the sensitivity factor α_u found. This is because the correlation influences the joint probability distribution function of correlated variables. Consequently, the sensitivity factors of the correlated normal Y -space, denoted as α_y , were derived in order to correctly highlight the contribution of a model parameter to the reliability index obtained. The importance factors α_u^2 and α_y^2 for the uncorrelated U -space and correlated Y -space, are defined as:

$$\alpha_{u,i}^2 = \frac{u_i^{*2}}{\beta_{HL}^2} \tag{42}$$

$$\alpha_{y,i}^2 = \frac{y_i^{*2}}{\|y^*\|^2} \tag{43}$$

Where:

- $\alpha_{u,i}$ Sensitivity factor in the uncorrelated normalised U -space [-]
- $\alpha_{y,i}$ Sensitivity factor in the elliptical/correlated normalised Y -space [-]
- β_{HL} Hasofer-Lind reliability index [-]

The reliability index β of the design point U^* generally does not exactly match the reliability target β_t . In order to compare the results from this study with the partial factors used in the original design, it was therefore necessary to slightly scale the reliability index. Since some input variables are correlated, the Cholesky decomposition L (Jiang et al., 2011; Lemaire, 2009; Melchers & Beck, 2018) was used directly to transform the results from the standard space U to the physical space X . The following transformation was applied in order to determine the design value of random variable x_i given a specific β_t (Lebrun & Dufloy, 2009a; Lebrun & Dufloy, 2009b).

$$U^* = \sqrt{\alpha_u^2 \beta_t^2} \quad (44)$$

$$Y^* = LU^* \quad (45)$$

$$[R] = [L][L]^{-1} \quad (46)$$

$$x_i^* = \mu_i^N + y_i^* \sigma_i^N \quad (47)$$

Where:

U^*	Design point, vector of design values, in the uncorrelated standardised U -space
Y^*	Design point, vector of design values, in the correlated normalised Y -space
R	Correlation matrix
L	Lower triangular matrix obtained by Cholesky decomposition of R
x_i^*	Design value of variable i in physical space X
μ_i^N	Mean value of equivalent normal distribution
σ_i^N	Standard deviation of equivalent normal distribution

The partial factors of the scaled design values x_i^* Eq. (47) were derived using Eq. (48). It should, however, be noted that this equation does not yet account for model uncertainties. Section 3.5.2 further discusses how model uncertainty can be taken into consideration.

$$\gamma_{m;i} = \frac{X_{k;i}}{X_{d;i}} \text{ and } \gamma_{f;i} = \frac{F_{d;i}}{F_{k;i}} \quad (48)$$

Where:

$\gamma_{f;i}$	Partial factor for load i , without accounting for model uncertainties [-]
$\gamma_{m;i}$	Partial factor for material property i , without accounting for model uncertainties [-]
$X_{d;i}$	Design value for material property i
$X_{k;i}$	Characteristic for material property i
$F_{d;i}$	Design value load i
$F_{k;i}$	Characteristic value load i

3.4 RESULTS OF RELIABILITY-BASED ASSESSMENTS OF QUAY WALLS

3.4.1 EVALUATION OF ABDO-RACKWITZ ALGORITHM OUTCOMES

Since coupling a reliability method to a finite element model can become a black box, its outcomes were compared with the results of other reliability methods and tools using Blum's analytical method (Section 3.3.1). In this study, the comparison was made for the structural limit states of the quay wall without the relieving platform Z_{yield} and $Z_{buckling}$. This is because both limit states can also be modelled using Blum's method (Chapter 4). The differences found appear to be fairly small (Table 3.5), and hence performing a finite element-based reliability assessment using the Abdo-Rackwitz algorithm seems a reasonable approach. Section 3.5.1 further discusses its performance.

Table 3.5. Comparison of lifetime reliability indices found using finite element-based and Blum-based reliability assessment for Z_{yield} and $Z_{buckling}$ of the quay wall without a relieving platform.

Design model	Reliability toolbox	Reliability method	Algorithm	Z_{yield}	$Z_{buckling}$
Plaxis Finite elements	ProbAna® ³ +OpenTURNS ⁴	FORM	Abdo-Rackwitz (1991)	3.76 ¹	3.64
Blum Analytical	Prob2B® ⁵	FORM	Rackwitz-Fiessler (1997)	3.87 ^{1,2}	3.49 ²
Blum Analytical	Matlab	Crude Monte Carlo	n/a	3.77 ²	3.58 ²

¹) The associated design point and sensitivity factors are listed in Appendix B.3.

²) The reader is referred to Chapter 4 for further details.

³) The reader is referred to (Laera & Brinkgreve, 2017) for further details.

⁴) The reader is referred to (Adrianov et al., 2007) for further details.

⁵) The reader is referred to (Courage & Steenbergen, 2007) for further details.

3.4.2 RESULTS OF FINITE ELEMENT-BASED RELIABILITY ASSESSMENTS

The reliability indices obtained for the two reference quay walls, without and with a relieving platform, are listed in Table 3.6. This table shows that, when model uncertainty and correlations are taken into account, the reliability index decreases. The reliability indices found differ per failure mode, indicating that only some structural components or failure modes are close to the target reliability index of RC2, which equals 3.8. It was not possible to locate the design point of the limit states Z_{strut} and Z_{grout} of the quay wall with a relieving platform, since soil failure occurs earlier in the finite element model. The results are further discussed in Section 3.5.1.

Table 3.6. Lifetime reliability index β for the two reference quay walls for the different limit state functions, with and without taking into account correlations and model uncertainty θ .

Correlations	Model uncertainty	Without relieving platform					With relieving platform			
		Z_{yield}	$Z_{buckling}$	Z_{strut}	Z_{grout}	Z_{GEO}	Z_{yield}	Z_{strut}	Z_{grout}	Z_{GEO}
Yes	Yes ($V=0.1$)	3.76	3.64	5.43	4.51	5.54	3.91	n/a^3	n/a^3	3.69
Yes	No	4.07	4.01 ¹	5.54	5.12	7.00 ²	4.32	n/a^3	n/a^3	4.49
No	No	4.51	4.14 ¹	5.80	5.14	7.62 ²	6.68 ²	n/a^3	n/a^3	4.84

¹) The model uncertainty related to the experiments conducted by Peters et al. (2017), denoted as $\theta_{m;buckling}$, was taken into account.

²) Beyond accuracy of FORM.

³) It was not possible to locate the design point because soil failure occurred in the hardening soil model.

Since some stochastic variables are correlated, the sensitivity factors $\alpha_{y,i}$, provide the most accurate description of their contribution to the reliability index found (Section 3.3.4). Table 3.7 includes the sensitivity factors α_y , taking model uncertainty into account, and only lists the values higher than 0.1. A high factor indicates that the variability in a model parameter contributes significantly to the probability of failure. Although the sensitivity factors can differ substantially per limit state function, the properties of the soil layers which largely influence the active and passive earth pressure acting on the quay wall are relatively influential, whereas the other soil layers show much lower sensitivity factors. Furthermore, uncertainty related to model uncertainty seems to play an important role. According to the sensitivity factors in Table 3.7, time-dependent random variables such as loads and water levels have quite low sensitivity factors and hence the reliability problem seems largely dominated by uncertainty in time-independent random variables, such as soil and grout properties. In addition, the limit state functions of the quay wall with the relieving platform are completely dominated by the uncertainty about the soil properties of one specific soil layer, i.e. the Pleistocene sand.

Table 3.7. Sensitivity factors $\alpha_y > 0.1$ for the quay walls without and with a relieving platform, taking into account correlations and model uncertainties.

Random variable	Time-dependent	Without platform					With platform	
		Z_{yield}	$Z_{buckling}$	Z_{strut}	Z_{grout}	Z_{GEO}	Z_{yield}	Z_{GEO}
Reliability index β		3.76	3.64	5.43	4.51	5.54	3.91	3.69
Materials X_i								
$E_{50;Backfill}$	No							
$E_{50;Clay}$	No							
$E_{50;Holocene}$	No	-0.24	-0.18	-0.25	-0.10	-0.14		
$E_{50;Reclamation}$	No	-0.17	-0.21		-0.10			
$E_{50;SandClay}$	No	n/a	n/a	n/a	n/a	n/a		
$E_{50;Pleistocene}$	No						-0.31	-0.24
$\varphi_{Backfill}$	No		-0.11		-0.18			
φ_{Clay}	No							
$\varphi_{Holocene}$	No	-0.44	-0.35	-0.72	-0.18	-0.31		
$\varphi_{Reclamation}$	No	-0.36	-0.38	-0.23	-0.21			
$\varphi_{SandClay}$	No	n/a	n/a	n/a	n/a	n/a		
$\varphi_{Pleistocene}$	No						-0.40	-0.76
$\gamma_{sat;Backfill}$	No			-0.11				
$\gamma_{sat;Clay}$	No							
$\gamma_{sat;Holocene}$	No	-0.34	-0.23	-0.50	-0.14	-0.32		
$\gamma_{sat;Reclamation}$	No	0.18	0.25		0.12			
$\gamma_{sat;SandClay}$	No	n/a	n/a	n/a	n/a	n/a		
$\gamma_{sat;Pleistocene}$	No						-0.21	-0.51
c_{Clay}	No							
$c_{SandClay}$	No	n/a	n/a	n/a	n/a			
$f_{y;combi-wall}^1$	No	-0.19	-0.22	n/a	n/a	n/a		n/a
$f_{y;anchor}^1$	No	n/a	n/a	-0.13	n/a	n/a	n/a	n/a
α_t	No	n/a	n/a	n/a	-0.55	n/a	n/a	n/a
q_c	No	n/a	n/a	n/a	-0.55	n/a	n/a	n/a
Loads F_i								
$Q_{surcharge}$	Yes	0.13	0.10	0.16	0.13		n/a	n/a
Q_{bulk}	Yes	n/a	n/a	n/a	n/a	n/a		
$F_{bollard}$	Yes						n/a	n/a
F_{crane}	Yes	n/a	n/a	n/a	n/a	n/a		
Geometry α_i								
h_{OWL}	Yes							
h_{GWL}	Yes							
h_{pile}^1	No						-0.16	-0.15

Table 3.7. Continued.

Random variable	Time-dependent	Without platform					With platform		
state		Z_{yield}	$Z_{buckling}$	Z_{strut}	Z_{grout}	Z_{GEO}	Z_{yield}	Z_{GEO}	
Reliability index β		3.76	3.64	5.43	4.51	5.54	3.91	3.69	
$h_{retaining}$	No	-0.18	-0.16	-0.13	-0.13				
t_{tube}^{-1}	No	-0.16	-0.21						
D_{tube}^{-1}	No	-0.21	-0.26	-0.10					
O_{grout}^{-1}	No	n/a	n/a	n/a	-0.17	n/a	n/a	n/a	
L_{grout}^{-1}	No	n/a	n/a	n/a	-0.17	n/a	n/a	n/a	
Model uncertainty θ_i									
θ_B	No	n/a	-0.46	n/a	n/a	n/a	n/a	n/a	
θ_M	No	0.42	0.30	n/a	n/a	n/a		n/a	
θ_N, θ_F	No				0.35	n/a		n/a	
$\theta_{\Sigma MSF}$	No	n/a	n/a	n/a	n/a	-0.74	n/a	-0.49	

¹⁾ Quality control procedures were taken into consideration.

3.4.3 SENSITIVITY ANALYSIS

The aim of the sensitivity analysis was to show the extent to which reliability indices are influenced by small variations in random variables. This section predominantly presents the results found for the limit state Z_{yield} . This is because this limit state is well-known, its outcomes are close to the reliability targets and it has been widely considered in other studies, which helps us to interpret the results obtained in this one. In accordance with other literature (Section 3.3.3), Fig. 3.4 shows that small changes in the variation coefficient of the soils' internal friction angle φ substantially influence the reliability index of Z_{yield} for both reference quay walls. The effect of the friction angle on the reliability index of the geotechnical limit states Z_{GEO} is generally even higher. Since the soil properties of the Pleistocene sand are quite dominant for the quay wall with a relieving platform, changing the type of distribution of its internal friction angle has more impact than changing the type of distribution functions of the quay wall without a relieving platform. Furthermore, Fig. 3.4 shows that neither changing the variation coefficient of the non-dominant loads nor their distribution function makes much of a difference for either reference quay wall.

In addition, Table 3.8 shows that slightly changing the variation coefficients of θ_M and $\theta_{\Sigma MSF}$ can also have a fairly high impact on the reliability index obtained.

During the service life of a quay wall, port authorities or terminals frequently ask to enhance its functionality by, for example, deepening the berth or increasing operational loads. Fig. 3.5 shows the effect of these functional changes on the reliability index and demonstrates that the reliability index is also significantly influenced by changing functional

requirements, while maintaining the same variation coefficient. Hence, a calculated reliability index is always relative to a certain functionality, as further discussed in Section 3.5.1.

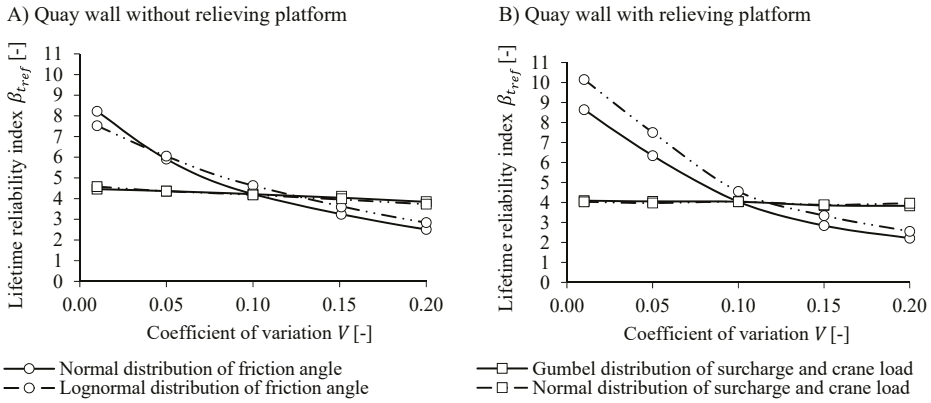


Fig. 3.4. Influence of angle of internal friction φ and live load Q on Z_{yield} for the reference quay wall without (A) and with (B) a relieving platform.

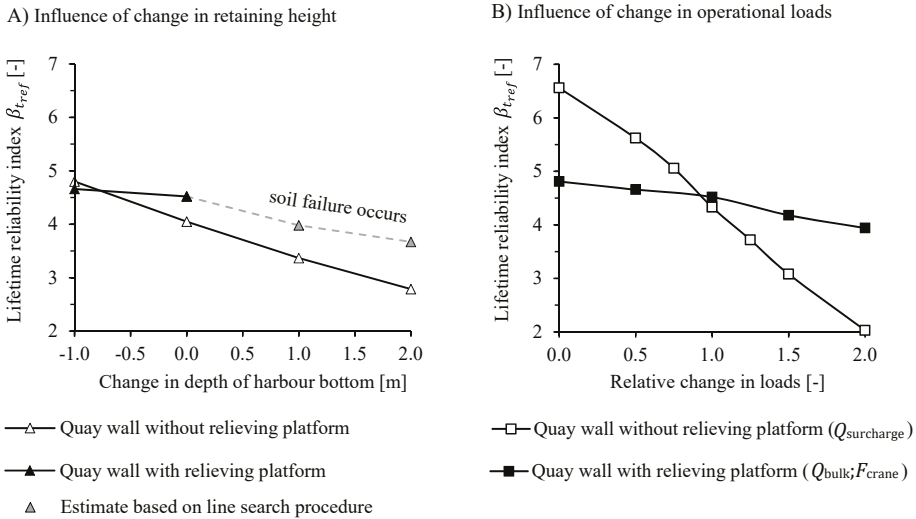


Fig. 3.5. Influence of deepening the harbour bottom (A) and changing the surcharge load (B) on the structural limit state Z_{yield}

Table 3.8. Influence of variation coefficient V_θ on Z_{yield} and Z_{GEO} for the quay wall without a relieving platform.

Limit state	Description	Variation coefficient V			Lifetime reliability index β
		θ_M	θ_N	$\theta_{\Sigma MSF}$	
Z_{yield}	Reference calculation	0.10	0.10	n/a	3.76
Z_{yield}	Recommended values for 'frames' (JCSS, 2001)	0.20	0.10	n/a	3.06
Z_{yield}	Recommended values for 'plates' (JCSS, 2001)	0.10	0.05	n/a	3.83
Z_{GEO}	Reference calculation	n/a	n/a	0.10	5.54
Z_{GEO}	Slightly lower variation coefficient	n/a	n/a	0.05	6.83

3.4.4 RESULTS: PARTIAL FACTORS OF SAFETY

When sensitivity factors are used to derive partial factors, they should ideally be based on several *FORM*-based assessments, the design points of which align with the required target reliability index. Table 3.6 shows that only some limit states are close to the reliability target $\beta_t=3.8$ of reliability class RC2 (NEN-EN 1990, 2011). This section presents the partial factors related to the limit state Z_{yield} of both reference quay walls, as well as Z_{GEO} of the quay wall equipped with the relieving platform. Table 3.9 lists the ratio between the characteristic value and the design value associated with RC2 while using the sensitivity factor α_u (Section 3.3.4). The material factors $\gamma_{m,i}$ lower than 1 indicate that the design values of the non-dominant soil layers are lower than the assumed characteristic values, but they are still higher than their expected values. Furthermore, the partial factor for the internal friction angle of the Pleistocene sand for the quay wall with the relieving platform is fairly high: approximately 1.3. This can be explained by the dominance of this specific soil layer, for which presumably an unrealistic combination of high strength properties and a high variation coefficient was assumed (Section 3.5), introducing an unrealistically low design value for $\varphi_{Pleistocene}$. The differences in sensitivity factors between the quay wall with and without a relieving platform can be explained by the difference in the number of dominant soil layers. In addition, fairly low partial load factors $\gamma_{f,i}$ were found; most were in the order of 1.1. Since the requirements for production tolerances of steel combi-walls in the port of Rotterdam are stricter than the regulations in NEN-EN 10029 (2010), fairly low geometrical factors were found for the structural dimensions. Table 3.9 also shows that the model factor applied to the bending moments has much more influence than applying a model factor to the normal forces for Z_{yield} , being approximately 1.15 for the quay wall without the relieving platform, whereas $\theta_{\Sigma MSF}$ significantly influences Z_{GEO} .

Table 3.9. Load and material factors for a fixed target reliability index, $\beta=3.8$, assuming that α_u is invariant and taking into account correlations.

Random variable	Characteristic values	Without platform		With platform			
		Z_{yield}		Z_{yield}		Z_{GEO}	
		with θ	without θ	with θ	without θ	with θ	without θ
Material properties	X_k	$\gamma_{m,i}$	$\gamma_{m,i}$	$\gamma_{m,i}$	$\gamma_{m,i}$	$\gamma_{m,i}$	$\gamma_{m,i}$
$E_{50;Backfill}$	$X_{5\%}$	0.71	0.73	0.71	0.70	0.72	0.69
$E_{50;Clay}$	$X_{5\%}$	0.74	0.75	0.72	0.71	0.71	0.72
$E_{50;Holocene}$	$X_{5\%}$	0.90	0.97	0.73	0.72	0.72	0.69
$E_{50;Reclamation}$	$X_{5\%}$	0.84	0.82	0.69	0.70	0.72	0.71
$E_{50;SandClay}$	$X_{5\%}$	n/a	n/a	0.75	0.74	0.72	0.72
$E_{50;Pleistocene}$	$X_{5\%}$	0.73	0.74	1.01	1.04	0.91	0.90
$\varphi_{Backfill}$	$X_{5\%}$	0.82	0.82	0.84	0.84	0.85	0.80
φ_{Clay}	$X_{5\%}$	0.84	0.85	0.84	0.83	0.82	0.80
$\varphi_{Holocene}$	$X_{5\%}$	1.03	1.15	0.85	0.85	0.85	0.82
$\varphi_{Reclamation}$	$X_{5\%}$	0.99	0.97	0.83	0.78	0.84	0.84
$\varphi_{SandClay}$	$X_{5\%}$	n/a	n/a	0.87	0.88	0.86	0.84
$\varphi_{Pleistocene}$	$X_{5\%}$	0.83	0.84	1.29	1.28	1.19	1.26
$\gamma_{sat; Backfill}$	μ	0.98	0.99	0.99	0.99	1.00	0.98
$\gamma_{sat; Clay}$	μ	1.01	1.01	1.00	1.00	0.99	1.00
$\gamma_{sat; Holocene}$	μ	1.04	1.07	1.00	1.00	1.00	0.99
$\gamma_{sat; Reclamation}$	μ	1.04	1.06	0.99	0.99	1.00	0.99
$\gamma_{sat; SandClay}$	μ	n/a	n/a	1.01	1.02	1.00	0.99
$\gamma_{sat; Pleistocene}$	μ	1.00	1.00	1.14	1.19	1.11	1.13
c_{Clay}	$X_{5\%}$	0.72	0.74	0.78	0.75	0.69	0.74
$c_{SandClay}$	$X_{5\%}$	n/a	n/a	0.75	0.74	0.75	0.94
$f_{y;CombiWall}^2$	$X_{5\%}$	1.01	0.97	0.95	0.95	n/a	n/a
Loads	F_k	$\gamma_{f,i}$	$\gamma_{f,i}$	$\gamma_{f,i}$	$\gamma_{f,i}$	$\gamma_{f,i}$	$\gamma_{f,i}$
$Q_{surcharge}$	Nominal	1.11	1.12	n/a	n/a	n/a	n/a
Q_{bulk}	Nominal	n/a	n/a	1.06	1.06	1.06	1.07
F_{crane}	Nominal	n/a	n/a	1.07	1.05	1.05	1.05
$F_{bollard}$	$X_{95\%}$	1.06	1.06	n/a	n/a	n/a	n/a
Geometry	$\Delta_{a,k}$	$\Delta_{a,i}$	$\Delta_{a,i}$	$\Delta_{a,i}$	$\Delta_{a,i}$	$\Delta_{a,i}$	$\Delta_{a,i}$
h_{OWL}	LLWS ³	0.00m ¹	-0.02m ¹	-0.01m ¹	0.00m ¹	0.00m ¹	-0.04m ¹
h_{GWL}	$h_{drainage}+0.3m$	0.04m ¹	0.01m ¹	-0.01m ¹	0.00m ¹	0.00m ¹	0.06m ¹
h_{pile}^2	μ	-0.01m ¹	-0.01m ¹	-0.04m ¹	-0.20m ¹	-0.22m ¹	-0.17m ¹
$h_{retaining}^4$	μ	-0.26m ¹	-0.29m ¹	-0.25m ¹	-0.10m ¹	-0.06m ¹	-0.10m ¹
t_{tube}^2	μ	-0.05cm ¹	-0.06cm ¹	-0.01cm ¹	-0.01cm ¹	0.00cm ¹	0.00cm ¹

Table 3.9. Continued.

Random variable	Characteristic values	Without platform		With platform			
		Z_{yield} with θ	Z_{yield} without θ	Z_{yield} with θ	Z_{yield} without θ	Z_{GEO} with θ	Z_{GEO} without θ
state							
D_{tube}^2	μ	0.00cm ¹	0.00cm ¹	0.92cm ¹	0.32cm ¹	0.01cm ¹	0.27cm ¹
Model uncertainty		$\gamma_{\theta;i}$	$\gamma_{\theta;i}$	$\gamma_{\theta;i}$	$\gamma_{\theta;i}$	$\gamma_{\theta;i}$	$\gamma_{\theta;i}$
θ_M	μ	1.14	n/a	1.04	n/a	n/a	n/a
θ_N	μ	1.04	n/a	1.02	n/a	n/a	n/a
$\theta_{\Sigma MSF}$	μ	n/a	n/a	n/a	n/a	0.82	n/a

¹) Geometrical change Δ_a in metres, which is added to the characteristic geometrical variable to obtain the design value.

²) Quality-control procedures were taken into consideration.

³) Low low water level at spring tide (De Gijt & Broeken, 2013).

⁴) Scour was not taken into consideration.

3.5 DISCUSSION ON PARAMETERS THAT INFLUENCE RELIABILITY AND PARTIAL FACTORS

3.5.1 EVALUATION OF RESULTS

Robustness and efficiency of the Abdo-Rackwitz algorithm

The reliability methods available in OpenTURNS were compared in terms of efficiency, robustness and accuracy. Performing finite element-based reliability assessments using the Abdo-Rackwitz *FORM* algorithm appeared to be quite efficient; in particular, convergence is more efficient in this case than with the gradient-free Cobyla algorithm (Powell, 1994), especially when many stochastic variables are taken into consideration. In general, roughly between two and ten iterations were needed to satisfy the convergence acceptance criteria. The one exception was the limit state function Z_{GEO} , for which the calculation time per evaluation and the number of iterations required were approximately a factor of four higher (Table 3.10). This was caused mainly by the presence of higher numerical noise in the global stability ratio ΣMsf . Using an appropriate finite difference step size ε (see Appendix B.2 for details) and robust numerical control settings for the hardening soil solver were crucial to achieve convergence (Laera & Brinkgreve, 2017). Although we were able to manage convergence using the Abdo-Rackwitz algorithm, this proved much more intensive for the quay wall with a relieving platform. The main reason for this was found to be the numerical variations in calculation output related to the quay wall’s complex geometry and the associated numerical mesh – due, for example, to the inclined wall, the embedded beams and the modelling of the relieving

platform – in combination with the accuracy of the finite element solver. Due to restrictions associated with the hardening soil constitutive model and limitations in OpenTURNS, it is not yet possible to perform finite element-based calculations for the reference quay walls using directional sampling. However, using a simplified finite element model shows that *FORM* is likely to outperform directional sampling and crude Monte Carlo with regard to computational efficiency. This is due mainly to the number of limit state evaluations required for relatively low failure probabilities, in combination with more than 25 model parameters, as Waarts (2000) also found. Furthermore, it is recommended that other reliability methods, such as ‘kriging’ (Sudret et al., 2017) and directional adaptive response sampling in combination with finite element models of quay walls (Waarts, 2000), be tested.

Table 3.10. Efficiency of the Abdo-Rackwitz algorithm.

Limit state	Without platform					With platform	
	Z_{yield}	$Z_{buckling}$	Z_{strut}	Z_{grout}	Z_{GEO}	Z_{yield}	Z_{GEO}
Reliability index	3.76	3.64	5.43	4.51	5.54	3.91	3.69
Number of variables	27	28	26	29	25	31	29
Iteration	2	2	9	3	n/a ¹	2	n/a ¹
Limit state evaluations	104	108	510	179	n/a ¹	127	n/a ¹
Residual error ²	<<0.1	<<0.1	<<0.1	<<0.1	<<0.1	<<0.1	<<0.1
Constraint error ²	<1%	<1%	<2%	<0.5%	<2.5%	<2%	<1%

¹) An alternative starting point was used, since the reliability index was fairly low. This was found by only activating the dominate variables, after performing approximately 30 iterations.

²) The reader is referred to [Appendix B.2](#) for additional information.

Comparison with original design

The results of the finite element-based reliability assessments correspond fairly well with the original design (Eijk, 2011; Timmermans, 2017), which requires a minimum reliability index of 3.8 for structural members to comply with the Eurocode standard (De Gijt & Broeken, 2013; NEN-EN 1990, 2011). Due to bearing capacity requirements, both quay walls have a relatively large installation depth. Consequently, the quay wall without a relieving platform has some margin in its geotechnical capacity (Z_{GEO}), whereas this is not the case for the quay wall with a relieving platform. In addition, the anchor systems (Z_{strut} and Z_{grout}) seem to be quite safe. The main reasons for this appear to be the low uncertainties due to the observance of strict test protocols and the fact that the original design takes into account failure of the neighbouring anchors. Taking correlations and model uncertainty into account, target reliability indices of 3.76 and 3.63 for Z_{yield} and $Z_{buckling}$ respectively were found for the quay wall without the relieving platform (Table 3.6). These are close to the target reliability index of 3.8. The reliability indices obtained for Z_{yield} and Z_{GEO} of the quay wall with a relieving platform were 3.91 and 3.69 respectively (Table 3.6), which are also fairly close

the reliability target. It should, however, be noted that extremely low design values for soil strength were sometimes obtained for Z_{yield} – for example, for the angle of internal friction of the Pleistocene sand.

Internal friction angle of soil

The reliability indices found are considered to be somewhat conservative, mainly because the reliability index is quite sensitive to changes in the variation coefficient of the internal friction angle of soil (Fig. 3.4). Interestingly, a previous study by Huijzer (1996) indicates that the mean value of the friction angle rises in line with an increasing soil deformation/strain rate, whereas the associated standard deviation decreases. The variation coefficient is therefore lower for soils with higher strength properties. This was also found by Cherubini (1999). In this study, the variation coefficient of soil strength was assumed to be 0.1 for all soil layers, in accordance with NEN-EN 1997 (2004), although Huijzer (1996) showed that the coefficient of variation of the sand layers in the Maasvlakte area of the port of Rotterdam is in the range 0.03-0.07, which would result in a much higher reliability index (Fig. 3.4). It is therefore highly recommended that further studies investigate the type of distribution function and the variation coefficient of the soil's internal friction angle, as well as its vertical correlation length.

Geometrical variations in soil layers

It was also found that the variation in soil-layer thickness had a negligible influence on the reliability index. Consequently, there seems to be no direct need to consider soil-layer thickness as a random variable when performing reliability-based assessments of soil-retaining walls with similar soil stratigraphy. This significantly reduces the number of model parameters, and hence the required calculation time. When we reduce the sand layers of the quay wall without the relieving platform – since they are fairly thick – by 50 per cent, the reliability index for Z_{yield} increases accordingly, from 4.07 to 4.55. This addresses the added value of soil investigation as well as site-specific knowledge (Schweckendiek et al., 2017).

3.5.2 EVALUATION AND DERIVATION OF PARTIAL FACTORS OF SAFETY

This section reflects upon the partial factors used in quay-wall engineering and discusses how correlations and model uncertainty influence the derivation of partial factors of safety. Before comparing and deriving partial factors, it must be clear how model uncertainty can be taken into account.

Options for implementation of model uncertainty

In accordance with NEN-EN 1990 (2011), a design is considered to be sufficiently safe if the design value of the resistance R_d is higher than the design value of the action effect E_d . These two values are defined as:

$$E_d = E(F_{d,i}, a_{d,i}, \theta_{d,i}) \quad (49)$$

$$R_d = R(X_{d,i}, a_{d,i}, \theta_{d,i}) \quad (50)$$

Where:

E_d	Design value of action effect
E	Action effect
R_d	Design value of resistance
R	Resistance
$F_{d,i}$	Design value of load i
$X_{d,i}$	Design value of material property i
$a_{d,i}$	Design value of geometric property i
$\theta_{d,i}$	Design value of model uncertainty i

In quay-wall engineering, however, material properties of soil layers – such as soil strength and weight density – can act simultaneously as resistance and load. Hence, the definition of the action effect must be reformulated as $E_d = E(F_{d,i}, X_{d,i}, a_{d,i}, \theta_{d,i})$. When deriving partial factors, two approaches can generally be distinguished: either model factors γ_{sd} and γ_{rd} can be applied to the representative load and resistance effect respectively (Eq. 51 and Eq. 52) or model factors γ_{sd} and γ_{rd} can be applied directly to individual load and resistance parameters using γ_f and γ_m respectively (Eq. 53 and Eq. 54).

$$E_d = \gamma_{sd} E \left(\gamma_f F_{rep,i}, \frac{X_{rep,i}}{\gamma_m}, a_{d,i} \right) \quad (51)$$

$$R_d = \frac{R \left(\frac{X_{rep,i}}{\gamma_m}, a_{d,i} \right)}{\gamma_{rd}} \quad (52)$$

or

$$E_d = E \left(\gamma_F F_{rep,i}, \frac{X_{rep,i}}{\gamma_M}, a_{d,i} \right) \quad (53)$$

$$R_d = R \left(\frac{X_{rep,i}}{\gamma_M}, a_{d,i} \right) \quad (54)$$

In which:

$$\gamma_F = \gamma_{sd} \gamma_f \text{ and } \gamma_M = \gamma_{rd} \gamma_m$$

Where:

γ_f	Partial factor for actions [-]
γ_F	Partial factor for actions, also accounting for model uncertainties [-]

γ_m	Partial factor for material properties [-]
γ_M	Partial factor for material properties, also accounting for model uncertainties [-]
γ_{Sd}	Partial factor associated with uncertainties in the action or the action-effect model [-]
γ_{Rd}	Partial factor associated with uncertainties in the resistance model [-]

Evaluation of partial factors used in the design without model uncertainty

When reflecting on the partial factors presently used, it is crucial to know if and how model uncertainty is accounted for in the design approach. The design reports on both reference quay walls (Eijk, 2011; Timmermans, 2017), and likewise the design manual (De Gijt & Broeken, 2013), show that no model factors are applied either to resistance or to action effects. If model uncertainty is accounted for in the design, it must be included in the partial load and material factors; that is, via γ_F and γ_M . It is, however, rather questionable whether γ_M includes model uncertainty; this is because the partial factors of soil properties are formulated on the basis of a code-calibration procedure (Calle & Spierenburg, 1991) specifically for reliability class RC2 in NEN-EN 1990 (2011), which does not provide any information regarding model uncertainty. Furthermore, this calibration report (Calle & Spierenburg, 1991) reveals that correlations are not taken into consideration.

Since Z_{yield} was included in the calibration report and the reliability index for the quay wall without the relieving platform was found in this chapter to be close to the reliability target for RC2, this limit state was used to determine partial factors of safety. Table 3.11 lists the partial material and load factors (γ_m and γ_q) found for Z_{yield} with and without correlations, in order to compare them with the partial factors in NEN-EN 9997 (2016). The partial factors for the other reliability classes were arrived at by scaling the reliability indices using the method described in Section 3.3.4.

Let us for now assume that model uncertainty was not taken into account in the procedure for calibrating the partial factors for soil properties (Calle & Spierenburg, 1991). If this is the case, then using the same limit state function Z_{yield} and the same model variables and type of distribution functions and coefficient of variation, slightly lower partial factors are found for soil properties and the surcharge variable load Q_v .

Since the internal friction angle φ is a dominant design variable, Table 3.11 shows that the material factors $\gamma_{m;\varphi}$ presently suggested for sheet pile walls in Table A.4b of NEN-EN 9997 (2016) will result in a fairly small differentiation between the reliability classes. Consequently, a design using the partial safety factor associated with RC1 is quite safe, whereas a design per RC3 is presumably too optimistic. Furthermore, the design value

found for soil stiffness E_{50} is fairly close to its mean value, and hence a partial factor of 1.3 seems unnecessary.

In the present design codes, correlations between soil properties are not taken into account and no distinction is made between dominant and non-dominant soil layers. Neglecting correlations could lead to an underestimation of the probability of failure, while assuming all soil layers to be dominant may lead to an overestimation. It is therefore recommended that correlations between soil properties be accounted for when defining partial factors, even though this will make the design process more complex.

Table 3.11. Partial factors γ_m and γ_q for Z_{yield} with and without correlations between soil conditions, for target reliability indices of 3.3, 3.8 and 4.3 respectively.

Model parameter	X_{rep} F_{rep}	V	Eurocode standard ⁶			Without correlations			With correlations		
			RC1	RC2	RC3	3.3 ⁴	3.8 ⁴	4.3 ⁴	3.3 ⁴	3.8 ⁴	4.3 ⁴
Reliability class											
Reliability target											
Correlations			No	No	No	No	No	No	Yes	Yes	Yes
Soil stiffness E_{50}	$X_{k;5\%}$	0.20	1.30	1.30	1.30	0.78 ¹	0.79 ¹	0.79 ¹	0.94 ¹	0.97 ^{1,5}	1.01 ¹
Tangent of friction angle φ	$X_{k;5\%}$	0.10	1.15	1.175	1.20	1.05 ¹	1.10 ¹	1.15 ¹	1.11 ¹	1.18 ^{1,5}	1.25 ¹
Weight density γ_{sat}	μ_x	0.05	1.00	1.00	1.00	0.97 ¹	0.97 ¹	0.97 ¹	1.06 ¹	1.07 ^{1,5}	1.08 ¹
Surcharge load Q	$F_{k,max}^2$	0.01	1.23 ³	1.36 ³	1.50 ³	1.10	1.11	1.12	1.11	1.12 ⁵	1.13

¹) Partial factor represents dominant Holocene sand layer and does not account for model uncertainty.

²) Operational limit as specified in service level agreement with the user.

³) This partial factor does not include model uncertainty and represents γ_q , which was derived by dividing γ_q by a model factor of 1.1 (NEN-EN 1990, 2011).

⁴) The target reliability index was scaled using the sensitivity factors in the U -space for Z_{yield} , associated with $\beta = 4.07$.

⁵) See fourth column of Table 3.9.

⁶) Based on NEN-EN 1990 (2011) and NEN-EN 9997 (2016).

Example of the derivation of partial factors with model uncertainty

This section presents the partial factors of safety derived from the results of the two reference quay walls, taking into account model uncertainty and correlations. They serve only as an example, since partial factors for codes and standards should ideally be derived from far more reliability-based assessments. Table 3.12 and Table 3.13 respectively list the partial factors found for the quay walls without and with a relieving platform, for the limit states of which the reliability indices found are close to the reliability target of RC2.

For both quay walls, lower partial factors were found for soil stiffness and the surcharge load than recommended in NEN-EN 9997 (2016) and NEN-EN 1990 (2011), respectively. Furthermore, partial factors for weight density and model factors need to be considered. It

should be noted, however, that the variation coefficient of all model factors was assumed to be 0.1, whereas really this value should preferably be based on experimental findings. The partial factors found for the soils' internal friction angle differ widely, both per failure mode and per reliability class. This is because the friction angle is a dominant variable and because the number of dominant soil layers present differs per failure mode. Again the results show lower and higher partial factors for the soils' friction angle than the values recommended in the design guideline for quay walls for RC1 ($\beta_t=3.3$) and RC3 ($\beta_t=4.3$) respectively (De Gijt & Broeken, 2013).

Table 3.12. Partial factors γ_m and γ_q for Z_{yield} and $Z_{buckling}$ with correlations between soil conditions for various target reliability indices, for the quay wall without a relieving platform.

Model parameter	X_{rep}, F_{rep}	SI	V		Z_{yield}			$Z_{buckling}$		
					3.3 ³	3.8 ⁴	4.3 ³	3.3 ³	3.8 ⁴	4.3 ³
Soil stiffness E_{50}	$X_{k,Low 5\%}$	-	0.20	γ_m	0.87	0.90 ^{1,5}	0.92 ¹	0.84 ¹	0.86 ¹	0.87 ¹
Tangent of friction angle φ	$X_{k,Low 5\%}$	-	0.10	γ_m	1.00	1.03 ^{1,5}	1.07 ¹	0.95 ¹	0.98 ¹	1.01 ¹
Weight density γ_{sat}	μ_x	-	0.05	γ_m	1.04	1.04 ^{1,5}	1.05 ¹	1.04 ¹	1.04 ¹	1.05 ¹
Surcharge load Q_y	$F_{k,max}^2$	-	0.10	γ_q	1.11	1.11 ⁵	1.12	1.09	1.09	1.10
Retaining height $h_{retaining}$	μ_a	cm	n/a	Δ_a	-0.23	-0.26 ⁵	-0.30	-0.20	-0.23	-0.26
Model factor θ_B	μ_θ	-	0.10	γ_{Rd}	n/a	n/a	n/a	0.83	0.81	0.78
Model factor θ_M	μ_θ	-	0.10	γ_{Sd}	1.12	1.14 ⁵	1.16	1.11	1.13	1.14

¹) Partial factor represents the Holocene sand layer for which the layer average of the internal friction angle is derived at 5% strain rate.

²) Operational limit as specified in service level agreement with user.

³) The target reliability index was scaled, while maintaining the sensitivity factors in the U -space.

⁴) The obtained reliability indices of 3.76 and 3.64 are very close to this target reliability index.

⁵) See third column of Table 3.9.

Table 3.13. Partial safety factors γ_m and γ_q for Z_{yield} and Z_{GEO} with correlations between soil conditions for various target reliability indices, for the quay wall with a relieving platform.

Model parameter	X_{rep}, F_{rep}	SI	Y_m	Z_{yield}			Z_{GEO}				
				V	3.3 ³	3.8 ⁴	4.3 ³	V	3.3 ³	3.8 ⁵	4.3 ³
Soil stiffness E_{50}	$X_{k;Low\ 5\%}$	-	Y_m	0.10 ⁴	0.98 ¹	1.01 ¹	1.05 ¹	0.20	0.88 ¹	0.91 ^{1,6}	0.94 ¹
Tangent of friction angle φ	$X_{k;Low\ 5\%}$	-	Y_m	0.07 ⁴	1.10 ¹	1.14 ¹	1.23 ¹	0.10	1.16 ¹	1.24 ^{1,6}	1.32 ¹
Weight density γ_{sat}	μ_x	-	Y_m	0.05	1.13 ¹	1.16 ¹	1.18 ¹	0.05	1.10 ¹	1.11 ^{1,6}	1.13 ¹
Surcharge load Q_y	$F_{k;max}^2$	-	Y_q	0.10	1.08	1.08	1.09	0.10	1.06	1.06 ⁶	1.06
Retaining height $h_{retaining}$	μ_a	cm	A_a	n/a	-0.06	-0.07	-0.07	n/a	-0.05	-0.06 ⁶	-0.07
Model factor θ_M	H_θ	-	Y_{sd}	0.10	1.05	1.06	1.07	0.10	n/a	n/a	n/a
Model factor $\theta_{\Sigma Msf}$	H_θ	-	Y_{rd}	0.10	n/a	n/a	n/a	0.10	0.84	0.82 ⁶	0.80

¹) Partial factor represents the Pleistocene sand layer for which the layer average of the internal friction angle is derived at 5% strain rate.

²) Operational limit as specified in service level agreement with user.

³) The target reliability index was scaled, while maintaining the sensitivity factors in the U -space.

⁴) The design point found using $V_{ES0} = 20\%$ and $V_\varphi = 10\%$ resulted in an unrealistically low design value for the angle of internal friction φ for Z_{yield} . Consequently, an additional probabilistic calculation was made using $V_{ES0} = 10\%$ and $V_\varphi = 7\%$, in accordance with the recommendations made by Huijzer. The reliability index thus obtained was approximately 4.3.

⁵) The obtained reliability index of 3.69 is very close to this target reliability index.

⁶) See seventh column of Table 3.9.

3.5.3 REFLECTION ON RESULTS FROM A PRACTICAL PERSPECTIVE

Since time-independent model parameters show high sensitivity factors (Table 3.7), this finding can be relevant when assessing service-proven quay walls (Allaix et al., 2018; Roubos et al., 2018). This is because the annual failure rate of a quay wall with a successful service history is likely to decrease over time in the absence of significant degradation. It is therefore likely that the remaining lifetime of many well-functioning quay walls can be extended. However, this aspect is not included in the existing codes of practice. It is therefore highly recommended that it be the subject of further study (Chapter 4).

Moreover, Fig. 3.5 shows that a reliability-based assessment can demonstrate the effect of changing functional requirements such as deepening the harbour bottom or enhancing operational loads. If the uncertainty over time is decreased by updating all the information available, then it seems possible to optimise the functionality of service-proven quay walls. Logically, though, there are limits. Although local conditions play an important role, it seems possible to deepen service-proven structures by approximately one metre without making structural adjustments, or to increase the loads they bear by about 20 per cent. This can be done using the data obtained from quay walls equipped with sensors, in combination with advanced reliability methods such as Bayesian updating. A further

functional increase is often not possible, because then the quay wall is most likely not able to withstand accidental limit states (ALS) such as extremely low outer water levels. It should be emphasised, too, that activating these 'hidden' capacities also requires extra attention from the user to prevent functional misuse – for example, overloading of the quay wall.

3.6 CONCLUSION AND RECOMMENDATIONS

The results of this chapter provide guidance on performing finite element-based reliability assessments of quay walls in realistic design conditions. Its most important findings are as follows.

- Finite element-based reliability assessments have been successfully performed using the gradient-based Abdo-Rackwitz *FORM* algorithm, which converges quite efficiently and accurately while taking into account a large number of stochastic variables.
- The reliability indices found for critical structural members align with the code requirements. However, they seem quite sensitive to changes in the variation coefficient of variables with a high sensitivity factor, such as the friction angle of soil.
- The structural failure modes of the combi-wall play an important role. In addition, the geotechnical stability of the quay wall equipped with a relieving platform has been found to be an important failure mode. Furthermore, the reliability of anchor systems seems to be fairly high.
- Neglecting model uncertainty and correlations between input variables leads to an underestimation of the probability of failure.
- The highest sensitivity factors were found for time-independent stochastic variables such as material properties of soil, steel and grout, as well as model uncertainty.
- The local soil stratigraphy and project-specific functional requirements, such as the retaining height and operational loads, can significantly influence the reliability of a quay wall. However, these stochastic variables show low sensitivity factors and hence require relatively low partial factors of safety.
- The differences between the partial factors found for the angle of internal friction of soil in the various reliability classes are greater than the recommended values in the Eurocode standard.

Since it is unclear if and how model uncertainty is accounted for in quay-wall engineering (De Gijt & Broeken, 2013), it is recommended that the partial factors presently used be re-evaluated and that, for instance, distinctions be drawn between dominant and non-dominant soil layers. In addition, the results of this chapter show that the variation in the soils'

angle of internal friction greatly influences quay-wall reliability. It is therefore recommended that a detailed study be conducted of relevant statistical properties, such as the type of distribution function and its variation coefficient. Although the reliability indices found for the anchor system are already quite high (Table 3.6), it is likely that dense sand layers contain additional capacity with regard to the grout body. This additional capacity can become relevant when deepening an existing berth or enhancing operational loads. Consequently, it is recommended that full-scale failure tests be performed on the grouted anchors in order to reveal their full capacity and to derive more insight into the statistical properties of α_c . Furthermore, it is highly recommended that new and existing quay walls be equipped with sensors to reduce the uncertainty related to modelling the soil-structure interaction. Studying this aspect will shed new light on model uncertainty and the actual capacity of a quay wall. The insights obtained will significantly benefit asset managers. Moreover, the data required is quite easy to obtain by simultaneously measuring deformations, water-level differences and anchor forces. This type of information can also be used in Bayesian reliability updating analyses.

The finding that time-independent random variables significantly influence the reliability index can play a crucial role in the assessment of existing quay walls, and presumably in that of all other service-proven geotechnical structures. It is therefore highly recommended that further investigation be conducted into the evolution of the probability of failure over time, including the effect of degradation, taking into account the successful service history of the quay walls. In the absence of degradation, e.g. by installing a system of cathodic protection, it is likely that the annual failure rate will decrease over time, and hence the service life of service-proven quay walls can safely be extended (Chapter 4).

4





THE EFFECT OF CORROSION ON THE RELIABILITY OF COMBI-WALLS

The sensitivity analysis presented in the previous chapter shows that quay-wall reliability is influenced by both the size and the variation of model parameters. In particular, the time-independent variables, such as retaining height, soil strength and material properties, greatly influence the reliability of a quay wall. As a result, the annual failure probability will decrease if the structure has survived in previous years, assuming that degradation is prevented; otherwise, the annual failure probability will increase. One of the main causes of quay-wall degradation is corrosion of steel structural members exposed to salt water. The aim of this chapter is to show the effect of corrosion-induced degradation on the reliability of steel combi-walls. The chapter outline is as follows. The principles of uniform and pitting corrosion are described in [Section 4.2](#), the methods used to assess the reliability of corroded combi-walls are addressed in [Section 4.3](#) and the results obtained are given in [Section 4.4](#). The results are further discussed in [Section 4.5](#) and conclusions are drawn in [Section 4.6](#). The effect of corrosion was slightly lower than expected a priori, and hence the insights obtained make it possible to safely extend the service lifetime of quay walls.

This chapter is based on the following publication: Roubos, A. A., Allaix, D., Schweckendiek, T., Steenbergen, R. D. J. M., & Jonkman, S. N. (2019), Time-dependent reliability analysis of service-proven quay walls subject to corrosion-induced degradation. Reliability Engineering & System Safety (submitted).

ABSTRACT

The assessment of service-proven quay walls subject to corrosion-induced degradation is inherently a time-dependent reliability problem. Two major challenges are the modelling of corrosion and taking into account the decrease of epistemic uncertainty throughout the quay wall's service life. The main objective of this chapter is to examine the probability of failure, despite successful past performance, when the quay wall is subject to corrosion and randomly imposed variable loads. The development of the annual failure rate is modelled using crude Monte Carlo and by performing a first-order system reliability analysis. The annual failure rates found for service-proven quay walls vary over time. For those with successful service histories and subject to low corrosion rates, the highest reliability indices are observed in the first year of the service life, whereas with higher corrosion rates the final year prevails. In general, it seems more practical to evaluate reliability on an annual basis rather than over longer time periods, since the latter will introduce an iterative procedure to determine the wall's remaining lifetime. The key findings of this chapter can be crucial for the lifetime extension of existing quay walls, and presumably also for other service-proven geotechnical structures subject to corrosion.

4.1 INTRODUCTION

Marine structures such as quay walls and jetties often suffer from corrosion-induced degradation. In the coming years, many such structures throughout the world will approach the end of their design lifetime and will be reassessed as part of lifetime-extension programmes (Roubos & Grotegoed, 2014). Steel structural members of quay walls generally show some degree of wall-thickness loss after a certain exposure period. This decrease in strength needs to be taken into consideration in the reassessment of quay walls. Two recent studies (Boero et al., 2012; Teixeira et al., 2016) show that the uncertainty in material loss due to corrosion-induced degradation significantly influences the reliability level of soil-retaining walls.

The parameters that influence corrosion can generally be classified into endogenous parameters related to the steel material, exogenous parameters related to the environment and a time-dependent component related to the exposure period (Houyoux et al., 2007). In the port of Rotterdam, corrosion rates depend mainly on geometry, orientation and the type of marine structure concerned, as well as site-specific environmental conditions (Jongbloed, 2008; Jongbloed, 2019). The wide diversity of deterioration agents, such as dissolved oxygen, salinity, water quality, temperature and exposure period, makes predicting the corrosion phenomenon a fairly complex process (Melchers & Jeffrey, 2008; Melchers & Wells, 2006). There tends to be a rather high level of uncertainty associated with the various influences (Melchers, 1999; Melchers, 2015; Melchers & Beck, 2018).

Consequently, millions of wall-thickness measurements and multiple destructive coupon tests have been performed in order to study the impact of uniform and pitting corrosion in the port of Rotterdam (Jongbloed, 2019). On the basis of this information, the Port of Rotterdam Authority has developed a practical method (Section 4.2) to assess the effect of corrosion on the remaining 'factor of safety' (*FoS*) using field observations. It is unclear, however, if a constant and time-independent factor of safety adequately covers the actual reliability level of a quay wall that has successfully been in service for a certain period of time, since in the absence of degradation it has become more likely that this structure will remain satisfactory and safe (Melchers & Beck, 2018).

Only a few studies have investigated the influence of corrosion on the reliability of steel soil-retaining walls (Houyoux et al., 2007; Osório et al., 2010; Schweckendiek et al., 2007), mainly using the first-order reliability method (*FORM*). None of these studies took successful past performance into account, however, and so they most likely overestimate the probability of failure of service-proven soil-retaining walls. This is because not all effects of the passage of time and service on structural reliability are negative (Hall, 1988). Hall (1988) found that the failure rate of non-deteriorating structures with successful service histories decreases significantly over time if the initial uncertainty in time-independent random variables is high.

Fig. 4.1-A shows that a structure without degradation has a constant failure rate if all the uncertainty involved is variability in time. By contrast, the failure rate of a structure will approach zero directly after completion if we assume that the uncertainty is exclusively epistemic in nature, since it only involves time-invariant random variables.

In reality, a quay wall will be subject to both time-dependent and time-independent sources of uncertainty, such as inherent natural variability in strength and loads (aleatory uncertainty), as well as lack of knowledge or insufficient information (epistemic uncertainty) (ISO 2394, 2015). In quay-wall engineering, time-independent uncertainties in soil properties and model uncertainty significantly influence the reliability level (Chapter 3). It is therefore expected that the annual failure rate of a service-proven and non-deteriorating quay wall will decrease during its early years of service and over time approach a constant value, since after a period of successful service only the time-dependent (aleatory) uncertainty remains (Fig. 4.1-A). If the effect of corrosion is included, the failure rate of the quay wall is expected to increase over time as the structure becomes subject to corrosion-induced degradation (Fig. 4.1-B). The extent of this effect will depend on the corrosion rate. In addition, Fig. 4.1-B shows that the beneficial effects of past performance can partly offset negative effects induced by corrosion.

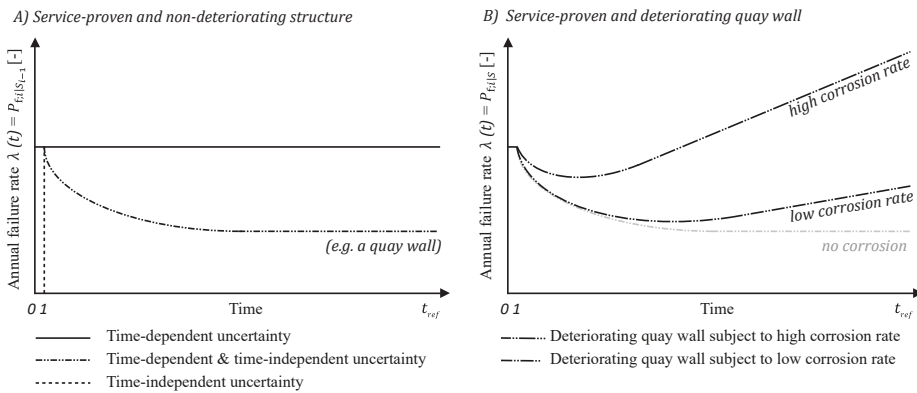


Fig. 4.1. Failure rate of service-proven and non-deteriorating structures (A), and the effect of service-proven deteriorating quay walls (B).

The primary aim of this chapter is to analyse the effect of corrosion-induced degradation on the reliability of steel structural members of quay walls. A secondary aim is to show how the overall factor of safety (FoS) and the reliability index (β) are related, and how they change over time for systems subject to corrosion. When assessing the impact of wall-thickness loss on structural reliability, our particular interest was to determine the annual failure rate of service-proven quay walls. In this chapter, a time-dependent reliability

analysis is performed by introducing time-independent and time-dependent uncertainty as random variables in order to account simultaneously for successful past performance and corrosion (Allaix et al., 2018; Roubos et al., 2018). In addition, a sensitivity analysis reveals the impact of the variability in dominant parameters, such as soil strength, yield strength, live loads and corrosion, on the evolution of the reliability index over time. The results of this chapter have been used to reflect on the ‘allowable stress-based’ method, which is presently used to assess combi-walls subject to corrosion-induced degradation in Rotterdam (Section 4.2).

4.2 ALLOWABLE STRESS-BASED METHOD TO ASSESS CORRODED COMBI-WALLS

This section describes the main principles of the ‘allowable stress-based’ method presently used by the Port of Rotterdam Authority to facilitate predictive asset management (Voogt, 2014), by evaluating the structural integrity of steel combi-walls, which represent about half of the quay walls in its port. For more in-depth details, the reader is referred to the corrosion handbook by Jongbloed (2019), which includes an overview of all research conducted into the phenomenon of corrosion at the port of Rotterdam.

A combined quay wall consists of steel primary elements such as H-profiles (Fig. 4.2-A) or tubular piles (Fig. 4.2-B), with sheet piles in between, which only have a soil retaining function. The corrosion rate of the primary steel element is usually higher due to a galvanic reaction with the secondary elements. This is because these elements generally have a higher steel quality, and hence are the less precious metal (Jongbloed, 2019). Furthermore, the wall-thickness loss on the landside of the primary elements appears to be negligible compared with the loss on the waterside, most likely because there is a lack of oxygen in the soil (Jongbloed, 2019). The wall-thickness reduction Δt is therefore only taken into account on the waterside of primary elements (Fig. 4.2).

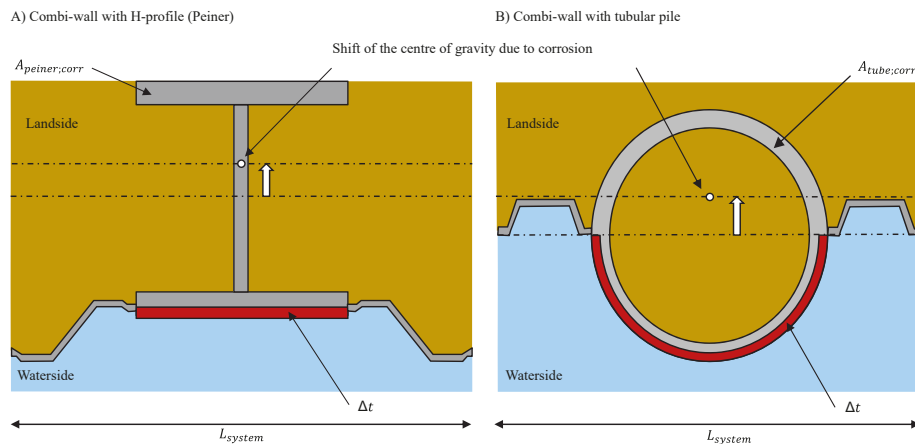


Fig. 4.2. Residual wall thickness and corrosion Δt of the primary combi-wall elements; cross-sections of Peiner system with H-piles (A) and of combi-tube system (B). The parts where corrosion is considered are highlighted in red.

The foundation for assessing corrosion-induced degradation relies on a strict in-situ test protocol using ultrasonic wall-thickness measurements and a procedure for measuring local corrosion pits (Roubos & Grotegoed, 2014). Significant pitting not only affects the structural failure modes but can also introduce geometrical openings which may cause soil erosion directly behind the quay wall. The field observations are examined statistically in order to assess both these failure modes.

Over the years, the Port of Rotterdam Authority has collected a large number of wall-thickness measurements in salt, brackish and fresh-water conditions. Although the corrosion rates found align with those described in the literature, it appears that predicting corrosion without field observations is fairly difficult. Even quay walls with similar geometries and in similar environmental conditions may show significant differences in corrosion rates (Jongbloed, 2019). Clear correlations between corrosion and other deterioration agents have not yet been identified. Jongbloed interpreted all the information available and developed dedicated typical corrosion curves (Fig. 4.3-B) for all the ports in the Netherlands (De Gijt & Broeken, 2013). If wall-thickness measurements have been taken after a certain exposure period, the representative corrosion curve can be selected and extrapolated to predict the evolution of corrosion over time. It should be noted that Jongbloed's curves represent the equivalent mean value of corrosion Δt_{eq} , which equals the sum of the mean uniform and pitting corrosion with an accuracy of approximately 1 mm during an exposure period of 50 years (Jongbloed, 2019). When developing these curves, however, data from the first ten years was lacking and so the curves have only been verified for longer-term exposures.

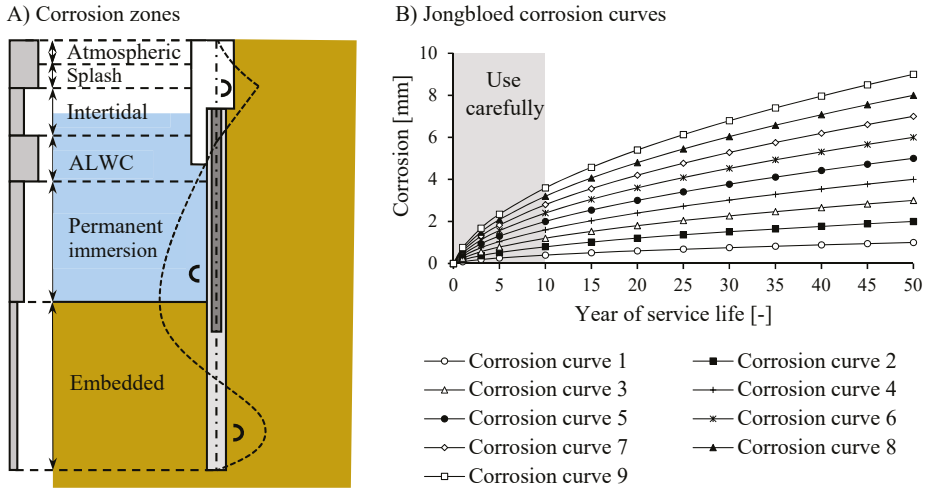


Fig. 4.3. Typical corrosion zones (A) and the Jongbloed corrosion curves (B).

The corrosion rates differ across the height of the quay wall, and therefore different corrosion zones are distinguished. These include the atmospheric, splash, intertidal, accelerated low-water corrosion (ALWC), permanent immersion and embedded zones (Fig. 4.3-A).

Geometrical openings induced by biochemical pitting corrosion generally occur in the ALWC zone (De Gijt & Broeken, 2013). Since the corrosion rates of the secondary sheet piles are fairly low, soil erosion due to geometric openings is not very likely in case of combi-walls and has yet to be observed in reality. This is because a hole in a tubular pile does not result directly in a geometrical opening, whereas the flange thickness of H-piles is relatively large. At present, the remaining service life is generally determined by ascertaining when the yield stress in the outer fibre of structural members subject to corrosion becomes excessive. These stresses largely depend on bending moments and axial forces (Eq. 55), and mostly prevail in the permanent immersion zone (Fig. 4.3-A). In order to assess the influence of pitting corrosion, a geometrical reduction is applied to the initial wall thickness ($t_0 - \Delta t_{eq}$), resulting in the 'equivalent wall thickness' t_{eq} (Eq. 57). This geometrical factor represents the decrease in the net capacity of the cross-section, and it depends on the ratio between pitting corrosion and residual wall thickness (Jongbloed, 2019). The structural assessment of corrosion relies on the *FoS* (Eq. 58).

$$\sigma_y(z, t_{eq}) = \frac{M_{wall}(z)}{W_{wall}(z, t_{eq})} + \frac{N_{tube}(z)}{A_{tube}(z, t_{eq})} \quad (55)$$

$$\sigma_{y;k,max}(z, t_{eq}) = \max(\sigma_{y;k}(z, t_{eq})) \quad (56)$$

$$t_{eq}(z) = t_0 - \Delta t_{eq}(z) \quad (57)$$

$$FoS = \frac{f_{y;k}}{\sigma_{y;k}} \quad (58)$$

Where:

t_{eq}	Equivalent wall thickness for a particular corrosion curve [m]
t_0	Initial wall thickness [m]
Δt_{eq}	Equivalent wall-thickness loss due to uniform and pitting corrosion [m]
FoS	Factor of safety [-]
$f_{y;k}$	Characteristic value yield strength related to characteristic loads and material properties [N/m ²]
σ_y	Stress in outer fibre of tube [N/m ²]
$\sigma_{y;k}$	Characteristic stress in outer fibre of tube [N/m ²]
M_{wall}	Bending moment in combi-wall [kNm/m ¹]
N_{tube}	Axial force at position of maximum bending moment in combi-wall [kNm/m ¹]
W_{wall}	Section modulus of combi-wall [m ³ /m ¹]
A_{tube}	Sectional area of tube [m ² /m ¹]
z	Depth [m]

Until the end of the twentieth century, the stresses σ_y were calculated using Blum's method (Blum, 1931). Nowadays, however, finite element models are available to model the soil-structure interaction more accurately. When using Blum's method, it was common practice to apply a factor of safety to $\sigma_{y;k}$ to verify the nominal yield strength $f_{y;k}$. The minimum FoS required in the design of a new quay wall was 1.5. This does not remain constant, however: asset managers distinguish different stages (Fig. 4.4) in a quay wall's service life. As long as the FoS remains higher than 1.3, an existing quay wall is considered to be sufficiently safe; if the remaining FoS is between 1.2 and 1.3, the wall-thickness loss is monitored more frequently. A FoS lower than 1.2 is considered unacceptable, because then the quay wall may not be able to withstand 'accidental' load combinations any more. In the latter case, the quay wall must be retrofitted or replaced.

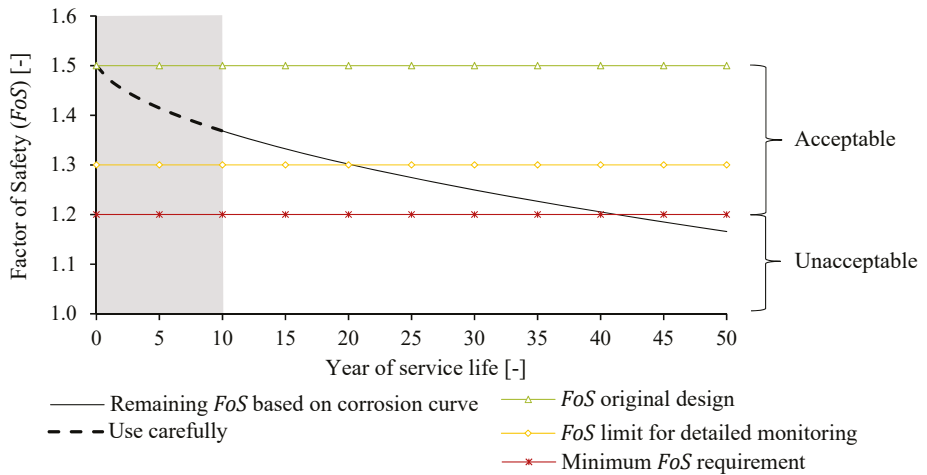


Fig. 4.4. Typical degradation curve due to corrosion and asset-management stages of steel combi-tubes in Rotterdam.

4.3 RELIABILITY-BASED METHOD TO ASSESS CORROSION-INDUCED DEGRADATION

4.3.1 INTRODUCTION

This section introduces the methods and input used to determine the effect of corrosion-induced degradation on the reliability of service-proven quay walls over time. In this chapter, a quay wall that has actually been built in Rotterdam serves as a reference (Fig. 4.5). This structure consists of a concrete slab and a combi-wall, and is equipped with grout anchors. The original design model and the as-built information were consulted (Timmermans, 2017). Fig. 4.5 shows the associated diagrams of the bending moments, the normal force and the horizontal deformation in ‘design’ conditions, which represent the fundamental ultimate limit state (ULS). It should be noted that the highest stresses occur at the position of the maximum bending moment in the span, which is in the ‘permanent immersion’ zone (Fig. 4.5).

The failure modes affected by corrosion were reformulated on the basis of limit state functions (Section 4.3.2) using random variables (Section 4.3.3).

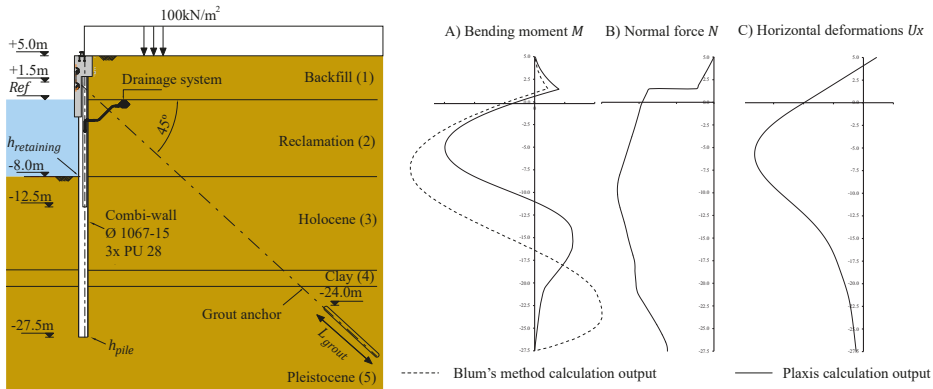


Fig. 4.5. Main dimensions of the reference quay wall, a combi-wall with grouted anchor (left), and its typical bending moment (A), normal forces (B) and deformation diagrams (C).

The assessment of service-proven structures is inherently a time-dependent reliability problem (Hall, 1988). The main objective is to determine the probability of failure, after successful past performance, while the quay wall is subject to corrosion-induced degradation and randomly imposed variable loads. This problem was solved numerically by performing a crude Monte Carlo analysis (Section 4.3.4) for each year of service life, with Blum's method used to model the quay wall analytically (Blum, 1931). It is well known that this method has some limitations, however, and so its calculation results were calibrated using a finite element model (Section 4.3.5).

4.3.2 LIMIT STATE FUNCTIONS OF COMBI-WALLS SUBJECT TO CORROSION

Since structural failure modes generally determine the remaining service life of a combi-wall subject to corrosion (Section 4.2), this study focuses on the limit states for 'yielding' and 'buckling'. Fig. 4.5 shows that the stresses in outer fibre on the waterside $\sigma_{y;water}$ are generally lower than on the landside $\sigma_{y;land}$ due to the presence of the axial force N_{tube} (Fig. 4.6). As a result, the landside of the combi-wall is more susceptible to local buckling, whereas the development of the stresses on the waterside is more sensitive to corrosion. The wall-thickness loss on the waterside results in a proportional increase of $\sigma_{y;water}$ and a slight increase of $\sigma_{y;land}$ (Fig. 4.6). This is caused by a decrease of A_{tube} , a shift of the centre of gravity and the reduction of the section modulus on the waterside $W_{wall;water}$. Consequently, the effect of corrosion on the yielding capacity of the combi-wall was studied for both the landside (Eq. 59) and the waterside (Eq. 60).

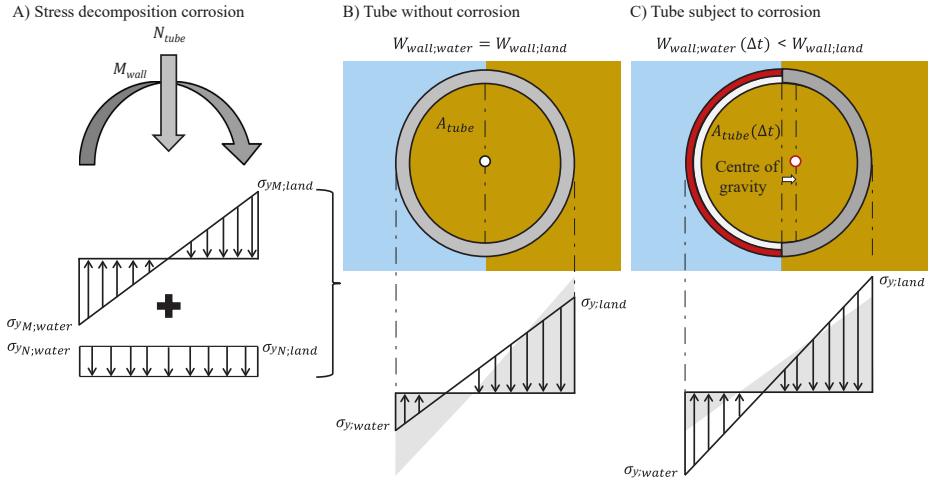


Fig. 4.6. Stress decomposition (A) over the cross-section of a combi-tube without (B) and subject to corrosion (C).

The formula to evaluate local buckling (Eq. 61) was derived from recent experiments, including the following empirical formula for the buckling factor f_B (Eq. 62), which represents the ratio between the actual and the theoretical bending moment capacity (Peters et al., 2017). The risk of local buckling is stress and strain level-dependent, and hence the parameter $D_{tube}/t_{tube} \varepsilon^2$ is generally used instead of D_{tube}/t_{tube} . The tubes' diameter D_{tube} and wall thickness t_{tube} represent the actual dimensions, and the yield strength f_y was based on tensile tests. Particularly because f_B was determined from experiments, in this study we included an additional stochastic factor θ_B to account for model uncertainty. In addition, the model factors θ_M and θ_N were applied to the calculated bending moments and axial forces. The following three state functions were considered as a reasonable approach:

$$Z_{yield;land}(z) = f_y - \max\left(\frac{\theta_M M_{wall}(z)}{W_{wall;land}(z)} + \frac{\theta_N N_{tube}(z)}{A_{tube}(z)}\right) \quad (59)$$

$$Z_{yield;water}(z) = f_y - \max\left(\frac{\theta_M M_{wall}(z)}{W_{wall;water}(z)} - \frac{\theta_N N_{tube}(z)}{A_{tube}(z)}\right) \quad (60)$$

$$\begin{aligned} Z_{buckling}(z) &= M_{Rd} - M_{Ed} \\ &= \min\left(\theta_B f_B f_y W_{tube}(z) \left(1 - \left(\frac{\theta_N N_{tube}(z) L_s}{N_{Rd}(z)}\right)^{1,7}\right) - \theta_M M_{wall}(z) L_s\right) \end{aligned} \quad (61)$$

Where:

$$f_B = 1.573e^{\frac{-0.0021 D_{tube} f_{y,measured}}{t_{tube} f_{y,ref}}} \quad (62)$$

And where:

$Z_{yield;land}$	State function, maximum stress in outer fibre of combi-wall on landside [kN/m ²]
$Z_{yield;water}$	State function, maximum stress in outer fibre of combi-wall on waterside [kN/m ²]
$Z_{buckling}$	State function, local buckling of tube [kNm/m ¹]
f_y	Yield strength [kN/m ²]
$f_{y;measured}$	Measured yield strength during full-scale tests [kN/m ²]
$f_{y;ref}$	Reference yield strength in accordance with NEN-EN1993 (2011) [kN/m ²]
M_{wall}	Bending moment in combi-wall [kNm/m ¹]
N_{tube}	Axial force at position of maximum bending moment in combi-wall [kNm/m ¹]
F_{anchor}	Anchor force [kN]
$W_{combi-wall}$	Section modulus, combi-wall [m ³ /m ¹]
W_{tube}	Section modulus, tube [m ³ /m ¹]
A_{tube}	Sectional area tube [m ² /m ¹]
M_{Ed}	Maximum bending moment [kNm/pile]
M_{Rd}	Reduced resisting bending moment [kNm/pile]
N_{Rd}	Maximum resistance for axial compressive force [kN/pile]
L_s	Centre-to-centre distance, combi-wall system [m]
f_B	Empirical formula based on experiments [-]
N_{Rd}	Maximum resistance for axial compressive force [kN/pile]
z	Depth across height of combi-wall
θ_B	Factor to account for model uncertainty related to buckling experiments [-]
θ_M	Factor to account for model uncertainty in bending moments [-]
θ_N	Factor to account for model uncertainty in axial forces [-]

4.3.3 DISTRIBUTION FUNCTIONS AND CORRELATIONS

This section presents the properties of the random variables used in this chapter (Table 4.1). The characteristic values employed comply with the original design (Timmermans, 2017), and for the most part the variation coefficients were determined in accordance with recommendations in literature (JCSS, 2001). Furthermore, time-dependent and time-independent random variables were taken into account. The methods used to perform the time-dependent reliability analysis are described in Section 4.3.4. The material properties and model uncertainty were considered to be time-independent variables, whereas water levels, operational loads and corrosion were assumed to vary over time.

The equivalent wall-thickness loss due to corrosion Δt_{eq} was modelled using Jongbloed's corrosion curves (Fig. 4.3-B), which represent the mean value of uniform and pitting corrosion combined. It should be noted that these curves, which are based on millions of wall-thickness measurements, exhibit higher corrosion rates when compared with other design guidance (Grabe, 2012; NEN-EN 1993-5, 2007). To illustrate the influence of different corrosion environments, this study examines the effect of all nine corrosion curves on the annual failure rate in the permanent immersion zone. The uncertainty related to corrosion-induced degradation was estimated using field measurements from the port of Rotterdam (De Jong, 2018). The variation coefficients found for distinctive corrosion environments range between 0.1 and 0.5, which is in accordance with other literature (Allaix et al., 2018; Boero et al., 2012; Roubos et al., 2018). The effect of the coefficient of variation on the reliability index was examined by performing a sensitivity analysis (Section 4.3.3).

Furthermore, the uncertainty in the corrosion rate was assumed to be fully correlated over time, since the experience with corrosion measurements is that the uncertainty is mainly epistemic in nature. In other words, the main uncertainty is usually which corrosion curve applies; but once the relevant curve has been determined using measurements, the development of corrosion mostly follows that curve throughout the quay wall's service life. In modelling terms, this means that the random variable representing the uncertainty in corrosion determines the position relative to the mean curve throughout the entire reference period being considered. Mainly to prevent simulation of unrealistically high or low corrosion rates during the crude Monte Carlo analysis, the respective probability distribution function was truncated; the effect of that on the results of this study was negligible, as demonstrated in the sensitivity analysis (Section 4.3.3). The reader is therefore referred to Chapter 3 for a detailed description of other random variables.

Table 4.1. Type of distribution and variation coefficient used in the Blum-based reliability assessment.

Design parameter	Time-dependent	SI	X_k	μ	Distribution	Variation coefficient V
Unit weight of soil γ_{sat}					Normal	
- Backfill (1)	No	kN/m ³	20.0	20.0		0.05 (Osório, 2010; Teixeira et al., 2016; NEN-EN 9997, 2016; Wolters et al., 2012)
- Reclamation sand (2)	No	kN/m ³	20.0	20.0		
- Holocene sand (3)	No	kN/m ³	20.0	20.0		
- Clay layer (4)	No	kN/m ³	17.0	17.0		
- Pleistocene sand (5)	No	kN/m ³	20.0	20.0		
Friction angle φ'_{rep}					Normal	
- Backfill (1)	No	°	32.5	38.9		0.10 ² (Osório, 2010; Teixeira et al., 2016; NEN-EN 9997, 2016; Wolters et al., 2012)
- Reclamation sand (2)	No	°	30.0	35.9		
- Holocene sand (3)	No	°	30.0	35.9		
- Clay layer (4)	No	°	22.5	26.9		
- Pleistocene sand (5)	No	°	32.5	38.9		
Cohesion c'	No	kPa	5.0	6.9	Lognormal	0.20 (Osório, 2010; Teixeira et al., 2016; NEN-EN 9997, 2016; Wolters et al., 2012)
Yield strength f_y	No	N/mm ²	485	510	Lognormal	0.07 (Osório, 2010; Teixeira et al., 2016; JCSS, 2001)
Tube diameter D_{tube}	No	m	1.067	1.067	Normal	0.05 ¹ (JCSS, 2001)
Wall thickness t_{tube}	No	m	0.15	0.15	Uniform	0.05 ¹ (JCSS, 2001)
Corrosion Δt_{eq}	Yes	m	n/a	variable ³	Truncated normal ⁷	0.50 (Boero et al., 2012; De Jong, 2018)
Outer water level ($h_{0(wr)}$)	Yes	m	-0.84 ⁴	-0.84	Gumbel	0.20 m ⁵
Ground water level ($h_{g(wr)}$)	Yes	m	-0.34 ⁴	-0.34	Gumbel	0.25 m ⁵ (Huijzer & Hannink, 1995)
Annual maximum load Q_{tt}	Yes	kN/m ²	n/a	72.1	Gumbel	0.14

Table 4.1. Continued.

Design parameter	Time-dependent	S_I	X_k	μ	Distribution	Variation coefficient V
Lifetime maximum load Q_{L50}	n/a	kN/m ²	100	104.8	Gumbel	0.10 (Calle & Spierenburg, 1991; Huijzer & Hannink, 1995; Huijzer, 1996; Osório et al., 2010)
θ_B	No	-	n/a	1	Normal	0.20 ⁴ (Peters et al., 2017)
θ_M	No	-	n/a	1	Lognormal	0.10 ⁶
θ_N	No	-	n/a	1	Lognormal	0.10 (JCSS, 2001)

¹) Based on production and execution tolerances, as well as project-specific acceptance criteria in the port of Rotterdam.

²) By analogy with NEN-EN 1997 (2004), considered at 5% strain rate (Huijzer & Hannink, 1995).

³) Depends on the selected corrosion curve.

⁴) Outer water level is based on low water at spring tide (LLWS); the groundwater level depends on the position of the drainage system. Water loads were considered as non-dominant loads, in accordance with the design report (Timmermans, 2017).

⁵) Geometrical standard deviation Δ_s based on the water-level measurements (Berg et al., 2018).

⁶) Factor is slightly lower than that recommended by the Probabilistic Model Code (JCSS, 2001) for modelling plates, which is 0.2; this is because measurements showed that the models used are conservative rather than optimistic (Adel, 2018; Huijzer & Hannink, 1995; Well, 2018).

⁷) Truncated by neighbouring corrosion curves.

In addition, dependency between input variables was taken into account in order to prevent underestimation of the probability of failure. Table 4.2 presents the correlation matrix considered. It is worth noting that the unsaturated (γ_{dr}) and saturated (γ_{sat}) soil weight densities were assumed to be fully dependent. This correlation was implemented automatically by applying a deterministic constant initial difference.

Table 4.2. Simplified correlation matrix.

	φ	γ_{sat}	c'	OWL	GWL	θ_M	θ_N
φ	-	0.50 ¹	-0.65 ¹	-	-	-	-
γ_{sat}	0.50 ¹	-	-0.09 ¹	-	-	-	-
c'	-0.65 ¹	-0.09 ¹	-	-	-	-	-
OWL	-	-	-	-	0.75 ²	-	-
GWL	-	-	-	0.75 ²	-	-	-
θ_M	-	-	-	-	-	-	1.00
θ_N	-	-	-	-	-	1.00	-

¹) Based on statistical analysis of a large dataset from Rotterdam (Wolters et al., 2012).

²) Approximated on the basis of statistical examination of the waterhead difference of a quay wall equipped with sensors in the port of Rotterdam (Berg et al., 2018). This correlation is only valid when waterhead differences are non-dominant loads.

4.3.4 NUMERICAL APPROACH TO TIME-DEPENDENT RELIABILITY ANALYSIS

This section describes the numerical approach to solve the time-dependent reliability problem. The solution to this problem was expressed as the probability of failure P_f . For each state function presented in Section 4.3.2, the probability of failure was defined as the probability of outcrossing the limit state $g(X)=0$ (JCSS, 2001). In this study, the failure probability P_f was directly related to the reliability index β on the basis of Eq. (64) (Cornell,1969; Hasofer & Lind, 1974). In addition, the conditional failure rate – which is defined as the probability of failure given that the structure has survived all previous years – was determined taking time-dependent effects on resistance $R(t)$ due to corrosion and variable loads $S(t)$ into account. When the instantaneous probability density functions of $R(t)$ and $S(t)$ are known, the instantaneous probability of failure $P_f(t)$ can be estimated. The basic formulation of the time-variant reliability problem is as follows:

$$g(X(t)) = R(t) - S(t) \tag{63}$$

$$P_f(t) = P(g(X(t)) \leq 0) = \int_{g(X(t)) \leq 0} f_{X(t)}(x(t)) dx(t) \tag{64}$$

$$P_f(t) = \Phi(-\beta(t)) \tag{65}$$

Where:

$g(X)$	State function of variable X
X	Vector of random variables
$R(t)$	Resistance function at time t
$S(t)$	Solicitation or load function at time t
$P_i(t)$	Instantaneous probability of failure at time t , assuming that the structure has survived the previous period [-]
$f_x(x)$	Joint probability density function of the vector X of random variables [-]
β	Reliability index [-]

This time-variant reliability problem was solved by performing a crude Monte Carlo analysis (Allaix et al, 2018). The evolution of the annual probability of failure $P_{f,i}$ was examined for different scenarios using Blum's analytical method (Section 4.3.5). The conditional probability of failure in year i was defined as the probability that failure occurs during year i , given that the structure has survived the previous period.

$$P_{f,i|S} = P(F_1) + P(F_2 \cap S_1) + P(F_3 \cap S_1 \cap S_2) + \dots + P(F_i \cap S_1 \cap \dots \cap S_{i-1}) \quad (66)$$

$$= P(F_i | S_1 \cap S_2 \cap \dots \cap S_{i-1})$$

Where:

$P_{f,i}$	Conditional probability of failure for year i , given that the structure has survived all previous years [-]
F_i	Failure in year i [-]
S_i	Survival in year i [-]

Analogous to equation Eq. (66), the cumulative probability of failure for a specific period was determined using Eq. (67) and Eq. (68). It should be noted that the term $P_{f,i|S}P_S$ represents the probability $P_{f_i} \cap P_S$, which is approximated by the conditional failure probability $P_{f,i|S}$. This is allowed since the probability of failure is fairly low.

$$P_{f,t_{ref}|S} = \sum_{i=1}^n P_{f,i|S}P_S \approx \sum_{i=1}^n P_{f,i|S} \quad (67)$$

$$P_{f,t_{sur}|S} = \sum_{i=1}^{n_{sur}} P_{f,i|S}P_S \approx \sum_{i=1}^{n_{sur}} P_{f,i|S} \quad (68)$$

$$P_{f,t_{rem}|S} = P_{f,t_{ref}|S} - P_{f,t_{sur}|S} \quad (69)$$

Where:

$P_{f;t_{ref} S}$	Probability of failure in the interval $[t_0, t_{ref})$ given that the structure has survived all previous years [-]
$P_{f;t_{sur} S}$	Probability of failure in the interval $[t_0, t_{sur})$ given that the structure has survived all previous years [-]
$P_{f;t_{rem} S}$	Probability of failure in the interval (t_{sur}, t_{ref}) given that the structure has survived all previous years [-]
P_S	Probability that the structure survived the previous period [-]
t_{ref}	Reference period [years]
t_{sur}	Period survived in service life [years]
t_{rem}	Remaining lifetime [years]
n	Number of years in service life [-]
n_{sur}	Number of years survived [-]

Practical application of crude Monte Carlo

In each simulation, the time-independent variables (Section 4.3.3) were generated once. In the case of time-dependent variables, new values were generated for each year of the service life. Furthermore, the time-dependent wall thickness, or in other words the increase of corrosion, was adjusted every year deterministically on the basis of a specific corrosion curve (Fig. 4.2). The crude Monte Carlo approach to solve the time-variant reliability problem starts by generating 10 million samples for the first year. The failures F_1 were used to estimate the annual failure rate $P_{f,1|S}$. Subsequently, only the survivals S_1 that did not cross the limit state continued to year two. Starting from the second year, the time-independent variables remained unchanged, whereas new samples were generated for time-dependent variables such as corrosion Δt_{eq} and the variable load Q_{tt} . Again, the failures F_2 determine the annual failure rate $P_{f,2|S}$. This process subsequently removes implausible realisations from the simulation (i.e. realisations in which the model predicts failure whereas the structure is supposed to survive) and was repeated for each year of the service life.

As an example, Fig. 4.7 presents the number of failures estimated on the basis of crude Monte Carlo. For this chapter a service life of 75 years was assumed, and consequently a total of approximately 750 million Blum-based evaluations was performed for each corrosion curve. However, Fig. 4.7 shows that the numerical noise for the situation without corrosion is still fairly high. This is because 750 million samples are too few to accurately calculate the failure rates in all individual years.

First-order system reliability analysis

In addition to crude Monte Carlo, a first-order approximation was performed to describe the development of the failure rate more accurately for fairly low failure rates. The annual

equilibrium, while performing a plasticity analysis to estimate the horizontal stresses in the soil (Eq. 71 and Eq. 72) (Bakker, 2000; Blum, 1931). Since Blum's method has some limitations, its outcome was evaluated using the finite element model Plaxis. This section discusses the calibration between Blum and the Plaxis hardening soil model.

$$K_{a,h} = \frac{\cos^2(\varphi)}{\left(1 + \sqrt{\frac{\sin(\delta + \varphi)\sin(\varphi)}{\cos(-\delta)}}\right)^2} \quad (71)$$

$$K_{p,h} = \frac{\cos^2(\varphi)}{\left(1 - \sqrt{\frac{\sin(\delta + \varphi)\sin(\varphi)}{\cos(-\delta)}}\right)^2} \quad (72)$$

Where:

$K_{a,h}$	Horizontal component of active earth-pressure coefficient [-]
$K_{p,h}$	Horizontal component of passive earth-pressure coefficient [-]
φ	Angle of internal friction [°]
δ	Wall-friction angle [°]

The deterministic outputs of the two models were compared for design conditions (Fig. 4.5-A). When using Blum's method, it is common practice to correct its calculation output (Grabe, 2012) since this method overestimates the bending moments and underestimates the anchor force. The calculation output of the finite element model shows a small rotation and translation at the toe (Fig. 4.5-C), whereas Blum assumes 'full fixation' of the combi-wall in the soil (Karamperidou, 2018; Steenepoorte, 1992). Moreover, Blum's method does not take into account vertical arching, assumes a rigid anchor support and neglects the structural rigidity of the combi-wall, as well as the backfilling of soil above the anchor. As a result, the bending moments and anchor forces derived using Blum are, respectively, higher and lower than those derived from the finite element model (Fig. 4.5-A). The differences between the deterministic finite element-based and Blum-based calculations are within acceptable limits assuming $\delta=0$ in combination with the following assumptions.

- The anchor force F_a calculated using Blum's method was increased by 15% (Hoesch, 1977).
- Blum's method does not return the normal force N_{wall} . Hence, this force was estimated using the Plaxis calculation output, which is approximately twice the horizontal anchor force F_a found using Blum.
- The maximum bending moment in the span M_{wall} was reduced by 30% (Leatemia & Heijndijk, 1998; Well, 2018).

In addition, the reliability index, the sensitivity factors and the design point found were also evaluated by performing Blum-based and finite element-based reliability assessments. The latter was undertaken using the reliability interface ProbAna® (Chapter 3), in which the gradient-based FORM algorithm Abdo-Rackwitz (1991) was selected. ProbAna® facilitates

the coupling between Plaxis and the open-source probabilistic toolbox OpenTURNS (Andrianov et al., 2007). Meanwhile, the Blum-based probabilistic analysis was conducted on the basis of the *FORM* and Monte Carlo. The *FORM* calculations are based on the Rackwitz-Fiessler algorithm (Rackwitz & Fiessler, 1997) using the reliability tool Prob2B (Allaix et al., 2017; Allaix et al., 2018). The results presented in the next section show that the reliability index, the design point and the associated sensitivity factors are quite similar.

4.4 RESULTS OF RELIABILITY ANALYSIS OF CORRODED COMBI-WALLS

4.4.1 COMPARISON OF BLUM-BASED AND FEM-BASED RELIABILITY ASSESSMENT

This section compares the results of the reliability-based assessments performed using the analytical Blum model and the finite element model of the reference quay wall. It should be noted that this comparison does not yet take corrosion into account, since the main objective here is to compare the lifetime reliability indices $\beta_{t_{50}}$ associated with the cumulative failure probability $P_{f,t_{50}}$ for a design lifetime of 50 years, as well as the annual reliability indices β_{t_1} related to $P_{f,t}$. The results obtained show fairly small differences (Table 4.3), and hence modelling using the calibrated Blum's method seems a reasonable approach to reveal the effect of corrosion-induced degradation on the reliability of a quay wall.

In addition, the marginal differences in the *FoS* found by performing the allowable stress-based assessments also align with the marginal differences of the established reliability indices. The detailed results for Z_{yield} are presented in Appendix C.1.

Table 4.3. *FoS*, lifetime reliability index and annual reliability index for Z_{yield} and $Z_{buckling}$

Design model		Reliability interface & method			$Z_{yield,landside}$	$Z_{yield,waterside}$	$Z_{buckling}$
Plaxis	Finite elements	n/a	n/a	<i>FoS</i>	1.49	2.64	1.51
Plaxis	Finite elements	ProbAna®	FORM-AbdoRackwitz	$\beta_{t_{ref}}$	3.76 ²	5.33 ²	3.63 ²
Blum	Analytical	Prob2B®	FORM-RackwitzFiessler	$\beta_{t_{ref}}$	3.87	5.05	3.49
Blum	Analytical	Matlab	Monte Carlo	$\beta_{t_{ref}}$	3.74	4.94 ¹	3.58
Plaxis	Finite elements	ProbAna®	FORM-AbdoRackwitz	β_{t_1}	4.39	5.79	n/a
Blum	Analytical	Prob2B®	FORM-RackwitzFiessler	β_{t_1}	4.44	5.68	3.84
Blum	Analytical	Matlab	Monte Carlo	β_{t_1}	4.36	5.18 ¹	3.94

¹) The number of samples is too low to determine the reliability index; a more accurate result should be obtained with a higher number of samples.

²) Results were derived in Chapter 3.

4.4.2 INFLUENCE OF CORROSION ON THE FoS AND THE RELIABILITY INDEX β

Corrosion-induced degradation reduces the FoS and reliability index β of the structural limit states. When assessing corroded combi-walls, the highest stresses typically develop in the permanent immersion zone (Fig. 4.3-A). For the reference quay wall, this zone corresponds with corrosion curve 3 (Section 4.1.5); Fig. 4.8 therefore presents its corresponding effect on the remaining FoS and the annual reliability index β . The FoS on the waterside is initially much higher than that on the landside due to the presence of axial force N_{tube} (Fig. 4.6). Furthermore, Fig. 4.8-A shows that the FoS for yielding on the landside and local buckling are quite similar (overlapping). By contrast, the results shown in Fig. 4.8-B indicate that the uncertainty in time-independent random variables significantly influences the limit state for local buckling of a service-proven quay wall, since the annual reliability index significantly increases in the early service period.

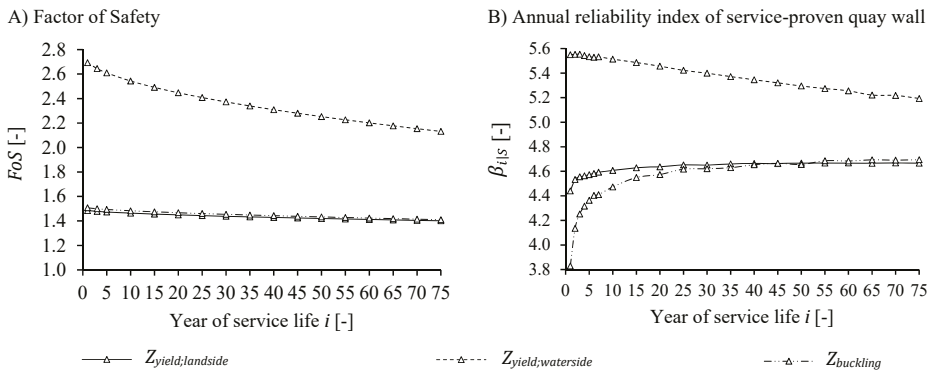


Fig. 4.8. Development of FoS (A) and annual reliability index (B) for Z_{yield} and $Z_{buckling}$ of a service-proven quay wall subject to corrosion curve 3 in the permanent immersion zone. The annual reliability curves are based on the first-order system analysis.

Fig. 4.9 shows the results of the Blum-based reliability assessment for the limit state yielding (Z_{yield}) on the landside; The main reason for focusing on this limit state is that it is well-known and is currently used in the allowable stress-based assessments of corroded quay walls (Section 4.2). The annual failure rates and the associated annual reliability index were determined using crude Monte Carlo for all nine corrosion curves, as well as for the situation without corrosion. Furthermore, the trendlines of the corrosion curves are based on a first-order system analysis (Section 4.3.3). The results clearly illustrate that the annual failure rate is not constant (Fig. 4.9). During its early years of service, the annual failure rate of a service-proven quay wall shows a downward trend, which is the result of successful resistance to past service loading (Hall, 1988). With low corrosion rates, the annual failure

rate keeps decreasing throughout the first 75 years, whereas with higher corrosion rates the annual failure rate will start increasing at some point during this time.

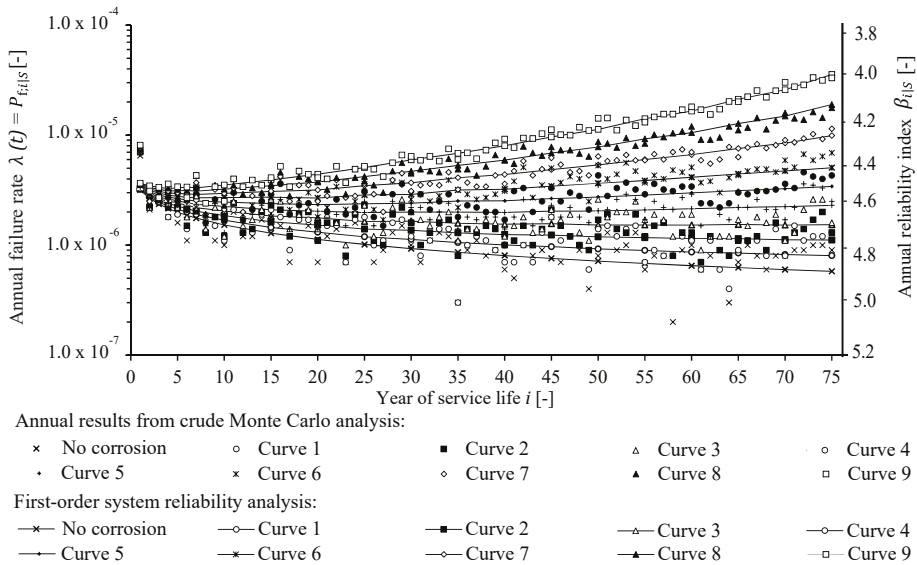


Fig. 4.9. Evolution of annual failure rate for different corrosion curves for the $Z_{yield;landside}$ in the permanent immersion zone.

Fig. 4.10-A shows the impact of corrosion on the FoS . As expected, the FoS decreases due to wall-thickness loss, which is directly related to the service life using the corrosion curves (Fig. 4.3). When a quay wall is undamaged, the FoS remains constant (Fig. 4.10-A) while the cumulative probability of failure of a service-proven uncorroded quay wall increases slightly over time (Fig. 4.10-C). This indicates that the allowable stress-based method is only related to the reference period t_{ref} via the corrosion curves, while a change in t_{ref} always results in a change in $P_{f;t_{ref}|S}$; This is because unfavourable time-dependent variables, such live loads, are more likely to occur during a longer service life.

In addition, Fig. 4.10-B shows that the annual reliability index for all curves increases in the early period of service due to past service performance. For the situation without corrosion and for corrosion curve 3, the annual reliability index keeps increasing as the quay wall ages successfully, whereas curves 6 and 9 show already show a decrease.

If we assume that the quay wall's service life is 75 years and that it has survived all previous service loads, its residual cumulative probability of failure for its remaining lifetime can be determined. Fig. 4.10-D shows that, despite corrosion, the residual cumulative probability of failure for a service-proven quay wall will decrease. When its remaining service life becomes short, e.g. $t_{rem} < 10$ years, Fig. 4.10-D shows an exponential decrease in the

cumulative probability of failure. This is a direct consequence of the decrease in uncertainty with regard to time-dependent variables, which play a much more dominant role in the remaining uncertainty compared with the uncertainty present during the design stage. Since unfavourable variable loads are less likely to occur during a shorter period of time, then where it has a successful service history the remaining cumulative probability of failure of a quay wall will decrease accordingly.

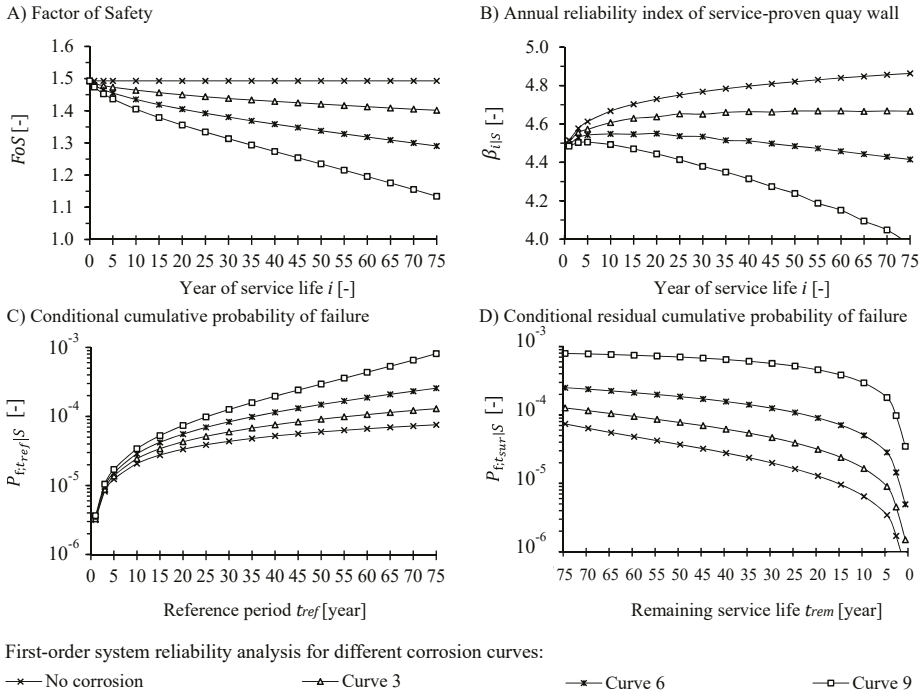


Fig. 4.10. Remaining factor of safety (A), development of annual reliability index (B), development of cumulative probability of failure (C) and remaining cumulative probability of failure (D) for $Z_{yield,tandside}$ of a service-proven quay wall in the permanent immersion zone.

4.4.3 SENSITIVITY ANALYSIS

This sensitivity analysis aims to reveal the impact of the variation coefficient of important random variables – such as the angle of internal friction φ (Fig. 4.11-A), the surcharge loads Q_{tz} (Fig. 4.11-B), the yield strength f_y (Fig. 4.11-C) and corrosion Δt_{eq} (Fig. 4.11-D) – on the conditional annual reliability index. In general, small variations in strength properties of soil have a higher impact on the annual reliability index than small variations in loads, yield strength and corrosion-induced degradation. Since the curves found overlap, Fig. 4.11-D illustrates that the variation coefficient of corrosion has almost no influence on the outcomes.

This can be explained by a fairly low sensitivity factor, e.g. approximately 0.05 for Δt_{eq} (see [Appendix C.2](#)). Furthermore, it was found that replacing the truncated normal with a normal distribution function had negligible effect on the outcome. The reader is referred to [Appendix C.2](#) for the comparison with and without truncated distribution function.

The variation coefficient of the soils' internal friction angle was directly applied to its expected value in order to determine the standard deviation, while the characteristic value for the live load was considered to be invariant, representing a return period of 50 years.

In addition, [Fig. 4.11-A](#) and [Fig. 4.11-B](#) show that the annual reliability index will become practically constant if Z_{yield} is dominated by uncertainty in time-dependent variables. By contrast, when time-independent random variables are dominant, the annual reliability index will increase during the early years of service. Furthermore, [Fig. 4.11-B](#) shows that a relatively small coefficient of variation for live loads only leads to a lower annual reliability index during the early service period. This is because the uncertainty in the live load Q_{tz} does not significantly influence the annual reliability indices – or, in other words, because the time-independent variables are dominant. Nevertheless, all the curves show higher annual reliability indices for lower variation coefficients of random variables, which is the direct result of a general decrease in the amount of uncertainty present in the reliability problem.

In general, the variation coefficient of random variables will determine the degree to which the reliability problem is time-variant, and hence whether the failure rate in the first or the final year of a reference period will prevail. This is discussed further in the next section.

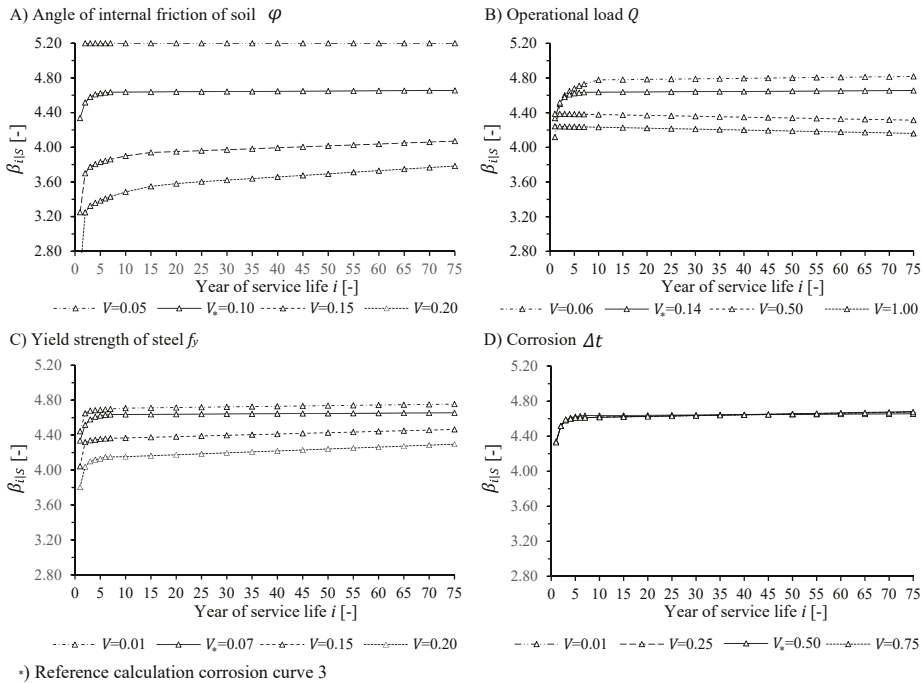


Fig. 4.11. Influence of variation coefficient of the soils' friction angle (A), surcharge load (B), yield strength (C) and corrosion (D) on the annual reliability index of a service-proven quay wall subject corrosion curve 3 in the permanent immersion zone. Trendlines are based on a crude Monte Carlo analysis.

4.5 DISCUSSION

4.5.1 INFLUENCE OF CORROSION ON FoS AND β OF REFERENCE QUAY WALL

Since the corrosion rate of the reference quay wall corresponds with corrosion curve 3 in the permanent immersion zone (Fig. 4.3-A), this section describes the impact of that curve on the FoS and β . Also discussed are the results obtained for non-deteriorated, service-proven quay walls, in order to be able to better interpret the influence of wall-thickness loss on the reliability of a quay wall.

When an uncorroded quay wall has shown the ability to function during a certain reference period, our confidence in its actual reliability level will increase. This is because it will be less likely that the strength properties of soil or steel, which show high sensitivity factors (Appendix C.1), are unfavourable. For quay walls subject to corrosion, this favourable

effect will also be present. However, the quay wall's reliability level will also be negatively influenced by corrosion-induced degradation.

The annual failure rate of a service-proven quay wall subject to corrosion curve 3 (Fig. 4.9) still shows a slightly downward trend after 75 years of successful service history. Successful service seems to reduce the remaining time-independent uncertainty. Consequently, it is unlikely that the end of the service life of this quay wall will be reached due to corrosion in the first 75 years. In this regard, the presence of the normal force induced by the vertical component of the anchor force plays a crucial role. It ensures that the stresses on the landside prevail over those on the waterside (Fig. 4.8). For quay walls without inclined anchors, it is highly likely that stresses on the waterside rather than the landside will determine the end of their service life. Furthermore, the annual reliability index (Fig. 4.10-B) of service-proven quay walls exposed to high corrosion rates, as in corrosion curves 6 and 9, will therefore continue to decrease.

4.5.2 INFLUENCE OF REMAINING SERVICE LIFE ON PROBABILITY OF FAILURE OF SERVICE-PROVEN QUAY WALLS

The annual failure rate found in this chapter generally shows a downward trend in the early years of service (Fig. 4.8-B). However, the further evolution of the failure rates depends on the rate of corrosion and the number of years survived. When assessing quay walls, therefore, either the first or the last year of the service life will prevail, for low and high corrosion rates respectively. The reference period of new quay walls is presently based on a design lifetime of 50 years, which is quite arbitrary. Changing this reference period will directly affect the cumulative probability of failure (Fig. 4.10-C), since the presence of higher loads and a higher degree of deterioration are more likely during a longer period of time. Furthermore, the uncertainty of time-independent variables such as soil or yield strength is not significantly affected by changing the reference period. In fact, the presence of fairly unfavourable time-independent variables becomes increasingly unlikely as a quay wall ages successfully.

When assessing a service-proven quay wall, it is possible to predict the end of its lifetime and the associated remaining service life. But this requires adjustment of the reference period. If we assume that a quay will be replaced after 75 years of service, for instance, we can determine the remaining cumulative probability of failure given its successful past performance (Fig. 4.8-D). Since reliability is always related to a certain reference period, and the remaining service lives of different existing quay walls will probably differ, deriving reliability targets for the remaining lifetime does not seem very efficient. In general, it appears more practical to evaluate reliability on an annual basis rather than for longer time periods, since the latter will introduce an iterative procedure to determine the remaining service life.

4.5.3 EVALUATION OF ALLOWABLE STRESS-BASED METHOD TO ASSESS CORRODED COMBI-WALLS

Before discussing the allowable stress-based method to assess corrosion-induced degradation of combi-walls (Section 4.2), it is worth noting that neither yielding nor local buckling failures have been identified in practice. This indicates that the method is rather conservative, a finding also supported by the decrease found in the annual failure rate (Fig. 4.9). Moreover, the allowable stress-based method presently features the assessment of single structural members, e.g. one tube in a combi-wall system. However, a combi-wall system generally has a some additional capacity to redistribute internal forces. As a result, it is almost impossible that only a single combi-tube will show yielding or local buckling. This redistribution has not yet been taken into account. Furthermore, despite the allowable stress-based method already distinguishing different corrosion zones across the height of the combi-wall (Fig. 4.3-A), it neglects spatial variation along the quay wall. It is therefore highly recommended that horizontal correlation lengths in the different corrosion zones be studied, because it seems unlikely that multiple tubes will show the same amount of pitting corrosion at the exact same position. Hence, it is expected that the actual reliability level of combi-walls is significantly higher.

Example

The differences between the allowable stress-based method and the probabilistic approach can best be discussed by presenting an example. However, our reference quay wall is subject to the relatively low corrosion rates of curve 3 and as a result its likely service lifetime is well beyond 75 years. Consequently, the end of the lifetime of the reference quay wall was predicted using the results from the more conservative corrosion curve 9, predominantly to demonstrate the differences and also to show the possible impact of corrosion on the stresses on the waterside. Predictions on the basis of the allowable stress approach show that the stresses on the waterside after approximately 50 years become higher than those on the landside, whereas following the probabilistic method shows that this is already likely after approximately 40 years (Fig. 4.12). Furthermore, the minimum required FoS is reached after 49 years. If we assume that the reference quay wall corresponds with RC1 of EN 1990 (2011), the minimum annual target reliability index is exceeded after 72 years (Table 4.4). In other words, using the probabilistic approach results in an increase of the remaining service life of approximately 35%. In addition, the residual cumulative probability of failure for the last three years is 2.85, which is higher than the minimum target reliability indices presented in literature (NEN-EN 1997, 2004; NEN-EN 8700, 2011; Roubos et al., 2018). This example illustrates the potential benefits of performing reliability-based assessments to safely extend the lifetime of service-proven quay walls. However, it should be noted that accidental load combinations, such as earthquake-induced ground motion and extreme

The effect of corrosion on the reliability of service-proven quay walls

tidal waterhead differences, were not taken into consideration in the present investigation (Section 1.5). Where loading events are infrequent, satisfactory past performance may not be a good indicator (Melchers & Beck, 2018).

Table 4.4. Exceeding of safety limits and annual reliability targets on the basis of the allowable stress and reliability-based assessments, respectively.

	Allowable stress-based assessment				Reliability-based assessment				
	FoS	$Z_{yield,landside}$	$Z_{yield,waterside}$	$Z_{buckling}$	β	$Z_{yield,landside}$	$Z_{yield,waterside}$	$Z_{buckling}$	
New design	< 1.5	Year 1	Year 36	Year 1	New design	< 4.2	Year 50	Year 43	Year 38
Intensive monitoring	< 1.3	Year 35	Year 47	Year 29	Repair works	< 3.8	> Year 75	Year 56	Year 66
Disapproval	< 1.2	Year 61	Year 53	Year 49	Disapproval	< 3.2	> Year 75	Year 72	> Year 75

¹⁾ NEN-EN 1990 (2011) and NEN-EN 1997 (2004).

²⁾ Roubos et al. (2018).

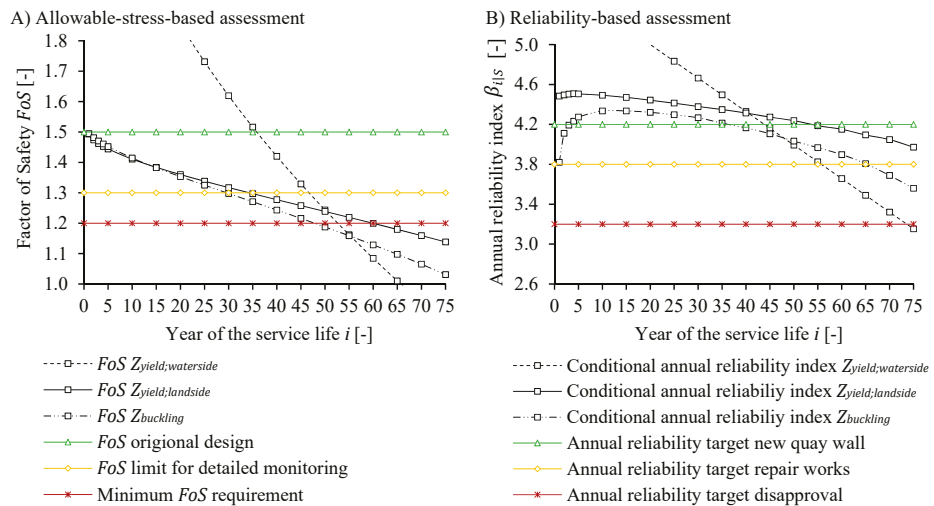


Fig. 4.12. Comparison of allowable stress-based (A) and reliability-based (B) assessments of a service-proven quay wall subject to corrosion curve 9 in the permanent immersion zone.

4.6 CONCLUSION AND RECOMMENDATIONS

The results of this chapter show the effect of corrosion-induced degradation on the reliability of service-proven combi-walls. Its most important findings are as follows:

- Annual failure rates and the associated reliability indices of service-proven quay walls are largely time-dependent. The failure rate of non-deteriorating quay walls decreases over time. For quay walls with successful service histories and subject to low corrosion rates, the highest annual reliability indices were typically observed in the first year of the service life, while for higher corrosion rates the final year is critical.
- The allowable stress-based method of assessing corrosion-induced degradation of combi-walls is conservative rather than optimistic in the case of service-proven quay walls.
- The ratio between the factor of safety and the reliability index changes over time and depends on the corrosion rate and the number of years survived. Hence, no generally applicable relationship was found.
- The reliability assessments performed using the calibrated Blum model show results similar to those from finite element-based reliability assessments.
- The variation coefficient of the angle of internal friction significantly influences the evolution of the annual failure rate over time.

Successful service, i.e. the survival of service loads, enables us to reduce time-independent uncertainties (Hall, 1988) such as uncertainty in soil strength of quay walls, leading to an increase in reliability. However, this positive effect will be less pronounced for quay walls exposed to rare extreme events such as earthquakes or accidental loading (Section 1.5). Hence, it is highly recommended that further investigation be undertaken into the influence of extreme events and accidental load combinations.

A reference period of one year enables us to evaluate quay-wall reliability, while taking into account the effects of past performance and degradation. Moreover, within a one-year reference period, the effects of past performance and degradation can be taken into account in an appropriate manner. These findings can play an important role in the evaluation of the reliability of an existing quay wall, since then its remaining service life and the associated reference period are generally unknown a priori. Hence, using annual target reliability indices is preferred.

Based on the findings of this chapter, the early application of a test load close to the characteristic/design load applied directly after completion of the structure can be an effective strategy to increase its reliability during its remaining service life (Hall, 1988; Melchers & Beck, 2018). The application of such a test load in a pre-posterior analysis is

therefore recommended. And if the outcomes are favourable in cost-benefit terms, so is the development of full-scale test protocols for new and service-proven quay walls.

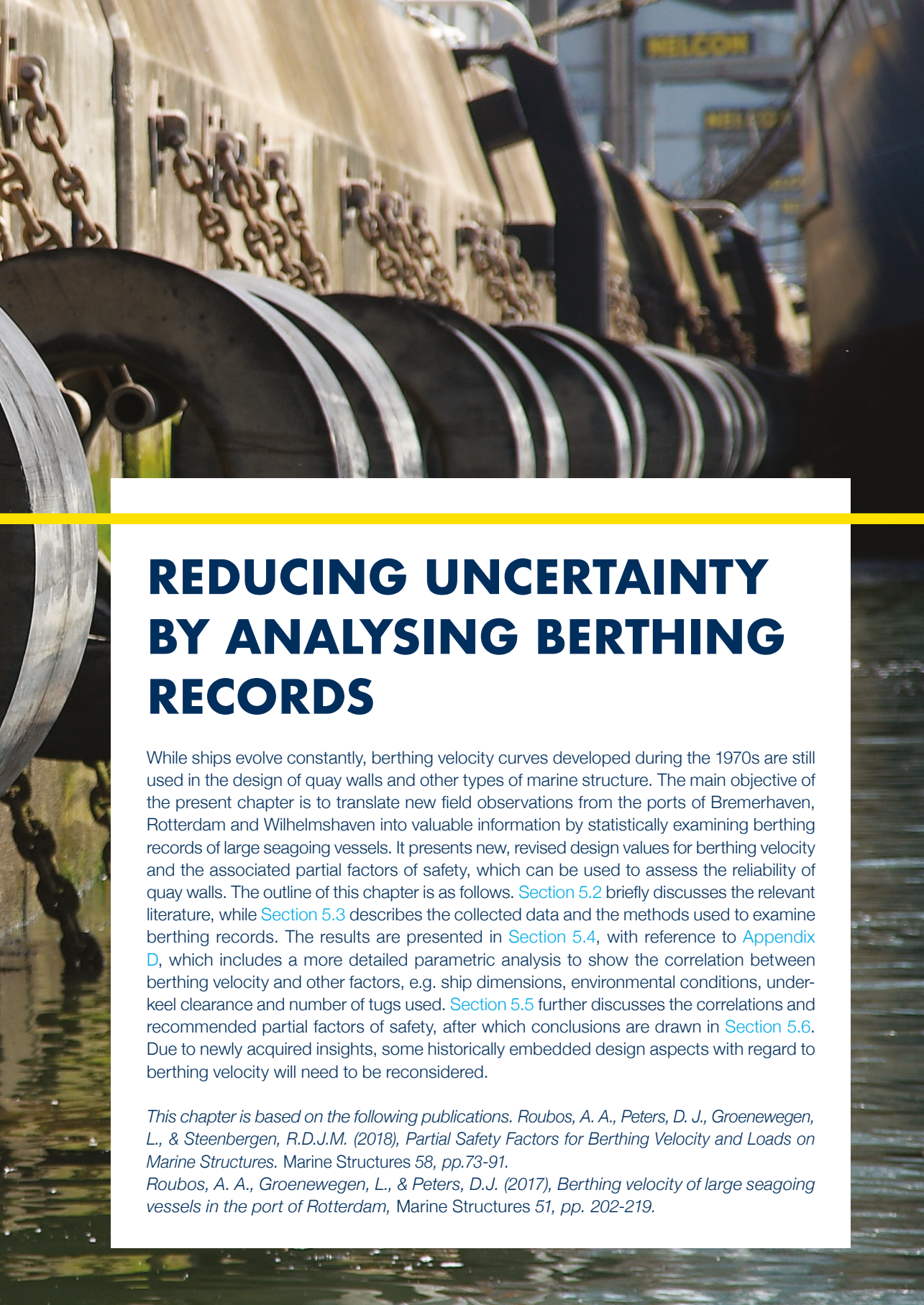
Furthermore, this chapter has shown that a calibrated Blum-based crude Monte Carlo analysis gives quite similar results to the finite-element-based *FORM* approximation. It would therefore be very interesting to compare these results with those obtained from other reliability methods, e.g. using response surfaces (a.k.a. surrogate models such as kriging (Sudret et al., 2017)) or directional adaptive response surface sampling (DARS) (Waarts, 2000), in order to verify the applicability of such methods for finite element-based and time-dependent reliability assessments.

In addition, further study of the development of pitting corrosion over time (position and propagation) (Kolios et al., 2014; Melchers & Jeffrey, 2008) is recommended, as is work to clarify how the combination of uniform and pitting corrosion can be taken into account when assessing combi-walls, e.g. by applying random field theory. Moreover, we suspect that truncating the probability distribution of corrosion does not always have a negligible effect on the outcome. This effect is probably much greater for sheet pile walls than for combi-walls, and hence we do not recommend truncation of the corrosion uncertainty as general practice.

Finally, the results of this chapter show that time-independent uncertainty decreases during the early years of a quay wall's service life. This finding can play a crucial role in the assessment of existing quay walls, and presumably in that of all other service-proven geotechnical structures. It is therefore highly recommended that practical guidelines be further developed, e.g. by updating the initial estimates of time-dependent random variables, in order to safely extend the service life of existing quay walls and other structures with similar features.

A large, bold yellow number '5' is centered on the left side of the image. The background is a photograph of a large, dark metal ring, possibly a component of a ship's anchor or a large pulley, with several heavy metal chains attached to it. The ring is suspended and its surface is highly reflective, showing distorted reflections of the surrounding environment, including what appears to be a body of water and a concrete structure. A thin yellow horizontal line is positioned below the number, extending across the width of the image.

5



REDUCING UNCERTAINTY BY ANALYSING BERTHING RECORDS

While ships evolve constantly, berthing velocity curves developed during the 1970s are still used in the design of quay walls and other types of marine structure. The main objective of the present chapter is to translate new field observations from the ports of Bremerhaven, Rotterdam and Wilhelmshaven into valuable information by statistically examining berthing records of large seagoing vessels. It presents new, revised design values for berthing velocity and the associated partial factors of safety, which can be used to assess the reliability of quay walls. The outline of this chapter is as follows. [Section 5.2](#) briefly discusses the relevant literature, while [Section 5.3](#) describes the collected data and the methods used to examine berthing records. The results are presented in [Section 5.4](#), with reference to [Appendix D](#), which includes a more detailed parametric analysis to show the correlation between berthing velocity and other factors, e.g. ship dimensions, environmental conditions, under-keel clearance and number of tugs used. [Section 5.5](#) further discusses the correlations and recommended partial factors of safety, after which conclusions are drawn in [Section 5.6](#). Due to newly acquired insights, some historically embedded design aspects with regard to berthing velocity will need to be reconsidered.

This chapter is based on the following publications. Roubos, A. A., Peters, D. J., Groenewegen, L., & Steenbergen, R.D.J.M. (2018), Partial Safety Factors for Berthing Velocity and Loads on Marine Structures. Marine Structures 58, pp.73-91.

Roubos, A. A., Groenewegen, L., & Peters, D.J. (2017), Berthing velocity of large seagoing vessels in the port of Rotterdam, Marine Structures 51, pp. 202-219.

ABSTRACT

Whilst design methods for quay walls have evolved into load and resistance factor design, existing partial factors of safety related to berthing velocity and loads have still not been verified and validated by measurement campaigns. In this chapter, field observations of modern seagoing vessels berthing at Bremerhaven, Rotterdam and Wilhelmshaven are used to evaluate partial factors of safety for berthing energy and berthing impact loads. Various types of vessel and navigation conditions are examined statistically. The results show that characteristic values of berthing velocity with a return period of 50 years are in line with design recommendations in literature. Design values of berthing velocity are sensitive to the number of berthing operations during the lifetime of a quay wall. Typical partial factors of safety for sheltered and exposed navigation conditions are derived by extrapolating distribution fits and applying extreme value theory. The probability of an uncontrolled berthing event is higher for exposed navigation conditions (strong tidal currents). In these circumstances, higher partial factors of safety for berthing velocity should be considered in the design of quay walls. When berthing aid systems are used, the probability of extreme berthing velocities is lower, resulting in lower partial factors of safety. The key findings of this chapter could be beneficial for the structural design of new quay walls and other types of marine structure and for the lifetime extension of existing ones.

5.1 INTRODUCTION

Numerous marine structures, such as quay walls, jetties and flexible dolphins, have been constructed all over the world to accommodate ships' berthing, mooring and loading operations. During the service life of a quay wall, its functional requirements may change. These changes often result in uncertainty regarding actual berthing energy and structural integrity, especially if the size of vessels using existing berthing facilities increases. Existing design guidance for assessing berthing energy, such as PIANC (2002), British Standards (BS 6349-4, 2016), the German EAU 2012 (Grabe, 2012) and the Spanish ROM (ROM 02-90, 1990), suggest applying an overall safety margin. But these guidelines do not include partial factor analyses of individual berthing parameters and their individual contributions to the uncertainty in berthing energy. It is often unclear how resultant fender forces derived from such analyses should be applied in accordance with the safety philosophy of Eurocode standards (NEN-EN 1990, 2011), which predominantly recommend applying a partial factor of safety to characteristic values of loads and resistance.

Metzger et al. (2014) state that load demands on berthing structures are not well understood due to a lack of information about berthing parameters. Hence, there is a strong need to determine design values of berthing parameters and partial factors of safety by using field observations. Although design guidelines recommend collecting sophisticated berthing records, little data of this kind is available. Ueda et al. (2010) have shown that berthing velocity is the most important design variable in defining berthing energy. The port authorities of Bremerhaven (Hein, 2014) and Rotterdam ([Appendix D.1](#)) therefore decided to start a measurement campaign for berthing velocity in order to evaluate and validate the performance of existing quay walls and the design guidance of EAU and PIANC. They wanted to know whether the berthing velocity curves of EAU and PIANC, as presented in [Fig. 5.1](#), are still representative of and safe for modern vessels.

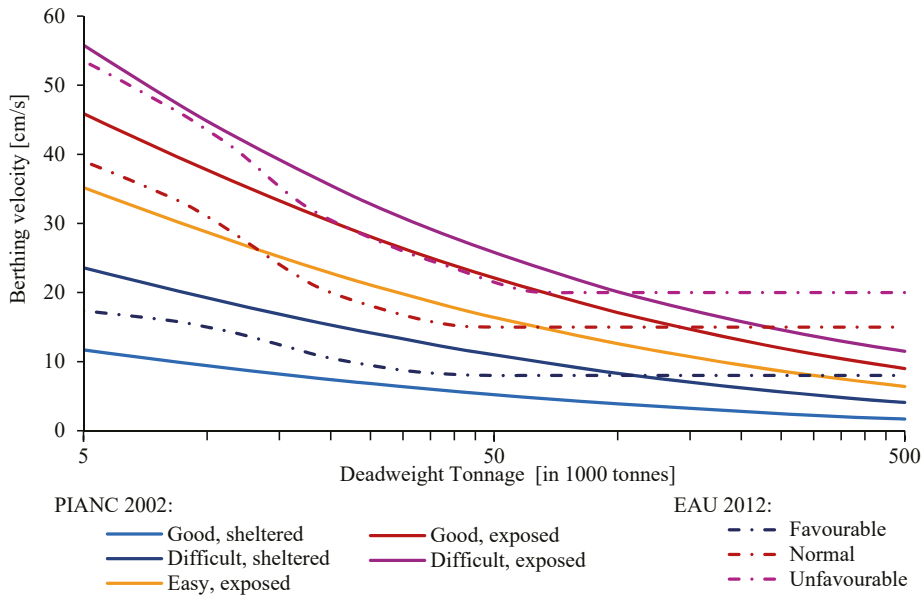


Fig. 5.1. Berthing velocity curves of PIANC 2002 (Brolsma curves) and EAU 2012 as a function of navigation conditions and vessel size.

The statistical meaning of berthing velocity curves is often unknown to or misinterpreted by designers and code writers of marine structures (Beckett Rankine, 2010). Where berthing records are available, existing design guidelines do not provide explicit recommendations with regard to the statistical examination of berthing velocities. For the most part, therefore, it is not clear how to use field observations.

This chapter aims to provide guidance to code developers and engineers on the use of field observations and the derivation of partial factors of safety for berthing velocity and loads on quay walls. The main focus is on deriving characteristic values and associated partial factors of safety for berthing velocity, because this is the dominant variable in assessing berthing impact (Ueda et al., 2010) on quay walls. Recently recorded field observations of berthing velocities in the ports of Bremerhaven, Rotterdam and Wilhelmshaven are used to determine theoretical design berthing velocities and corresponding partial factors of safety in accordance with the Eurocode standard (NEN-EN 1990, 2011). The characteristic and design berthing velocities found are compared with the design guidance presently in use. Furthermore, partial factors of safety have been derived using large datasets for sheltered and exposed navigation conditions. The results of this chapter show that further research could introduce new business and other opportunities by, for example, allowing larger vessels to berth at existing quay walls and/or extending the service life of these marine structures.

5.2 BERTHING VELOCITY IN LITERATURE

5.2.1 GENERAL PRINCIPLES OF BERTHING ENERGY AND IMPACT

The objective of this section is to elucidate the general principles of and methods used to account for berthing energy and the resulting berthing impact loads in structural design. Berthing energy is generally calculated on the basis of a large number of parameters, in line with the following equation:

$$E_{kin} = 1/2 Mv^2 C_m C_s C_c C_E \quad (73)$$

Where:

E_{kin}	Kinetic energy [kNm]
M	Mass of vessel/water displacement [tonnes]
v	Total translation velocity of centre of mass at time of first contact (includes component parallel and perpendicular to berthing line) [m/s]
C_m	Virtual mass factor [-]
C_s	Ship flexibility factor [-]
C_c	Waterfront structure attenuation factor [-]
C_E	Eccentricity factor [-]

Eq. (73) is embedded in most design guidelines, or they refer to PIANC (2002). PIANC berthing velocity curves are widely used by the industry to determine 'normal' berthing energy. Given a normal berthing energy, an abnormal berthing impact factor C_{ab} is applied to derive an abnormal berthing energy. In fact, C_{ab} is an overall safety margin, but since the introduction of the Eurocodes this has been used as a partial factor of safety for variable berthing impact loads together with design values of resistance parameters.

$$E_{abnormal} = C_{ab} E_{normal} \quad (74)$$

Where:

$E_{abnormal}$	Abnormal berthing energy [kNm]
C_{ab}	Abnormal berthing factor [-]
E_{normal}	Normal berthing energy [kNm]

The berthing impact load F to which a quay wall is subjected is a function of the kinetic energy absorbed by the berthing system and of its deformation characteristics δ . Given a

certain berthing velocity, the resulting berthing impact load largely depends on the stiffness of the structure and the soil conditions (ROM 02-90, 1990).

$$E_{kin} = \int_0^{\delta_{max}} F(\delta) d\delta \quad (75)$$

The deformation characteristics of a berthing system can be linear or non-linear. Eq. (79) shows that a berthing impact load in a linear system (e.g. flexible dolphins without fenders) is proportional to berthing velocity. The effect of linear and non-linear behaviour is further discussed in Section 5.5.1. In the case of linear-elastic behaviour, a berthing impact load can generally be derived by applying the following equations:

$$E_{kin} = \frac{1}{2} F \delta \quad (76)$$

$$\delta = \frac{F}{k} \quad (77)$$

$$F = \sqrt{2E_{kin}k} \quad (78)$$

$$F = v \sqrt{M C_m C_s C_c C_e k} \quad (79)$$

Where:

F	Berthing impact load [kN]
δ	Deflection of berthing structure [m]
k	Stiffness of berthing structure and soil [kN/m]

Eurocode standards do not recommend using an overall safety margin, but advise applying partial factors of safety to characteristic design variables. Partial factors of safety are predominantly related to both loads and resistance. Within the framework of this chapter, the load component is of particular interest and partial load factors define the ratio between the design value for load S_d and its characteristic value S_k .

$$S_d = \gamma_Q S_k \quad (80)$$

Where:

S_d	Design value for variable load [kN]
S_k	Characteristic value for variable load [kN]
γ_Q	Partial factor of safety for variable load [-]

It should be noted that the partial factor for variable loads γ_Q already takes account of the possibility of unfavourable deviations as well as uncertainties in modelling the effects of loads.

5.2.2 RETURN PERIODS OF BERTHING VELOCITY CURVES

The berthing velocity curves presented in Fig. 5.1 are frequently used to determine berthing impact loads in the design of quay walls. In this section, return periods of berthing velocity curves in literature are summarised in order to provide an insight into the reliability of berthing impact loads used in practice.

The German recommendations for waterfront structures, EAU 2012 (Grabe, 2012), do not include information on the reliability of velocity curves but instead refer to ROM 0.2-90 (1990). The berthing velocity tables of the Spanish ROM appear to be based on a return period of 50 years. The general recommendation of the Japanese OCDI (2009) and Eurocode NEN-EN 1990 (2011) do not cover this topic. Brolsma's original curves have been reproduced and slightly modified over time, and published in PIANC (2002) and BS 6349-4 (2014). The authors noted that Brolsma's berthing velocity curves are often not applied correctly. In particular, the term 'mean design', included in PIANC 2002, is misinterpreted. This value is not equal to the mean berthing velocity of a vessel. Scrutiny of the original Brolsma paper reveals that the measurements were extrapolated. The associated berthing velocity curves were derived for a berthing frequency of 3000 vessels during a reference period of 30 years. This is equal to 100 berthings per year, assuming two very large crude carrier (VLCC) vessels per week.

5

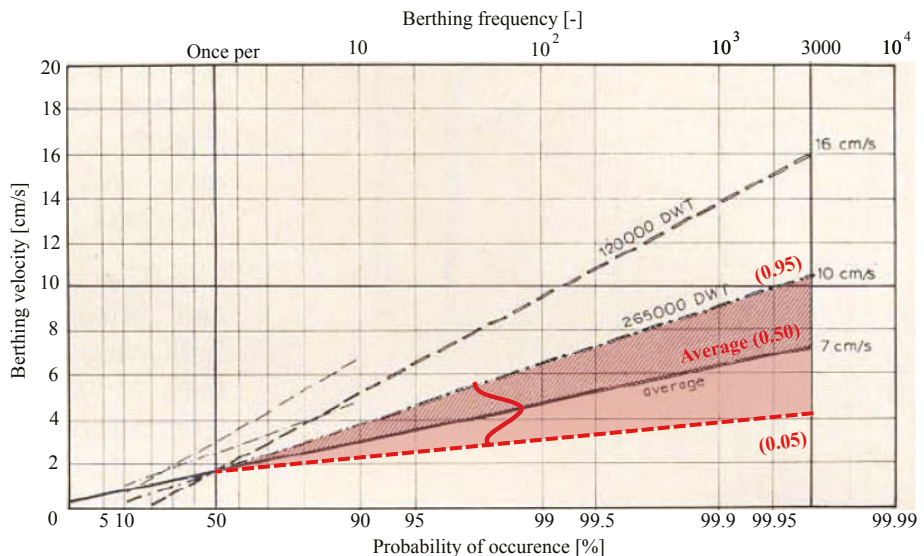


Fig. 5.2. Extrapolation of 150 measurements derived by Brolsma et al. (1977).

Fig. 5.2 was included in the original paper by Brolsma et al. (1997) and shows an extrapolation of berthing velocities up to 3000 berthings. Brolsma showed that the average value (solid line representing the 0.50 quantile in Fig. 5.2) of a VLCC tanker (265,000 DWT)

in a reference period of 30 years was approximately 7 cm/s. The berthing velocities with a 5% probability of exceedance in a reference period of 30 years (dashed lines representing the 0.95 quantile in Fig. 5.2) were approximately 10 cm/s and 16 cm/s for VLCC tankers and Aframax tankers (120,000 DWT), respectively. A reference period close to 30 years is in line with industry practice values for the design lifetime of a quay wall in the 1970s. An overview of return periods of berthing velocity curves in relevant literature is given in Table 5.1.

Table 5.1. Overview of return periods of berthing velocity curves in literature.

SI	PIANC (2002)	BS 6349-4 (2014)	EAU (2012)	ROM (1990)	OCDI (2009)	NEN-EN 1990 (2011)	
T_r	year	30 ¹	30 ¹	50 ²	50	-	-

¹) Based on berthing frequency published by Broisma et al. (1997).

²) Based on ROM 0.2-90 (1990).

5.2.3 ABNORMAL BERTHING AND LOAD FACTORS

When the backgrounds of the berthing velocity curves are known, the abnormal berthing factors C_{ab} and partial factors of safety γ_Q are compared in order to gain an insight into the actual reliability of relevant literature. Given a general cargo vessel, BS 6394-4 (2014) recommends using an abnormal berthing factor equal to $C_{ab}=1.5$. For LNG, LPG and ferries, $C_{ab}=2.0$ is recommended. EAU 2012 (Grabe, 2012) recommends applying a factor of safety to characteristic berthing energy to account for exceptional berthing manoeuvres. These factors of safety correspond to the abnormal berthing factors in PIANC (2002). An overview of abnormal berthing factors in literature is given in Table 5.2.

Table 5.2. Abnormal berthing factor C_{ab} in literature.

Ship type	Size	PIANC (2002)	EAU (2012)	BS 6349-4 (2014)	ROM (1990)	OCDI (2009)	NEN-EN 1990 (2011)
Tankers	Largest-smallest	1.25-2.00	1.25-2.00 ¹	-	2.00	-	-
Bulkers	Largest-smallest	1.25-2.00	1.25-2.00 ¹	-	2.00	-	-
Container	Largest-smallest	1.50-2.00	1.50-2.00 ¹	-	2.00	-	-
General Cargo	-	1.75	1.75 ¹	1.50 ²	2.00	-	-
Roro, ferries	-	≥ 2.00	≥ 2.00 ¹	-	2.00	-	-
Tugs, workboats	-	2.00	2.00 ¹	-	2.00	-	-
LNG, LPG	-	-	-	2.00	2.00	-	-
Island berth	-	-	-	2.00	2.00	-	-

¹) Based on PIANC (2002).

²) Continuous quay handling of conventional cargo vessels.

As indicated, berthing energy is absorbed by the deflection of a marine structure and the hull of a vessel, resulting in a berthing impact load on the marine structure. BS 6349-4 (2014) therefore recommends also applying additional partial factors of safety to a resulting berthing impact load. The partial factors for normal and abnormal berthing impact loads are $\gamma_Q=1.35$ (persistent situation) and $\gamma_Q=1.2$ (transient situation), respectively.

BS 6394-1-2 (2016) considers an uncontrolled berthing procedure to be an accidental design situation, and so the consequences of failure of a fender system being overloaded (e.g. direct and indirect future losses) must be taken into consideration. According to the British Standards, typical return periods of extreme environmental events for permanent structures are 50-100 years in persistent design situations and 500-1000 years in accidental ones. The recommended design lifetimes for quay walls and fender systems are 50 and 15 years, respectively. Replacement of fenders during the lifetime of the structure is thus considered normal practice.

The German EAU 2012 distinguishes permanent, transient and accidental design situations and is consistent with Eurocode NEN-EN 1990 (2011). The partial factors of safety γ_Q of loading classes 1, 2 and 3 for unfavourable variable loads are 1.0, 1.3 and 1.5, respectively. No exceptional/accidental berthing impacts (collisions/loss of control) need to be taken into consideration. The partial factors of safety for loads related to berthing manoeuvres in the design of quay walls are in line with these values, but the partial factors in the design of flexible dolphins are all set at 1.0 in accordance with Table R218-1 of EAU 2012 (Grabe, 2012).

The Spanish ROM 0.2-90 (1990) determines berthing loads as variable dynamic impact loads and also accounts for accidental berthing impacts (mechanical failures of tugs or vessels, mooring line breakage, sudden environmental condition changes, human error, etc.). Typical return periods of accidental impact loads are 1000 years and they are classified as 'abnormal' impacts. In this case, it is recommended that a factor of safety for berthing energy of $C_{ab}=2.0$ be applied. The recommended partial factor of safety for a berthing impact load is $\gamma_Q=1.5$, which needs to be combined with other permanent and variable loads on marine structures (ROM 0.0, 2002).

The Japanese OCDI design code for marine structures considers serviceability, restorability and safety (Nagao et al., 2009). Its design philosophy emphasises minimum port performance requirements and does not prescribe reliability standards. The general recommendation is to use a return period of 50 years for the derivation of characteristic variable loads. The OCDI suggests that a variable action with an annual exceedance probability of at least 1% should be the basic performance requirement. In fact, this probability is a threshold and represents a minimum return period of 100 years. The OCDI recommends using the threshold carefully, as it is only a guide for situations in which a design working life is in accordance with design standards.

Eurocode NEN-EN 1990 (2011) does not provide specific recommendations for the design of marine structures. In the case of environmental loads, a characteristic value with a return period of 50 years is recommended. The partial factors of safety γ_Q of reliability classes RC1, RC2 and RC3 are 1.35, 1.5 and 1.65 for unfavourable variable loads, respectively. An overview of return periods T_R and partial factors of safety γ_Q in literature is given in Table 5.3.

Table 5.3. Return periods and partial factors of variable and berthing impact loads in literature.

	SI	PIANC	BS 6394-1-2	EAU	ROM	OCDI	EN 1990
		(2002)	(2015)	(2012)	(1990)	(2009)	(2011)
Variable loads (in general)¹							
T_R SLS	Year	-	50-100	50	50	50	50
T_R ALS	Year	-	500-1000	-	1000	-	- ²
γ_Q ULS	-	-	1.35-1.50	1.3-1.5	1.50	-	1.35/1.5/1.65
Berthing impact							
γ_Q (persistent)	-	-	1.35	1.00 ³	-	-	-
γ_Q (transient)	-	-	1.20	1.00 ³	-	-	-

¹) Design codes do not uniformly describe SLS, ULS and ALS and are not completely consistent.

²) In the case of earthquakes, characteristic values with return periods in the range of 475-2475 years are recommended.

³) In the case of flexible dolphins.

5.3 METHODS TO EXAMINE BERTHING VELOCITY

5.3.1 DATA COLLECTION

Approximately 1393 records of berthing operations were collected in Germany and about 555 Netherlands (Appendix D.1). The field observations regarding these berthing operations are further described by Hein (2014) and in Appendix D.1. Various types of vessel, berth and navigation conditions were represented in the datasets. All berthing records were collected in well-organised port environments, namely Bremerhaven (1235), Rotterdam (555) and Wilhelmshaven (158). An overview of the collected data is given in Table 5.4. The berths in Bremerhaven were classified as exposed and berthing operations seemed to be influenced by strong tidal currents; the tidal range there is typically about 3.8 m, with tidal currents of 2.5-3.5 knots. All other berths were classified as sheltered.

Table 5.4. Overview of field observations of berthing velocity.

Ship type [-]	n [-]	v_{μ} [cm/s]	v_{\max} [cm/s]	Berth type [-]	Berthing aids [-]	Wind [-]	Waves [-]	Current [-]
Container	□ 177	4.0	10	Closed quay	None	High	Sheltered	Low
Tanker	○ 329	4.3	12	Jetty/dolphin	PPU/docking system	High	Sheltered	Low
Bulker	◇ 144	4.4	13	Closed quay	Portable pilot units	High	Sheltered	Low
Container	□ 1235	6.6	26	Closed quay	None	High	Exposed	High

The vessels were differentiated by ship type into container vessels, tankers and bulkers. They were then further differentiated into specific vessel classes in order to illustrate their differences or similarities. The classification was based largely on the international Lloyds database of vessels. All container vessels berthed at closed quay walls equipped with either hard buckling or soft cylindrical fender systems. Bulkers berthed at closed quay walls equipped with rigid timber beams. The tanker berths were equipped with flexible breasting dolphins fitted with buckling fender systems. Studies by Yamase et al. (2014) and [Appendix D.1](#) have shown that berthing velocities are not influenced by the type of marine structure being berthed or the type of fendering used.

5.3.2 PARTIAL FACTORS OF SAFETY

A probabilistic study by Ueda et al. (2010) showed that the contribution of berthing velocity to the uncertainty in kinetic berthing energy was approximately 85%, indicating that factors of safety should be applied predominantly to berthing velocity. When defining kinetic berthing energy, berthing velocity is assumed to be the only stochastic variable in [Eq. \(73\)](#). The partial factors of safety derived in the present chapter were therefore applied to a characteristic value of berthing velocity. The partial factor γ_v was defined as the ratio between a design berthing velocity v_d and a characteristic berthing velocity v_k . The following equation was then used to determine partial factors of safety for berthing velocity:

$$\gamma_v = \frac{v_d}{v_k} \tag{81}$$

Where:

- γ_v Partial factor of safety for berthing velocity [-]
- v_d Design value of berthing velocity [cm/s]
- v_k Characteristic value of berthing velocity [cm/s]

Characteristic and design berthing velocities were considered to be extreme events and were derived by extrapolating distribution fits and applying extreme value theory. For this chapter, characteristic berthing velocities had a return period of 50 years, representing a time-variant berthing velocity with a 2% probability of being exceeded during a reference period of one year. It should be noted that this is not equal to a 2% probability that a single berthing operation will exceed the characteristic berthing velocity. This insight is important, since a quay wall accommodates multiple vessels per year. It is further emphasised that a return period is not the same as a reference period. The probability that an event with a return period of 50 years will occur in a reference period of one year is 2%, and in a reference period of 50 years it is 63.5%.

A design value for berthing velocity is typically selected such that a quay wall has sufficient reliability (or a sufficiently low probability of failure). Assuming a normal distribution, this is written as follows:

$$P_f = \Phi(-\beta_d) \text{ or } \beta_d = \Phi^{-1}(P_f) \quad (82)$$

Where:

P_f	Probability of failure of an event [-]
β_d	Target reliability index [-]
Φ^{-1}	Inverse of standard normal distribution function [-]

Target reliability indices β_d are generally prescribed in design codes, such as the Eurocode standards (NEN-EN 1990, 2011). The derivation of design berthing velocities with a probability of exceeding a certain threshold is further explained in [Section 5.3.4](#), in accordance with the following principle:

$$P(v > v_d) = \Phi(-\alpha_s \beta_d) \quad (83)$$

Where:

v	Berthing velocity [cm/s]
v_d	Design value of berthing velocity [cm/s]
α_s	Sensitivity factor for load/solicitation [-]. When the load is a dominant variable this factor equals -0.7. For non-dominant loads this factor equals -0.28 (ISO 2394, 2015).

When establishing extreme berthing velocities from field observations, the size of the datasets was of significant importance, especially as the objective was to derive a set of generalised partial factors of safety. Partial factors are preferably derived using large

datasets, because extreme berthing velocities are influenced by the fit of the low probability tail of an extreme value distribution to field observations. In the present chapter, three large datasets were developed, namely ‘All tankers’, ‘All sheltered’ and ‘All exposed’. ‘All tankers’ is a subset of ‘All sheltered’ and represents the use of berthing aid systems, such as portable pilot units (PPU) and fixed shore-based laser docking systems. The use of berthing aid systems should reduce the probability of extreme/uncontrolled berthing events. Moreover, the available data was subdivided into ‘sheltered’ and ‘exposed’ navigation conditions. An overview of the datasets is given in [Table 5.5](#).

Table 5.5. Large datasets.

Large datasets [-]	n [-]	v_{μ} [cm/s]	v_{max} [cm/s]	Berth type [-]	Berthing aids [-]	Wind [-]	Waves [-]	Current [-]
All tankers ◦ ¹	392	4.6	12	Open	PPU/docking system	High	Sheltered	Low
All sheltered Δ	713	4.4	13	Mixture	Mixture	High	Sheltered	Low
All exposed □	1235	7.1	26	Closed	None	High	Exposed	High
All data	1948	6.6	26	Mixture	Mixture	High	Mixture	Mixture

¹) Dataset is a subset of ‘All sheltered’.

5.3.3 DATA ANALYSIS

This section describes the methods used to derive berthing velocities with low probabilities of exceedance in order to determine partial factors of safety. In [Appendix D.1](#) and in the OCDI (2009), field observations of single berthing velocities are examined statistically. Both studies show that a distribution fit of the low-probability tail is closer to a Weibull distribution $F(x;\lambda,k)$ than to a normal or lognormal distribution. For this chapter, the collected berthing velocities were therefore described using a Weibull distribution fit on the basis of maximum likelihood estimation. Typical distribution fits for all ‘sheltered’ and ‘exposed’ data are illustrated in [Fig. 5.3](#) and [Fig. 5.4](#).

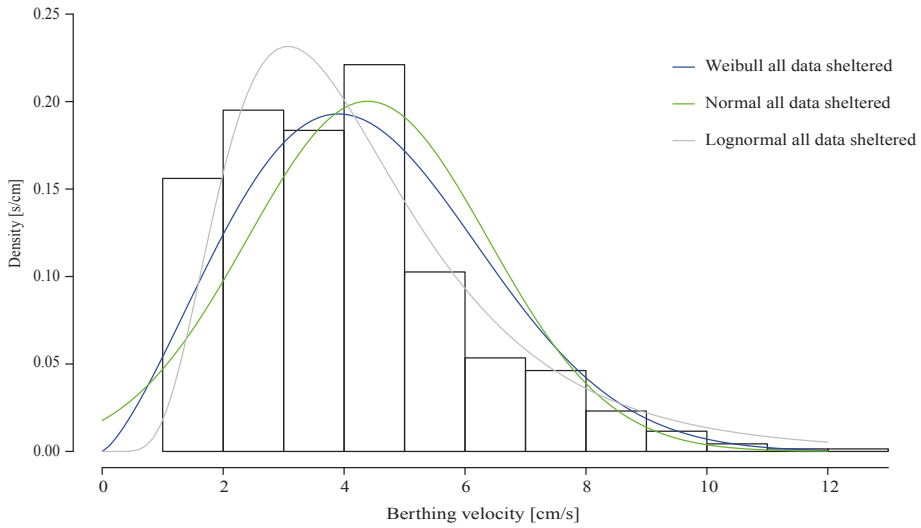


Fig. 5.3. Histogram and probability density functions of all ‘sheltered’ berthing records (n=713).

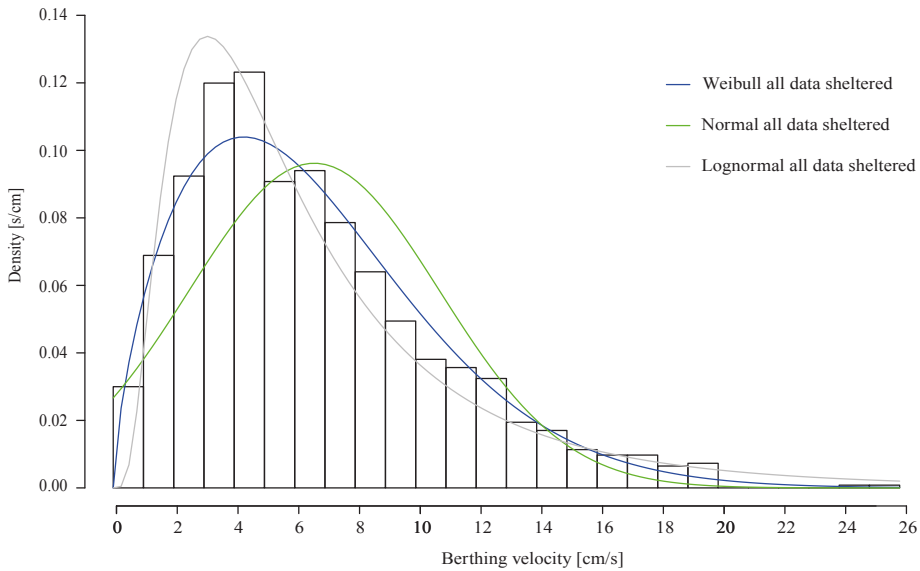


Fig. 5.4. Histogram and density functions of all ‘exposed’ berthing records (n=1235).

Characteristic and design berthing velocities were derived on the basis of extreme value theory, using the following methods.

- A direct assessment performed by extrapolating the Weibull distribution fit to the original dataset.
- An indirect assessment based on the use of normal distributions only, in line with the method often used for load extrapolations as per the Eurocode by applying a two-step extreme value analysis of annual and lifetime maxima.

The first method was based on the extrapolation of a distribution fit to the original data. Assuming that the number of berthings per year and the required target reliability during a certain reference period are known, characteristic v_k and design berthing velocities v_d were established by extrapolating the Weibull distribution fit. The probability that a berthing velocity X was higher than a particular berthing velocity x was calculated by generating corresponding berthing velocities directly from the Weibull distribution function $P(X > x) = 1 - F(x)$:

$$F(x; \lambda, k) = 1 - \exp\left(-\left(\frac{x}{\lambda}\right)^k\right) \quad (84)$$

$$\left(\frac{x}{\lambda}\right)^k = -\ln(1 - F_x(x)) = -\ln(P(X > x)) = \ln\left(\frac{1}{P(X > x)}\right) \quad (85)$$

$$\left(\frac{x}{\lambda}\right) = \left(\ln\left(\frac{1}{P(X > x)}\right)\right)^{\frac{1}{k}} \quad (86)$$

$$x = \lambda \left(\ln\left(\frac{1}{P(X > x)}\right)\right)^{\frac{1}{k}} \quad (87)$$

Where:

$F(..)$	Probability distribution function [-]
x	Berthing velocity [cm/s]
μ	Mean value [cm/s]
σ	Standard deviation [cm/s]
λ	Scale parameter in Weibull distribution [cm/s]
k	Shape parameter in Weibull distribution [-]

Given the number of berthings within a year, n berthing velocities with a certain probability of exceedance during a reference period expressed by a return period T_R , were calculated using the following equation:

$$v(T_R, n) = \lambda \left(\ln\left(\frac{1}{P(X > x)}\right)\right)^{\frac{1}{k}} = \lambda (\ln(T_R n))^{\frac{1}{k}} \quad (88)$$

Where:

T_R	Return period [years]
n	Number of berthings per year [-]

The second method is based on extreme value theory and is suggested in the *Implementation of Eurocodes* handbook (Leonardo da Vinci Pilot Project, 2005). In the case of time-dependent loads, distributions of annual and lifetime maxima were used to account for alternative reference periods or target reliability indices in order to determine and generalise partial factors of safety. In this study, the probability that all berthing operations during a certain reference period would be lower than or equal to a particular berthing velocity was calculated by examining distributions of extreme berthing velocities. As in the Eurocodes, the extreme value distributions were called distributions of annual and lifetime maxima. The following general mathematical principles of extreme value theory were applied:

$$F_{x_n^n} = P(x_1 \leq x \cap x_2 \leq x \cap \dots \cap x_n \leq x) \tag{89}$$

$$= P(x_1 \leq x)P(x_2 \leq x) \dots P(x_n \leq x)$$

$$F_{x_n^n} = (F_{x(x)})^n \tag{90}$$

The parameters x_1, \dots, x_n represent field measurements of berthing velocities v_1, \dots, v_n and were assumed to be independent Weibull distributed random variables:

$$F(x; \lambda, k) = 1 - \exp\left(-\left(\frac{x}{\lambda}\right)^k\right) \tag{91}$$

From the typical Weibull distribution fit, random berthing velocities corresponding to a certain reference period were generated. The maximum berthing velocities during this reference period were selected and stored.

$$P(X > x) = P(\max(v_1, v_2, \dots, v_n) > x) \tag{92}$$

This process was repeated at least 200 times to ensure an appropriate population of maximum berthing velocities. In this way a new distribution of maxima was formed, which appeared to be a normal distribution (Fig. 5.5). The fit to the tail of this distribution was of significant importance when deriving berthing velocities with low probabilities of occurrence. The dark blue dashed line in Fig. 5.5 is the distribution of annual maxima and represents the distribution of maximum berthing velocities during a reference period of one year. The red dashed line is the lifetime maxima and represents the maximum berthing velocity during a reference period of 50 years.

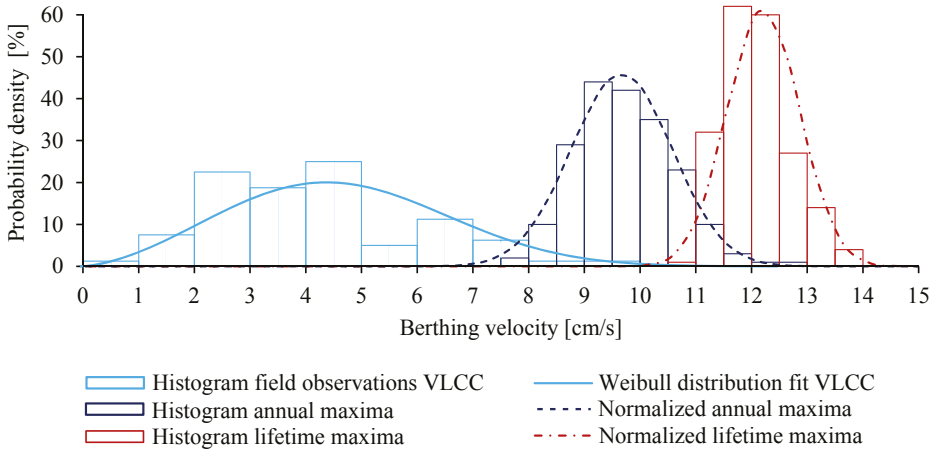


Fig. 5.5. Distribution of annual and lifetime maxima ($t_{ref}=50$ years) for VLCC vessels at Rotterdam.

It should be noted that the second method was also influenced by the number of berthings during a certain reference period. An increase in berthings resulted in an increase in the mean value and a decrease in the coefficient of variation. This insight is essential to interpret the results of extreme value theory and the influence of berthing frequency.

5

5.3.4 CHARACTERISTIC AND DESIGN BERTHING VELOCITIES

The magnitude of extreme berthing velocities largely depends on the number of berthings during a certain reference period. Some design codes explicitly provide recommendations on target reliability β_d index and other codes on return period T_R . Given a target reliability index for a certain reference period, the corresponding return period was calculated with the following equations:

$$P_d = 1 - \left(1 - \frac{1}{T_R}\right)^{t_{ref}} \tag{93}$$

$$T_R = \frac{1}{1 - (1 - P_d)^{\frac{1}{t_{ref}}}} = \frac{1}{1 - (1 - \Phi(-\alpha_S \beta_d))^{\frac{1}{t_{ref}}}} \tag{94}$$

Where:

- P_d Lifetime probability of failure of an event [-]
- T_R Return period of variable load [years]
- t_{ref} Reference period [years]
- α_S Sensitivity factor for dominating load/solicitation [-]
- β_d Prescribed target reliability index [-]

In this study, the principles of ISO 2394 (2015) were applied in order to comply with existing design codes and standards. The safety philosophies of Eurocodes (NEN-EN 1990, 2011) and OCDI (2009) are both based on the principles of ISO 2394, and British Standards, EAU and ROM are consistent with Eurocodes. ISO 2394 recommends applying sensitivity factors to dominant and non-dominant loads. In this study, both load and strength were assumed to be important and only dominant loads were taken into consideration. Non-dominating loads were not taken into account because, in the case of load combinations, modern design codes generally recommend applying a set of combination factors to transform dominating loads into non-dominating loads. The importance of berthing velocity was expressed by applying a sensitivity factor $\alpha_s = -0.7$ to dominating variable loads. It should be noted that α_s has a negative value and could be verified by a probabilistic assessment. Consequently, the probability of a dominating variable berthing velocity exceeding a design berthing velocity was evaluated by Eq. (83).

Eurocode standard NEN-EN 1990 defines target reliability indices β_d for reliability classes RC1, RC2 and RC3. Other design guidelines incorporate recommendations for return periods T_R (Section 5.2.2). The theoretical return periods of the target reliability indices of EN 1990 for dominant loads ($\alpha_s = -0.7$) for a reference period of 50 years were determined by applying Eq. (94) and are listed in Table 5.6.

Table 5.6. Theoretical return periods for variable loads during a reference period of 50 years according to EN 1990.

	SI	RC1	RC2	RC3
β_d	-	3.3	3.8	4.3
α_s	-	-0.7	-0.7	-0.7
P_d	%	1.05	0.40	0.13
T_R	year	4750	12,500	38,250

In the present study, extreme berthing velocities for different return periods were derived in order to compare field observations with existing design guidelines. Design berthing velocities corresponding to return periods of 100, 475, 1000, 4750, 12,500 and 38,250 years were derived. It should be noted that the codes are intended not to cover the incidence of such very rare events, but to create a low probability that structures will fail under the conditions of a reasonably rare incident during their service lifetime, also taking into account all sources of errors and adverse conditions not explicitly covered by the partial factors. Characteristic berthing velocities represented a return period of 50 years. For comparison, the number of berthings was set at approximately 100 berthings of a design vessel per year. This is similar to the underlying assumption of the berthing velocity curves derived by Brolsma et al. (1977).

Characteristic berthing velocities were derived by directly extrapolating the Weibull distribution fit (method 1) and by examining distributions of annual maxima (method 2). The distribution of annual maxima appeared to be a normalised distribution with a mean value and standard deviation $(\mu_{v_k}, \sigma_{v_k})$ (Fig. 5.7). Given $n=100$ berthings per year, the reliability of $T_R=50$ years corresponds to once per 5000 berthings ($T_R \cdot n$). The inverse of $T_R=50$ years is a probability of 2% being exceeded in a reference period of one year, and the corresponding annual reliability index therefore equals $\beta_{2\%}=2.054$. In this study, the following equations were used to determine berthing velocities with a return period of 50 years:

$$v_k = \lambda (\ln(T_R n))^{\frac{1}{k}} = \lambda (\ln(5000))^{\frac{1}{k}} \quad (\text{method 1}) \quad (95)$$

$$v_k = \mu_{v_k} + \beta_{2\%} \times \sigma_v = \mu_{v_k} (1 + 2.054 \times V_{v_k}) \quad (\text{method 2}) \quad (96)$$

The design berthing velocities for different return periods and the probability of exceedance were derived using the same methods. Design berthing velocities according to method 1 were derived by using Eq. (97). In the case of normalised distributions of lifetime maxima (method 2), the corresponding design berthing velocities were found by applying Eq. (98).

$$v_d = \lambda \left(\ln \left(\frac{n}{1 - (1 - \Phi(-\alpha_S \beta_d))^{\frac{1}{t_{ref}}}} \right) \right)^{\frac{1}{k}} \quad (\text{method 1}) \quad (97)$$

$$v_d = \mu_{v;d} - \alpha_S \beta_d \sigma_{v;d} = \mu_{v;d} (1 - \alpha_S \beta_d V_{S;d}) \quad (\text{method 2}) \quad (98)$$

Where:

$\mu_{v;d}$	Mean value of lifetime maxima [cm/s]
$\sigma_{v;d}$	Standard deviation of lifetime maxima [cm/s]
α_S	Sensitivity factor for berthing velocity [-]. When the berthing impact load is a dominant variable this factor equals -0.7. For non-dominant variables this factor equals -0.28.
$V_{S;d}$	Covariation of lifetime maxima [-]

5.4 DESIGN VALUES FOR BERTHING VELOCITY AND PARTIAL FACTORS

5.4.1 EXTREME BERTHING VELOCITIES

As an example, the population of VLCCs with a deadweight tonnage of 260,000-319,000 was examined statistically by using direct extrapolation of the Weibull distribution fit (method 1) and extreme value distributions (method 2).

An extrapolation of the Weibull distribution fit based on 80 field measurements of VLCC tankers was used to determine extreme berthing events (Fig. 5.6). Assuming 100 berthings

of a design vessel per year, the characteristic berthing velocity v_k was approximately 11.9 cm/s. The design berthing event corresponding to a target reliability equal to $\beta_d=3.8$ and a sensitivity factor equal to $\alpha_s=-0.7$ had a probability of exceedance equal to $P(v \leq v_d) \approx 0.4\%$. In practice, this means a 0.4% chance of exceedance during a period of 50 years, which corresponds to a theoretical return period of 12,500 years and a probability of exceedance of 1/1,250,000. A design berthing velocity v_d of approximately 14.4 cm/s was found (Fig. 5.6).

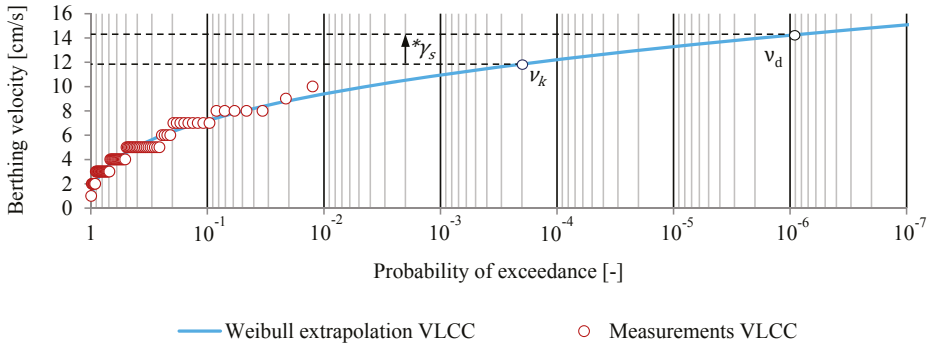


Fig. 5.6. Extrapolation of Weibull distribution fit to VLCC tankers (method 1).

The *Implementation of Eurocodes* handbook (Leonardo da Vinci Pilot Project, 2005) uses extreme value theory to determine appropriate partial factors of safety. The same principles were applied in this study. They are illustrated in Fig. 5.7. The solid blue line represents the probability density function of a Weibull distribution fit to the original dataset. The dashed blue and red lines are the normalised extreme value distributions of annual maxima and lifetime maxima, respectively. The mean value of lifetime maxima was higher and the probability density function was steeper than the density function of annual maxima.

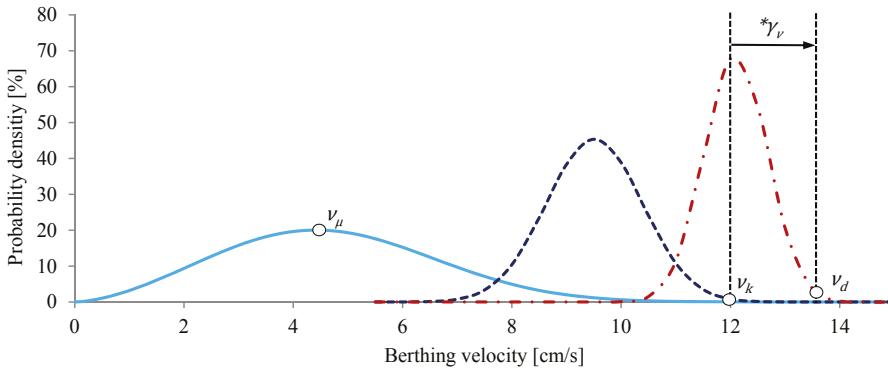


Fig. 5.7. Extreme value distributions of annual maxima and lifetime maxima ($t_{ref}=50$ years) for VLCC tankers (method 2).

On the basis of 80 VLCC berthing operations, a single berthing had a mean berthing velocity v_{μ} of approximately 4.5 cm/s. The characteristic berthing velocity v_k with a theoretical return period of 50 years was equal to approximately 12 cm/s. Assuming 5000 VLCC berthings and a 0.4% chance of exceedance during a reference period of 50 years, a design berthing velocity v_d of approximately 13.6 cm/s was found (Fig. 5.7).

This example showed that similar design berthing velocities v_d were found by applying direct extrapolation (method 1) and indirect extreme value distributions (method 2). The small differences were caused mainly by inadequate modelling of the low-probability tail of both normalised annual and lifetime maxima distributions. The typical shape and scale parameters of the Weibull distribution fits and distributions for annual and lifetime maxima are given in Appendix D.2. An overview of calculation results for both methods is given in Table 5.7. It should be noted that the derived berthing velocities were based on a berthing frequency of 100 berthings per year, a sensitivity factor $\alpha_s=-0.7$ and a reference period of 50 years.

Table 5.7. Extreme berthing velocities for individual vessel classes (cm/s).

T_R [Years]	$P(v \leq v_d)$ [%]	$kDWT$	n^1	max^2	Extrapolation of Weibull distribution fit										
					63.50	39.50	10.00	4.88	1.05	0.40	0.13	38,250	50	63.50	10.00
Tankers ◦															
		60-85	23	9	12.6	12.9	13.6	13.9	14.5	14.8	15.2	12.6	14.1	14.3	14.5
		Aframax ³	175	12	11.1	11.4	12.1	12.4	13.0	13.4	13.8	10.8	12.8	13.0	13.3
		Suezmax	95	11	11.5	11.9	12.6	12.9	13.5	13.9	14.2	11.2	13.0	13.2	13.4
		VLOC	80	10	11.9	12.3	13.0	13.3	14.0	14.4	14.8	12.0	13.4	13.6	13.8
		Fix. Laser	19	7	8.9	9.1	9.7	9.9	10.4	10.6	10.9	8.6	9.9	10.1	10.2
Bulkers ◊															
		150-205	107	13	15.3	16.0	17.4	18.0	19.2	19.9	20.8	14.9	18.4	18.8	19.2
		205-365	37	10	12.8	13.3	14.3	14.7	15.6	16.1	16.7	12.5	15.4	15.7	16.0
Containers □															
		7 - 15	37	10	12.7	13.0	13.5	13.8	14.3	14.6	14.9	12.6	13.9	14.1	14.3
		Feeders	31	9	12.2	12.6	13.3	13.7	14.3	14.7	15.2	12.0	14.1	14.4	14.6
		Panamax	31	8	10.8	11.1	12.0	12.3	13.1	13.5	14.0	10.1	12.9	13.1	13.4
		Post Panamax	60	7	10.3	10.7	11.6	12.1	12.9	13.4	13.9	10.1	12.3	12.5	12.8
		New Panamax ³	18	3	3.8	3.9	4.1	4.1	4.3	4.4	4.5	3.7	4.2	4.3	4.3
Containers □															
		Coasters	177	20	29.8	31.4	34.8	36.4	39.6	41.5	43.7	27.7	38.1	39.1	40.1
		Feeders	250	20	29.4	30.9	34.2	35.7	38.7	40.6	42.6	28.4	37.3	38.2	39.2
		Panamax	104	19	26.9	28.0	30.5	31.6	33.8	35.2	36.6	26.1	31.8	32.5	33.1
		Post Panamax	288	25	28.7	30.1	33.0	34.3	37.0	38.6	40.4	27.7	35.1	35.9	36.7
		New Panamax	150	20	26.9	28.1	30.7	31.8	34.2	35.6	37.1	25.7	32.8	33.5	34.3
		ULCV	171-195	266	26	26.7	28.2	31.4	32.8	35.8	37.6	22.9	33.6	34.4	35.2
Large datasets															
		All tankers ◦	932	12	11.5	11.8	12.6	12.9	13.5	13.9	14.3	11.1	13.0	13.2	13.4
		All sheltered △	7-365	13	12.6	13.1	14.0	14.4	15.2	15.7	16.3	12.1	15.0	15.3	15.6
		All exposed □	1235	26	26.4	27.7	30.4	31.6	34.1	35.6	37.2	25.2	32.6	33.4	34.2
		All data	1948	26	25.0	26.3	29.1	30.4	32.9	34.4	36.2	22.7	31.8	32.6	33.5

¹⁾ Number of field observations.

²⁾ Maximum measured berthing velocity.

³⁾ Dataset is most likely too optimistic (Appendix D).

⁴⁾ Dataset is most likely too conservative (Appendix D).

5.4.2 CHARACTERISTIC BERTHING VELOCITIES

In Fig. 5.8, the berthing velocities of individual vessel classes representing a return period of 50 years are compared with those in EAU 2012 (Grabe, 2012) and PIANC (2002). It should be noted that the berthing velocity curves in EAU 2012 represent berthing velocities with a return period of 50 years, while those in PIANC 2002 represent berthing velocities with a return period of 30 years. The characteristic values of berthing velocity v_k of individual vessel classes were determined by using existing design practice and by interpreting the results derived in Section 5.4.1.

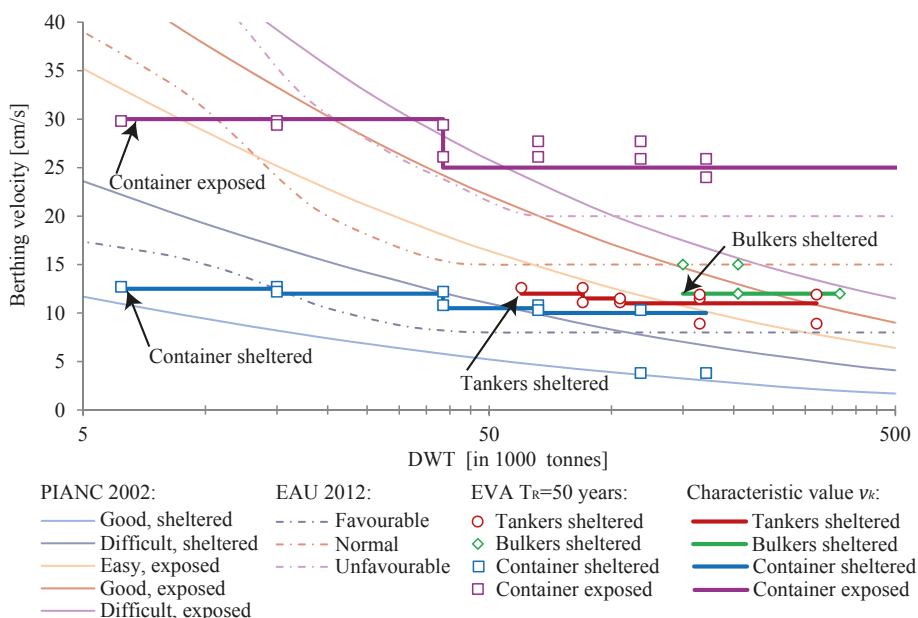


Fig. 5.8. Characteristic berthing velocities compared with PIANC 2002 and EAU 2012.

In the statistical examination of extreme berthing velocities, no real correlation between berthing velocity and the mass of the vessel was found for tankers in sheltered conditions. The goodness of fit of the Weibull distribution function to the individual dataset of Aframax tankers was low and should be used with care (Appendix D.1). In practice, characteristic values of berthing velocity are generally higher than 10 cm/s. If a shore-based docking system has been installed, characteristic berthing velocities of 8 cm/s are more common. Similar values were found in Section 5.4.1. It should be noted that individual datasets for bulk carriers most likely contain overestimated berthing velocities at the moment of impact (Appendix D.1). For large seagoing bulkers, no real correlations were found. Characteristic berthing velocities of 12 cm/s for large bulkers in sheltered conditions were typically used

in practice. A small correlation between vessel size and berthing velocity was found for container vessels in sheltered conditions. The berthing velocities were influenced by type of manoeuvre/landing procedure and berthing policy (Appendix D.1). Berthing velocities of large seagoing container vessels in exposed navigation conditions showed no real correlation with vessel size (Hein, 2014). The berthing velocities were higher than in EAU velocity curves, but due to very low berthing angles (always between 0° and 1°) deflection of the fenders showed that the actual berthing energy was still less than the design energy (Hein, 2014). It should be noted that for most individual vessel classes there was insufficient data to determine partial factors of safety per vessels class and therefore large datasets were developed.

5.4.3 PARTIAL FACTORS OF SAFETY FOR BERTHING VELOCITY γ_v

In this study, partial factors of safety were defined as the ratio between a design value and a characteristic value of berthing velocity, and they were derived by direct interpolation of a Weibull distribution fit (method 1) to large datasets. The results are given in Table 5.8. It is important to realise that partial factors of safety for time-dependent design berthing velocities are theoretically inconstant. Partial factors are influenced by the uncertainty and importance of a berthing velocity, as well as the target probability of failure during a certain reference period.

Table 5.8. Partial factors of safety for berthing velocity γ_v by applying method 1, extrapolation of Weibull distribution fit.

	SI	Reliability class of EN 1990		
		RC1	RC2	RC3
All tankers ○	-	1.17	1.20	1.24
All sheltered Δ	-	1.21	1.25	1.29
All exposed □	-	1.29	1.34	1.41
All data	-	1.31	1.38	1.44

Fig. 5.9 shows that the Weibull distribution fits to the datasets ‘All tankers’ and ‘All sheltered’ slightly underestimate low-probability berthing velocities. This was considered acceptable because the highest measured berthing velocities were caused by overly conservative measurements of, for example, small seagoing tankers and large seagoing bulkers (Appendix D.1). The dataset ‘All exposed’ contains numerous berthing velocities just below 20 cm/s, as well as two higher ones of 25 and 26 cm/s (Fig. 5.9). The Q-Q probability plot in Fig. 5.10 shows that the theoretical and empirical quantiles of the two extreme berthing velocities measured in Bremerhaven were almost identical.

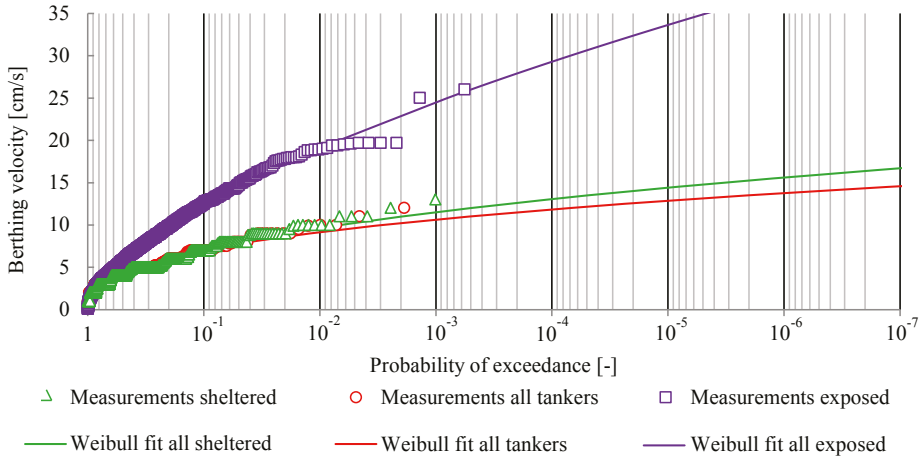


Fig. 5.9. Probability of exceedance plot for large datasets.

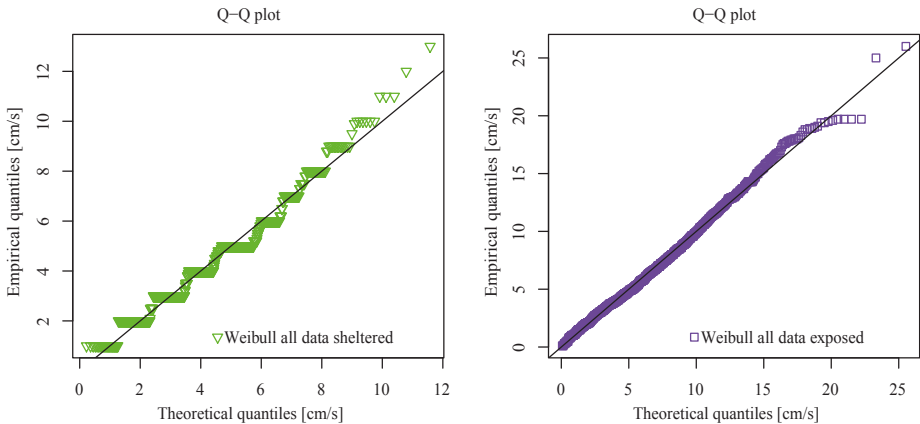


Fig. 5.10. Probability distribution plots for all 'sheltered' and all 'exposed' data

5

5.5 DISCUSSION ON HOW TO DETERMINE DESIGN VALUES FOR BERTHING VELOCITY

5.5.1 HOW TO USE BERTHING VELOCITY RECORDS AND PARTIAL FACTORS IN THE DESIGN

This section discusses how to implement field observations of berthing velocity and partial factors of safety in structural assessments of berthing impact loads on quay walls. As explained in Section 5.2.1, the berthing impact load to which a marine structure is subjected

largely depends on the type of berthing structure; that is, whether it has linear or non-linear deformation characteristics. The effect of linear and non-linear behaviour on berthing impact load F is further explained by the following simplified equation to illustrate the effect of difference in performance:

$$F = k\delta^N \quad (99)$$

Where:

F	Berthing impact load [kN]
δ	Deflection of fender + berthing structure [m]
k	Stiffness of berthing structure and soil [kN/m]
N	Coefficient for linearity [-]

Examples of berthing structures showing linear and non-linear structural behaviour are given in Table 5.9. When, for instance, a pneumatic or cylindrical fender system is installed on a rigid quay wall, the berthing energy is absorbed by fender deflection, showing non-linear hardening ($N > 1$). Flexible dolphins equipped with timber fendering absorb berthing energy by deflection, showing an approximately linear-elastic behaviour ($N = 1$). When a buckling-type fender system is installed on a flexible dolphin, structural behaviour often shows softening ($N < 1$), but when the capacity of a fender system is exceeded, the response of a berthing structure will be similar to a situation without fendering ($N = 1$) – for example, during the full compression of a fender equipped with a fender stop. If buckling-type fender systems are installed on rigid quay walls, the amount of energy absorbed by the marine structure itself is negligible. In this case, the fender system absorbs most of the berthing energy by deflection and the resulting berthing impact load is influenced mainly by fender characteristics, showing typically ideal plastic behaviour ($N \approx 0$).

Table 5.9. Examples of linear and non-linear behaviour of marine structures.

Range	Behaviour	Examples
$N > 1$	Non-linear hardening	Rigid marine structure (quay wall) + cylindrical/pneumatic type fender system Flexible dolphin + cylindrical/pneumatic type fender system
$N = 1$	Linear elastic	Flexible dolphin without energy-absorbing fender system (timber fendering)
$N < 1$	Non-linear softening	Flexible dolphin + buckling-type fender system
$N \approx 0$	Ideal plastic	Rigid marine structure (quay wall) + buckling-type fender system

The process to derive a design berthing impact load by simultaneously applying the two design approaches described in Section 5.2.1 is illustrated in Fig. 5.11. The principal difference is the application of a partial factor of safety to either a characteristic berthing velocity γ_v or a characteristic berthing impact load γ_Q . The flowchart starts with the determination of a characteristic berthing velocity v_k by using field observations. Typical characteristic berthing velocities measured at well-organised ports are presented in Fig. 5.8. It should be noted that the berthing frequency influences the characteristic berthing velocity. This is further discussed in Section 5.5.3. The derivation of partial factor of safety γ_v was based on a statistical examination of sophisticated datasets from representative field observations. The partial factor of safety γ_v does not take into account uncertainty in modelling the effects of loads, while partial factor of safety γ_Q complies with design codes and standards, such as NEN-EN 1990 (2011), and already includes model uncertainty. In line with the Eurocode standard, Eq. 6.2 of NEN-EN 1990, an additional partial factor of safety γ_{sd} for berthing impact load F_v needs to be applied. It should be noted that the governing berthing impact load F_d depends on the type of berthing structure and the values of partial factors γ_v , γ_{sd} and γ_Q .

Fig. 5.12 shows that a partial factor of safety for berthing velocity γ_v is only proportional to a partial factor of safety for berthing impact load γ_Q for linear-elastic behaviour ($N=1$). If we assume that $\gamma_v = \gamma_Q$, then in the case of non-linear softening ($N < 1$) the partial factor of safety for berthing impact load γ_Q will result in the governing berthing impact load F_d . Conversely, in the case of non-linear hardening ($N > 1$) a partial factor of safety for berthing velocity γ_v will result in the governing berthing impact load F_d . The effect of uncertainty in modelling the load effect is illustrated by applying γ_{sd} to F_v .

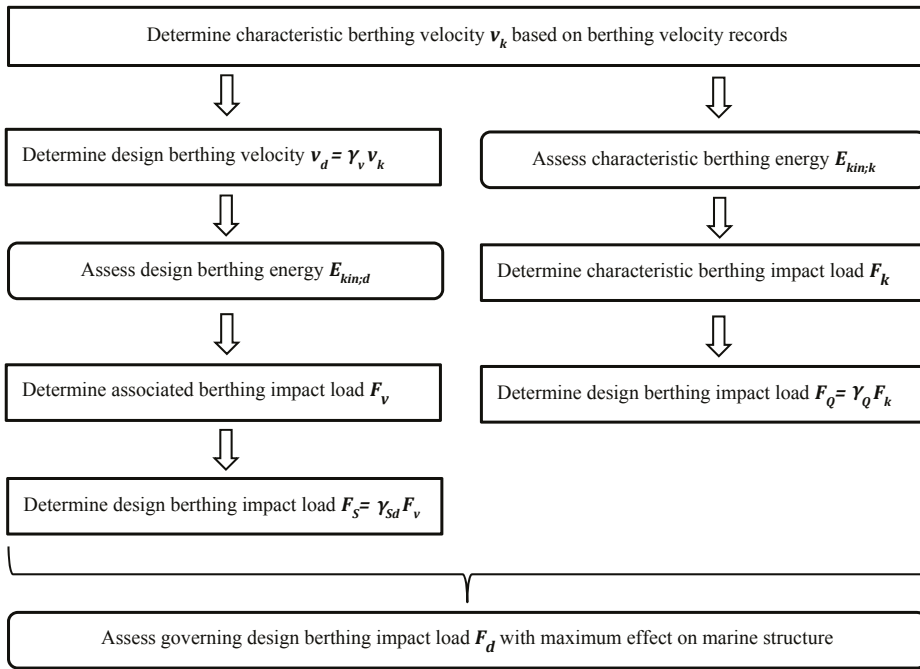


Fig. 5.11. Global flowchart assessing berthing impact on a marine structure.

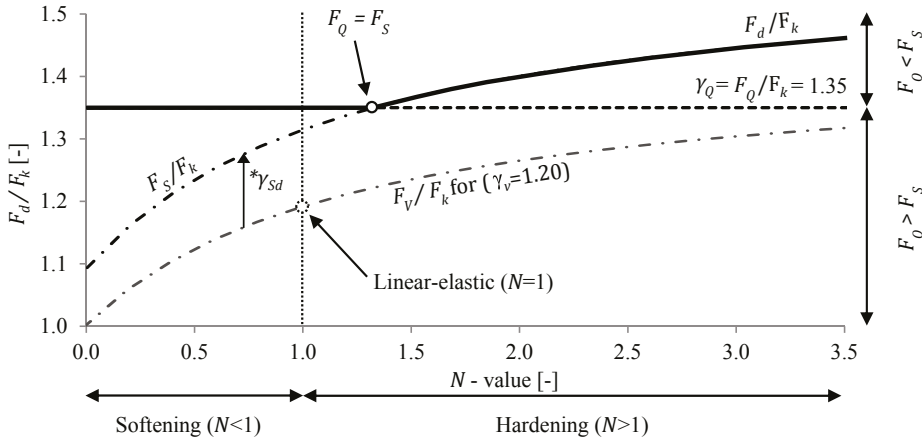


Fig. 5.12. Influence of linear and non-linear behaviour on design berthing impact load.

If large datasets are available for a statistical approach, it is recommended that partial factors of safety be determined by evaluating extreme berthing velocities. Table 5.10 presents generalised partial factors of safety for berthing velocities γ_v as concluded in

this study. It should be noted that γ_v is proportional to $\sqrt{C_{ab}}$. For the dataset of sheltered navigation conditions, partial factors of safety are lower than in the dataset of exposed navigation conditions (strong tidal currents). The use of berthing aid systems resulted in even lower design velocities and lower partial factors of safety.

Table 5.10. Partial factor of safety γ_v for berthing velocity (v_k) and abnormal berthing factor C_{ab} for berthing energy (E_k), given well-organised navigation conditions.

Navigation conditions	Pilot assistance	Symbol	Reliability class EN 1990		
			RC1	RC2	RC3
Sheltered and monitored ¹	Yes	γ_v	1.15	1.20	1.25
		C_{ab}	1.35	1.45	1.55
Sheltered	Yes	γ_v	1.20	1.25	1.30
		C_{ab}	1.45	1.55	1.70
Exposed ²	Yes	γ_v	1.30	1.35	1.40
		C_{ab}	1.70	1.80	2.00

¹) Pilots are aware of the allowable berthing velocity and use berthing aid systems, such as portable pilot units.

²) Strong tidal currents.

When significant softening ($N < 1$) occurs between a characteristic berthing impact load (service limit state) and a design berthing impact load (ultimate limit state), a reduction of the partial factor of safety γ_Q could be considered. The effect of softening on energy absorption due to linear and non-linear behaviour is illustrated in Fig. 5.13. When the hatched areas below the linear (left) and non-linear (right) load-deflection curve are equal, the design berthing impact load F_Q is lower in the case of softening.

$$E_{kin;linear} = E_{kin;non-linear} = \int_0^{\delta_{max}} F(\delta) d\delta \quad (100)$$

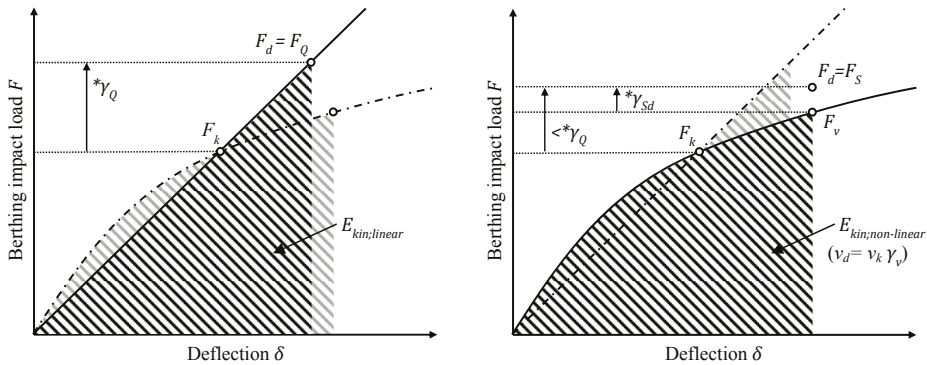


Fig. 5.13. Linear system (left) and non-linear system with significant softening (right).

In case of non-linear softening, the partial factor of safety is smaller than γ_Q . The berthing impact load should be derived by using a partial factor of safety γ_v on berthing velocity, based on the assumption that an ultimate limit state is a theoretical situation/event which has a very low probability of occurrence during the service life. In the case of repetitive loading above a service limit state situation, the effect of softening should not be applied or should be used carefully. The partial factor γ_{sd} applied to berthing impact load F_v , was suggested in order to comply with the safety philosophy of the Eurocode standard (NEN-EN 1990, 2011). It should be noted that all partial factors of safety in that standard were derived by accounting for uncertainties in modelling the effect of loads, and γ_{sd} was generally assumed to be equal to approximately 1.1. Applying γ_{sd} to resulting berthing impact loads acting on marine structures should be done with great care, because additional factors of safety are already considered in the determination of berthing energy as well as in the design of fender systems. It is recommended that further research be conducted into the application of γ_{sd} in the case of berthings with and without pilot assistance.

5.5.2 EVALUATION OF PARTIAL FACTORS OF SAFETY

Although existing design guidelines do not differentiate between sheltered and exposed navigation conditions, the partial factors of safety listed in Table 5.10 are in the range of the recommended values in literature (Table 5.2). BS 6394-4 (2014) recommends using $C_{ab}=1.5$ for situations with a low risk profile and $C_{ab}=2.0$ for situations with a high risk profile. Given the absence of field observations, an abnormal berthing factor equal to $C_{ab}=1.5$ must be used in the case of general cargo vessels. This is quite similar to the results found in Section 5.4.1 for sheltered berthings in RC2. For LNG, LPG and ferries, $C_{ab}=2.0$ is recommended; this is close to the abnormal berthing factor for exposed conditions in RC3. The reason for this increase is not explicitly given in BS 6394-4. For an LNG or LPG berth, a higher consequence class with a higher reliability index could be considered. One explanation for $C_{ab}=2.0$ for ferry berths

could be their higher berthing frequency, combined with the fact that captains of ferries do not make use of pilot or tug assistance and they have large numbers of passengers on board.

PIANC (2002) and EAU 2012 (Grabe, 2012) recommend applying lower abnormal berthing factors, approximately $C_{ab}=1.25$, for large seagoing tankers and bulkers. In this study, higher abnormal berthing factors were found for these vessels. This could be due to the higher target reliability index in the Eurocodes, or to the use of shore-based docking systems. PIANC is aware of the influence of the low reliability level and, for berths with very low approach velocities, recommends using a higher confidence level in the case of normal berthing (Section 4.2.8.4 of PIANC (2002)). PIANC and EAU 2012 suggest that there is a correlation between vessel size and abnormal factor of safety C_{ab} . Although berthing policy (e.g. use of berthing aid systems, pilot and tug assistance) was to some extent related to vessel size, in this study no correlation was found between type and size of vessel and partial factor of safety γ_v .

BS 6349-4 (2014) also recommends applying an additional partial factor of safety to the resulting berthing impact load. The partial factors of safety representing normal (characteristic) and design situations given in the code are 1.35 for persistent situations and 1.2 for transient ones. The values found were quite similar to the partial factor of safety of exposed and sheltered navigation conditions. Although without accounting for non-linear softening, following BS 6349-4 could result in a conservative design.

5.5.3 INFLUENCE OF BERTHING FREQUENCY

As explained, partial factors γ_v were based on a berthing frequency of 100 design vessels per year. The Spanish ROM (ROM 02-90, 1990) already addresses the importance of berthing frequency. Logically, if fewer arrivals are expected during a reference period then the design berthing velocity will decrease, because theoretically each berthing operation has a probability of exceeding the design berthing velocity. There are two ways to deal with this effect: apply either an alternative characteristic berthing velocity v_k or a correction factor to partial factor γ_v . If used correctly, both methods should result in the same design berthing velocity. The influence of berthing frequency on partial factor γ_v was calculated by applying a correction factor $C_{berthing}$:

$$C_{berthing} = \frac{\gamma_a}{\gamma_v} = \frac{v_a}{v_d} \quad (101)$$

Where:

$C_{berthing}$	Correction factor for γ_v [-]
γ_a	Alternative partial factor of safety [-]
v_a	Alternative berthing velocity [cm/s]

The alternative berthing velocity v_a was derived by using Eq. (97). The correction factors for the datasets 'All tankers', 'All sheltered' and 'All exposed' are given in Table 5.11 and illustrated in Fig. 5.14.

Table 5.11. Correction factor $C_{berthing}$ for partial factor of safety γ_v given an alternative berthing frequency n .

n	1	2	5	10	25	50	100	200	1000
All tankers \circ	0.863	0.886	0.915	0.936	0.962	0.981	1.000	1.018	1.058
All sheltered \triangle	0.840	0.866	0.900	0.924	0.955	0.978	1.000	1.021	1.069
All exposed \square	0.782	0.817	0.862	0.895	0.938	0.969	1.000	1.030	1.099
All data	0.776	0.812	0.858	0.892	0.936	0.968	1.000	1.031	1.102

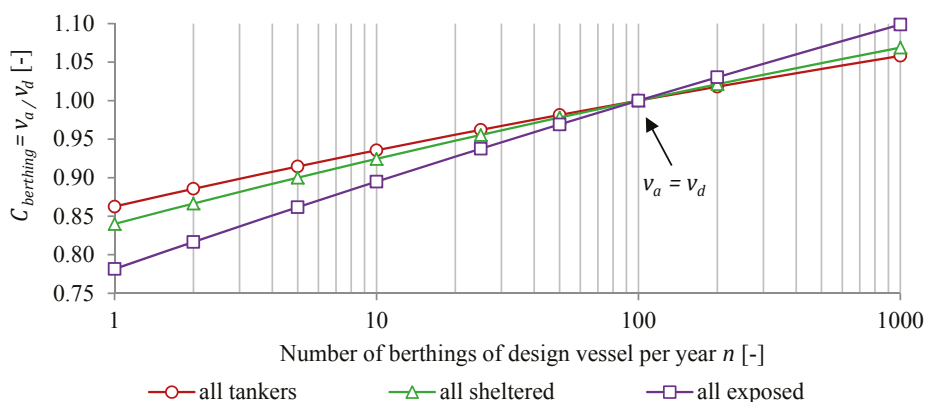


Fig. 5.14. Influence of alternative numbers of berthings on partial factor of safety γ_v given a reference period of 50 years.

5.6 CONCLUSIONS AND RECOMMENDATIONS

This chapter has provided guidance on the use of field observations and partial factors of safety for berthing velocity and loads on quay walls and other types of marine structure. The results have been used to evaluate existing design guidance. The most important conclusions from this are as follows.

- The measured berthing velocities were low, compared with current recommendations on design values. Typically, the mean values for individual vessel classes varied between 4 and 7 cm/s. The maximum observed berthing velocities were 13 cm/s and 26 cm/s, in sheltered and exposed navigation conditions respectively. Characteristic values of berthing velocities found in this chapter were generally in the range of recommendations in literature. Only the derived characteristic berthing velocity of large seagoing vessels in exposed navigation conditions (strong tidal currents) was higher, but these berthings appeared to have very low berthing angles at the moment of impact, resulting in less fender compression.

- A characteristic value of berthing velocity with a return period of 50 years based on a berthing frequency of 100 berthings per year shows a close correlation with existing recommendations for the design of new quay walls. When assessing quay walls, actual berthing frequency needs to be taken into consideration.
- The collected data does not confirm the historical assumption that berthing velocities of large seagoing vessels are strongly related to ship dimensions. No evidence was found to suggest that berthing velocities are influenced by the vessel's draught or under-keel clearance, or the type of marine structure they are berthing at. Nor was any correlation found between wind speed (environmental factors) and berthing velocity. However, berthing velocities do depend strongly on berthing policy (type of landing, experienced and well-trained pilots, tug assistance, berthing aid systems, etc.).
- A partial factor of safety for berthing velocity is not a fixed value, as it is influenced by the prescribed probability of failure during a reference period and by variations in berthing velocity. The partial factors of safety found in this chapter did not show a correlation with vessel size. Higher partial factors of safety were found for exposed navigation conditions (strong tidal currents), and lower ones when berthing aids were applied.
- The existing design guidelines were considered to be safe for most situations. Applying the British Standards (BS 6349-4, 2014) could result in a conservative design. When using the recommendations of PIANC (2002) and EAU (Grabe, 2012), applying an abnormal berthing factor C_{ab} lower than 1.5 should be done with great care.

If site-specific data is not available, partial factors of safety for berthing velocity γ_v as derived in this chapter could be used instead of applying an overall safety margin. It is recommended that further study be undertaken into the risk of high berthing velocities in the case of navigation conditions with strong tidal currents. In particular, the effect of a second berthing impact could reduce the amount of energy transferred if berthing angles are low. Sophisticated datasets and partial factors of safety for the berthing velocity of inland barges and smaller seagoing coasters are still lacking. It is therefore recommended that field observations of such smaller vessels be collected in order to better account for the human influence on berthing velocity, which is believed to be greater when berthings are not assisted by well-trained pilots. The presented methods for deriving characteristic and design values for berthing velocity are easy to apply and could be beneficial for assessing existing quay walls (e.g. capping beams and fender systems) and other types of marine structure. Given the distribution characteristics listed in [Appendix D.2](#), the effect of lower target reliabilities, alternative reference periods and berthing frequencies could be accounted for by using [Eq. \(97\)](#). This will generally result in lower design berthing velocities.

6





CONCLUSION AND RECOMMENDATIONS

“Knowledge is an unending adventure at the edge of uncertainty.”

Jacob Bronowski

This thesis has addressed some important aspects to consider in reliability-based assessments of quay walls. It shows how to derive target reliability indices and to perform reliability analyses using finite element models. Moreover, the evolution of the failure rate over time was examined, taking into account the effects of past service performance and degradation. The findings have enhanced our understanding of quay walls' reliability, enabling us to determine their residual lifetime more accurately and so make better use of these assets.

This chapter presents the main findings and overall conclusion of this thesis ([Section 6.1](#)). It also summarises the detailed findings of each chapter ([Section 6.2](#)). Furthermore, recommendations for follow-up research and practical implementation are proposed ([Section 6.3](#)). In addition to its scientific value, the output of this research should benefit end users such as port and terminal authorities, engineers, asset managers and code writers. Based on its findings, a series of improvements to several national and international standards and design manuals have already been implemented ([Section 6.4](#)).

6.1 MAIN FINDINGS

The main objective of this thesis was to show how quay-wall reliability can be evaluated and what aspects should be considered. Of these, especially important is how a quay wall's evolution affects its probability of failure over time. The five main findings of this thesis are listed below.

1. For the commercial quay walls considered in this study, it was found that the economic risk-acceptance criterion prevails when deriving reliability targets, provided that the requirements concerning human safety are met via the marginal lifesaving cost principle. Allocating reliability targets dedicated to the specific risk profile of a quay wall is essential when performing reliability-based assessments. The lifetime reliability targets obtained for a reference period of fifty years were in the range of values recommended in literature. Furthermore, it was found that the failure rate of quay walls evolves significantly over time ([Finding 3](#)), whereas the design codes currently in use, such as the Eurocode (NEN-EN 1990, 2011), implicitly assume that rate to be constant. As a result, the annual reliability targets found are lower than those in the Eurocode. Moreover, within a one-year reference period, the effects of past performance and degradation can be taken into account in an appropriate manner. These findings can play an important role in the evaluation of the reliability of an existing quay wall, since then its remaining service life and the associated reference period are generally unknown a priori. Hence, using annual target reliability indices is preferred.
2. Despite highly non-linear soil behaviour and complex soil-structure interaction (e.g. due to inclined retaining walls or relieving platforms), the reliability level of a quay wall can be estimated successfully by performing finite element-based reliability assessments using the Abdo-Rackwitz algorithm, which is a gradient-based first order reliability method (*FORM*). This method proved to be able to evaluate various failure modes considering twenty nine random variables. In general, two to ten iterations were needed to satisfy the convergence acceptance criteria. The resulting reliability indices for the critical failure modes of two real-life quay walls were fairly close to the reliability target of the original design, which corresponds with reliability class RC2 in NEN-EN 1990 (2011).
3. Time-independent stochastic variables, such as material properties of soil, steel and grout, as well as model uncertainty, influence the evolution of the failure probability over time. This finding is crucial when assessing existing quay walls, since (epistemic) uncertainty in time-independent variables decreases over time for quay walls with successful past service performance. In the absence of significant degradation, the failure rate of a service-prove quay wall therefore decreases over time. Consequently,

- not only is the quay wall's actual reliability higher than assumed in its early service period, but the net present value of the residual risk also decreases, and hence reliability targets derived from an economic perspective will decrease accordingly.
4. In the event of non-deteriorating quay walls, the probability of failure of a structure with a successful service history decreases over time, resulting in a higher reliability level compared to the reliability level in the early years of service. In this context, it was found that for service-proven combi-walls¹ subject to low corrosion rates, the highest failure rates occur in the first year of the service life, while for high corrosion rates the final year prevails. Since many existing combi-walls are subject to low corrosion rates near the maximum bending moment, this finding indicates that, despite some degradation, their remaining lifetime is longer than previously assumed based on past performance.
 5. Berthing velocity, the speed at which a ship approaches the quay wall, and the dimensions of seagoing vessels are not strongly correlated. However, well-established design recommendations, such as PIANC (2002), assume a strong negative correlation. Consequently, the associated design values for berthing impact loads acting on quay walls induced by small and large seagoing vessels are too conservative and too optimistic, respectively. By contrast, the berthing velocity depends mainly on the berthing policy (e.g. type of landing, experience of pilots, and the use of tug assistance or berthing aid systems). These design guidelines should be revised.

In addition to the five main findings, reliability is always related to a reference period and a certain functionality, such as water depth or operational activities. Both factors are important preconditions when evaluating quay-wall reliability.

In summary, the applicability of finite element-based reliability assessments in quay-wall engineering has increased considerably. The methods developed to evaluate quay-wall reliability can be used to determine the remaining service life, to make better use of existing structures, and to improve the design of new quay walls. The main findings of this thesis can play a crucial role in the assessment of existing quay walls and, presumably, all other service-proven geotechnical structures subject to degradation.

¹ combi-walls are quay walls consisting of king piles with sheet pile walls between them

6.2 DETAILED FINDINGS

6.2.1 RISK-BASED RELIABILITY TARGETS FOR QUAY WALLS

When performing reliability-based assessments, it is essential to allocate an appropriate reliability target. This thesis has derived reliability targets from different risk perspectives, such as the acceptance criteria associated with economic optimisation, individual risk, group risk and the life quality index. For commercial quay walls, it was found that target reliability indices can generally be determined on the basis of economic optimisation. The annual and lifetime target reliability indices obtained were in the range 2.8–3.5 and 2.5–3.3, respectively. However, it should be noted that the individual and group risk are relevant if failure consequences reach far beyond the quay wall itself: for instance, if failure leads to the release of hazardous substances or large explosions.

Although the reliability criteria in codes and standards presently used in civil engineering differ significantly, it was found that the allocation of reliability targets appears to be fairly consistent and uniform throughout the world if the assessment criteria and the associated reliability targets from ISO 2394 (2015) are applied systematically. The framework of ISO 2394 therefore forms a solid basis for assessing quay walls' reliability. However, this thesis has also revealed that this framework will become richer and more interpretable if it is extended with considerations regarding the type of failure, the likelihood of warning signals, concepts of functional and structural redundancy and indirect impacts such as damage to the reputation of a port or terminal.

It is vitally important to allocate reliability targets for quay walls and other geotechnical structures that suit their risk profile, since the degree and sources of time-dependent and time-independent uncertainty – such as inherent natural variability in strength and loads (aleatory uncertainty), as well as lack of knowledge or insufficient information (epistemic uncertainty) – differ from the recommendations for buildings and bridges currently in use, as do the consequences of failure. It is therefore recommended to add an appendix to Eurocode NEN-EN 1990 that provides specific guidance for the design of quay walls, e.g. examples for the classification (CC1, CC2 or CC3) and partial factors of safety.

6.2.2 FINITE ELEMENT-BASED RELIABILITY ASSESSMENT OF QUAY WALLS

One objective of this thesis was to develop a method to perform a finite element-based reliability assessment of a quay wall, while realistically modelling the soil-structure interaction. The reliability indices for relevant failure modes of two real-life quay walls in Rotterdam were therefore estimated by coupling probabilistic methods with finite element models. In spite of a fairly complex soil-structure interaction, the presence of numerical noise and a fairly large number of stochastic variables, finite element-based reliability assessments could be performed successfully using the algorithm named Abdo-Rackwitz, which converged

quite efficiently and accurately. In general, between two and ten iterations were needed to satisfy the convergence acceptance criteria.

The reliability indices found for prevailing failure modes correspond fairly well to the prescribed target reliability for RC2 of Eurocode NEN-EN 1990 (2011). Furthermore, the results show that model uncertainty and correlations between input variables, such as the correlation between the stiffness, weight density and friction angle of soil layers, must be taken into account, since otherwise the failure probability is significantly underestimated.

In addition, this thesis has provided insight into parameters that influence quay-wall reliability by presenting the obtained sensitivity factors for all stochastic input variables. These factors show that quay-wall reliability is largely dependent on uncertainty in time-independent variables, such as the material properties of soil, steel and grout. By contrast, much lower sensitivity factors were found for loads and geometrical variables, such as the soil-retaining height. Despite their fairly low sensitivity factors, changing the quay wall's retaining height and operation loads can substantially affect the quay walls' reliability level, since the estimated reliability index is conditional upon a certain functionality. In this context it should be noted that variability (aleatory uncertainty) in these functional preconditions does not significantly influence the quay wall's reliability level, and hence they require fairly low partial factors of safety. Likewise, fairly low required partial factors were found for soil stiffness by comparison with the recommendations in the Eurocode.

Regarding the determination of design values of strength variables, the results suggest that the differentiation in the partial factors of safety from Eurocode 7 (NEN-EN 9997, 2016) for the soil's internal friction angle is fairly low for the distinguished reliability classes. As a result, a design using the partial factors of safety associated with reliability class RC1 is relatively safe, whereas a design for RC3 is presumably too optimistic. Furthermore, the current set of partial factors suggested by Eurocode 7 does not account for correlations. As a result, the influence of dominant soil layers on the reliability of quay walls is underestimated, whereas there is an overestimation in the case of non-dominant layers in the guidelines presently used in quay-wall design.

6.2.3 THE EFFECT OF CORROSION ON THE RELIABILITY OF SERVICE-PROVEN QUAY WALLS

The assessment of service-proven quay walls subject to corrosion-induced degradation is inherently a time-dependent reliability problem. Two major challenges here are modelling corrosion and taking into account the decrease in epistemic uncertainty throughout the quay wall's service life. This thesis has examined the probability of failure given successful past performance, while the quay wall is subject to corrosion and randomly imposed variable loads. The annual failure rates found for service-proven quay walls vary over time, and they decrease over time in the case of non-deteriorating quay walls. Although corrosion

results in an increase in the failure rate, this thesis has concluded that some corrosion of combi-walls can be allowed; this is because this phenomenon occurs mainly on the waterside (Jongbloed, 2019), while the stress on the landside prevails during the initial design process. Consequently, the initial reliability level of a combi-wall is higher on the waterside and so some corrosion is acceptable. Only in the event of severe corrosion rates (corrosion curves 6-9 in Fig. 4.3) does the probability of failure increase significantly.

In addition, the ratio between the reliability index and the factor of safety (this factor is commonly used in allowable-stress-based assessments to evaluate the residual capacity of existing quay walls) is not constant over time. Due to corrosion, the strength of a combi-wall decreases while at the same time our confidence in a quay wall that has survived all previous years increases. Both these aspects influence the reliability level, while the factor of safety is influenced only by loss of wall thickness. As a result, the actual failure probability of an existing quay wall will be lower than presently assumed when performing an allowable stress-based analysis. Consequently, in spite of corrosion-induced degradation, it is expected that the remaining service life of many service-proven quay walls can be extended safely and responsibly by performing a time-dependent reliability analysis.

6.2.4 CUSTOMISED DESIGN VALUES FOR BERTHING VELOCITY TO ENHANCE QUAY WALL RELIABILITY

While the dimensions and propulsion systems of vessels have evolved considerably, no comprehensive research has been conducted on berthing velocities and the associated berthing impact loads acting on quay walls since the 1970s (Beckett Rankine, 2010). In this thesis, the berthing velocity of large seagoing vessels was examined statistically using new berthing records provided by the port authorities of Bremerhaven, Rotterdam and Wilhelmshaven. The distribution functions found can serve as input for reliability-based assessments of quay walls and for allocating tolerable design values for berthing velocity.

Although the berthing velocity curves (Brolsma et al., 1977) presently used in the design of fender systems suggest that there is a strong negative correlation between berthing velocity and the size of a vessel, this dependency could not be confirmed in this study. By contrast, the results show that berthing velocities depend on the berthing policy, which indirectly includes the influence of the type of landing procedure, the experience of pilots and captains and the use of tug assistance or docking aid systems. Furthermore, no evidence was found that berthing velocity is greatly affected by the vessels' draft, the type of vessel, the wind speed or the under-keel clearance.

The maximum tolerable berthing velocity depends on the prescribed reliability target, the influence of the berthing impact force on the failure mode being evaluated and the variation expected in the berthing velocities of individual arrivals. In addition, the berthing frequency and the reference period play an important role. However, none of these aspects

is yet explicitly taken into account in the methods presently in use to assess berthing impact loads. This thesis therefore offers a new formula Eq. (97), based on a Weibull distribution fit, which can be used to customise design values for berthing velocity aiming for a specific reliability target. On the basis of both the data available and this formula, a generic set of partial factors of safety has been determined for favourable and unfavourable navigation conditions in accordance with the reliability requirements of NEN-EN 1990 (2011).

When assessing berthing impact loads acting on existing quay walls, a lower target reliability level will generally be required than for new structures, the actual berthing frequency can be estimated more accurately and the reference period will be shorter. As a result, a lower partial factor of safety can be applied to the characteristic berthing velocity, which makes it possible to allow larger vessels to berth onto existing fender systems or to extend their service life.

6.3 RECOMMENDATIONS

6.3.1 RELIABILITY TARGETS AND FAILURE CONSEQUENCES

1) Allocate appropriate target reliability indices

Since reliability methods have become more robust and efficient, it is expected that they will be used more frequently. However, it is quite remarkable that less effort has been put into customising target reliability indices for different types of civil engineering works. Consequently, the results of advanced reliability-based assessments have to be compared with fairly general reliability targets, which were derived predominantly for buildings. It is therefore recommended that design codes and standards, such as ISO 2394 (2015) and the Eurocodes (NEN-EN 1990, 2011), be improved in order to allocate appropriate reliability targets for quay walls and other civil engineering works.

In addition, this thesis has shown that it is more practical to use annual target reliability indices when assessing existing quay walls, since otherwise an iterative procedure to determine the quay wall's remaining lifetime will be required. In the case of new quay walls, however, the reference period is known. Consequently, both annual or lifetime reliability indices can be used in the design of quay walls. Furthermore, in literature it is often not very clear whether targets are assigned to the structure as a whole or to structural components. Since quay-wall systems are fairly long structures, it is recommended that there be a focus on component reliability and the associated failure consequences. However, quay walls that are part of a larger system, such as a primary flood-defence system, should take account of the length effect (Calle & Spierenburg, 1991; Janssen, 2012; Roubos & Grotegoed, 2014; STOWA, 2011; TAW, 2003) in order guarantee the reliability of the system.

2) Classify all marine structures in a port

Allocating an appropriate reliability class is crucial to prevent service-proven structures from being unjustly condemned. In this thesis, it has been found that unavailability of a single berth generally results in fairly low indirect economic damage for ports and terminals. However, there are also special berths that may influence the performance of several other terminals or companies. It is therefore recommended that all berths in a port be consciously classified and that functional redundancy in the port be assessed when a berth is temporarily unavailable. Moreover, as revealed by natural disasters in Japan (Iai et al., 1996), the efficiency of the recovery of the port and its hinterland must also be considered in the classification of berths, e.g. by investing in the ability of port infrastructure to withstand severe earthquakes, tsunamis and/or other disasters (OCDI, 2009). From these perspectives, a higher reliability class can be assigned strategically.

3) Develop a database and a model to describe quay-wall failures

The damage that occurs when a quay wall is temporarily unavailable or collapses plays an important role in defining an acceptable reliability target. Predicting direct and indirect impacts, such as social consequences and damage to the reputation of a port, is often beyond the expertise of engineers. In addition, records of actual quay-wall failures are lacking. This thesis has shown that the failure consequences may differ considerably depending on the failure mode. Presently, neither a database with past failures nor a model is available to accurately predict social and economic repercussions. It is therefore recommended that such a database be developed, along with a damage estimation model targeted at a better understanding of the causes and consequences of failure in order to determine custom reliability targets for critical structural members or failure modes. This will prevent erroneous conclusions based on excessively generic criteria, e.g. the conclusion that a quay wall has insufficient reliability or needs to be replaced when in fact it meets all relevant requirements.

6.3.2 REDUCING UNCERTAINTY IN STRENGTH

4) Develop methods to account for past performance

This thesis has shown that uncertainty in the soil-structure interaction greatly influences the reliability of quay walls. Since local soil conditions differ, it is recommended that a soil-structure interaction log be developed for all new quay walls; this should include sensor-based information about the quay walls' structural response to loading, e.g. by measuring deformations, water levels and anchor forces. Doing so will shed new light on model uncertainty and the actual strength of a quay wall. In addition, it is particularly recommended that the variability in and correlations between soil properties be investigated. In this context,

it is important to realise that what is relevant is not the point-to-point variation, but rather the uncertainty in the average strength of a soil layer associated with the soil volumes affected by the different failure modes. By reducing these uncertainties, it is expected that the functionality of many quay walls can be enhanced, e.g. by allowing bigger vessels to berth or the installation of larger cranes.

Many existing quay walls in the port of Rotterdam are in good condition and have a successful service history. However, they regularly do not comply with modern code requirements developed for new structures. The main reason for this is that these guidelines do not yet account for past performance, and hence neglect the decrease in epistemic uncertainty. It is therefore recommended that further study of this effect on quay-wall reliability be carried out, taking degradation into consideration, and also that new design guidance for the assessment of existing quay walls be developed.

Based on the findings of this thesis, it appears that the early application of a test load close to the maximum design load directly after completion of new quay walls can be an effective strategy to increase their reliability during their remaining service life. It is therefore recommended that the effectiveness of a test load in such a pre-posterior analysis be investigated. If the outcomes are favourable, full-scale test protocols for new quay walls should be developed. In addition, it is recommended that a test procedure be developed to increase the functionality of existing quay walls by gradually applying a well-controlled test load and simultaneously logging the associated quay-wall behaviour – for instance, deformations and strains. In this case, the quay wall would not be tested until failure in order to maintain the structure after the test. Another option is to test a quay wall nominated for replacement in the near future until failure. Yet another is to develop a quay wall fully equipped with sensors dedicated to testing.

5) Modelling corrosion-induced degradation

The quay-wall monitoring system (KMS) used by the Port of Rotterdam Authority presently assesses the stresses in single structural members subject to corrosion-induced degradation, such as the king piles of a combi-wall system. It is worth noting that KMS includes corrosion curves, which were developed from millions of wall-thickness measurements (Jongbloed, 2019). These curves enable the Port of Rotterdam Authority to manage the relatively high coefficient of variation in wall-thickness measurements. It is therefore recommended that other port authorities also start measurement campaigns and develop a similar method to take corrosion induced degradation into consideration. This thesis, however, has found that quay walls generally ensure redistribution of structural forces. As a result, it is almost impossible that a single member will display yielding or buckling. This redistribution has not yet been included in KMS. While KMS already distinguishes between different corrosion zones across the height of the combi-wall, spatial variation of these zones along the quay

wall is not yet taken into consideration. It is therefore recommended that horizontal correlation lengths of the distinctive corrosion zones be subject to further study. Both these factors show that the current version of KMS is conservative and most likely underestimates the actual structural capacity of steel combi-walls subject to pitting corrosion.

6.3.3 REDUCING UNCERTAINTY IN LOADS

6) Perform reliability-based assessments for quay walls subject to earthquakes and large tidal differences

The methods developed in this thesis have been applied successfully to the quay walls in the port of Rotterdam. However, this port has a relatively favourable geographical location with regard to earthquakes and tidal loads. It is therefore recommended that the results and conclusions be verified in other load environments, since it is not yet possible to exclude the possibility that time-independent loads also dominate the failure modes of quay walls subject to earthquakes and/or extreme water heads. If such loads do heavily influence quay-wall reliability, then it is likely that another set of safety factors will apply to these structures.

7) Manage and predict accidental load combinations

When assessing existing quay walls, partial factors of safety applied to characteristic values of loads are generally reduced. However, clear guidance on how to deal with extreme loads, such as accidental load combinations for which the partial factors in the original design are already equal to one, is still lacking. It may therefore be that an existing structure complies with these standards but nevertheless is unable to withstand accidental load combinations. If engineers blindly follow the existing standards, they may create dangerous situations. It is therefore recommended that code writers revise these standards by explicitly addressing how to deal with accidental load combinations.

Although this thesis has found that failure modes exhibit warning signals, it is recommended that port authorities be alert to the potential functional misuse of quay walls while they are subject to extreme environmental conditions, such as a very low outer water level. In this context, it is recommended that quay-wall deformations be verified regularly, along with the functioning of the drainage system and the presence of scour, and also that visual checks for overloading be performed prior to such extreme conditions (or that quay walls be equipped with sensors to measure the terminal loads). Predicting accidental load combinations seems possible when real-time data is available and is coupled to predictive models.

8) Start collecting berthing records of inland barges

Several guidelines include design values for the berthing velocity of inland vessels. However, these values are inconsistent and it is unclear how they were derived. As there are many

berths for inland barges throughout the world, it is recommended that measurement campaigns be started to collect up-to-date data. Ideally, a new PIANC working group should start collecting these measurements throughout the world. It is likely that the landings of inland barges will also be influenced by human behaviour, and it is therefore recommended that work be undertaken to reveal the extent to which captains' behaviour can be influenced in this regard – for instance, by showing the maximum permissible berthing velocity on a display.

9) *Statistically examine mooring loads*

During its service life, one frequently asked question is whether larger vessels may be allowed to berth onto an existing quay wall. At multiple berths in the port of Rotterdam, mooring loads are already registered. However, this data is not yet used to assess the reliability of quay walls; moreover, it could also be used to optimise or validate the models used for performing static and dynamic mooring analyses. In addition, specific safety factors for mooring loads can be determined by statistically examining the data available. It is therefore recommended that examining mooring loads be the subject of further study. A second recommendation is to equip bollards and quick release hooks with sensors to receive real-time information, which would make it possible to predict whether a dangerous situation might arise by using the available data from wind and/or vessel-traffic models. It is expected that these suggestions will enhance the functionality (e.g. larger ships at higher wind speeds) of marine structures as well as the safety within a port.

6.4 RELEVANCE AND IMPLICATIONS

In addition to presenting its scientific results, this thesis has devoted particular attention to the implementation of its main findings and the methods developed in order to ensure that its outcomes benefit both industry and society, e.g. port and terminal authorities, engineers, asset managers and code writers. Consequently, it has proposed practically applicable formulas, new methods and concrete recommendations to improve design guidance, and these have already been implemented in revisions of national and international design guidelines. The formula derived in [Chapter 5](#) to establish customised design values for berthing velocity based on field measurements has been included in the PIANC guideline *Berthing velocities analysis of seagoing vessels over 30 kDWT* (PIANC, 2019) and in the design manual *Flexible Dolphins* (Roubos, 2018). Moreover, this formula has already been used by the Port of Rotterdam Authority to make better use of existing marine structures by allowing larger vessels to berth onto existing facilities. Furthermore, based on the main findings of this thesis specific recommendations have been written for the allocation of

reliability targets to marine structures, and these are now included in the Dutch annex of NEN-EN 1990 (2019) as well as in the design manuals *Quay Walls* (De Gijt & Broeken, 2018), *Jetties and Wharfs* (Broeken, 2018) and *Flexible Dolphins* (Roubos, 2018).

In collaboration with the firm Plaxis, the reliability interface ProbAna[®] has been developed to calculate the reliability of a quay wall in a finite element environment. Since January 2017, a commercial version of this interface has been available (Laera & Brinkgreve, 2017); it is now used to assess not only quay walls, but also hydraulic structures and the Dutch primary flood-defence system. Due to the robustness and efficiency of this interface, the practical application of finite-element-based reliability assessments has increased considerably.

Another finding of this thesis – the lack of correlation between the size of a vessel and its berthing velocity – has led to a reconsideration of the historically embedded berthing velocity curves developed by Brolsma (1977), which have been used since 1977 in the design of maritime constructions throughout the world. In this regard, the new working group PIANC WG211 will review the recommendations presently used for assessing berthing energy and the associated berthing impact force (PIANC, 2019). Furthermore, during this research no background documents or berthing velocity measurements were found to support the design recommendations' current values for inland barges, which immediately led Rijkswaterstaat (the Dutch national public works agency) and the Port of Rotterdam Authority to start new measurement campaigns.

By illuminating the aspects that influence quay walls' reliability, this thesis has discovered new opportunities to make better use of these structures. The Port of Rotterdam Authority is now using these insights to optimise its monitoring programme and to perform specific tests on its quay walls. New ideas have also arisen to increase the functionality of existing quay walls and jetties by applying structural modifications (Schutte, 2017). By contrast, it seems possible to optimise the functionality of existing quay walls, such as by deepening berths or installing larger cranes, without structural adjustments. Based on the results of this thesis, it is expected that the nautical guaranteed depth (NGD) and operational loads of quay walls in Rotterdam can be increased by approximately 0.5-1.0 metres and 10-20%, respectively. A further increase would be inappropriate, because then the ability of a quay wall to withstand accidental load combinations would be insufficient. It should, however, be noted that searching for operational limits with regard to safety is not without risks and also requires additional efforts to prevent overloading and functional misuse.

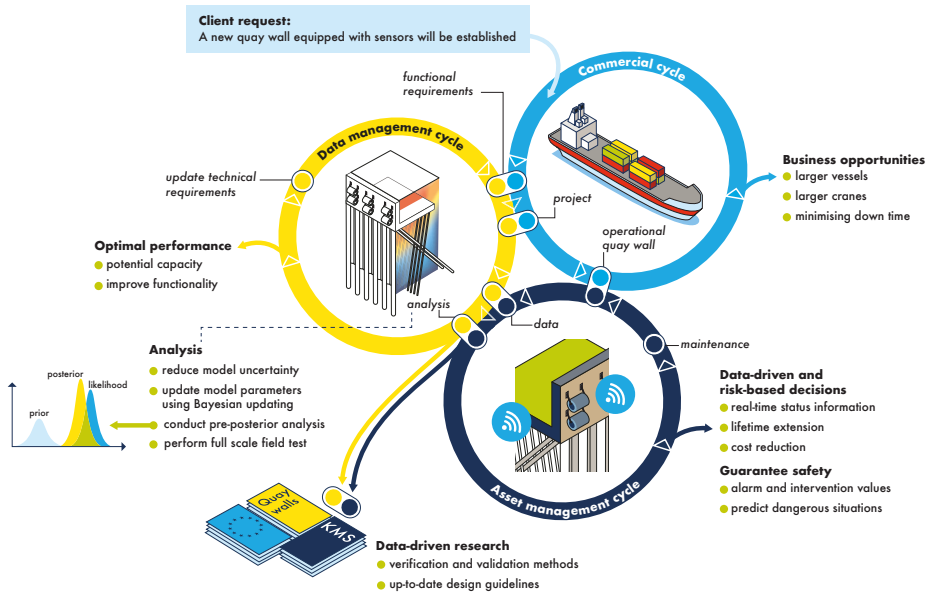


Fig. 6.1. Optimising functionality, maintenance and guidelines using quay-wall data

Since quay walls are increasingly equipped with sensors, a great deal of data has become available. This can serve as input for the methods developed in this thesis, thus facilitating predictive modelling and fostering reliability and safety. Fig. 6.1 shows how port authorities or terminals can make better use of sensor data and reliability-based assessments by distinguishing and connecting commercial, asset-management and data-management cycles. In the asset-management cycle, sensor data allows us to lay foundations for data-driven and risk-based decisions to optimise the required maintenance. In addition, data-driven information will enable us to continuously improve our understanding of quay walls and can be used in the application of Bayesian updating. In the data-management cycle, data analytics in combination with finite element models can be used to update the functional requirements of a specific quay wall, which boosts the commercial cycle, e.g. by creating new business opportunities. Furthermore, data-driven research is of the utmost importance to maintain design guidelines and to validate new methods.

In summary, the methods developed in this thesis enable reliability-based assessments of quay walls. However, it is of the utmost importance that engineers do not rely solely on these advanced methods, and keep using their engineering sense and expert judgement as well.

REFERENCES

- Abdo, T., & Rackwitz R. (1991), *A New Beta-Point Algorithm for Large Time-Invariant and Time-Variant Reliability Problems*. Munich, Germany.
- Adel, N. (2018), *Load Testing of a Quay Wall: An Application of Bayesian Updating*. MSc thesis. Delft, The Netherlands: Delft University of Technology.
- Allaix, D., Steenbergen, R. D. J. M., & Wessels, J. F. M. (2017), *Target Reliability Levels for the Design of Quay Walls*. Delft, The Netherlands: TNO.
- Allaix, D., Steenbergen, R. D. J. M., & Wessels, J. F. M. (2018), *Target Reliability Levels for Existing Quay Walls*. Delft, The Netherlands: TNO.
- Andrianov, G., Burriel, S., Cambier, S., Dutfoy, A., Dutka-Malen, I., Rocquigny, E. de, Sudret, B., Benjamin, P., Lebrun, R., Mangeant, F., & Pendola, M. (2007), Open TURNS, an open source initiative to Treat Uncertainties, Risks 'N Statistics in a structured industrial approach. *Proceedings of the European Safety and Reliability Conference 2007, ESREL 2007 – Risk, Reliability and Societal Safety 2*.
- Armijo, L. (1966), Minimization of Functions Having Lipschitz Continuous First-Partial Derivatives. *Pacific J. Math* 16, pp. 1-3.
- Ang, A. H. S., & De Leon, D. (1997), Determination of Optimal Target Reliabilities for Design and Upgrading of Structures. *Structural Safety* 19, pp. 91-103.
- Arangio, S. (2012), Reliability Based Approach for Structural Design and Assessment: Performance Criteria and Indicators in Current European Codes and Guidelines. *Int. J. Lifecycle Performance Engineering* 1, pp. 64-91
- ASCE 7-10 (2010), *Minimum Design loads for buildings and other structures*.. Reston, USA: American Society of Civil Engineers. ISBN 978-0-7844-1085-1
- Bakker, K. J. (2000), *Soil Retaining Structures*. Doctoral thesis. Delft, The Netherlands: Delft University of Technology. ISBN 9058093204.
- Beckett Rankine (2010), *Berthing Velocities and Brotsma Curves*. London, United Kingdom: Beckett Rankine.
- Berg, van der J. W., Seesing, B. A. S., Greef J., Jaspers Focks, D. J., & Quist, P. (2018), *Quay Wall of the Future: Comparison report*. Rotterdam, The Netherlands: Smartport. RT780-49/18-007.302.
- Bezih, K., Chateauneuf, A., Kalla, M., & Bacconnet, C. (2015), Effect of soil-structure interaction on the reliability of reinforced concrete bridges. *Ain Shams Engineering Journal* vol. 6, pp. 755-766.
- Bhattacharya, B., Basu, R., & Ma, K. (2001), Developing target reliability for novel structures: the case of the Mobile Offshore Base. *Marine Structures* 14, pp. 37-58.
- Blum, H. (1931), *Einspannungsverhältnisse bei Bohlwerken*. Berlin, Germany: W. Ernst und Sohn.
- Böckmann, J., & Grünberg, J. (2009), Determination of safety levels for quay wall structures. *Proceedings of the 7th International Probabilistic Workshop*, pp. 327-341.

- Boero, J., Schoefs, F., Yanez-Godoy, H., & Capra, B. (2012), Time-function reliability of harbour infrastructures from stochastic modelling of corrosion. *European Journal of Environmental and Civil Engineering* 16, pp.1187-1201.
- Bötger, E., & Linde, A. (2014), Verschillende perspectieven op de nieuwe waterveiligheidsnormen. Utrecht, The Netherlands.
- Bochen, D. (2012), *Berthing velocities and fender design*. Delft, The Netherlands: UNESCO-IHE.
- Broeken, M. L. (2018), *Jetties & Warfs*. Delft, The Netherlands: CROW. ISBN 978-90-5367-657-8
- Brolsma, J. U., Hirs, J. A., & Langeveld, J. M. (1977), *Paper on Fender Design and Berthing Velocities*. Leningrad, USSR, PIANC World Congress.
- BS 6349-1-2 (2016), *Maritime Works: General – Code of Practice for Assessment of Actions*. London, United Kingdom. ISBN 978-0-580-76229-1.
- BS 6349-4 (2014), *Maritime Works: Code of Practice for Design of fendering and Mooring Systems*. London, United Kingdom. ISBN 978-0-580-66969-9.
- BS 6349-2 (2010), *Maritime Works – Part 2: Code of Practice for the Design of Quay Walls, Jetties and Dolphins*. London, United Kingdom. ISBN 978-0-580-73243-0
- Buijs, F. A., Hall, J. W., Sayers, P. B., & Van Gelder, P. H. A. J. M. (2009), Time-dependent reliability analysis of flood defences. *Reliability Engineering & System Safety* 94. pp. 1942-1953.
- Buijs, F. A., Sayers, P. B., Hall, J. W., & Van Gelder, P. H. A. J. M. (2009), *Time-Dependent Reliability Analysis of Anchored Sheet Pile Walls*. Flood Risk Management: Research and Practice. London, United Kingdom: Taylor & Francis Group. ISBN 978-0415485074.
- Buijsingh, P. (2013), *ALARP Guide*. Rijswijk, The Netherlands: Shell. SR.13.14005
- Burkhardt, E., & Matakis, K. (2013), Collection of Berthing Velocities and Resulting Design Recommendations by PIANC Working Group MarCom 145. *ASCE Ports 2013*, pp. 670-678.
- Calle, E. O. F., & Spiereburg, S. E. J. (1991), *Veiligheid van damwandconstructies – Onderzoeksrapportage deel 1, for CUR committee C69*. Delft, The Netherlands: Deltares, report CO-31690/12
- Cherubini, C. (1999), Probabilistic approach to the design of anchored sheet pile walls. *Computers and Geotechnics* 26, pp. 309-330.
- Chryssanthopoulos, M. K., Janssens, V., & Imam, B. (2011), *Modelling of Failure Consequences for Robustness Evaluation*. London, United Kingdom: IABSE-IASS Symposium – Taller, Longer, Lighter.
- Cho, S. E. (2007), Effects of spatial variability of soil properties on slope stability. *Engineering Geology* 92, pp. 97-109.
- Cork, S., & Chamberlain, N. (2015), *CIRIA C746: Old Waterfront Walls*. London, United Kingdom. ISBN 978-0860177517.
- Cornell, C. A. (1969), A probability-based structural code. *ACI Journal* vol. 66, pp. 974-985.

References

- Courage, W. M. G., & Steenbergen, H. M. G. M. (2007), *Prob2B™: Variables, Expressions and Excel® Installation, and Getting Started*. Delft, The Netherlands.
- CUR 190 (2000), *Kansen in de civiele techniek – Deel 1: probabilistisch ontwerpen in theorie*. Gouda, The Netherlands: CUR. ISBN 9037601022.
- Das, M. R., & Das, S. K. (2010), Reliability based optimum design of sheet pile wall using a simple optimization tool. *Indian Geotechnical Conference*. Mumbai, India.
- Diamantidis, D. (2017), A Critical View on Environmental and Human Risk Acceptance Criteria. *International Journal of Environmental Science and Development* vol. 8, no. 1, pp. 62-68.
- DNV (1992), *Structural Reliability Analysis of Marine Structures*. Høvik, Norway: Det Norske Veritas. Classification notes NO. 30.6.
- Eijk, R. A. van der (2011), *Design Report: Quay Wall for a New Bulk Terminal at Maasvlakte Rotterdam*. Rotterdam, The Netherlands: Port of Rotterdam Authority.
- Faber, M. H., & Virguez-Rodríguez, E. (2011), Supporting decisions on global health and life safety investments. *Applications of Statistics and Probability in Civil Engineering – Proceedings of the 11th International Conference on Applications of Statistics and Probability in Civil Engineering*, pp. 434-443.
- Fenton, A. G., Naghibi, F., Dundas, D., Bathurst, J., & Griffiths D. V. (2016), Reliability-based geotechnical design in 2014 Canadian Highway Bridge Design Code. *Canadian Geotechnical Journal* 53, pp. 236-251.
- Fischer, K., Barnardo-Viljoen, C., Faber, M. H. (2012), Deriving target reliabilities from the LQI. *LQI Symposium in Kgs. Lyngby*, Denmark.
- Fischer, K., & Faber, M. H. (2012), The LQI acceptance criterion and human compensation costs for monetary optimization – a discussion note. *LQI Symposium in Kgs. Lyngby*, Denmark.
- Fischer, K., Virguez, E., Sánchez-Silva, M., & Faber, M. H. (2013), On the assessment of marginal life saving costs for risk acceptance criteria. *Structural safety* 44, pp. 37-46.
- Franks, A. (2017), *A Simplified Approach to Estimating Individual Risk*. Westbrook, United Kingdom: Amy Vectra Ltd.
- Gaba, A., Hardy, S., Doughty, L., Powrie, W., Selemetas, D., & Skanska. C. (2017), *C760 Guidance on Embedded Retaining Wall Design*. London, United Kingdom: CIRIA. ISBN 978-0860177647.
- Gijt, J. G. de, (2010), *A History of Quay Walls*. The Hague, The Netherlands. ISBN 9789059810327.
- Gijt, J. G. de, & Vinks, R. (2011), Cost of quay walls including life cycle aspects. *MTEC Singapore, Proceedings of the International Maritime-Port Technology and Development Conference*, pp. 135-139.
- Gijt, J. G. de, (2003), *Quay Walls, First Edition*. Gouda, The Netherlands: SBRCURnet. ISBN 0415364396.
- Gijt, J. G. de, & Broeken, M. L. (2013), *Quay Walls, Second Edition*. Delft, The Netherlands: SBRCURnet. ISBN 987-1138000230.

- Gijt, J. G. de, & Broeken, M. L. (2018), *Errata – Quay Walls, Second Edition*. Delft, The Netherlands: SBRCURnet.
- Grabe, J. (2012), *Recommendations of the Committee for Waterfront Structures, Harbours and Waterways EAU 2012*, ninth edition. Hamburg, Germany. ISBN 978-3433031100.
- Grave, P. (2002), *Validation Partial Factors from 'Probabilistic Analysis' Sheet Pile Walls*. Delft, The Netherlands: Delft University of Technology.
- Gulvanessian, H., & Holický, M. (2005), Eurocodes: using reliability analysis to combine action effects. *Structures & Buildings* 158, pp. 243-252.
- Hall, W. B. (1988), Reliability of service-proven structures. *Structural Engineering* 114, pp. 608-624.
- Hannink, G. (2008), *Van onzekerheid naar betrouwbaarheid: Handreiking voor geotechnisch ontwerpers*. Gouda, The Netherlands. ISBN 978-90-376-0509-9.
- Hasofer, A. M., & Lind N. C. (1974), An exact and invariant first order reliability format. *J. Eng. Mech. Div. ASCE* 100, pp. 111-121.
- Health and Safety Executive (2001), *Reducing Risks, Protecting People*. Norwich, United Kingdom: HSE. ISBN 0-7176-2151-0.
- Health and Safety Executive (2009), *Societal Risk: Initial Briefing to Societal Risk Technical Advisory Group*. Norwich, United Kingdom: HSE.
- Hein, C. (2014), *Berthing velocity of large container ships*. San Francisco, USA: PIANC World Congress.
- Hoesch (1977), *Spundwand-Handbuch Berechnung*. Dortmund, Germany: Hoesch.
- Holícký, M. (2011), The target reliability and design working life. *Safety and Security Engineering IV*, pp. 161-169.
- Houyoux, C., Alberts, A., Heeling, A., Benaissa, B., & De Cristofaro, N. (2007), *Design Method for Steel Structures in Marine Environment Including the Corrosion Behaviour*. European Commission Report EUR22433EN. ISBN 927903768.
- Huijzer, G. P., & Hannink, G. (1995), The construction of parameterized subsurface models. *Proceedings, Eleventh European Conference on Soil Mechanics and Foundation Engineering*. Copenhagen, Denmark.
- Huijzer, G.P. (1996), *Eindrapport probabilistische analyse damwand constructies*. Rotterdam, The Netherlands: Port of Rotterdam Authority.
- Iai, S., Ichii, K., & Morita, T. (1996), *Analysis of damage to Quay Walls during 1995 Great Hanshin Earthquake, Japan*. Yokosuka, Japan: Eleventh World Conference on Earthquake Engineering. ISBN 0080428223.
- ISO 2394 (1998), *General Principles on Reliability for Structures*. Geneva, Switzerland: International Organisation for Standardisation.
- ISO 2394 (2015), *General Principles on Reliability for Structures*. Geneva, Switzerland: International Organisation for Standardisation.

References

- ISO 13822 (2010), *Bases of Design of Structures – Assessment of Existing Structures*. Geneva, Switzerland: International Organisation for Standardisation.
- Janssen, H. L. (2012), *CUR 166: Sheet Pile Walls, Sixth edition*. Gouda, The Netherlands: SBRCURnet. ISBN 9037600368.
- JCSS (2001), *Probabilistic Model Code, Part 1*. Joint Committee on Structural Safety, www.jcss.byg.dtu.dk.
- Jiang, P., Basudhar, A., & Missoum, S. (2011), Reliability assessment with correlated variables using support vector machines. *52nd AIAA/ASME/ASCE/AHS/ASC Structures, Structural Dynamics and Materials Conference – Proceedings*.
- Johansen, I.L. (2010), *Foundations and Fallacies of Risk Acceptance Criteria*. NTNU. ISBN 978-82-7706-2281
- Jong, S. (2018), *Technical Report: Corrosion and Pitting on Quay Structures*. Rotterdam, The Netherlands: Port of Rotterdam Authority.
- Jongbloed, B. P. (2008), *End Report: Causes of Corrosion in the Port of Rotterdam*. Rotterdam, The Netherlands: City of Rotterdam.
- Jongbloed, B. P. (2019), *From Inspection to Prediction of Corrosion-Induced Degradation of Quay Walls in Port of Rotterdam*. Rotterdam, The Netherlands: Port of Rotterdam Authority.
- Jongejan, R. (2008), *How Safe is Safe Enough? The Government's Response to Industrial and Flood Risks*. Delft, The Netherlands: Delft University of Technology.
- Jongejan, R., Jonkman, S. N., & Maaskant, B. (2009), The potential use of individual and societal risk criteria within the Dutch flood safety policy (part 1): Basic principles. *Reliability, Risk and Safety: Theory and Applications, Proceedings from ESREL 2009*.
- Jonkman, S. N., Jongejan, R., & Maaskant, B. (2011), The Use of Individual and Societal Risk Criteria Within the Dutch Flood Safety Policy – Nationwide Estimates of Societal Risk and Policy Applications. *Risk Analysis* 31, pp. 282-300.
- Jonkman, S. N., Gelder P. H. A. J. M. van, & Vrijling J. K. (2003), An overview of quantitative risk measures for loss of life and economic damage, *Journal of Hazardous Materials* A99, pp. 1-30.
- Jonkman, S. N., & Schweckendiek, T. (2015), Developments in Levee Reliability and Flood Risk Analysis in the Netherlands. In: Schweckendiek, T., et al. (eds.), *Geotechnical Safety and Risk V*. IOS Press. ISBN 978-1-61499-579-1
- Jonkman, S. N., Steenbergen, R. D. J. M., Morales-Nápoles, O., Vrouwenvelder, A. C. W. M., & Vrijling, J. K. (2015), *Probabilistic Design: Risk and Reliability Analysis in Civil Engineering*. Delft, The Netherlands.
- Johnston, R. (2010), *Structural Reliability of Retaining Walls Designed to AS 4678 for Permanent, Imposed and Seismic Loads*. Sydney, Australia.
- Karamperidou, A. (2018), *Parametric Analysis of Quay Walls with Relieving Platform by Means of Elastic Supported Beam and Finite Element Method*. MSc thesis. Delft, The Netherlands: Delft University of Technology.

- Kolios, A., Srikanth, S., & Salonitis, K. (2014), Numerical simulation of material strength deterioration due to pitting corrosion. *Procedia CIRP* 13, pp. 230-236.
- Kubler, O. (2006), *Applied Decision-Making in Civil Engineering*. Zurich, Switzerland.
- Kunz, C. (2015), Ein Konzept für Teilsicherheitsbeiwerte für bestehende Wasserbauwerke. *Bautechnik* 92, pp. 549-556.
- Leatemia, F. L., & Heijndijk, P. (1998), *Design Guideline: Quay Walls, Port of Rotterdam*. Rotterdam, The Netherlands.
- Lebrun, R., & Dutfoy, A. (2009a), A generalization of the Nataf transformation to distribution with copula. *Probabilistic Engineering Mechanics* 24, pp. 172-178.
- Lebrun, R., & Dutfoy, A. (2009b), Do Rosenblatt and Nataf isoprobabilistic transformation really differ? *Probabilistic Engineering Mechanics* 24, pp. 577-584.
- Laera, A., & Brinkgreve, R. B. J. (2017), *Plaxis Probabilistic Analyses 2017; ProbAna*. Delft, The Netherlands: Plaxis bv.
- Lemaire, M. (2009), *Structural Reliability*. London, United Kingdom: Wiley. ISBN 978-1848210820.
- Lentz, A. (2007), Acceptability of civil engineering decisions involving human consequences. Munich, Germany: Technical University of Munich.
- Leonardo da Vinci Pilot Project (2005), *Implementation of Eurocodes – Handbook 2 – Reliability Backgrounds*. Prague, Czech Republic. CZ/02/B/F/PP-134007.
- Leveson, N. (2004), New Accident Model for Engineering Safer Systems. *Safety Science* 42, pp. 237-270.
- Ligtvoet, A., & Lei, T. van der, (2012), *Analyse bedrijfswaarden HbR*. Delft, The Netherlands: Delft University of Technology.
- Lindenberg, J. (2008), *Van onzekerheid naar betrouwbaarheid: Handreiking voor geotechnisch ontwerpers*. Gouda, The Netherlands: CUR. ISBN 978-9037605099.
- Liu, P. L., & Der Kiureghian, A. (1990), Optimization algorithms for structural reliability. *Structural Safety* 9, pp. 161-177.
- Losada, M., & Benedicto, M. (2005), Target Design Levels for Maritime Structures. *J. Waterway, Port, Coastal, Ocean Eng.*, pp. 171-180.
- Low, B. K., & Phoon, K. K. (2002), Practical first-order reliability computations using Spreadsheet. *Probabilistics In Geotechnics*. Graz, Austria.
- Luenberger, D. G. (1986), *Introduction to Linear and Nonlinear Programming*. Stanford, USA: Springer. ISBN 978-0387745022
- Lunne, T., Robertson, P. K., & Powell, J. J. M., (1997), *Cone Penetration Testing in Geotechnical Practice*. London, United Kingdom: E & FN Spon Press. ISBN 978-0419237501.

References

- Makhdoumi, H., Keshtegar, B., & Sahahraki, M. (2017), A comparative study of first-order reliability method-based steepest descent search directions for reliability analysis of steel structures. *Advances in Civil Engineering* 2017.
- Manoj, N. R. (2017), *Reliability-Based Ultimate Limit State Design in Finite Elements and Compliance with Eurocode 7*. Delft, The Netherlands: Delft University of Technology.
- McCann, M. W., & Paxson, G. (2016), Uncertainty in dam failure consequence estimates. *FLOODrisk 2016 – Third European Conference on Flood Risk Management*. eISSN: 2267-1242
- Melchers, R. E. (1999), Corrosion uncertainty modelling for steel structures. *Journal of Constructional Steel Research* 52, pp. 3-19.
- Melchers, R. E., & Jeffrey, R. J. (2008), Probabilistic models for steel corrosion loss and pitting of marine infrastructure. *Reliability Engineering and System Safety* 93, pp. 423-432.
- Melchers, R. E., & Wells, T. (2006), Models for the anaerobic phases of marine immersion corrosion. *Corrosion Science* 48, pp. 1791-1811.
- Melchers, R. E., Jeffrey, R. J., & Usher, K. M., (2014), Localized corrosion of steel sheet piling. *Corrosion Science* 79, pp. 139-174.
- Melchers, R. E. (2015), Long-term immersion corrosion of steels in seawaters with elevated nutrient concentration. *Corrosion Science* 81, pp. 110-116.
- Melchers, R. E., & Beck, A. J., (2018), *Structural Reliability Analysis and Prediction*. Wiley. ISBN 978-1119266075.
- Melchers, R.E. (2007), Structural reliability theory in the context of structural safety. *Civil Engineering and Environmental Systems* 24, pp. 55-96.
- Metzger, A.T., Hutchinson, J., & Kwiatkowski, J. (2014), Measurement of marine vessels berthing parameters. *Marine Structures* 39, pp. 350-372.
- Nagao, T., Watabe, Y., Kikuchi, K., & Honjo, Y. (2009), Recent revision of Japanese Technical Standard for Port and Harbour Facilities based on a performance based design concept. *Geotechnical Risk and Safety*, pp. 39-47. London. United Kingdom.
- NEN-EN 1990 (2011), *Eurocode – Basis of Structural Design*. Brussels, Belgium: European Committee for Standardisation.
- NEN-EN 1990 (2019), *Eurocode – Basis of Structural Design + Dutch Appendix*. Delft, The Netherlands: Netherlands Standardisation Institute. ICS 91.010.30; 91.080.01.
- NEN-EN 1993-1 (2011), *Eurocode 3: Design of Steel Structures – Part 1-1: General Rules and Rules for Buildings*. Brussels, Belgium: European Committee for Standardisation.
- NEN-EN 1993-5 (2007), *Eurocode 3: Design of Steel Structures – Part 5: Piling*. Brussels, Belgium: European Committee for Standardisation.
- NEN-EN 1997 (2004), *Eurocode 7: Geotechnical Design – Part 1: General Rules*. Brussels, Belgium: European Committee for Standardisation.

- NEN-EN 1998-1 (2004), *Design of Structures for Earthquake Resistance - General Rules, Seismic Actions and Rules for Buildings*. Brussels, Belgium: European Committee for Standardisation.
- NEN-9997-1 (2016), *National Annex, Eurocode 7: Geotechnical Design – Part 1: General Rules*. Delft, The Netherlands: NEN. ICS 91.080.01.
- NEN-EN 10029 (2010), *Hot-Rolled Steel Plates 3 mm Thick or Above – Tolerances on Dimensions and Shape*. Brussels, Belgium: European Committee for Standardisation.
- NEN 6700 (2005), *Technische grondslagen voor bouwconstructies – TGB 1990 – Algemene basiseisen*. Delft, The Netherlands. ICS: 91.080.01.
- NEN-EN 8700 (2011), *Basis of Structural Assessment of Existing Structures – Buildings: The Minimum Safety Level*. Delft, The Netherlands: NEN.
- Nocedal, J., & Wright, S. J. (2000), *Numerical Optimization*. New York, USA: Springer. ISBN 0387303030.
- Norme Tecniche per le Costruzioni (2008), *Infrastrutture*. Rome, Italy: NTC.
- NORSOK Z-013N (2001), *Risk and Emergency Preparedness Analysis* Norsok Standard. Oslo, Norway.
- OCDI (2009), *Technical Standards and Commentaries for Port and Harbour Facilities in Japan*. Tokyo, Japan: The Overseas Coastal Area Development Institute.
- Osório, P., Odenbreit, P., & Vrouwenvelder, T. (2010), Structural reliability analysis of quay walls with sheet piles. *PIANC MMX Congress*. Liverpool, United Kingdom.
- Paltrinieri, N., & Khan, F. (2016), *Dynamic Risk Analysis in the Chemical and Petroleum Industry: Evolution and Interaction with Parallel Disciplines in the Perspective of Industrial Application*. Elsevier. ISBN 9780128037652.
- Peters, D. J., Sadowski, A., Rotter, M., & Taras, A. (2017), Calibration of Eurocode design models of thin-walled cylinder under bending with full scale tests. *Eurosteel 2017* 1, pp. 3729-3740. Copenhagen, Denmark.
- Phoon, K. K., & Kulhawy, F. H. (1999), Characterization of geotechnical variability. *Canadian Geotechnical Journal* 36. pp. 612-624.
- Phoon, K. K., & Retief, J. V. (2016), *Reliability of Geotechnical Structures in ISO239*. CRC Press. ISBN 978-1138029118.
- PIANC (2002), *Guideline for Design of Fender Systems*. Brussels, Belgium: PIANC. ISBN-2-87223-125-0
- PIANC (2019), *Berthing velocities analysis of seagoing vessels over 30 kDWT*. Brussels, Belgium: PIANC.
- Powell, M. J. D. (1994), A direct search optimization method that models the objective and constraint functions by linear interpolation. *Advances in Optimization and Numerical Analysis* 275, pp. 51-67.
- Rackwitz, R., & Fiessler, B. (1997), Structural reliability under combined random load sequences. *Computers and Structures* 9, pp.489-494.
- Rackwitz, R. (2000), Optimization – the basis of code making and reliability verification. *Structural Safety* 22, pp. 27-60.

References

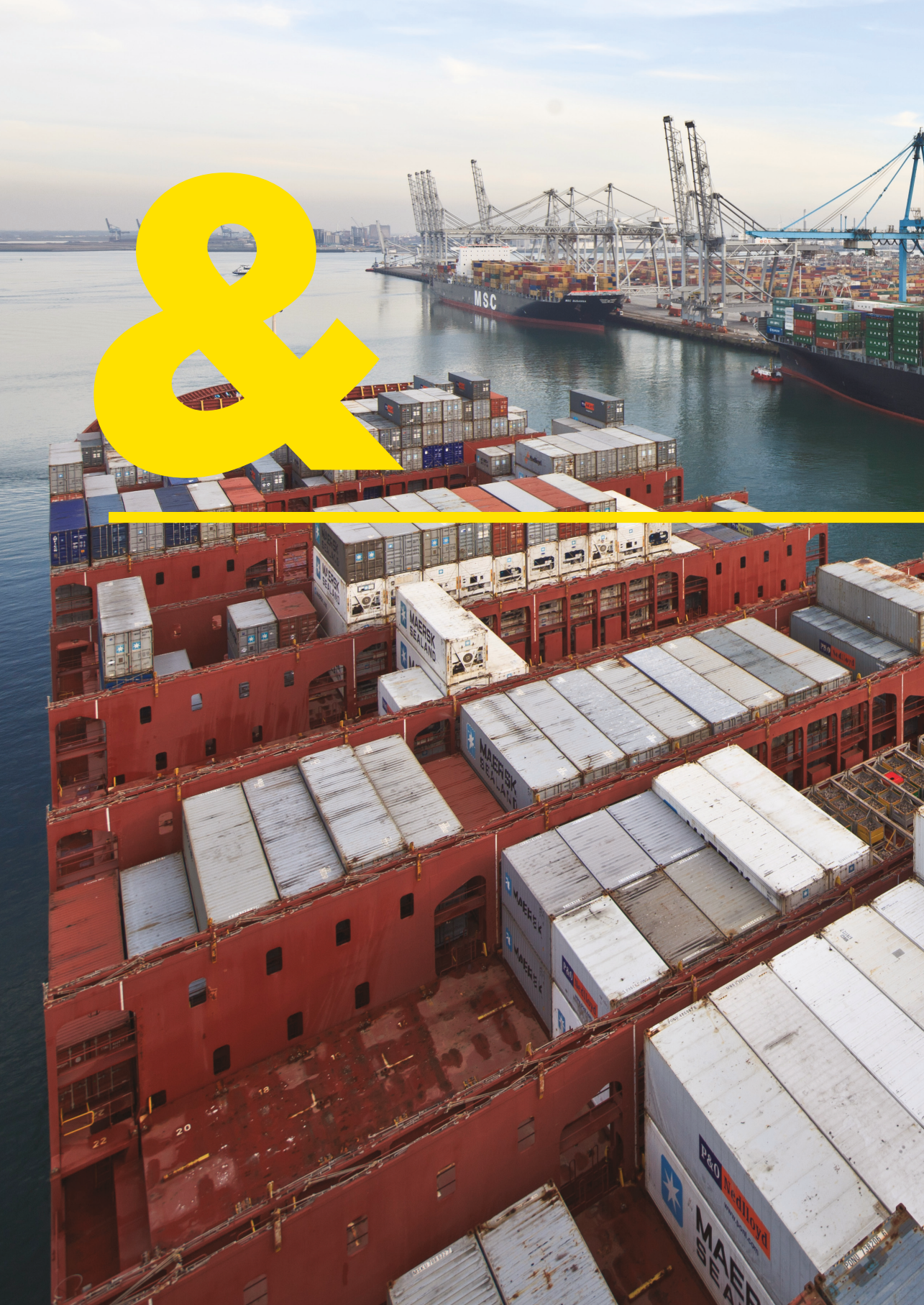
- Rackwitz, R. (2001), Reliability analysis – a review and some perspectives. *Structural safety* 23, pp. 365-395.
- Rackwitz, R. (2002), Optimization and risk acceptability based on the Life Quality Index. *Structural Safety* 24, pp. 297-331.
- Rackwitz, R. (2004), Optimal and acceptable technical facilities involving risks. *Risk Analysis* 24, pp. 675-695.
- Rackwitz, R., Lentz, A., & Faber, M. (2005), Socio-economically sustainable civil engineering infrastructures by optimization. *Structural Safety* 27, pp. 187-229.
- Rackwitz, R. (2006), The effect of discounting, different mortality reduction schemes and predictive cohort life tables on risk acceptability criteria. *Reliability Engineering & System Safety* 91, pp. 469-484.
- Rackwitz, R. (2008), *The Philosophy Behind the Life Quality Index and Empirical Verification*. Joint Committee on Structural Safety.
- Rath, S. A. H. (2012), *Method of Approach Measurements, Rotterdam*. Rotterdam, The Netherlands: Rotterdam University of Applied Sciences.
- Rausand, M. (2013), *Risk Assessment Theory, Methods, and Applications*. Wiley. ISBN 978-0-470-63764-7.
- Rippi, A., & Teixeira, A. (2016), Reliability-based assessment of a retaining wall using FEM. 25th *European Young Geotechnical Engineers Conference*. Sibiu: Romania.
- ROM 0.0 (2002), *General Procedure and Requirements in the Design of Harbor and Maritime Structures*. Madrid, Spain. ISBN 978-84888975309.
- ROM 0.2-90 (1990), *Maritime Works Recommendations: Actions in the Design of Maritime and Harbour Works*. Madrid, Spain: Puertos del Estado. ISBN 978-8488975003.
- ROM 0.5-05, (2008), *Geotechnical Recommendations for the Design of Maritime and Harbour Works*. Madrid, Spain: ROM. ISBN 978-8488975622.
- Roscoe, K., Diermanse, F., & Vrouwenvelder, T. (2018), System reliability with correlated components: accuracy of the equivalent planes method. *Structural Safety* 57, pp. 53-63.
- Rosenblatt, M. (1952), Remarks on a multivariate transformation. *The Annals of Mathematical Statistics* 23, pp. 470-472.
- Roubos, A. A., & Grotegoed, D. (2014), *Urban Quay Walls*. Delft, The Netherlands: SBRCURnet. ISBN 978-1138000230.
- Roubos, A. A., Jaspers Focks, D. J., & Peters, D. J. (2016), *Innovation Flexible Dolphins by Full-Scale Field Test Laterally Loaded Tubular Piles*. Rio de Janeiro, Brazil: PIANC COPEDEC.
- Roubos, A. A., Groenewegen, L., & Peters, D. J. (2017), Berthing velocity of large seagoing vessels in the port of Rotterdam. *Marine Structures* 51, pp. 202-219.
- Roubos, A. A., Steenbergen, R. D. J. M., Schweckendiek, T., & Jonkman, S. N. (2018), Risk-based target reliability indices of quay walls. *Structural Safety* 75, pp. 89-109.

- Roubos, A. A., Allaix, D., Fischer, K., Steenbergen, R. D. J. M., & Jonkman, S. N. (2018), *Target reliability indices for existing quay walls derived on the basis of the LQI criterion..* Ghent, Belgium: IALCC
- Roubos, A. A., Allaix, D., Schweckendiek, T., Steenbergen, R. D. J. M., & Jonkman, S. N. (2019), Time-dependent reliability analysis of service-proven quay walls subject to corrosion-induced degradation. *Reliability Engineering & System Safety* (submitted).
- Roubos, A. A., Schweckendiek, T., Brinkgreve, R., Steenbergen, R. D. J. M., & Jonkman, S. N. (2019), Finite element-based reliability assessment of quay walls. *Georisk: Assessment and Management of Risk for Engineered Systems and Geohazards* (submitted).
- SANS 10160-1 (2010), *Basis of Structural Design and Actions for Buildings and Industrial Structures, Part 1: Basis of Structural Design.* Pretoria, South Africa. ISBN 978-0-626-24757-7
- Santos, S. R., Matioli, L. C., & Beck, A. T. (2012), New optimization algorithms for structural reliability analysis. *Computer Modeling in Engineering & Sciences* 83, pp. 23-55.
- Saurin, B. F. (1963), Berthing forces of large tankers. *Proceedings of Sixth World Petroleum Congress, Frankfurt*, Section VII – Paper 10.
- Schutte, J. (2017), *Deepening of Existing Combi Walls.* Rotterdam, The Netherlands: Rotterdam University of Applied Sciences.
- Schweckendiek, T., Krogt, M. van der, Rijnveld, B., & Teixeira, A. M. (2017), *Handreiking Faalkansanalyse Macrostabieliteit.* Delft, The Netherlands: Deltares.
- Schweckendiek, T., Courage, W. M. G., & Gelder, P. H. A. J. M. van (2007), Reliability of sheet pile walls and the influence of corrosion – structural reliability analysis with finite elements. *Proceedings of the European Safety and Reliability Conference 2007 (ESREL 2007)*, pp. 1791-1799. Stavanger, Norway.
- Schweckendiek, T., Vrouwenvelder, A. C. W. M., Calle, E. O. F., Jongejan, R. B., & Kanning, W. (2012), Partial factors for flood defenses in the Netherlands: modern geotechnical codes of practice – development and calibration. In: Arnold, P., et al. (eds), *Special Geotechnical Publication.* Taylor & Francis.
- Skjong, R., Vanem, E., & Endresen, Ø. (2007), *Risk Evaluation Criteria: Technical Report.* SAFEDOR -D-4.5.2 DNV.
- Sluis, J. J. M. (2012), *Validation of Embedded Pile Row in PLAXIS 2D.* MSc thesis. Delft, The Netherlands: Delft University of Technology.
- Smit, C. F. (2014), *Reliability Based Optimization of Concrete Structural Components.* Stellenbosch, South Africa.
- Sørensen, J. D. (2004), *Notes in Structural Reliability Theory And Risk Analysis.* Aalborg, Denmark: Institute of Building Technology and Structural Engineering.
- Steenbergen, R. D. J. M., & Vrouwenvelder, A. C. W. M. (2010), Safety philosophy for existing structures and partial factors for traffic loads on bridges. *Heron* 55, pp. 123-139.
- Steenbergen, R. D. J. M., Sýkora, M., Diamantidis, D., Holický, M., & Vrouwenvelder, A. C. W. M. (2015), Economic and human safety reliability levels for existing structures. *Structural Concrete* 16, pp. 323-332.

References

- Steenepoorte, C. (1992), *Het ontwerp van een kademuurconstructie voor container overslag in de Amazonehaven op de Maasvlakte*. MSc thesis. Delft, The Netherlands: Delft University of Technology.
- STOWA (2011), *Leidraad Waterkerende Kunstwerken in regionale waterkeringen*. Amersfoort, The Netherlands: Technische adviescommissie waterkeringen. ISBN 978-90-5773-529-5
- Structural Concrete (2012), *Textbook on Behaviour, Design and Performance, Second Edition, Volume 5*. Lausanne, Switzerland. ISBN 978-2-88394-102-1
- Sudret, B. (2008), Analytical derivation of the outcrossing rate in time-variant reliability problems. *Structures and Infrastructure Engineering* 4, pp. 353-362.
- Sudret, B. (2011), Time-variant reliability problems. In: Baroth, J., Schoefs, F., and Breysse, D. (eds), *Construction Reliability – Safety, Variability and Sustainability*, pp. 187-206 (chapter 10). ISTE/Wiley.
- Sudret, B., Marelli, S., & Wiart, J. (2017), Surrogate models for uncertainty quantification: an overview. *Eleventh European Conference on Antennas and Propagation*. Paris, France.
- Sýkora, M., & Holický, M. (2011), Target reliability levels for the assessment of existing structures. *Proc. ICASPII*, pp. 1048-1056.
- Sýkora, M., Holický, M., Lenner, R., & Manas, P. (2014), Target reliability levels for existing bridges considering emergency and crisis situations. *Advances in Military Technology* 9.
- Sýkora, M., Diamantidis, D., Holický, M., & Jung, K. (2017), Target reliability for existing structures considering economic and societal aspects. *Structure and Infrastructure Engineering* 13-1, pp. 181-194.
- TAW (2003), *Leidraad kunstwerken*. Delft, The Netherlands: Technische adviescommissie voor de waterkeringen. ISBN 90-369-5544-0
- TAW (1985), *Enkele gedachten aangaande een aanvaardbaar risiconiveau in Nederland*. The Hague, The Netherlands: Technische adviescommissie voor de waterkeringen.
- Terwel, K. C. (2014), *Structural Safety, Study into Critical Factors in the Design and Construction Process*. Delft, The Netherlands. ISBN 978-94-6259-174-5
- Teixeira, A., Rippi, K., Schweckendiek, T., Brinkman, H., Nuttall, J., Hellebrandt, L., & Courage, W. (2016), *Soil-Structure Interaction – Reliability Analysis of a Retaining Wall, 2015*. Delft, The Netherlands: Deltares & TNO. 11200575-016.
- Timmermans, A. L. J. (2017), *Final Design, Combi-Wall for Inland Barges, Report Number 101*. Project i.000770, Offshore terminal SIF. Rotterdam, The Netherlands: Port of Rotterdam Authority.
- ThyssenKrupp GfT Bautechnik (2007), *Spundwand-Handbuch – Berechnung*. Gelsenkirchen, Germany: ThyssenKrupp GfT Bautechnik.
- Ueda, S., Yamase, S., & Okada, T. (2010), Reliability Design of Fender Systems for Berthing Ship. *Proc. Of Intl'. Navig. Congr. No. 79*.
- USACE (1999), *Risk-Based Analysis in Geotechnical Engineering for Support of Planning Studies*, ETL1110-2-556. Washington DC, United States

- Vasco Costa, F. (1968), *Berthing Manoeuvres of Large Ships*. The Dock and Harbour Authority XLVIII, pp. 351-358.
- Voogt, H. (2014), Proactive and predictive waterfront asset management – Port of Rotterdam experience. *Proceedings, PIANC*. San Francisco, United States.
- Vriend, A. C. (2015), *LBBR: Rapportage bezwijkproeven op zelfborende groutinjectiepalen*. Jetmix, 15566-r-003. Rotterdam, The Netherlands: Port of Rotterdam Authority.
- Vrouwenvelder, A. C. W. M., Holický, M., Tanner, C. P., Lovegrove, D. R., & Canisius, E. G. (2001), *Risk Assessment and Risk Communication in Civil Engineering*. CIB Report: Publication 259. ISBN 90-6363-026-3
- Vrouwenvelder, A. C. W. M., & Siemens, A. J. M. (1987), Probabilistic calibration procedure for the derivation of partial factors of safety for the Netherlands building codes. *Heron*, pp. 9-29.
- Vrouwenvelder, A. C. W. M., & Scholten, N. (2010), Assessment Criteria for Existing Structures. *Structural Engineering International* 20, pp. 62-65.
- Vrouwenvelder, A. C. W. M. (2002), Developments towards full probabilistic design codes. *Structural Safety* 24, pp. 417-432.
- Vrouwenvelder, A. C. W. M. (2001), The fundamentals of structural building codes. *Proceedings of the International Conference on Structural Engineering, Mechanics and Computation*, volume 1, pp. 183-193. Cape Town, South Africa. ISBN 0-08 -043948-9.
- Vrouwenvelder, A. C. W. M. (2017), Theory and applications of structural reliability analysis. *ICOSSAR 2017, 12th International Conference on Structural Safety & Reliability*.
- Vrijling, J. K. (2001), Probabilistic design of water defense systems in the Netherlands. *Reliability Engineering and System Safety* 74, pp. 337-344.
- Vrijling, J. K., Hengel, W. van, & Houben, R. J. (1998), Acceptable risk as a basis for design. *Reliability Engineering and System Safety* 59, pp. 141-150.
- Vrijling, J. K., & Gelder, P. H. A. J. M. van (2000), An analysis of the valuation of a human life. *Proceedings of ESREL 2000, SARS and SRA-Europe Annual Conference*, pp. 197-200.
- Waarts, P. H. (2000), *Structural Reliability Using Finite Element Analysis – an Appraisal of DARS: Directional Adaptive Response Sampling*. Delft, The Netherlands.
- Well, T. J. van der (2018), *Reliability-Based Assessment of Quay Walls*. Delft, The Netherlands: Delft University of Technology.
- Wolters, H. J., Bakker, K. J., & Gijt, J. G. de (2012), *Reliability of Quay Walls Using Finite Element Analysis*. Delft, The Netherlands: Delft University of Technology.
- Yamase, S., Ueada, S., Okada, T., Arai, A., & Shimizu, K. (2014), *Characteristics of Measured Berthing Velocity and the Application for Fender Design of Berthing Ship*. San Francisco, USA. PIANC World Congress.
- Zhang, Y., & Kiureghian, A. der (1995), Two improved algorithms for reliability analysis. *Proceedings of the Sixth IFIP – WG7.5, Reliability and Optimization of Structural Systems*.





APPENDICES

- A1. Derivation of analytical formulas
- A2. Probability distribution functions
- B1. Additional information on reference quay walls
- B2. Abdo-Rackwitz *FORM* algorithm
- B3. Comparison of Blum & Prob2B with Plaxis & OpenURNS
- C1. Comparison of reliability methods
- C2. Comparison with and without truncation
- D1. Berthing velocity of large seagoing vessels in Rotterdam
- D.1.1 Berthing records and data analysis
- D.1.2 Results data analysis berthing records Rotterdam
- D.1.3 Discussion berthing records port of Rotterdam
- D.1.4 Conclusion berthing velocity of large seagoing vessels in Rotterdam
- D2. Typical distribution functions berthing velocity



APPENDIX A1. DERIVATION OF ANALYTICAL FORMULAS

In this appendix, analytical formulas of the objective function C_{Total} and the associated derivative have been derived to determine the discounted future failure costs in each year of the reference period. The analytical formulas were also used in the sensitivity analyses (Sections 2.5.2 and 2.5.4). It should be noted that the Hasofer-Lind reliability index β is the decision parameter.

$$\min\{C_{Total} = C_{Investments}(\beta) + C_{CapitalisedRisk}(\beta)\} \quad (102)$$

$$\frac{\partial C_{Total}(\beta^*)}{\partial \beta} = 0 \quad (103)$$

$$C_{Total} = C_0 + C_m\beta + C_f P_{f;t_0} + C_f \cdot \sum_{n=1}^{n_{ref}} \frac{\Delta P_{f;t_n}}{(1+r)^n} \quad (104)$$

Where:

$C_{Investments}$	Investments in safety measures [€]
$C_{CapitalisedRisk}$	Present value of future failure costs [€]
β	Decision parameter [-]
β^*	Optimum reliability index [-]
C_0	Initial construction costs independent of reliability level [€]
C_m	Marginal construction cost dependent on reliability level [€]
C_f	Summation of direct and indirect costs of failure [€]
$P_{f;t_0}$	Part of the probability of failure not influenced by time interval $[0, t_{ref})$ [-]
ΔP_f	Reference period, dependent increase in cumulative probability of failure in the year n [-]
n	Number of years [-]
n_{ref}	Number of years in the reference period [-]
r	Real annual discount rate [-]

The probability of failure was determined on the basis of a standard normal distribution. Hence, the following equations were used:

$$\phi(\beta) = f(\beta) = \frac{1}{\sqrt{2\pi}} e^{-\frac{1}{2}\beta^2} \quad (105)$$

$$\Phi(\beta) = F(\beta) = \int_{-\infty}^{\beta} \frac{1}{\sqrt{2\pi}} e^{-\frac{1}{2}x^2} dx = \frac{1+Erff\left(\frac{\beta}{\sqrt{2}}\right)}{2} \quad (106)$$

$$Erff(\beta) = F(\beta) = \frac{2}{\sqrt{\pi}} \int_0^{\beta} e^{-t^2} dt \quad (107)$$

Where:

$\phi(\beta)$	Probability density function of normal distribution [-]
$\Phi(\beta)$	Cumulative distribution function of normal distribution [-]
$\text{Erf}(\beta)$	Error function [-]

In this appendix the following properties of the standard normal distribution were used:

$$\Phi(-\beta) = 1 - \Phi(\beta) \text{ for } \beta \in \mathbb{R} \quad (108)$$

$$\Phi^{-1}(p) = -\Phi^{-1}(1 - p) \text{ for } p \in (0,1) \quad (109)$$

$$\Phi(0) = 0.5 \quad (110)$$

$$\frac{\partial \Phi(\beta)}{\partial \beta} = \phi(\beta) = \frac{1}{\sqrt{2\pi}} e^{-\frac{1}{2}\beta^2} \quad (111)$$

$$\frac{\partial \Phi^{-1}(p)}{\partial p} = \left(\frac{\partial \Phi(\beta)}{\partial \beta} \right)^{-1} = \frac{\sqrt{2\pi}}{e^{-\frac{1}{2}\beta^2}} \quad (112)$$

The mathematical notation of time-variant reliability problems is well described by Sudret (2008; 2011) and Rackwitz (2001). In addition to the formulation of the limit state function (Section 2.3.2), time-dependent uncertainty such as deterioration or due to variable loads must also be taken into account. The failure probability in the time interval $(t, t+\Delta t)$ is defined in accordance with the notation of Sudret and Rackwitz as:

$$P_f(t, t + \Delta t) = \mathbb{P}(\exists t \in [t, t + \Delta t]: Z \leq 0) \quad (113)$$

When the time interval $(t, t+\Delta t)$ approaches zero, the point-in-time instantaneous probability of failure – in other words, the failure rate – can be found (Sudret, 2008). The probability of failure at time instant t is defined as:

$$P_{f,i}(t) = \mathbb{P}(Z \leq 0) \quad (114)$$

Eq. (115) shows the classical upper and lower bounds of the probability of failure in the time interval $(t, t+\Delta t)$ (Rackwitz, 2001).

$$\max_{t \in (t, t+\Delta t)} P_{f,i}(t_i) \leq P_f(t, t + \Delta t) \leq P_{f,0} + E[N^+(t, t + \Delta t)] \quad (115)$$

Where:

$P_f(t, t + \Delta t)$	Probability of failure in interval $(t, t+\Delta t)$ [-]
$P_{f,i}(t_i)$	Probability of failure at time instant t_i [-]
$P_{f,0}$	Part of the probability of failure being independent of time interval $(t, t+\Delta t)$ [-]

Appendix A1. Derivation of analytical formulas

N^+	Number of outcrossings of the limit state [-]
Z	State function [-]

The usual approach to a time-variant reliability problem is based on the computation of the outcrossing rate $E[N^+(t, t + \Delta t)]$ of the limit state under consideration (Sudret, 2008). However, in this study the upper and lower bounds were not used. Instead, the probability of failure in time interval $P_f(t, t + \Delta t)$ was defined by subdividing $P_{f;t_n}$ into a block that is largely time-independent $P_{f;0}$ and a block that is fully time-dependent $\sum \Delta P_{f;t_n}$ (Fig. 2.5).

$$P_{f;t_n} = P_{f;0} + \sum \Delta P_{f;t_n} \quad (116)$$

$$P_{f;t_{ref}} = P_{f;0} + \sum_{n=1}^{n_{ref}} \Delta P_{f;t_n} \quad (117)$$

The main difference between a time-invariant and a time-variant reliability problem is that in the latter case one does not know when a failure occurs (Sudret, 2011). When t_{eq} is determined, the marginal change in probability of failure in each year can be established by subtracting the cumulative probability of failure in the intervals $[0, t_n)$ and $[0, t_{n-1})$ using Eq. (118). This equation is a function of the probability of failure during a reference period of one year $P_{f;t_1}$ (Fig. 2.6). The cumulative failure probability in the time interval $[0, t_n)$ was derived by transforming Eq. (7) into Eq. (118), and the time-independent part using Eq. (120). The equations are illustrated in Fig. 2.6. When $P_{f;t_1}$, t_{eq} and t_{ref} are known, $P_{f;t_{ref}}$ and $\Delta P_{f;t_n}$ can be derived by the following equations:

$$\Delta P_{f;t_n} = P_{f;t_n} - P_{f;t_{n-1}} \quad (118)$$

$$P_{f;t_n} = 1 - (1 - P_{f;t_1})^{an+b} \quad (119)$$

$$P_{f;t_0} = 1 - (1 - P_{f;t_1})^b \quad (120)$$

$$a = \frac{n_{eq} - 1}{n_{ref} - 1} \quad (121)$$

$$b = \frac{n_{ref} - n_{eq}}{n_{ref} - 1} \quad (122)$$

The probability of failure over a certain time interval $(t, t+\Delta t)$ can be described using the cumulative distribution function $F(\beta)$.

$$P(X > x) = 1 - F(\beta) \quad (123)$$

$$P_{f;t_1} = P(X > x) = 1 - F(\beta) = \Phi(-\beta_{t_1}) \quad (124)$$

$$1 - P_{f;t_1} = \Phi(\beta_{t_1}) \quad (125)$$

The above transformation was applied to Eq. (119).

$$P_{f;t_n} = 1 - (\Phi(\beta_{t_1}))^{an+b} \quad (126)$$

$$P_{f;t_{n-1}} = 1 - (\Phi(\beta_{t_1}))^{a(n-1)+b} \quad (127)$$

$$\Delta P_{f;t_n} = P_{f;t_n} - P_{f;t_{n-1}} = \left(1 - (\Phi(\beta_{t_1}))^{an+b}\right) - \left(1 - (\Phi(\beta_{t_1}))^{a(n-1)+b}\right) \quad (128)$$

If one implements the following denotation:

$$\Phi(\beta_{t_1}) = \Phi_1 \quad (129)$$

ΔP_f is defined as:

$$\Delta P_f = -\Phi_1^{an} \Phi_1^b + \Phi_1^{an} \Phi_1^{-a} \Phi_1^b \quad (130)$$

$$\Delta P_f = \Phi_1^{an} \Phi_1^{-a} \Phi_1^b - \Phi_1^{an} \Phi_1^b \quad (131)$$

$$\Delta P_f = \Phi_1^{an} \Phi_1^b (\Phi_1^{-a} - 1) \quad (132)$$

Consequently, the following formula of $C_{CapitalisedRisk}$ was found:

$$C_{CapitalisedRisk} = C_f \sum_{n=0}^{n_{ref}} \frac{\Phi_1^{an} \Phi_1^b (\Phi_1^{-a} - 1)}{(1+r)^n} \text{ for } n \in [0, n_{ref}] \quad (133)$$

$$C_{CapitalisedRisk} = C_f \Phi_1^b (\Phi_1^{-a} - 1) \sum_{n=0}^{n_{ref}} \left(\frac{\Phi_1^a}{1+r}\right)^n \quad (134)$$

$$C_{CapitalisedRisk} = C_f (\Phi_1^{b-a} - \Phi_1^b) \sum_{n=0}^{n_{ref}} \left(\frac{\Phi_1^a}{1+r}\right)^n \quad (135)$$

If one separates the part $P_{f;0}$ – being not influenced by a change in reference period – from the part $\sum \Delta P_{f;t_n}$ – which depends on the reference period – the following equation is obtained:

$$C_{CapitalisedRisk} = C_f P_{f;0} + C_f (\Phi_1^{b-a} - \Phi_1^b) \sum_{n=1}^{n_{ref}} \left(\frac{\Phi_1^a}{1+r}\right)^n \text{ for } n \in [1, n_{ref}] \quad (136)$$

Now the following transformation rule is used:

$$\sum_{i=0}^{n_{ref}} Ax^i = A \frac{1 - x^{n_{ref}+1}}{1 - x} \quad (137)$$

And thus:

$$\begin{aligned} \sum_{i=0}^{n_{ref}} Ax^i &= Ax^0 + \sum_{i=1}^{n_{ref}} Ax^i = Ax^0 + \sum_{i=0}^{n_{ref}-1} Ax^{i+1} = Ax^0 + \sum_{i=0}^{n_{ref}-1} Ax^i x \\ &= Ax^0 + Ax \frac{1 - x^{n_{ref}}}{1 - x} \end{aligned} \quad (138)$$

Appendix A1. Derivation of analytical formulas

Where:

$$x = \frac{\Phi_1^a}{1+r} \text{ (in fact, this an adjusted grow rate)} \quad (139)$$

$$A = C_f(\Phi_1^{b-a} - \Phi_1^b) \quad (140)$$

Consequently, the following formula of $C_{CapitalisedRisk}$ was found:

$$C_{CapitalisedRisk} = C_f P_{f;0} + A(x) \frac{1 - (x)^{n_{ref}}}{1 - (x)} \quad (141)$$

$$C_{CapitalisedRisk} = C_f P_{f;0} + C_f(\Phi_1^{b-a} - \Phi_1^b) \left(\frac{\Phi_1^a}{1+r} \right) \frac{1 - \left(\frac{\Phi_1^a}{1+r} \right)^{n_{ref}}}{1 - \left(\frac{\Phi_1^a}{1+r} \right)} \quad (142)$$

$$C_{CapitalisedRisk} = C_f P_{f;0} + C_f \frac{(\Phi_1^b - \Phi_1^{b+a})}{1+r} \frac{1 - \left(\frac{\Phi_1^a}{1+r} \right)^{n_{ref}}}{1 - \left(\frac{\Phi_1^a}{1+r} \right)} \quad (143)$$

$$C_{CapitalisedRisk} = C_f(1 - \Phi_1^b) + C_f \frac{(\Phi_1^b - \Phi_1)}{1+r} \frac{1 - \left(\frac{\Phi_1^a}{1+r} \right)^{n_{ref}}}{1 - \left(\frac{\Phi_1^a}{1+r} \right)} \quad (144)$$

The analytical formula of the objective function now becomes:

$$f(\beta) = C_0 + C_m \beta_{t_1} + C_f(1 - \Phi_1^b) + C_f c(\Phi_1^b - \Phi_1) \frac{1 - (c\Phi_1^a)^{n_{ref}}}{1 - c\Phi_1^a} \quad (145)$$

Where:

$$\Phi_1 = \Phi(\beta_{t_1}) \quad \text{Standard normal cumulative distribution function [-]}$$

The derivative of the objective function was used to determine the optimum reliability index β^* and to derive insight into the sensitivity of the input variables, such as the discount rate r , the absolute value, C_p , marginal costs of safety measures C_m and the reference period t_{ref}

$$\frac{\partial C_{Investments}(\beta^*)}{\partial \beta_{t_1}} + \frac{\partial C_{CapitalisedRisk}(\beta^*)}{\partial \beta_{t_1}} = 0 \quad (146)$$

$$C_m + \frac{\partial C_{CapitalisedRisk}(\beta^*)}{\partial \beta_{t_1}} = 0 \quad (147)$$

$$\frac{\partial C_{CapitalisedRisk}(\beta^*)}{\partial \beta_{t_1}} = -C_m \quad (148)$$

The formula of $C_{CapitalisedRisk}$ was rearranged as follows:

Appendix A1. Derivation of analytical formulas

$$c = 1/(1 + r) \quad (149)$$

$$C_{\text{CapitalisedRisk}} = C_f(1 - \Phi_1^b) + C_f c (\Phi_1^b - \Phi_1) \frac{1 - (c\Phi_1^a)^{n_{ref}}}{1 - c\Phi_1^a} \quad (150)$$

$$C_{\text{CapitalisedRisk}} = c(\Phi_1(x)^b - \Phi_1(x)) \frac{1 - (c\Phi_1(x)^a)^{n_{ref}}}{1 - c\Phi_1(x)^a} \quad (151)$$

$$C_{\text{CapitalisedRisk}} = \frac{c(\Phi_1(x)^b - \Phi_1(x))(1 - (c\Phi_1(x)^a)^{n_{ref}})}{1 - c\Phi_1(x)^a} \quad (152)$$

$$= \frac{c \left(\left(0.5 + 0.5 \operatorname{erf} \left(\frac{x}{\sqrt{2}} \right) \right)^b - \left(0.5 + 0.5 \operatorname{erf} \left(\frac{x}{\sqrt{2}} \right) \right) \right) \left(1 - \left(c \left(0.5 + 0.5 \operatorname{erf} \left(\frac{x}{\sqrt{2}} \right) \right) \right)^a \right)^{n_{ref}}}{1 - c \left(0.5 + 0.5 \operatorname{erf} \left(\frac{x}{\sqrt{2}} \right) \right)^a} \quad (153)$$

The derivative of $C_{\text{CapitalisedRisk}}$ was derived using a derivative calculator.

$$\begin{aligned} \frac{\partial C_{\text{CapitalisedRisk}}}{\partial \beta_{t_1}} &= -C_f b \phi_1 \Phi_1^{b-1} \\ &+ C_f \left(\frac{c(b\phi_1 \Phi_1^{b-1} - \phi_1)(1 - (c\Phi_1^a)^{n_{ref}})}{1 - c\Phi_1^a} + \frac{ac^2 \phi_1 (1 - \Phi_1^a)(1 - (c\Phi_1^a)^{n_{ref}})}{(1 - c\Phi_1^a)^2} \right. \\ &\left. - \frac{ac n_{ref} \phi_1 (\Phi_1^{b-1} - 1)(c\Phi_1^a)^{n_{ref}}}{(1 - c\Phi_1^a)} \right) \end{aligned} \quad (154)$$

Where:

$$\phi_1 = \phi(\beta_{t_1}) \quad \text{Standard normal probability density function [-]}$$

$$\Phi_1 = \Phi(\beta_{t_1}) \quad \text{Standard normal cumulative distribution function [-]}$$

The derivative of $C_{\text{Investments}}$ is presented in Eq. (156).

$$C_{\text{Investments}}(\beta_{t_1}) = C_0 + C_m \beta_{t_1} \quad (155)$$

$$\frac{\partial C_{\text{Investments}}(\beta_{t_1})}{\partial \beta_{t_1}} = C_m \quad (156)$$

The solution to the optimisation problem was found using the following equations:

$$\begin{aligned} \min \{C_{\text{Total}}(\beta_{t_1})\} &= \{C_{\text{Investments}}(\beta_{t_1}) + C_{\text{CapitalisedRisk}}(\beta_{t_1})\} \\ \frac{\partial C_{\text{Investments}}(\beta_{t_1})}{\partial \beta_{t_1}} + \frac{\partial C_{\text{CapitalisedRisk}}(\beta_{t_1})}{\partial \beta_{t_1}} &= 0 \rightarrow \beta^* \end{aligned} \quad (157)$$

$$\frac{\partial C_{\text{CapitalisedRisk}}(\beta^*)}{\partial \beta_{t_1}} = -C_m \quad (158)$$

$$\begin{aligned} -C_f b \phi_1 \Phi_1^{b-1} + C_f \left(\frac{c(b\phi_1 \Phi_1^{b-1} - \phi_1)(1 - (c\Phi_1^a)^{n_{ref}})}{1 - c\Phi_1^a} + \frac{ac^2 \phi_1 (1 - \Phi_1^a)(1 - (c\Phi_1^a)^{n_{ref}})}{(1 - c\Phi_1^a)^2} \right. \\ \left. - \frac{ac n_{ref} \phi_1 (\Phi_1^{b-1} - 1)(c\Phi_1^a)^{n_{ref}}}{(1 - c\Phi_1^a)} \right) &= -C_m \end{aligned} \quad (159)$$

APPENDIX A2. PROBABILITY DISTRIBUTION FUNCTIONS

Table A2.1. Type of distribution and variation coefficient (CoV) of important model parameters.

Design parameter	Soil layer	SI	μ	Distribution	CoV
Unit weight of soil γ_{sat}	Backfill ¹	kN/m ³	20	Normal	0.05 ²
	Reclamation sand ¹	kN/m ³	20	Normal	0.05 ²
	Holocene sand ¹	kN/m ³	20	Normal	0.05 ²
	Clay layer ¹	kN/m ³	19	Normal	0.05 ²
	Pleistocene sand ¹	kN/m ³	20	Normal	0.05 ²
Friction angle φ'_{rep}	Backfill ¹	°	39	Normal	0.10 ^{2,3}
	Reclamation sand ¹	°	36	Normal	0.10 ^{2,3}
	Holocene sand ¹	°	36	Normal	0.10 ^{2,3}
	Clay layer ¹	°	27	Normal	0.10 ^{2,3}
	Pleistocene sand ¹	°	39	Normal	0.10 ^{2,3}
Cohesion c'	Clay layer ¹	kpa	7	Lognormal	0.20 ²
Soil stiffness $E_{50,ref}$	Backfill ¹	Mpa	50	Lognormal	0.20 ²
	Reclamation sand ¹	Mpa	30	Lognormal	0.20 ²
	Holocene sand ¹	Mpa	30	Lognormal	0.20 ²
	Clay layer ¹	Mpa	5	Lognormal	0.20 ²
	Pleistocene sand ¹	Mpa	60	Lognormal	0.20 ²
Yield strength f_y		N/mm ²	510 ⁵	Lognormal	0.07 ⁴
Tube diameter D_{tube}		m	1.62 ⁵	Normal	0.01
Wall thickness t_{tube}		m	0.23 ⁵	Uniform	0.05
Annual live loads Q_{t1}		kN/m ²	26 ⁵	Gumbel	0.20
Lifetime live loads Q_{t50}		kN/m ²	42 ⁵	Gumbel	0.10

¹)Top levels of backfill sand, reclamation sand, Holocene sand, clay layer and Pleistocene sand are MSL +5.0 m, MSL -0.0 m, MS -8.0 m, MSL -20.0 m and MSL -21.0 m, respectively, where MSL = mean sea level.

²) Value is based on soil investigation in accordance with Eurocode 7 (NEN-EN 9997-1, 2016).

³) Value represents the average variability of the soil layer and is verified by the research by Huijzer (Huijzer & Hannink, 1995; Huijzer 1996).

⁴) Value is based on Peters et al. (2017) and the probabilistic model code (JCSS, 2001).

⁵) Value is based on a quay wall situated in the Maasvlakte area of the port of Rotterdam.

APPENDIX B1. ADDITIONAL INFORMATION ON REFERENCE QUAY WALLS

Table B.1. Structural properties and modelling of the reference quay walls.

	SI	Without relieving platform	With relieving platform
Combi-wall		Plate element	Plate element
Steel quality tube	-	X70	X65
Steel quality sheet pile	-	S355GP	S355GP
E steel	GPa	210	210
EI	kNm ² /m	5.466E05	1.031 E6
EA	kN/m	3.476E06	6.058 E6
System length	m	2.995	3.724
Anchor		Grout anchor	Grout anchor
Strut	-	Note to node	Node to node
Grout	-	Embedded beam row	Embedded beam row
Steel quality	-	E470	AC600D
Strut diameter	mm	101.6	82.5
Wall thickness strut	mm	17.5	22.2
Centre to centre	m	1.47	2.735
Level	-	NAP+1.50m	NAP+0.9m
EA	kN per pile	9.7E5	n/a
..	kN/m	n/a	310.5 E3
E grout body	kN/m ² per pile	7E6	n/a
..	kN/m ² /m	n/a	2.10 E8
τ_{skin}	kN/m	750	330
Inclination	°	45	18
Foundation piles		n/a	Embedded beam row
Inclination	-	n/a	1:3.5
Diameter	m	n/a	0.560/0.650
Centre to centre	m	n/a	2.28
EI	kNm ² /m	n/a	21.17 E3
EA	kN/m	n/a	1.08 E6
τ_{skin}	kN/m	n/a	100

APPENDIX B2. ABDO-RACKWITZ FORM ALGORITHM

When conducting finite element-based *FORM* assessments, understanding the background of the algorithm used is crucial in order to increase calculation robustness. However, clear descriptions of the Abdo-Rackwitz algorithm are lacking in the literature. This appendix describes the algorithm used in our study.

Like other *FORM*-based algorithms, Abdo-Rackwitz models the uncertainties regarding the random variables x using a random vector X with joint cumulative distribution function F_x . The vector X is converted into a standard normal vector U by means of isoprobabilistic transformation $T(X)=U$, e.g. using the Nataf or the Rosenblatt transformation (Andrianov et al., 2007; Lebrun & Dufloy, 2009a; Rosenblatt, 1952). OpenTURNS has implemented the following objective function and equality constraint (Andrianov et al., 2007):

$$f(u) = \frac{1}{2} \|u\|^2 = \frac{1}{2} \|\sqrt{u^T u}\|^2 = \frac{1}{2} \sum U_i^2 = \frac{1}{2} \sum (\alpha_{u,i} \beta)^2 = \frac{1}{2} \beta^2 \quad (160)$$

$$\text{subject to } g(u) = 0 \quad (161)$$

Where:

$f(u)$	Objective function [-]
u	Vector of input variables in standard space [-]
$g(u)$	State function or level function [-]
β	Reliability index [-]
$\alpha_{u,i}$	Sensitivity factor in the U -space [-]

One advantage of this objective function is that its derivative equals the identity function $\nabla f(u) = u$, which simplifies the optimisation process. The limit state criterion is approximated point-wise, by a tangent hyperplane $g(u)=0$ in the standard space during the iteration process (Rackwitz & Fiessler, 1997). From geometrical representation, it follows that the vector β is perpendicular to the hyperplane, which in turn is tangential to the linearised failure surface $g(u)=0$ in the point closest to the origin (u^*). This is the maximum probable point (MPP) (Hasofer & Lind, 1974) of failure and is associated with the minimum distance to the hypersphere, which is equal to $\beta = \|u^*\|$. The point u^* can be found by:

$$u^* = \underset{g(u)=0}{\operatorname{argmin}} f(u) \quad (162)$$

In order to find u^* , the projected gradient-based Abdo-Rackwitz algorithm was used. This includes a line search based on exact penalisation of the constraint $g(u)=0$. To a lesser extent, the algorithm is also influenced by the number of random variables. But there is no need to know the exact formulation of $g(x)$ (Abdo & Rackwitz, 1991). Nor does it require

determination of the precise ‘Hessian’ (Lemaire, 2009), so that consequently the iteration process is quite efficient. However, detailed information about its settings is lacking in the literature. To support future users, the modifications applied to this algorithm and the settings used are therefore briefly explained. In addition, the settings for hardening soil were further studied in order to improve the applicability and efficiency of ProbAna® (Laera, & Brinkgreve, 2017).

The iteration process of the Abdo-Rackwitz algorithm is quite similar to that of the Rackwitz-Fiessler (1997) algorithm (abbreviated HL-RF) (Zhang & Der Kiureghian, 1995), if $\alpha^k = 1$. HL-RF generally results in a higher convergence rate, but can also cause unstable results (Makhduomi et al., 2017). From the present iterate, the next one was found by determining a search direction d and step length a :

$$u^{k+1} = u^k + a^k d^k \quad (163)$$

Where:

u	Vector of input variables in the standard space [-]
a	Step size or step length, initially 1 and then gradually shrinking by a factor of τ [-]
d	Directional vector [-]
k	Iteration number [-]

At iteration k , the algorithm first computes the search direction (Eq. 164) (Liu & Der Kiureghian, 1990), and the partial derivatives of the constraint function (Eq. 165), which determine the gradient $\nabla g(x)$ on the basis of ‘centred’ finite differences. The difference interval $dx_i = 2\epsilon_i$ should be large enough to allow some numerical noise induced by the finite difference solver of the hardening soil model, whereas fairly low values will not assure global convergence. If numerical noise dominates the calculation output of the finite element model, the prediction of the gradient will become inaccurate. Consequently, it will be pure luck if this gradient is in a descent direction (Nocedal & Wright, 2000). Evaluating the finite difference interval is highly recommended, in order to improve the efficiency of the backtracking line-search procedure.

$$d^k = \frac{\nabla g(u^k)^T \cdot u^k - g(u^k)}{\|\nabla g(u^k)\|^2} \nabla g(u^k) - u^k \quad (164)$$

$$\frac{\partial g(x)}{dx} \approx \frac{g(X_i + \epsilon_i) - g(X_i - \epsilon_i)}{2\epsilon_i} \quad (165)$$

Where:

d	Directional vector [-]
-----	------------------------

Appendix B2. Abdo-Rackwitz FORM algorithm

k	Iteration number [-]
$g(\underline{u}^k)$	Linearised limit state function in the standard space at the point \underline{u}^k [-]
$\nabla g(\underline{u}^k)$	Gradient of limit state function in the standard space at the point \underline{u}^k [-]
U_i	Input variable in standard space [-]
n	Number of input variables [-]
ε_i	Finite difference step for each dimension i in the original space [-]

Secondly, the algorithm initiates a line search by approximately solving the exact penalisation of the optimisation problem (Eq. 160) in the direction d^k to obtain the most ideal step length (Lemaire, 2009). This exact penalisation transforms the constrained optimisation problem into an unconstrained one by introducing a merit of the objective function $m(\underline{u})$ (Eq. 171). Since this merit function includes a penalty coefficient c and does not involve the gradient of the constraint function $g(\underline{u})$, it requires less computation effort. The line search starts by updating c in order to ensure a descent direction:

$$c^{k+1} = \max(1 + c^k, \text{Smooth} \frac{\|\underline{u}^k\|}{\|\nabla g(\underline{u}^k)\|}) \quad (166)$$

It should be noted that, if c is large enough, the solution of the line search is fairly close to the exact solution of the constrained problem. Zang and Kiureghian (1995) have proved that d^k is in a descent direction and results in global convergence if:

$$c > \frac{\|\underline{u}^k\|}{\|\nabla g(\underline{u}^k)\|} \quad (167)$$

The loop to determine the ideal step size starts at $j=0$ by assuming an initial step size equal to $\tau^0=1$. Subsequently, this step size is gradually reduced with a multiplicative factor τ , in accordance with:

$$a_j^k = \tau^j \text{ for } \tau \in (0,1) \quad (168)$$

The loop continues until one of the following two exit conditions is satisfied:

$$a_j^k < \frac{\varepsilon_{\text{max;absolute}}}{\|d^k\|} \quad (169)$$

$$m(\underline{u}_{j+1}^k) \leq m(\underline{u}_j^k) + a_j^k \cdot \omega \cdot \nabla m(\underline{u}_j^k)^T \cdot d^k \quad (170)$$

Where:

$$m(u) = \frac{1}{2}u^T u + c|g(u)| \quad (171)$$

$$\nabla m(u) = u + c \cdot \text{sign}(g(u)) \cdot \nabla g(u) \quad (172)$$

Where:

$m(u)$ Merit function of the objective function $f(u)$ at point u [-]

ω Armijo factor [-]

c Penalty coefficient [-]

$\varepsilon_{\text{max,absolute}}$ Allowable absolute error between two iterates [-]

Eq. (169) represents the maximum allowable step size per iteration k , whereas Eq. (170) determines the minimum improvement to be made to the penalised objective function during the line search. This merit function $m(u)$ (Zhang & Der Kiureghian, 1995) includes the Armijo rule (Armijo, 1966; Luenberger, 1986). This loop guarantees an appropriate decrease of the next iterate u^{k+1} .

The influence of the Armijo factor ω appeared to be marginal, so the default value (recommended in literature, i.e. Nocedal & Wright, 2000) 10^{-4} was used. Furthermore, the absolute value of τ in the range 0.5-0.8 generally leads to an acceptable calculation time. During this study it was found that the first step in the line-search procedure was quite large, frequently introducing soil failure into the finite element model. This was mitigated by adapting the finite difference interval ε_i and by adjusting the loop to determine the ideal step size (Laera & Brinkgreve, 2017).

After the line-search procedure, the allowable convergence errors were evaluated in order to verify whether or not the iteration process was finished. The iteration process stops if one of the following two convergence acceptance criteria has been satisfied:

$$\varepsilon_{\text{absolute}} < \varepsilon_{\text{max,absolute}} \cap \varepsilon_{\text{relative}} < \varepsilon_{\text{max,relative}} \quad (173)$$

$$\varepsilon_{\text{residual}} < \varepsilon_{\text{max,residual}} \cap \varepsilon_{\text{constraint}} < \varepsilon_{\text{max,constraint}} \quad (174)$$

Where:

$$\varepsilon_{\text{absolute}} = \|u^{k+1} - u^k\| \quad (175)$$

$$\varepsilon_{\text{relative}} = \frac{\|u^{k+1} - u^k\|}{\|u^{k+1}\|} = \frac{\varepsilon_{\text{absolute}}}{\|u^{k+1}\|} \quad (176)$$

$$\varepsilon_{\text{residual}} = \left\| u^k + \frac{g(u^k) - \nabla g(u^k)^T \cdot u^k}{\|\nabla g(u^k)\|^2} \right\| \quad (177)$$

$$\varepsilon_{\text{constraint}} = |g(u^k)| \quad (178)$$

Appendix B2. Abdo-Rackwitz FORM algorithm

Where:

$\varepsilon_{absolute}$	= absolute error of two successive iterates[-]
$\varepsilon_{relative}$	= relative error of two successive iterates [-]
$\varepsilon_{residual}$	= orthogonality error at the point u^k [-]
$\varepsilon_{constraint}$	= absolute error of the constraint function $g(u)$ [-]

In this study, the second of the two acceptance criteria was used (Eq. 174). This is because otherwise the Abdo-Rackwitz algorithm did not necessarily converge to a global solution. When the residual error is fairly low, it is highly likely that the solution is a global minimum, whereas a low absolute error could also represent a local minimum. Since the absolute error influences the backtracking line-search procedure, the maximum allowable error was set at 0.01, because values lower than 0.001 appeared to be in the range of the numerical noise of the calculation output of the finite element model. The relative error was set lower than 0.00001 in order to urge the algorithm to converge to a global solution.

The maximum residual error was set at 0.01. The constraint error depends on the limit state under consideration. A maximum constraint error of 0.05 times $g(u)$ was acceptable, and generally higher than the numerical noise around the Plaxis calculation output.

APPENDIX B3. COMPARISON OF BLUM & PROB2B WITH PLAXIS & OPENTURNS

Table B3.1. Comparison of Blum & Prob2B with Plaxis & OpenURNS in respect of lifetime reliability index, the design points in physical space X^* and normal space U^* and the sensitivity factor α for Z_{yield} *

		Blum & Prob2B			Plaxis & OpenURNS		
Reliability index β		3.87			3.76		
Parameter	SI	X^*	U^*	$\alpha_{u-space}$	X^*	U^*	$\alpha_{u-space}$
$E_{50;Backfill}$	MPa	n/a	n/a	n/a	50.9	0.19	0.05
$E_{50;Reclamation}$	MPa	n/a	n/a	n/a	25.7	-0.68	-0.19
$E_{50;Holocene}$	MPa	n/a	n/a	n/a	24.3	-0.96	-0.26
$E_{50;Clay}$	MPa	n/a	n/a	n/a	4.8	-0.07	-0.02
$E_{50;Pleistocene}$	MPa	n/a	n/a	n/a	49.2	0.02	0.01
$\varphi_{Backfill}$	°	39.4	0.13	0.03	39.7	0.16	0.04
$\varphi_{Reclamation}$	°	33.1	-0.78	-0.20	30.6	-1.34	-0.37
$\varphi_{Holocene}$	°	24.7	-3.11	-0.80	29.4	-1.60	-0.44
φ_{Clay}	°	26.6	-0.12	-0.03	26.7	-0.07	-0.02
$\varphi_{Pleistocene}$	°	38.6	-0.06	-0.02	39.3	0.09	0.03
$\gamma_{sat;Backfill}$	kN/m ³	20.3	0.32	0.08	20.5	0.41	0.11
$\gamma_{sat;Reclamation}$	kN/m ³	20.0	0.45	0.12	19.3	0.17	0.05
$\gamma_{sat;Holocene}$	kN/m ³	17.8	-0.77	-0.20	18.6	-0.39	-0.11
$\gamma_{sat;Clay}$	kN/m ³	17.0	0.00	0.00	16.9	-0.06	-0.02
$\gamma_{sat;Pleistocene}$	kN/m ³	20.0	0.01	0.00	20.1	0.03	0.01
h_{OWL}	m	-0.82	0.06	0.01	-0.84	0.01	0.00
h_{GWL}	m	-0.27	-0.24	-0.06	-0.31	-0.22	-0.06
Q_{t50}	kN/m ²	116	1.12	0.29	112	0.61	0.17
$h_{retaining}$	m	n/a	n/a	n/a	0.25	-0.72	-0.20
t_{tube}	mm	14.6	-0.53	-0.14	14.5	-0.67	-0.18
D_{tube}	m	1.029	-0.72	-0.19	1.021	-0.86	-0.24
f_y	N/mm ²	479.7	-0.84	-0.22	473.8	-1.74	-0.48
θ_M	-	1.10	0.96	0.25	1.14	1.36	0.37
θ_N	-	1.02	0.24	0.06	1.04	0.36	0.10

APPENDIX C1. COMPARISON OF RELIABILITY METHODS

Table C1.1. Comparison of Blum&Prob2B with Plaxis & OpenURNS in respect of lifetime reliability index, the design points in physical space X^* and normal space U^* and the sensitivity factor α for $Z_{yield,landside}$ *

		Blum & Prob2B			Plaxis & OpenURNS		
Reliability index β		3.87			3.77		
Parameter	SI	X^*	U^*	$\alpha_{u-space}$	X^*	U^*	$\alpha_{u-space}$
$E_{50;Backfill}$	MPa	n/a	n/a	n/a	47.9	-0.12	-0.03
$E_{50;Reclamation}$	MPa	n/a	n/a	n/a	25.6	-0.70	-0.19
$E_{50;Holocene}$	MPa	n/a	n/a	n/a	24.7	-0.88	-0.23
$E_{50;Clay}$	MPa	n/a	n/a	n/a	4.8	-0.09	-0.02
$E_{50;Pleistocene}$	MPa	n/a	n/a	n/a	47.6	-0.15	-0.04
$\varphi_{Backfill}$	°	39.4	0.13	0.03	39.7	0.26	0.07
$\varphi_{Reclamation}$	°	33.1	-0.78	-0.20	29.2	-1.74	-0.46
$\varphi_{Holocene}$	°	24.7	-3.11	-0.80	28.4	-1.93	-0.51
φ_{Clay}	°	26.6	-0.12	-0.03	27.5	0.24	0.06
$\varphi_{Pleistocene}$	°	38.6	-0.06	-0.02	39.7	0.26	0.07
$\gamma_{sat;Backfill}$	kN/m ³	20.3	0.32	0.08	20.2	0.20	0.05
$\gamma_{sat;Reclamation}$	kN/m ³	20.0	0.45	0.12	19.2	-0.23	-0.06
$\gamma_{sat;Holocene}$	kN/m ³	17.8	-0.77	-0.20	18.5	-0.36	-0.10
$\gamma_{sat;Clay}$	kN/m ³	17.0	0.00	0.00	17.1	0.11	0.03
$\gamma_{sat;Pleistocene}$	kN/m ³	20.0	0.01	0.00	20.0	-0.02	-0.00
h_{OWL}	m	-0.82	0.06	0.01	-0.83	0.06	0.02
h_{GWL}	m	-0.27	-0.24	-0.06	-0.29	-0.25	-0.07
Q_{t50}	kN/m ²	116	1.12	0.29	112	0.56	0.15
$h_{retaining}$	m	n/a	n/a	n/a	0.23	-0.66	-0.18
t_{tube}	mm	14.6	-0.53	-0.14	14.3	-0.91	-0.24
D_{tube}	m	1.029	-0.72	-0.19	1.035	-1.03	-0.27
f_y	N/mm ²	479.7	-0.84	-0.22	503.5	-0.72	-0.19
θ_M^{-1}	-	1.10	0.96	0.25	1.15	1.52	0.40
θ_N^{-1}	-	1.02	0.24	0.06	1.03	0.33	0.09

1) The model uncertainties θ_M and θ_N are assumed to be independent.

APPENDIX C2. COMPARISON WITH AND WITHOUT TRUNCATION

Table C2.1. Comparison between truncated normal distribution and normal distribution in respect of lifetime reliability index, the design points in physical space X^* and normal space U^* and the sensitivity factor α for corrosion curve 3 of $Z_{yield,landside}$

		Truncated normal distribution for Δt_{eq}			Normal distribution for Δt_{eq}		
Reliability index β		4.30			4.29		
Parameter	SI	X^*	U^*	$\alpha_{u-space}$	X^*	U^*	$\alpha_{u-space}$
$\varphi_{Backfill}$	°	39.5	0.15	0.03	39.4	0.12	0.03
$\varphi_{Reclamation}$	°	33.1	-0.78	-0.18	32.9	-0.82	-0.19
$\varphi_{Holocene}$	°	24.1	-3.29	-0.77	24.1	-3.28	-0.76
φ_{Clay}	°	26.6	-0.13	-0.03	26.6	-0.13	-0.03
$\varphi_{Pleistocene}$	°	38.6	-0.06	-0.01	38.5	-0.08	-0.02
$\gamma_{sat; Backfill}$	kN/m^3	20.4	0.38	0.09	20.4	0.36	0.08
$\gamma_{sat; Reclamation}$	kN/m^3	20.0	0.50	0.12	20.0	0.49	0.12
$\gamma_{sat; Holocene}$	kN/m^3	17.6	-0.85	-0.20	17.6	-0.85	-0.20
$\gamma_{sat; Clay}$	kN/m^3	16.9	-0.01	-0.01	17.0	0.01	0.00
$\gamma_{sat; Pleistocene}$	kN/m^3	20.0	-0.01	-0.01	20.0	0.01	0.00
c_{Clay}	kPa	6.66	-0.00	-0.00	6.64	-0.01	-0.00
h_{OWL}	m	-0.83	0.13	0.03	-0.83	0.14	0.03
h_{GWL}	m	-0.28	-0.29	-0.07	-0.28	-0.28	-0.06
Q_{t1}	kN/m^2	90.5	1.54	0.36	89.8	1.49	0.35
t_{tube}	mm	14.36	-0.66	-0.15	14.36	-0.66	-0.15
D_{tube}	m	1.029	-0.73	-0.17	1.028	-0.72	-0.17
f_y	N/mm^2	478	-0.89	-0.21	478	-0.89	-0.21
θ_M	-	1.13	1.27	0.30	1.13	1.27	0.30
θ_N	-	1.13	0.00	0.00	1.13	0.00	0.00
Δt_{eq}	mm	3.12	0.16	0.04	3.52	0.35	0.08

APPENDIX D1. BERTHING VELOCITY OF LARGE SEAGOING VESSELS IN ROTTERDAM

This appendix is based on the following publication: Roubos, A. A., Groenewegen, L., & Peters, D. J. (2017), Berthing velocity of large seagoing vessels in the port of Rotterdam. Marine Structures 51, pp. 202-219.

Introduction

During their service life, marine structures such as quay walls, jetties and flexible dolphins have to ensure the effective, safe and efficient handling of ships. In the coming years, many marine structures at the port of Rotterdam will be upgraded as part of a lifetime extension programme. The actual performance and reliability of quay walls depend largely on the ratio between the actual loads acting on these structures, the original design values and the deterioration of the facility. The loads associated with berthing impact need to be taken into consideration in the structural analysis. Ueda et al. (2010) showed that the contribution of berthing velocity to the uncertainty in kinetic berthing energy was approximately 85%, which provides an indication of the need for further investigation on berthing velocity.

At the 1953 International Navigation Congress in Rome, Prof. A. L. L. Baker examined berthing velocity based on field observations of exposed locations in the United Kingdom and the Arabian Gulf. His work was extended by Saurin (1963) and Brolsma et al. (1997), and resulted in the so-called Brolsma curves. The Brolsma curves included in the design guideline of fender systems (PIANC, 2002) are shown in [Fig. 5.1](#). Brolsma collected field measurements from shore-based docking systems at three berths in Rotterdam and one in Scotland. The proposed mean design values of the berthing velocities were called normal berthings and represent a return period of 30 years based on 100 arrivals per year. Over time, Brolsma's original curves were reproduced, slightly modified and published in PIANC (2002) and BS 6349-4 (2014). The German recommendations for waterfront structures, EAU 2012 (Grabe, 2012), and the Spanish ROM 0.2-90 (1990) both provide recommendations for characteristic values of berthing velocities. The berthing velocity of large seagoing vessels with a DWT greater than approximately 50,000 tonnes was assumed to be independent of the size and type of vessel. Three categories of navigation conditions were distinguished ([Fig. 5.1](#)).

The Japanese OCDI (2009) presented mean berthing velocities of approximately 5 cm/s related to single berthings of small seagoing vessels, based on a survey by Moriya et al. The highest observed berthing velocity was 15 cm/s. A data collection published by Ueda and Shirashi in 1992 was also included. The measurements included in the dataset consisted of 738 berthing operations of oil tankers with a DWT of approximately 200,000 tonnes at offshore berths. These displayed a Weibull distribution:

Appendix D1. Berthing velocity of large seagoing vessels in Rotterdam

$$F(x; \lambda, k) = 1 - e^{-\left(\frac{x}{\lambda}\right)^k} \quad (\text{Weibull distribution}) \quad (179)$$

Where:

λ	Scale parameter in Weibull distribution [m/s] $\lambda \approx 0.04$ m/s
x	Velocity [m/s]
k	Shape parameter in Weibull distribution [-] $k \approx 2$

The highest recorded berthing velocity was 13 cm/s and a design value of 14.5 cm/s with a return period of once per 1000 arrivals was recommended.

Relatively little data on berthing velocity has been collected since the 1970s, and measurements of large seagoing container vessels have been completely lacking (Beckett Rankine, 2010). PIANC therefore initiated a new working group, MarCom 145, with the objective of producing a report providing data on actual vessel approaches for a range of environmental conditions and presenting clear and uniform guidelines on the use of design berthing velocities (PIANC, 2019). The Port of Rotterdam Authority supported this PIANC initiative and decided to develop a measurement programme to collect new observations. This programme was subsequently extended to various ports in the United States (Burkhart & Matakis, 2013). A detailed description of the method can be found in Rath (2012). Similar initiatives were undertaken in Germany, South Asia and Japan, as described by Hein (2014) and Jamase et al. (2014). Berthing operations of ferry-class vessels were conducted in the ports of Juneau and Seattle (Metzger et al., 2014). Typically, mean berthing velocities of 5 cm/s were found. The maximum berthing velocity measured was 13 cm/s.

This appendix considers the most relevant parameters which could influence berthing velocities. The historical assumption that berthing velocity is correlated to the dimensions of large seagoing vessels is not supported by all design guidelines. Remarkably, the variety in types of vessel, their propulsion systems, berthing policies and pilot experience is not included in any guideline. For berths with a relatively low under-keel clearance and/or a relatively closed type of marine structure (e.g. a quay wall), lower berthing velocities are to be expected due to the so-called water cushion effect. Hence, the main focus of this appendix is the correlation between berthing velocity and ship dimensions, type of fendering, water cushion effect, type of marine structure, environmental factors, berthing policy and navigation aids. Its main objective is to enhance understanding of landing procedures and berthing velocities. The probability distribution functions of berthing velocity are of particular interest, as they provide a solid base for future reliability-based assessments of quay walls. It was expected that actual berthing velocities would most likely be lower than in the current design guidance, because existing quay walls are still in good condition. The results of this appendix could contribute to new business opportunities, e.g. to allow larger vessels to berth at existing quay walls and/or to extend the service life of quay walls and other types of marine structure.

Appendix D1. Berthing velocity of large seagoing vessels in Rotterdam

D.1.1 BERTHING RECORDS AND DATA ANALYSIS

Type of vessel and project location in Rotterdam

Berthing velocities of small and large seagoing container vessels, tankers and bulkers were of interest. Unfortunately it was impossible to measure the berthing velocity of small vessels with limited freeboard. To acquire more insight into the correlation between berthing velocity and type of vessel, a differentiation was made between container vessels, tankers and bulkers. Subsequently, each of these vessel types was subdivided into specific vessel classes. The classification of vessels was largely based on the international Lloyds database. Various berth types were involved. All container vessels moored at closed quay walls equipped with either hard buckling or soft cylindrical fender systems. Bulkers berthed at closed quay walls where rigid timber beams were installed. At tanker berths, flexible mooring dolphins with buckling fender systems were utilised adjacent to open jetties. The geographical location of the berths is indicated in Fig. D.1.



Fig. D.1. Berths associated with either PPU data, mobile or shore-based laser observations in the Maasvlakte area of the port of Rotterdam.

Data collection

Several methods were used for collecting data on berthing velocities. Interviews and questionnaires appeared to be less efficient and vessels' automatic identification systems (AIS) did not provide enough accuracy. A berthing velocity accuracy of mm/s was preferred for this study, with at least cm/s being required. Container vessels were measured using a

Appendix D1. Berthing velocity of large seagoing vessels in Rotterdam

portable laser system provided by Trelleborg Marine Systems, called SmartDock® laser LITE (Fig. D.2). With this, tracking records of actual berthing operations were collected during the windy season (Oct.-Dec. 2011). In total, 178 measurements of relatively large seagoing container vessels were recorded. These were collected by the Port of Rotterdam Authority in close co-operation with KRVE (the Royal Boatmen's Association Eendracht in the Port of Rotterdam) and the Dutch Pilotage Service. This appeared to be an efficient and safe way to gather a large amount of data in a short period of time. Following this data-gathering campaign, the method developed for it was also used in several ports in the United States.



Fig. D.2. SmartDock® laser LITE and software interface.

A typical berthing operation recorded with portable lasers is illustrated in Fig. D.3. Firstly, the point of maximum fender deflection and zero (berthing) velocity was determined. Because the distance between the portable workstation and the fender line is known, the exact moment of impact and corresponding berthing velocity were established relatively easily. It should be noted that, in this case, the container vessel rebounds a little shortly after its first contact with the fender. A few moments later, a second impact is visible. In this particular case, the first impact was predominant. For small feeder, tanker and bulker berthings, the velocity of the second impact was often higher.

Appendix D1. Berthing velocity of large seagoing vessels in Rotterdam

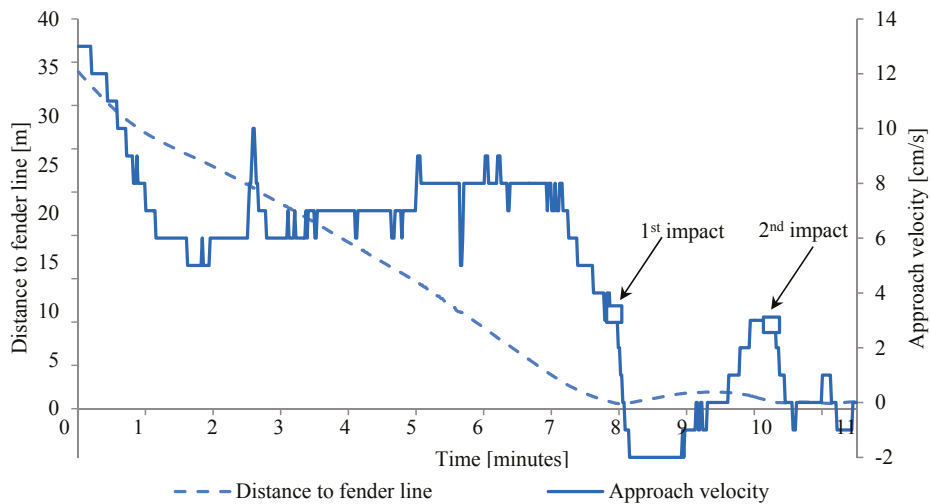


Fig. D.3. Approach velocity of Post-Panamax container vessel to moment of impact, recorded with SmartDock® portable workstation.

As well as the portable laser data, the Dutch Pilotage Service provided approximately 222 portable pilot unit (PPU) tracking records and two terminals provided data from five jetties equipped with shore-based docking aid systems, covering approximately 161 berthings. The accuracy of these measurements was cm/s for the shore-based systems and mm/s for the PPU data. PPU's are only installed on vessels with a draught greater than 17m, because they have to sail very accurately through the main port channels. A total of 225 tanker berthing measurements were collected, and 144 for bulkers.

According to the GPS tracking records, even moored vessels are always in motion. It was therefore extremely difficult to determine the berthing velocity at the moment of impact if fender systems were installed on flexible dolphins. The GPS position of the fender line could not be compared directly with the location of first impact, and a second berthing impact often predominated over the first due to the yaw motion of the tanker. This issue was resolved by finding the maximum berthing velocity within a range of 0.8 m (based on actual measured deformations of the dolphins). The extreme events deduced from PPU data are therefore most likely slightly conservative, especially those for bulk carriers. Verification showed that no correction was made for the PPU tracking records of bulkers berthing at closed quay walls equipped with rigid fender beams. The extreme berthing velocities of bulkers are therefore most likely overestimated, because there is negligible deflection of quay walls and rigid fender beams.

It was envisaged at the start of this test programme that a clear distinction would have to be made between various berthing and navigation parameters. A large database was

developed including all available and most likely relevant data which might influence berthing velocity. Besides observations of berthing velocity, the following data was collected.

- General data (date and arrival time).
- Measured data (berthing velocity and angle).
- Geometric conditions (type of terminal, number of bollards, type of waterfront structure, design depth/level of harbour bottom, berthing condition, type of fendering, exposed or sheltered).
- Vessel characteristics (name, type, length, width, maximum draught, actual draught, type of thrusters for main propeller, stern and bow thrusters, bow radius).

Data analysis

Several hypotheses, mainly regarding correlations between berthing velocity and other berthing parameters, were tested using linear regression analyses. This section provides an overview of the statistical methods used to acquire insight into the key parameters influencing berthing velocity.

For various types of vessel, the mean value, standard deviation and the maximum observed berthing velocity were established in order to verify the hypothesis that berthing velocity correlates with the size of the vessel. All vessel classes were individually analysed with normal, lognormal and Weibull cumulative distribution functions. One important disadvantage of such a differentiation into populations of individual vessel classes is a significant decrease of the number of measurements within a certain population. The volume of data within a population sometimes becomes too low for empirical analysis. The following probability distribution functions were applied to the datasets of the collected berthing velocities:

$$F(x; \mu, \sigma) = \frac{1}{2} \left(1 + \operatorname{erf} \left(\frac{x - \mu}{\sigma\sqrt{2}} \right) \right) \quad (\text{normal distribution}) \quad (180)$$

$$F(x; \mu, \sigma) = \frac{1}{2} \left(1 + \operatorname{erf} \left(\frac{\ln(x) - \mu}{\sigma\sqrt{2}} \right) \right) \quad (\text{lognormal distribution}) \quad (181)$$

$$F(x; \lambda, k) = 1 - \exp \left(- \left(\frac{x}{\lambda} \right)^k \right) \quad (\text{Weibull distribution}) \quad (182)$$

Where:

$F(\cdot)$	Probability distribution function [-]
x	Berthing velocity [cm/s]
μ	Mean [cm/s]
σ	Standard deviation [cm/s]
λ	Scale parameter in Weibull distribution [m/s]
k	Shape parameter in Weibull distribution [-]

Appendix D1. Berthing velocity of large seagoing vessels in Rotterdam

It should be noted that if a single extreme berthing velocity was measured in a small population, the Weibull fit could be excessively influenced by that one extreme value and this could easily lead to unrealistic and unreliable extreme berthing velocities. The influence of the maximum observed berthing velocities was investigated with a Weibull fit for the data points with a peak over threshold (POT) of 95%. These principles are illustrated in Fig. D.16. If the fit of the distribution had a lower coefficient of correlation than $R^2 < 0.85$, the results of the data analysis were carefully studied and should be neglected in future extreme value analysis. An adequate fit of the tail of the distribution functions to the dataset is of the utmost importance. The dataset of tanker berthings was enlarged with the measurements from those in Germany, which resulted in larger populations. This location had navigation conditions and a berthing policy similar to those in Rotterdam.

Most of the data which could influence berthing velocity was in the public domain or already registered by the Port of Rotterdam Authority (e.g. actual draught, water levels, wind power and direction, type of berth, etc.). The methods used to collect this data were all relatively basic and reliable. Because the actual draught, actual bottom level and actual water level are known, a regression analysis between the under-keel clearance (UKC) of container vessels was carried out in order to measure the water cushion effect adjacent to closed quay walls.

$$UKC = h_w - h_{bottom} - d_{act} \quad (183)$$

Where:

UKC	Under-keel clearance [m]
h_w	Actual water level [m + MSL]
h_{bottom}	Actual bottom level [m + MSL]
d_{act}	Actual draught [m]

The influence of wind speed and wind direction on the berthing velocity of container vessels was examined during the windy season. The position of the berth relative to the wind direction was registered in a central database (Bochen, 2012). Logically, the windage area of a vessel strongly depends on its actual draught. The lateral wind force acting on the vessels was quantified in order to find out whether wind was influencing berthing velocity by using the following equations:

$$P_{lat} = q A_{act} \sin(\alpha) = \frac{1}{2} \rho v_w^2 \sin(\alpha) \quad (184)$$

$$A_{act} = A_{min} + (T_{max} - T_{act})LBP \quad (185)$$

Where:

P_{lat}	Lateral wind force [kN]
q	Dynamic pressure [kN/m ²]
A_{act}	Actual windage area [m ²]
A_{min}	Minimum windage area [m ²]
α	Angle between wind and the hull [°]
ρ	Air density [kg/m ³]
v_w	Wind velocity [m/s]
T_{act}	Actual draught [m]
T_{max}	Maximum draught [m]
LBP	Length between perpendiculars [m]

In the Rotterdam datasets for tankers and bulkers, both fore and aft velocities of the berthing records are listed. That data includes a combination of translational and angular velocity just before the first moment of impact. At the moment of maximum fender compression, the translational berthing velocity at the point of contact becomes zero and the ship maintains angular momentum. During the manoeuvre, tugs may change the angular position of the vessel. A model based only on translational velocities of the centre of mass of vessels seemed inaccurate, especially at low velocities and low berthing angles. Although low angles seemed to be favourable, greater approach angles could contribute to a reduction in the amount of energy to be absorbed by the fender system. If vessels are berthed in a direction perpendicular to the line connecting the centre of gravity of the ship and the point of contact of the fender system, the amount of energy absorbed by the fender will be reduced. A negative rotation of the vessel during the final landing procedure will also reduce the berthing impact. This type of berthing could be efficient in the case of berths with high currents. The berthing angle during this type of landing must be larger in order to allow enough time to reduce the vessel's rotational velocity, otherwise the second impact could be more severe than the first. The following formula is included in the EAU 2012 (Grabe, 2012):

$$E_{kin} = 1/2 m v C_m C_s C_c C_E \quad (186)$$

$$E_{kin} = \frac{m C_m C_s C_c (v^2 (k^2 + r^2 \cos^2 \phi) + 2v\omega r k^2 \sin \phi + \omega^2 r^2 k^2)}{2(k^2 + r^2)} \quad (187)$$

Before the first impact, the measured fore and aft perpendicular velocities include rotational effects. During evaluations of the Rotterdam measurements, the maximum fore and aft velocities were treated conservatively as translation velocities perpendicular to the

Appendix D1. Berthing velocity of large seagoing vessels in Rotterdam

berthing line. Only a part of the ship's energy is absorbed by the fender during the first impact, which is dominated by translation movements by the vessel. The second impact is dominated by rotation and also contains angular momentum, and can be more severe compared to the first. Typically, the translational velocity of the first impact is close to the mean berthing velocity, while the velocity of the second impact is approximately 2-3 cm/s higher. This depends on the type of landing, the direction of vessel movements and the rotational component (Fig. D.4). The C_E factor of the rotational component is smaller and the landing will generally be smoother than the impact dominated by translation (Vasco Costa, 1986).

$$C_E = \frac{k^2+r^2\cos^2\phi}{k^2+r^2} + \frac{\omega r}{v} \cdot \frac{2k^2\sin\phi}{k^2+r^2} + \frac{\omega^2 r^2}{v^2} \cdot \frac{k^2}{k^2+r^2} \quad (\text{translation and rotation}) \quad (188)$$

$$C_E = \frac{k^2+r^2\cos^2\phi}{k^2+r^2} \quad (\text{translation only}) \quad (189)$$

$$C_E = \frac{k^2}{k^2+r^2} \quad (\text{rotation only}) \quad (190)$$

The estimate of the radius of gyration was obtained from the OCDI (2009):

$$k = \frac{\sqrt{I}}{L} = \frac{L}{\sqrt{12}} = 0.29 L \text{ with } B < \frac{1}{6} L \quad (191)$$

$$k = L (0.19C_B + 0.11) \text{ for } C_B < 1 \quad (192)$$

Where:

E_{kin}	Kinetic energy [kJm]
m	Mass of vessel/water displacement [tonnes]
k	Radius of gyration of vessel [m]
r	Distance of vessel's centre of gravity from point of contact with marine structure [m]
v	Total translation velocity of centre of mass at time of first contact (includes component parallel and perpendicular to berthing line) [m/s]
v_t	Component of the translation velocity perpendicular to the berthing line [m/s]
v_r	Perpendicular velocity due to vessel rotation considered at a distance equal to the radius of gyration from the vessel's centre of gravity [m/s].
ω	Vessel's angular velocity at time of first contact with fender [rad/s]
ϕ	Angle between velocity vector v and distance r [°]
α	Berthing angle [°]

Appendix D1. Berthing velocity of large seagoing vessels in Rotterdam

L	Length of vessel [m]
B	Width of vessels [m]
C_B	Block coefficient, $C_B \approx 0.72-0.85$ for bulkers or $C_B \approx 0.85$ for tankers [-]
C_m	Virtual mass factor [-]
C_s	Vessel flexibility factor [-]
C_c	Waterfront structure attenuation factor [-]
C_E	Eccentricity factor, $C_E \approx 0.4-0.6$ for quarter-point and $C_E \approx 0.6-0.8$ for third-point berthing [-]

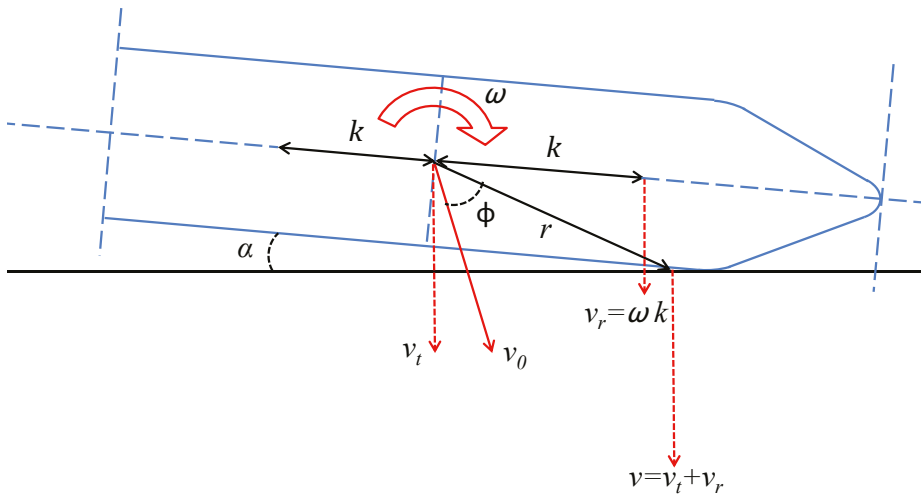


Fig. D.4. Principles of translational and angular velocity during first impact.

An overview of typical design berthing velocities was developed for various design vessels in order to compare the new measurements with the currently recommended design guidance. Logically, these values were established by a desk study of the programme of requirements and relevant design reports. The desk study was limited to the most important berths constructed between 1990 and 2015. All marine structures involved are owned by the Port of Rotterdam Authority.

D.1.2 RESULTS OF DATA ANALYSIS OF ROTTERDAM BERTHING RECORDS

Measurements were collected for various berths in several port basins. In an attempt to increase understanding of the recorded berthing velocities, differentiating factors were accounted for by vessel characteristics, environmental aspects and berthing policy. The key findings of that exercise are presented in this section.

Appendix D1. Berthing velocity of large seagoing vessels in Rotterdam

Ship dimensions and characteristics

The mean berthing velocity of large seagoing vessels was approximately 4 cm/s and the maximum measured velocity from 555 berthings was 13 cm/s (Table D.1). Almost all arrivals were assisted by tugs and guided by pilots.

Table D.1. Collection of berthing velocity survey from measurements.

Ship type	n	v_{μ} [cm/s]	v_{max} [cm/s]	Berth type	Berthing aids	Wind	Waves	Current
Container	178	4.0	10	closed quay	None	high	sheltered	low
Tanker	225	4.3	12	jetty/dolphin	Portable pilot units/shore-based docking aids	high	sheltered	low
Bulker	144	4.4	13	closed quay	Portable pilot units	high	sheltered	low

The frequency of arrivals was set at 100 berthings by the design vessel per year, in line with the recommendations made by Brolsma et al. (1977). The berthing velocity corresponding to a return period of 50 years was derived by extrapolating the Weibull distribution fit of individual vessel classes (Fig. D.5).

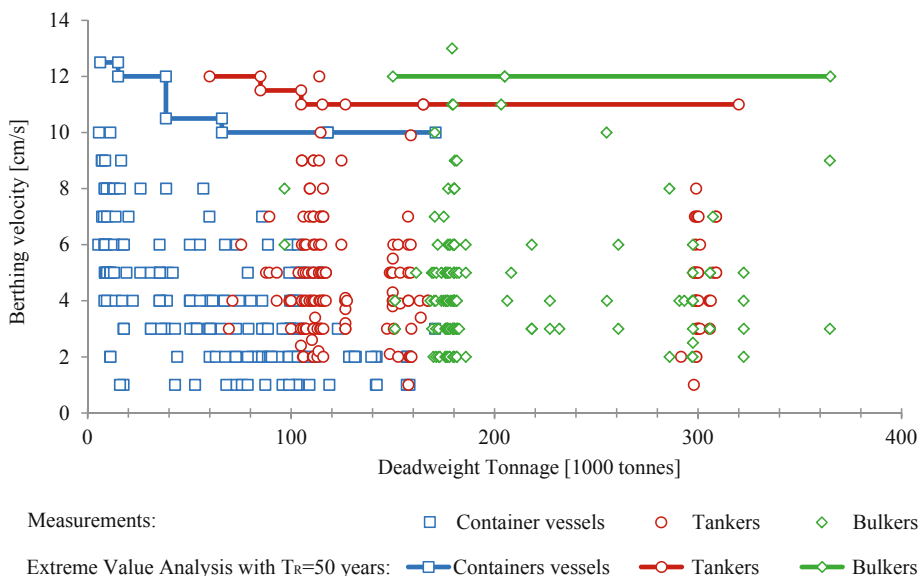


Fig. D.5. Field measurements of berthing velocity against extreme berthing velocities with a return period of 50 years.

Appendix D1. Berthing velocity of large seagoing vessels in Rotterdam

The berthing velocities of individual vessel classes with a return period of 50 years were compared with the design curves in EAU 2012 (Grabe, 2012) and PIANC (2002), as shown in Fig. D.6. The values in the EAU graphs are characteristic values with a return period of 50 years. The PIANC curves represent a return period of 30 years.

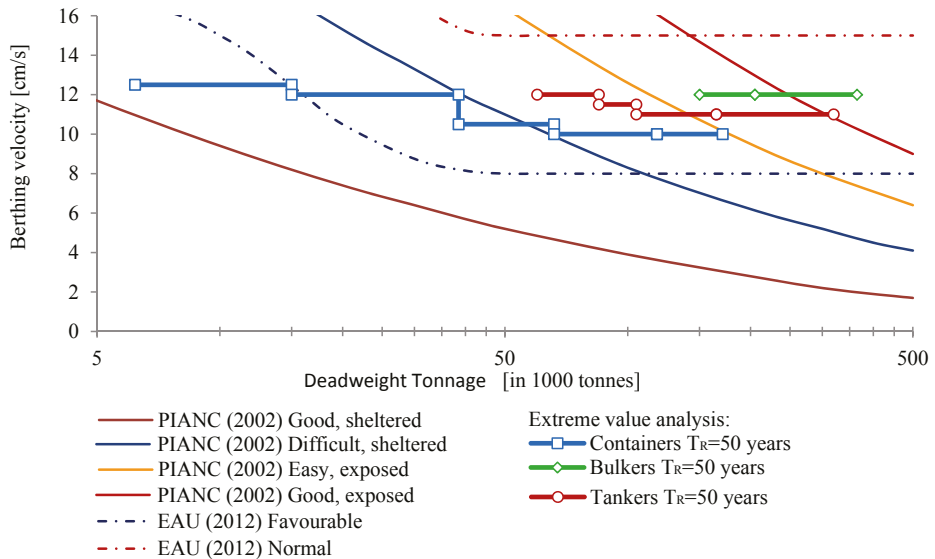


Fig. D.6. Berthing velocities with a return period of 50 years against EAU 2012 and PIANC 2002.

According to the new measurements, tankers showed a very small correlation between berthing velocity and vessel mass. Large seagoing bulkers did not show any correlation. A gentle correlation was found only for container vessels. It should be stressed that the volume of data obtained for some vessel classes was too small to be able to draw a final conclusion. Furthermore, no difference was found between the actual water displacement and the maximum water displacement of the vessel.

The ratio between the actual draught and maximum draught was further studied by means of linear regression analysis. The dataset showed a high degree of dispersion and no real correlation was found.

Despite the fact that the datasets were too small to draw strong conclusions, the trend suggests that berthing velocity does not vary for different vessel draughts within the considered range. As an example, the under-keel clearances of Post-Panamax arrivals are shown in Fig. D.7. The median value of the under-keel clearance of all container vessels was approximately 6 m, and the water cushion effect did not significantly influence the berthing velocities of container vessels. Moreover, no correlation between berthing velocity and under-keel clearance was found for bulkers and tankers.

Appendix D1. Berthing velocity of large seagoing vessels in Rotterdam

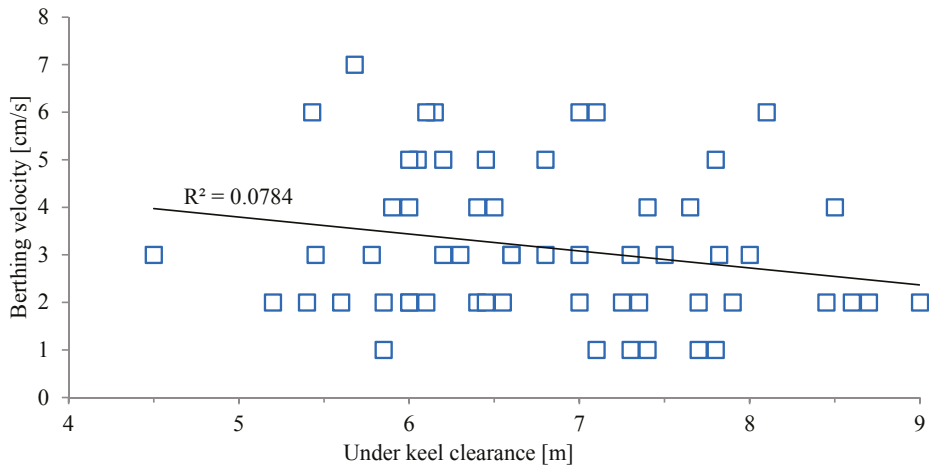


Fig. D.7. Relationship between UKC and berthing velocity for Post-Panamax class container vessels.

A comparison of the various locations showed that the distribution of berthing velocities for container vessels was more or less constant for the port basins in the Maasvlakte area of the port of Rotterdam. The basins' geometric characteristics (wide or narrow) had no effect on the distribution of berthing speeds. Nor did occupancy of the surrounding berths have any significant influence. Typical distributions for container vessels are shown in Fig. D.8.

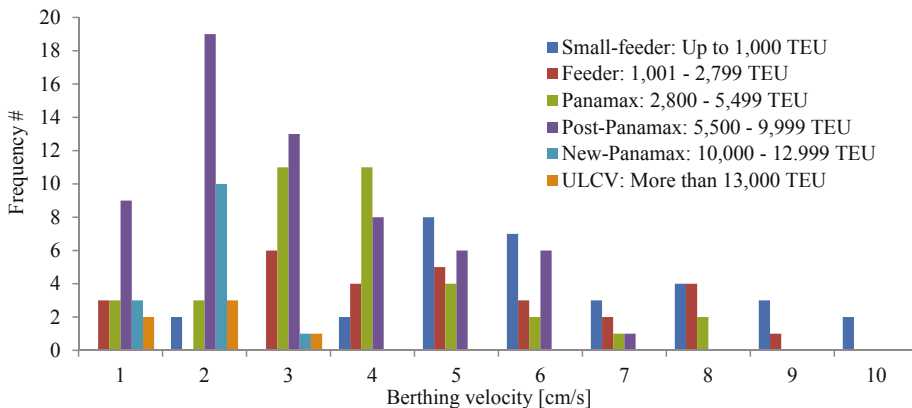


Fig. D.8. Histogram of berthing velocities of individual container vessel classes.

Environmental conditions

The relevant berths in the port of Rotterdam are classified as sheltered with respect to currents and waves (Fig. D.1). Nevertheless, manoeuvres at them by large container vessels with high freeboards and large numbers of containers on deck are still potentially highly

Appendix D1. Berthing velocity of large seagoing vessels in Rotterdam

wind-sensitive. Almost all nautical experts agreed on this. For several types of container vessels, the lateral wind force acting on the vessel was calculated. The results for the Panamax and Post-Panamax classes are shown in Fig. D.9. Generally, the coefficient of correlation was negligible or small for container vessels. No real correlations were found for small feeders and Panamax vessels, but Post-Panamax vessels do show a small correlation.

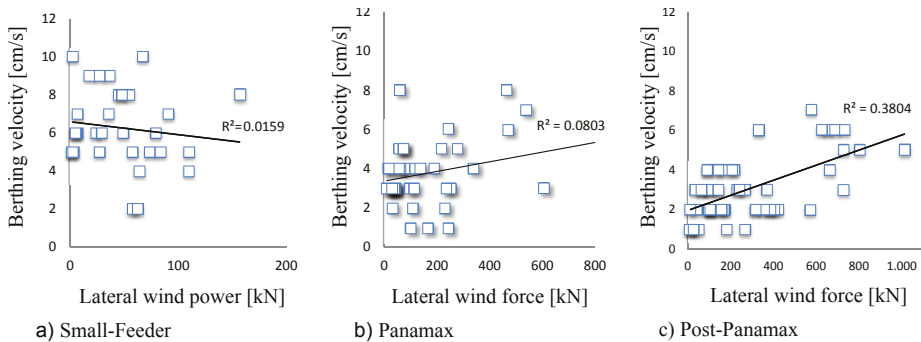


Fig. D.9. Lateral wind force versus berthing velocity for small feeders (a), Panamax (b) and Post-Panamax (c) vessels.

Fig. D.10 shows that wind does not have a major influence on berthing velocity. In this figure, measurements for container vessels are divided into three categories according to weather conditions: favourable (wind speed < 7 m/s), normal (wind speed 8-12 m/s) and unfavourable (wind speed > 12 m/s) conditions. It should be noted that tankers and bulkers may not enter the port of Rotterdam when wind speeds exceed Beaufort force 8 (< 20.7 m/s) unless the wind direction is favourable, when the maximum is Beaufort force 9 (< 24.4 m/s). Container vessels may not enter the port when wind speeds exceed Beaufort force 6 (< 13.8 m/s). No clear distinction between categories was observed.

Appendix D1. Berthing velocity of large seagoing vessels in Rotterdam

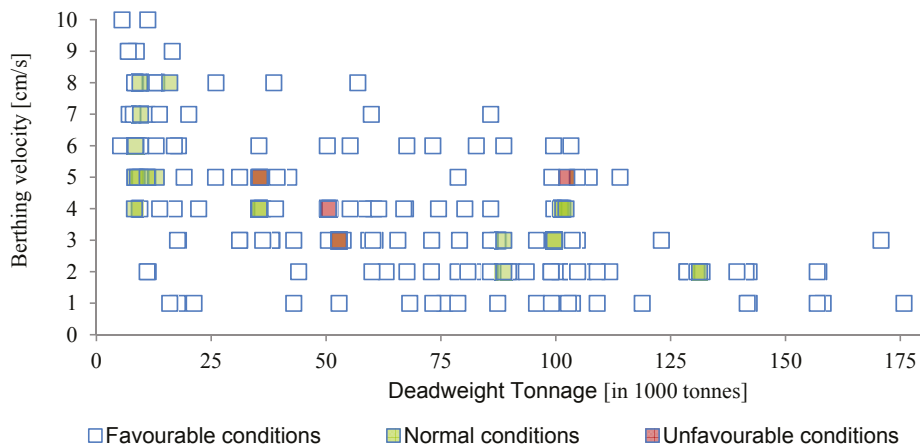


Fig. D.10. Influence of wind on the berthing velocity of container vessels.

Tug assistance

The individual container vessel classes were compared in terms of tug assistance (Table D.2). Generally, the number of tugs required depends on the type of vessel (size, actual draught), the navigation conditions (occupancy of the berths) and the environmental conditions (lateral wind force). Although there was not enough data to derive reliable correlations between number of tugs and all these parameters, some trends were apparent.

- The number of tugs used does not affect berthing velocity;
- There was a significant difference between small feeders and feeders (Fig. D.11). In order to explain this, the tracking records were studied in more detail. It was found that the significant change was caused by a different type of landing procedure.

Table D.2. Number of tugs used by individual container vessel classes and mean value of berthing velocity (cm/s).

Vessel type	No tugs			One tug			Two tugs			Three tugs		
	n	v	DWT	n	v	DWT	n	v	DWT	n	v	DWT
Small feeder	29	6.1	9004	2	8.5	7617						
Feeder	12	5.7	16250	11	4.5	21771	3	3.3	36583			
Panamax				15	3.8	42424	22	3.6	55120	2	5.5	55170
Post-Panamax	1	3.0	104696	13	2.8	87340	37	3.1	90029			
New-Panamax				4	3.0	114327	18	3.1	114277	2	3.0	116733
ULCV							5	1.8	153552	4	1.5	153140

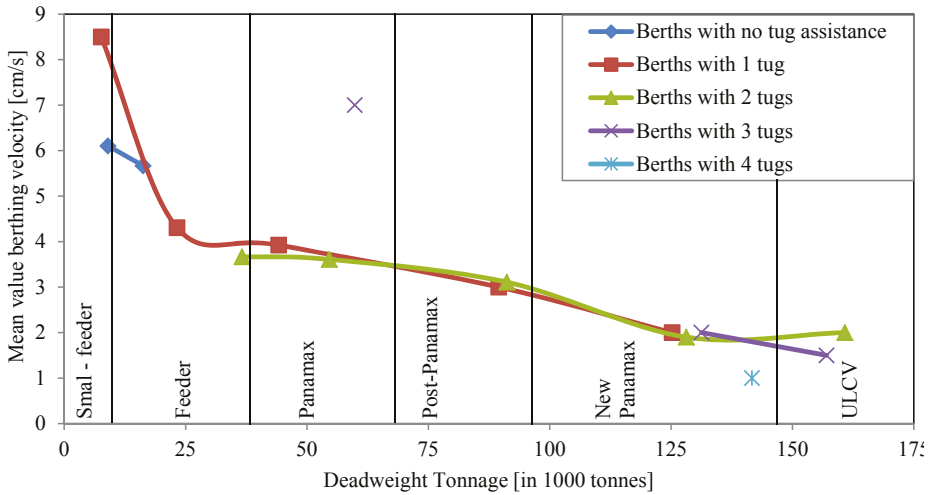


Fig. D.11. Correlation between tug assistance and dimensions of container vessels for mean berthing velocities and DWT.

Type of landing

Small feeders and feeders (DWT < 38,500 tonnes) appeared to have higher berthing velocities, as assumed in most of the design codes. Studying these particular berthing records showed that the smaller vessels were unable to accomplish parallel landing operations. Their angle of approach was much higher and fewer tugs were used. The berthing angle at the moment of impact usually remained between 0° and 1.5° (Fig. D.12), and sometimes the second berthing impact was dominant. Large container vessels always used tug assistance and were equipped with bow and stern thrusters, which allowed them to berth almost parallel to the fender line. Container vessels with large displacements (DWT > 38,500 tonnes) were stopped 20-30 m from the berth and parallel to it. Consequently, their angle of approach during the landing procedure remained small. Initial approach velocities measured at some distance from the berthing line were generally in the order of approximately 10-40 cm/s (Table D.3). The tracking records showed that captains still seemed to have some influence over the landing procedure in the final metres. Berthing velocities at the moment of impact for various container vessel types generally remained between 0 and 10 cm/s. All records of berthing operations of container vessels showed berthing angles, typically of 1.5° or less (Fig. D.12).



Appendix D1. Berthing velocity of large seagoing vessels in Rotterdam

Table D.3. Approach velocity during berthing manoeuvres of container vessels at Maasvlakte, Rotterdam.

Distance to fender line [m]	Approach velocity [cm/s]
20-50	10-30
5-20	10-20
0-5	5-15
0	0-10

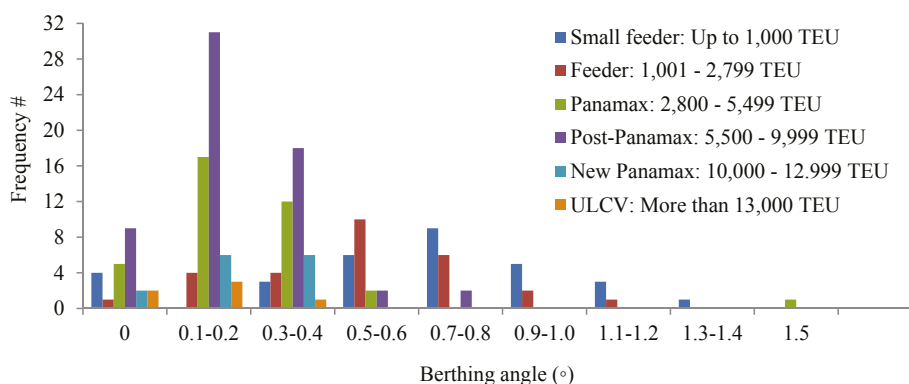


Fig. D.12. Distributions of berthing angles of container vessels at Maasvlakte, Rotterdam.

For tankers and bulkers, only the velocities at the moment of impact were available. Landing operations of large seagoing tankers and bulkers showed similarities with those of small container vessels. For the datasets of tankers and bulkers, the angular velocity was calculated. The perpendicular component of the angular velocity $v_r = \omega k$ was plotted against the translational velocity perpendicular to the berthing line (Fig. D.13). This component is not exactly the same as the rotational component of the actual berthing velocity, due to the fact that the distance from the point of impact to the centre of mass is not necessarily the same as the radius of gyration. The translational component parallel to the berthing line was not recorded. The latter value has an effect on the velocity angle ϕ and thus on the C_E factor. It was noted that, on average, an angular velocity term of 2-3 cm/s was added. The dependency on the translational velocity was weak. For bulk carriers, measurements of the berthing angles were available (Fig. D.14). A slight effect of higher angular velocities at small berthing angles was observed.

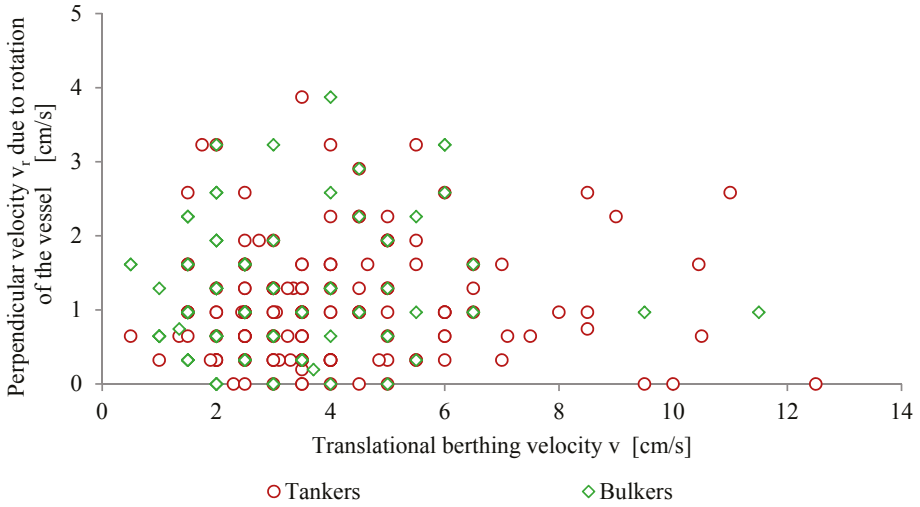


Fig. D.13. Measured rotational and translational velocities for tankers and bulkers.

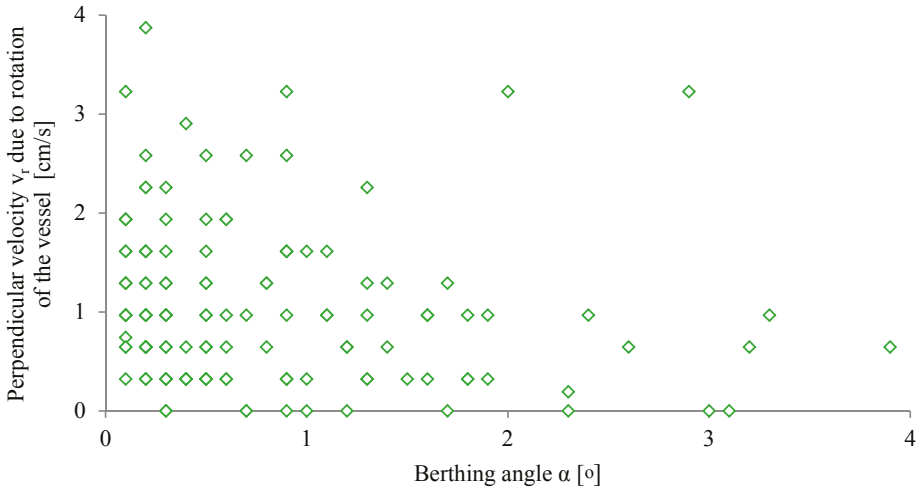


Fig. D.14. Measured rotational velocity for bulk carriers versus berthing angle.

Distribution of berthing velocities

An adequate fit of the low-probability tail of the distribution to the dataset was made in order to estimate extreme berthing velocities. The accuracy of the fit of the tail was investigated for normal, lognormal and Weibull distributions (Fig. D.15). In addition, a Weibull fit for the data points with a peak over threshold (POT) of 95% was conducted. The parameters for the best fit with normal, lognormal and Weibull and Weibull POT 95% probability distributions functions are listed in Table D.4, per vessel class.



Appendix D1. Berthing velocity of large seagoing vessels in Rotterdam

Table D.4. Cumulative distribution functions for various vessel classes.

Ship type	kDWT	n	max	Normal			Lognormal		Weibull		Weibull POT 95%	
				μ_s	σ_s	V_s	$Ln(\mu_s)$	$Ln(\sigma_s)$	λ	k	λ	k
Tankers												
Panamax	60-85	23	0.09	0.055	0.018	0.33	-2.96	0.339	0.063	3.09	0.059	2.82
Aframax ¹	85-105	175	0.12	0.044	0.018	0.40	-3.21	0.469	0.050	2.68	0.031	1.26
Suezmax	115-165	95	0.11	0.047	0.018	0.39	-3.13	0.395	0.053	2.75	0.057	2.49
VLCC	260-319	80	0.10	0.047	0.019	0.40	-3.15	0.422	0.053	2.65	0.044	1.91
Fixed laser	260-319	19	0.07	0.035	0.013	0.36	-3.40	0.348	0.041	2.77	0.019	0.92
Bulkers												
Capesize	150-205	107	0.13	0.045	0.022	0.50	-3.22	0.449	0.050	1.91	0.046	1.51
VLBC	205-365	37	0.10	0.042	0.019	0.44	-3.25	0.405	0.048	2.18	0.048	1.85
Containers												
Coasters	7-15	37	0.10	0.063	0.019	0.31	-2.83	0.360	0.071	3.68	0.063	2.74
Feeders	15-42	31	0.09	0.047	0.019	0.41	-3.17	0.496	0.054	2.63	0.058	2.99
Panamax	42-70	31	0.08	0.036	0.016	0.46	-3.46	0.510	0.041	2.22	0.034	1.51
Post Panamax	70-118	60	0.07	0.030	0.015	0.52	-3.66	0.540	0.034	1.93	0.036	2.27
New Panamax	118-171	18	0.03	0.018	0.006	0.33	-4.06	0.361	0.021	3.60	0.010	0.92
Rotterdam data	7-365	555	0.13	0.043	0.021	0.59	-3.29	0.594	0.046	2.28	0.044	1.72
All data	7-365	713	0.13	0.044	0.020	0.45	-3.24	0.498	0.049	2.28	0.043	1.75

¹⁾ The fit of the Weibull distribution to the measured data resulted in an underestimation of the highest actual measured berthing velocities with the use of PPU's. Although the reliability of the maximum values measured with the PPU was analysed carefully, these values are probably unsafe to use for determining the design berthing velocity.

Generally, the fit of the Weibull distribution of the berthing velocity of a single berthing operation provided the most appropriate description of the tail, by comparison with a normal or lognormal distribution. This is illustrated by the theoretical density functions and the Q-Q probability plot (Fig. D.15).

Appendix D1. Berthing velocity of large seagoing vessels in Rotterdam

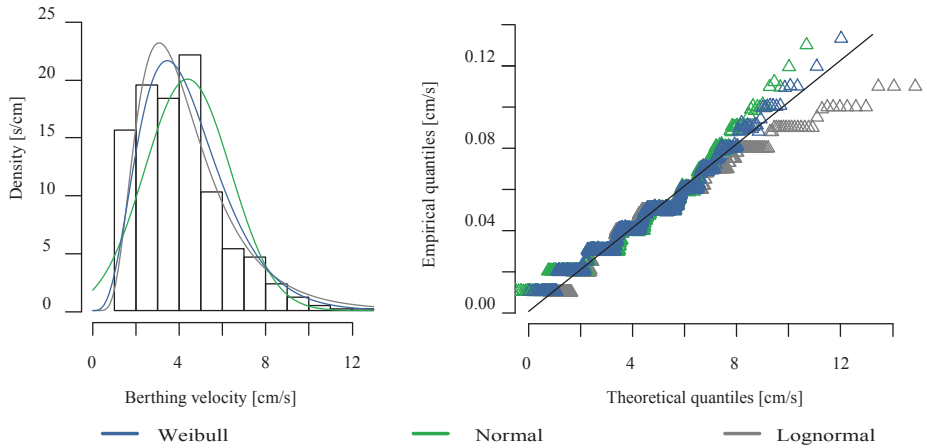


Fig. D.15. Histogram of theoretical density functions (left) and Q-Q probability plot (right) of all 713 observations.

Only the Aframax tankers had a coefficient of correlation less than $R^2 < 0.85$, meaning that the results should be treated with caution. The lognormal distribution was not convincing as a realistic estimation of the low-probability tail and overestimated the extreme berthing velocities with a small probability of exceedance (Fig. D.16). Conversely, the normal distribution regularly resulted in an underestimation of the maximum measured berthing velocity. The shape of the POT distribution fits is useful, but not reliable for small populations.

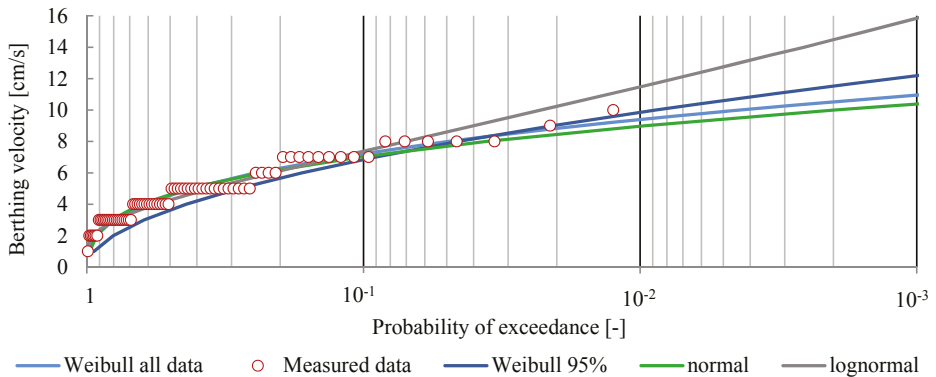


Fig. D.16. Probability distribution functions for 80 observations of VLCC tankers (260 - 319 kDWT) measured in Germany and Rotterdam.

The number of berthings during the service life of each berth may differ. Design berthing velocities are in fact time-dependent. It should be noted that extreme berthing conditions were therefore most likely not included in small data populations. The probability of exceedance in Fig. D.16 is related to a single berthing operation and not to the return

Appendix D1. Berthing velocity of large seagoing vessels in Rotterdam

period of a certain berthing velocity during the design lifetime. The number of arrivals during the lifetime will influence the relevant design berthing velocities for a marine structure. For example, according to a Weibull distribution the velocity of a single berthing with a probability of exceedance of approximately 1% ($P = 0.01$) is approximately 9.4 cm/s. This corresponds to a return interval of once per 100 arrivals. Note that the maximum observed velocity in a population of 80 observations of VLCCs was 10.0 cm/s. If 1000 arrivals are to be expected during the lifetime, the berthing velocity with a return interval of once per 1000 berthings is approximately 11.0 cm/s ($P = 0.001$). This indicates the importance of the distribution of the extreme values and the frequency of arrivals during a certain reference period.

D.1.3 DISCUSSION OF BERTHING RECORDS AT THE PORT OF ROTTERDAM

Performance of berthing facilities and fender systems

In order to correctly interpret the collected data, the performance of marine structures during the service life was discussed briefly with nautical experts, pilots and asset managers from the port of Rotterdam. The asset managers explained that some berthing facilities are approaching the end of their design lifetime. Most of the marine structures still appear to be in good condition. Quay walls equipped with soft cylindrical fenders require significantly less maintenance than those with hard buckling fenders. Reported damage to fender systems was often related to chains, stairs and panels. Damage of this type is usually not caused directly by excessively high berthing velocities. The asset managers also noted that berths which are suitable for both seagoing vessels and inland barges showed much more local damage to their fender systems. Local damage to fender panels was caused mainly by irregularities of the ship's hull or by inappropriate use of mooring lines. The timber structures installed on bulker quay walls appeared to be subjected to frequent uncontrolled manoeuvring by inland barges (pusher/towboats). These do not absorb energy, resulting in high hull pressures. Assuming that an increase in hull pressure is undesirable, berthing velocity was expected to be lower. The measurements for bulkers showed slightly lower mean values (Table D.4), but the coefficient of variance and maximum/extreme berthing velocities appeared to be higher. This could be explained by the overestimation of berthing velocities from the PPU tracking records. Generally, no significant differences were found between the berthing velocities of various fender systems at container terminals. The pilots confirmed that they do not consider the type of fender system in their berthing policy.

Navigation aids and target berthing velocity

In recent decades, there has been an increase in the use of navigation aids such as portable pilot units (PPUs) and fixed shore-based docking systems. In Rotterdam, pilots and boatmen are all well-trained and have ample experience. It is their job to moor and unmoor

Appendix D1. Berthing velocity of large seagoing vessels in Rotterdam

vessels in a safe and efficient manner. The pilots and boatmen confirmed that modern tools, which have introduced real-time monitoring of vessel movements, increase their control and confidence during the berthing process. According to nautical experts, uncontrolled berthings of large seagoing vessels are not likely to happen in well-organised ports.

In most situations, the pilots and captains are not aware of the design berthing velocity. Generally, their objective is to land with a berthing velocity of approximately 3-4 cm/s. A berthing velocity of 8 cm/s was mentioned as unlikely to happen when using pilot and tug assistance. Five jetties for liquid bulk carriers are equipped with shore-based docking aid systems to assist in reducing berthing velocities. Generally, the determination of such a target resulted in increased confidence concerning the condition of the marine structure. On the one hand, a pilot may observe a berthing facility that is in a relatively poor condition. In this case, they seem likely to adopt a lower approach velocity. On the other hand, although there is often less experience with brand new berthing facility in its first months in service, its condition is relatively good. In this case, pilots may consider a higher berthing velocity. Typical target berthing velocities for onshore docking systems are shown in [Table D.5](#).

Table D.5. Target berthing velocities for onshore docking systems at tanker berths in the port of Rotterdam.

Target berthing velocity [cm/s]			Traffic light	Explanation
Terminal 1 ¹	Terminal 2 ²	Terminal 3		
0-7	0-4	0-6	Green zone	Safe
7-11	4-6	6-10	Orange zone	Too high
> 11	> 6	> 10	Red zone	Unsafe/damage

¹⁾ Vessels with a DWT > 150,000 tonnes have to berth in the green zone. The landing of vessels with a DWT < 150,000 may incidentally exceed the green zone.

²⁾ If the velocity is higher than 8 cm/s, an alarm signal is given.

In cases where approach velocities exceeded the limit, a red signal was visible. If the manoeuvre was continued, the captain of the vessel would be held responsible for any damage. At some berths, vessels with less water displacement were allowed to berth in the orange zone. Note that the measurements taken were almost perfectly in line with these target berthing velocities. The pilots explained that they try to reach the upper limit of the green light range rather than aiming for 3-4 cm/s. Establishing a target berthing velocity may prevent extreme velocities, but could result in higher mean values.

The 'human factor', expressed in terms of captains' experience and knowledge of local environmental as well as navigation conditions is an important parameter with regard to berthing velocity. For large seagoing vessels, human influence will most likely result in fewer extreme events. If the pilots intuitively classify an approach velocity as too high, adequate

Appendix D1. Berthing velocity of large seagoing vessels in Rotterdam

measures will be taken or the berthing operation will be aborted immediately. Conversely, the opposite could be the case regarding smaller seagoing vessels and inland barges, due to less experience or captains' greater responsibility. The human factor could result in an increase of extreme events or higher values for uncontrolled berthing velocities. Small seagoing vessels and inland barges berthing without tug assistance and pilot assistance should therefore have a greater margin of safety.

Vessel characteristics and water cushion effect

For tankers and bulkers with relatively large water displacements, i.e. a DWT > 100,000 tonnes, the correlation between ship mass and velocity seems insignificant. This is more or less in line with the recommendations given in the EAU and ROM. Although there was a weak correlation between the dimensions of a container vessel (DWT) and its berthing velocity, the collected data did not confirm the historical assumption that berthing velocities correlate strongly with ship dimensions (Fig. D.6). The mean berthing velocities of large seagoing vessels were between 3 and 4 cm/s (Table D.4), which is in accordance with the objective of the pilots. It should be noted that the maximum values were still below the design velocities (for 'abnormal' berthing operations). The maximum berthing velocities were generally caused by vessels smaller than the design vessel (Fig. D.17). The abnormal berthing velocities were established by multiplying the normal berthing velocities by $\sqrt{C_{ab}}$, C_{ab} , this being the abnormal berthing impact factor as concluded from design recommendations (PIANC, 2002). It should also be noted that a value of 10 cm/s was implemented as a lower limit for 'normal' berthing velocities.

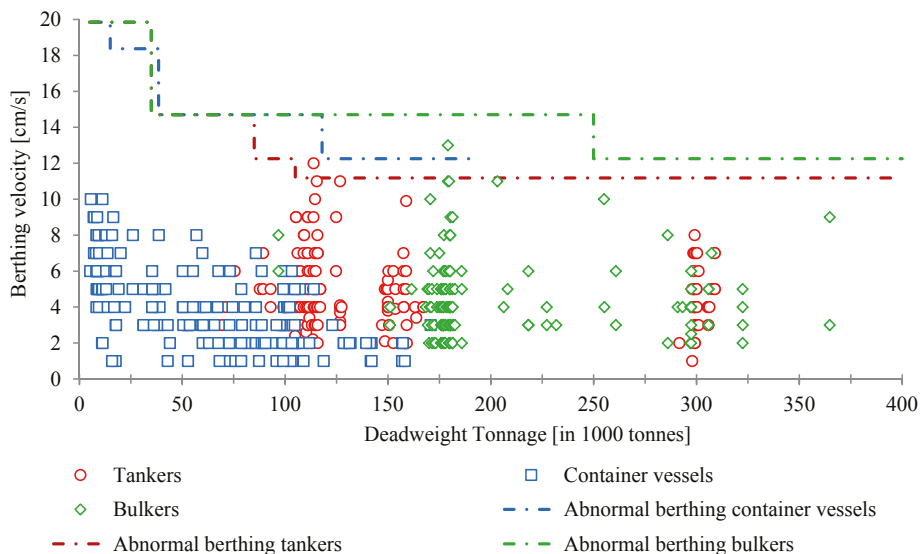


Fig. D.17. Field observations versus currently recommended abnormal berthing velocities.

Appendix D1. Berthing velocity of large seagoing vessels in Rotterdam

The pilots suggested that, due to low approach velocities, advanced propulsion systems, the parallel landing procedure and their ability to stop a container vessel even at one metre in front of the berth, the influence of the cushion effect did not play a dominant role in the berthing velocities of container vessel arrivals. To underline their experience, the pilots mentioned that they are actually able to ‘feel’ the water cushion at specific bulker berths. The water cushion was only felt during the final metre of the landing procedure for vessels with low under-keel clearance at closed quay walls. The *UKC* effect was most likely excluded due to the overestimation from the PPU tracking records. The influence of the water cushion effect most likely existed only in the case of very low *UKC* (Bochen, 2012).

The maximum berthing velocities measured were slightly higher than the maximum of 8 cm/s mentioned by the pilots. It should be emphasised that the extreme berthing velocities of tankers and bulkers measured using PPUs are likely to be slightly conservative. The higher extreme velocities were mostly caused by a second berthing impact due to yaw motion and the angular velocity of vessels. This has also been found at other ports, in Germany (Hein, 2014) and Japan (Yamase et al., 2014). The observations of approximately 1500 large container vessel arrivals in Bremerhaven were compared with the measurements in Rotterdam (Fig. D.18).

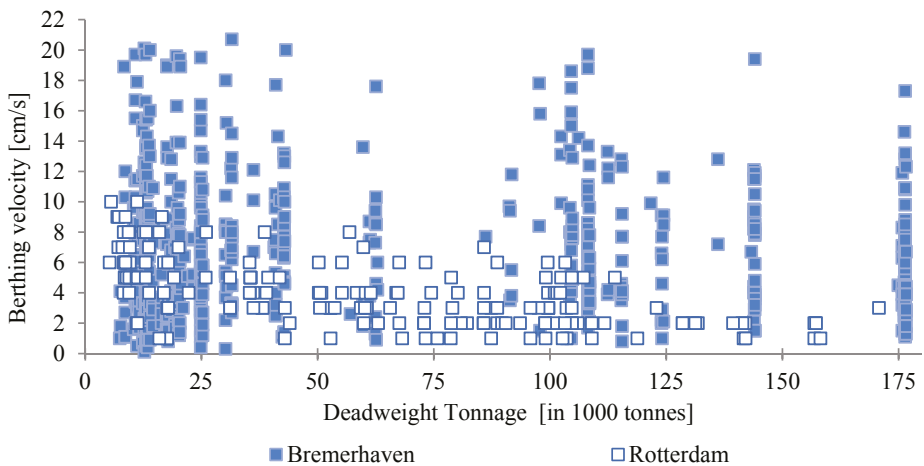


Fig. D.18. Measurements of container vessels in Bremerhaven and Rotterdam versus PIANC 2002.

The berthing velocities measured at Bremerhaven deviate significantly from those for the same individual container vessel classes as measured in Rotterdam. After consulting the German and Dutch pilots, it was concluded that a reasonable explanation for this discrepancy is that it is most likely caused by variations in angular velocity due to different environmental conditions (strong tidal currents) and types of landing procedure.

Appendix D1. Berthing velocity of large seagoing vessels in Rotterdam

Environmental conditions and type of landing

All berths in the Maasvlakte area of the port of Rotterdam have high degrees of shelter to waves and currents. At Rotterdam, the manoeuvring of container vessels is influenced mainly by wind. For this reason, berthing operations of such vessels were deliberately recorded during the windy season. However, examination of the resulting data showed that wind did not influence berthing velocities, either directly or indirectly. Similar conclusions were drawn from filed observations of onshore container berths in Japan and other parts of Asia (Yamase et al., 2014). One plausible explanation for the fact that wind is not of major influence may be found in the berthing policy used. Harbour masters and pilots adjusted this depending on environmental conditions.

The measurements conducted at the port of Bremerhaven have enhanced understanding of the effects of currents, since this port has relatively exposed navigation conditions. The German pilots take the tidal current of the River Weser into account in their landing strategy. In particular, the angle approach during the berthing procedure is high. At the final moment of impact, however, the berthing angle is always less than 1 degree. Fig. D.18 shows that the effects of strong currents can double or even triple berthing velocities (sum of transverse and angular velocity component), compared with the parallel landing procedure applied in Rotterdam. With the use of tug assistance and the early attachment of mooring lines during the final landing, at Rotterdam container vessels practically always berth parallel to the quay wall (Rath, 2012).

The berthing angles at the moment of impact in Rotterdam and Bremerhaven were significantly smaller than in the literature (Table D.6). It should be noted that the angle of approach was higher in Bremerhaven, but the berthing angle at the moment of impact was small. For large seagoing container vessels, the maximum measured berthing angle in a population of 1500 berthings was 0.82°. The average angle was approximately 0.24° (Hein, 2014).

Table D.6. Comparison of measured berthing angles of container vessels with guidelines.

Design codes	Ship dimensions	Berthing angle without tugs	Berthing angle with tugs
PIANC (2002)	> 50,000 DWT	-	Smaller than 5-6°
	Coasters	8°-10°	-
	Barges	15°	-
EAU (2012)	All	10°-15°	Smaller than 6°
ROM 0.2-90 (1990)	All	5°-15°	7°-10°
Measurements (2011)	> 50,000 DWT	-	0°-1°
	Coasters	0°-1.5°	-

Appendix D1. Berthing velocity of large seagoing vessels in Rotterdam

The current design guidelines tend to prescribe rather conservative values for berthing angles. For some vessels and quay types, these high angles are very unlikely and do not correspond with observed practice. In many cases the vessel would hit the quay wall or cranes before it touches the fender system. If the berthing angle is relatively small, the vessel might touch more than one fender, which is of course favourable for energy absorption. For parallel berthing against flexible dolphins at dedicated positions, this will often not be the case. Generally, engineers assess the most onerous condition where all the berthing energy is absorbed by a single fender with a minimum berthing angle. More fenders will be activated simultaneously only at very low berthing angles. However, this approach needs to be reconsidered for closed quay walls in the case of container berths. An improved understanding of actual berthing angles is relevant for assessments of fender spacing and offset relative to marine structures, in order to avoid collisions between ships and quays. Further analysis on this aspect is recommended so as to optimise design values.

Differences between tankers and container vessels

Seagoing tankers displayed berthing velocities 20-30% higher than those of large seagoing container vessels with similar dimensions (water displacement), even though the same pilots, boatmen and environmental conditions were involved. One plausible explanation could be that most tankers were berthing at berths with shore-based docking aid systems. Captains and pilots were therefore aware of allowable/target berthing velocities. Moreover, most tankers arrived with PPU assistance as well. The pilots therefore had an enhanced confidence level and aimed for target berthing velocities. Generally, there was no cushion effect at tanker berths, whereas all container vessels berthed at closed quay walls. Also, the added mass of tankers could be larger and their greater angle of approach causes the water between a sloped revetment and a jetty to be squeezed out. Additional rotational velocity was therefore excluded. Tankers are not equipped with bow thrusters. The availability of these thrusters give captains of container vessels more control during berthing operations, and they are used to reduce angles of approach. Berthing angles adjacent to container berths are often restricted due to interfaces between the bow flare angles of vessels and container cranes, or occupancy of berths. The allowable hull pressure of tankers is probably higher due to safety requirements in vessel design guidance (this needs further investigation). The total duration of general berthing procedures for tankers appears to be two to three times longer (durations are 1 hour for Aframax, 1 hour for VLCC and 20-30 minutes for containers). Due to greater inertia, tankers have to stay in motion in order to guarantee manoeuvrability, while container vessels can be stopped in a parallel position a few metres in front of the fender line. Note, too, that stopping a tanker will consume an extra 15-20 minutes, compared with stopping a container vessel. Tankers have a smaller freeboard and windage area. Within the port of Rotterdam, the berthing policy regarding container vessels depends heavily on weather

Appendix D1. Berthing velocity of large seagoing vessels in Rotterdam

conditions. The governing wind conditions probably occurred during navigation through main channels, and an extra tug was probably available to assist during the final landing.

D.1.4 CONCLUSIONS ON BERTHING VELOCITIES OF LARGE SEAGOING VESSELS IN ROTTERDAM

Since the development of the Broisma curves in the 1970s, new measurements of berthing velocities have been provided by the port of Rotterdam. And data analyses have resulted in a better understanding of various factors influencing berthing velocity. The most important conclusions are as follows.

- The measured berthing velocities were low, compared with current recommendations on design values. Typically, the mean values for individual vessel classes varied between 3 and 5 cm/s. The maximum observed velocity during 555 berthings was 13 cm/s.
- The collected data does not confirm the historical assumption that berthing velocities of large seagoing vessels are strongly related to ship dimensions. No evidence was found to suggest that berthing velocities of fully-laden vessels are lower than those of empty or partly ballasted ones.
- No evidence was found to suggest that berthing velocity is influenced by the type of marine structure or type of fender system.
- No correlation between wind speed (environmental factors) and berthing velocity was found in the sheltered (no waves and currents) port basins of Rotterdam.
- Berthing velocities depend heavily on berthing policy (type of landing, experienced and well-trained pilots, tug assistance, berthing aid systems, etc.)
- Establishing a target berthing velocity results in a decrease of extreme berthing events, but does not necessarily reduce berthing velocity during regular/normal berthing operations.
- The theoretical distribution of the low-probability tail of the measurements is closer to a Weibull distribution than to a normal or lognormal distribution.

In the design of marine structures berthing impact loads largely influence the reliability of fender systems, reinforcement of capping beams and (flexible) dolphins. Berthing velocity seemed to be the dominant design parameter for fender systems. Nominal values for the mass of a vessel and the accompanying water displacement could be considered for structural assessments of marine structures. The measured berthing angles were much lower at the moment of impact, compared with the design guidance. Further investigation of these aspects is recommended. It is also recommended that a rotational velocity component should be considered if no parallel landing operation is guaranteed. Strong tidal and non-tidal currents, in particular, may result in far higher berthing velocities. The factors affecting berthing velocity may change during the life of hydraulic structures. These factors include the experience of captains and pilots and the condition of the berthing facility.

APPENDIX D2. TYPICAL DISTRIBUTION FUNCTIONS FOR BERTHING VELOCITY

Table D2.1. Typical distribution parameters in Weibull fit and annual and lifetime maxima distributions.

Ship type	Size	n^1	Max ²	Weibull fit		Annual maxima			Lifetime maxima		
				λ	k	$\mu_{v;1}$	$\sigma_{v;1}$	$V_{S;1}$	$\mu_{v;50}$	$\sigma_{v;50}$	$V_{S;50}$
[-]	[kDWT]	[-]	[cm/s]	[cm/s]	[-]	[cm/s]	[cm/s]	[-]	[cm/s]	[cm/s]	[-]
Tankers ○											
Panamax	60-85	23	9	6.3	3.09	10.61	0.90	0.085	12.83	0.56	0.044
Aframax ³	85-105	175	12	5.0	2.68	9.24	0.74	0.080	11.42	0.61	0.053
Suezmax	115-165	95	11	5.3	2.75	9.58	0.81	0.085	11.75	0.54	0.046
VLCC	260-319	80	10	5.3	2.65	9.51	0.88	0.093	12.10	0.58	0.048
Fix. laser	260-319	19	7	4.1	2.77	7.26	0.64	0.088	8.95	0.43	0.048
Bulkers ◇											
Capesize ⁴	150-205	107	13	5.0	1.91	11.44	1.20	0.105	15.73	1.14	0.073
VLBC ⁴	205-365	37	10	4.8	2.18	10.10	0.95	0.094	13.31	0.90	0.067
Containers □											
Coasters	7 - 15	37	10	7.1	3.68	11.05	0.80	0.072	12.86	0.47	0.037
Feeders	15 -42	31	9	5.4	2.63	10.37	1.10	0.106	12.56	0.68	0.054
Panamax	42-70	31	8	4.1	2.22	8.45	0.78	0.092	11.15	0.74	0.066
Post Panamax	70-118	60	7	3.4	1.93	7.83	1.00	0.128	10.56	0.74	0.070
New Panamax ³	118-171	18	3	2.1	3.60	3.36	0.25	0.074	3.86	0.16	0.041
Containers □											
Coasters	7 - 15	177	20	7.2	1.50	21.10	3.23	0.153	31.40	2.90	0.092
Feeders	15 -42	250	20	7.4	1.55	21.29	3.46	0.162	30.84	2.78	0.090
Panamax	42-70	104	19	8.5	1.86	20.62	2.67	0.130	27.73	1.78	0.064
Post Panamax	70-118	288	25	8.0	1.68	21.24	3.15	0.148	29.86	2.28	0.076
New Panamax	118-171	150	20	8.1	1.79	20.10	2.71	0.135	27.82	2.14	0.077
ULCV	171-195	266	26	6.2	1.47	18.76	3.13	0.167	28.04	2.39	0.085
Large datasets											
All tankers ○	60-319	392	12	5.2	2.69	9.40	8.4	0.089	11.67	0.58	0.049
All sheltered △	7-365	713	13	4.9	2.28	10.05	9.9	0.098	13.00	0.85	0.065
All exposed □	7-195	1235	26	7.4	1.61	20.44	29.1	0.142	29.04	2.44	0.084
All data	60-319	1948	26	6.4	1.57	17.83	23.5	0.132	26.19	2.41	0.092

¹⁾ Number of field observations.

²⁾ Maximum measured berthing velocity.

³⁾ Dataset is most likely too optimistic (Appendix D.1).

⁴⁾ Dataset is most likely too conservative (Appendix D.1).

CURRICULUM VITAE

18/01/1983

Born at Zwijndrecht, The Netherlands.

Education

2004-2006

MSc Civil Engineering and Geosciences, Hydraulic Structures section, Delft University of Technology, The Netherlands.

Thesis: *Dealing with uncertainties in the design of bottom protection near quay walls.*

Supervisor: Prof.dr.s.ir. J.K. Vrijling.

2001-2004

BSc Civil Engineering and Geosciences, Delft University of Technology, The Netherlands.

1995-2001

VWO pre-university education, Develstein College, Zwijndrecht, The Netherlands.

Employment

2016-present

Researcher, Hydraulic Structures and Flood Risk, Delft University of Technology, The Netherlands.

2013-present

Senior Port Engineer, Port Development, Port of Rotterdam Authority, The Netherlands.

2013-present

Tutor, postgraduate courses, Delft, The Netherlands.

2011-2013

Project Manager, Port Engineering, City of Rotterdam, The Netherlands.

2009-2011

Tutor, Rotterdam University of Applied Sciences, Rotterdam, The Netherlands.

2006-2011

Consultant, Port Engineering, City of Rotterdam, The Netherlands.

2005

Consultant, Unipartners Delft, Delft, The Netherlands.

Awards

2007

Paepe Willems Award, PIANC.

2007

Nominated for Dutch Hydraulic Engineering *Award* (Waterbouwprijs).

Committees

2019-present

CROW Working Group: CUR 166 Sheet Pile Walls

2019-present

PIANC WG 211: Design of Fender Systems.

2017-present

PIANC WG 164: Deepening of Existing Berths.

2017-present

CROW Working Group: Dutch Port Infrastructure Committee.

2015-present

CROW Working Group: Hydraulic Loads and Effects of Ship Propulsion Systems.

2010-2019

PIANC WG 145: Berthing Velocities in Well-Organised Ports.

2012-2017

Executive Committee, PIANC Dutch Young Professionals.

2012-2018

SBRCURNET C206: Flexible Dolphins.

2012-2014

SBRCURNET C186: Urban Quay Walls.

2009-2013

SBRCURNET C211: Quay Walls, second edition.

2008

CUR F50: Geotextile Tubes Filled with (Contaminated) Dredging Materials.

LIST OF PUBLICATIONS

The following publications are related to this thesis:

PEER-REVIEWED JOURNAL PAPERS

Roubos, A. A., Groenewegen, L., & Peters, D. J. (2017), Berthing velocity of large seagoing vessels in the port of Rotterdam. *Marine Structures* 51, pp. 202-219.

Roubos, A. A., Peters, D. J., Groenewegen, L., & Steenbergen, R. D. J. M. (2018), Partial Safety Factors for Berthing Velocity and Loads on Marine Structures. *Marine Structures* 58, pp. 73-91.

Roubos, A. A., Steenbergen, R. D. J. M., Schweckendiek, T., & Jonkman, S. N. (2018), Risk-based target reliability indices of quay walls. *Structural Safety* 75, pp. 89-109.

Roubos, A. A., Schweckendiek, T., Brinkgreve, R., Steenbergen, R. D. J. M., & Jonkman, S. N. (2019), Finite element-based reliability assessment of quay walls. *Georisk: Assessment and Management of Risk for Engineered Systems and Geohazards* (submitted).

Roubos, A. A., Allaix, D. L., Schweckendiek, T., Steenbergen, R. D. J. M., & Jonkman, S. N. (2019), Time-dependent reliability analysis of service-proven quay walls subject to corrosion-induced degradation. *Reliability Engineering & System Safety* (submitted).

Roubos, A. A., Allaix, D. L., Schweckendiek, T., Steenbergen, R. D. J. M., & Jonkman, S. N. (2019), Target reliability indices for existing quay walls derived on the basis of economic optimisation and human safety requirements. *Structure and Infrastructure Engineering* (submitted).

PEER-REVIEWED BOOKS AND BOOK SECTIONS

Roubos, A. A., & Grotegoed, D. (2014), *Urban Quay Walls*. Delft, The Netherlands: SBRCURnet. ISBN 978-1138000230.

Roubos, A. A., (2018), *Flexible Dolphins*. Delft, The Netherlands: CROW. ISBN 987-90-5367-656-1.

Roubos A. A., (2019), *Berthing velocities analysis of seagoing vessels over 30 kDWT*. PIANC Working Group Report 145. Brussels, Belgium: PIANC.

List of publications

Roubos, A. A., Peters, D. J., & Steenbergen, R. D. J. M. (2018), *Appendix: Risk-Based Reliability Differentiation; Quay Walls, Second Edition*. Delft, The Netherlands: SBRCURnet. ISBN 987-1138000230.

Roubos, A. A., Peters, D. J., & Steenbergen, R. D. J. M. (2018), *Appendix: Risk-Based Reliability Differentiation; Jetties & Wharves*. Delft, The Netherlands: CROW. ISBN 978-90-5367-657-8.

Roubos A. A., (2019), *Deepening Existing Berths*. PIANC Working Group Report 164, chapter 2. Brussels, Belgium: PIANC.

Roubos A. A., (2019), Working Group Report 145: Berthing velocity analysis of seagoing vessels over 30kDWT; Chapter 8. Brussels, Belgium: PIANC.

Roubos, A. A., Peters, D. J., & Steenbergen, R. D. J. M. (2019), Appendix B: Table NB.21 – B1 – Voorbeelden van toepassingen gevolklassen. In: *NEN-EN1990 Eurocode: Grondslagen van het constructief ontwerp*. Delft, The Netherlands: NEN.

CONFERENCES

Roubos, A. A., Jaspers Focks, D. J., & Peters, D. J. (2016), *Innovation Flexible Dolphins by Full-Scale Field Test Laterally Loaded Tubular Piles*. Rio de Janeiro, Brazil: PIANC COPEDEC.

Roubos, A. A., Groenewegen, L., Ollero, J., Hein, C., & Wal, E. van der (2017), *Design Values for Berthing Velocity of Large Seagoing Vessels*. Panama City, Panama: PIANC 34th World Conference.

Roubos, A. A., Allaix, D., Fischer, K., Steenbergen, R. D. J. M., & Jonkman, S. N. (2018), *Target Reliability Indices for Existing Quay Walls Derived on the Basis of the LQI Criterion*. Ghent, Belgium: IALCC.

Roubos, A. A., Peters, D. J., & Steenbergen, R. D. J. M. (2019), *Target Reliability Indices for Quay Walls, Jetties and Flexible Dolphins*. Pittsburgh, United States: Ports 2019.

Matic, I., Nijs, R. de, Vos, M. de, & **Roubos, A. A.** (2019), *Full-scale load testing on long prefabricated concrete piles in the Port of Rotterdam*. Reykjavik, Iceland: ECSMGE 2019.

Weisstein, R., Gijt, J. G. de, Heeres, O. M., & **Roubos, A. A.** (2019), *Relationship between the construction costs and the reliability index of quay walls*. Stuttgart, Germany: EACEF 2019.

ACKNOWLEDGEMENTS

In 2015 I was asked to comment on the roadmap *Futureproof Port Infrastructure*. Reviewing this research plan from the Smartport community, aiming for a sustainable port in 2030, inspired me to come up with new ideas. On behalf of Smartport, Egbert van der Wal and Robert van der Linden asked me to briefly describe and share those ideas. So that is what I did, and both of them were immediately so enthusiastic that they asked me whether I was willing to conduct the necessary research myself.

While it was never my intention to do a PhD at this stage in my career, I decided to start this research based mainly on the experiences of and advice from Bas Jonkman, Jarit de Gijt and Tiedo Vellinga. This decision was not an easy one, however, since I am an engineer who loves working on unique projects and undertaking civil engineering works. More importantly, I recently became a father and I have promised my children that I will always be there for them. Since I enjoy working in a team, I was worried that conducting research would be too lonely for me. Fortunately, this did not turn out to be the case because I have been in close contact with my peers and colleagues since day one. Whether I had a question or just needed someone to share my ideas with, there was always somebody within my network willing to help. I am unable to describe how it feels to receive your support and always positive feedback. I am glad to have this opportunity to thank all of you for motivating and encouraging me.

Starting with my supervisors, Bas Jonkman and Raphaël Steenbergen. Bas has the ability to provide me, and presumably all his students, with the right feedback at the right time, without being too directive. This helped me to structure this research and to maintain progress. Since I was not familiar with the Eurocode, I discussed my results with Professor Steenbergen. Raphaël was immediately willing to help and taught me about reliability theory and the derivation of partial factors of safety. Thank you both for guiding me during this interesting period of my life.

I am indebted to Timo Schweckendiek, who provided me with great feedback. Timo is one of a kind, since he has the ability to understand within minutes a problem that would take anyone else hours to apprehend. In addition, I am always impressed by the creativity and knowledge of Dirk Jan Peters. When no-one else could answer my questions, Dirk Jan would often point me in the right direction. During this research, I was also fortunate to meet Diego Allaix. I am deeply grateful to him. We had a lot of interesting discussions about Plaxis, Diana and Blum's method, but also about time-dependent reliability problems. Timo, Dirk Jan and Diego: thank you for helping me to become a better researcher and please, never lose your enthusiasm!

I would like to thank all the companies and organisations involved in this study – and Smartport and the Port of Rotterdam Authority in particular – for their support, funding

Acknowledgements

and hospitality. I received unconditional support from Piet Louwen, Annemagreet Schouten and Egbert van der Wal. Without your support I would never have completed this thesis. I also want to thank Jarit de Gijt, who has transferred to me his passion for quay walls and other marine structures. I received one of my best tips from Tiedo Vellinga. He said, “Do not make the mistake of being the project manager of your PhD. You have to be independent and should not be responsible for the budget.” This led me to decide to ask my friend and colleague Matthijs Tromp to take on that task. Matthijs, I am so grateful for your contribution and for never letting me down.

During this research, I have been in constant contact with experts from the industry. Without their support, feedback and reviews, the practical application of my findings would have not been possible. Sharing our knowledge is crucial if we are to move forward. My conversations with Cornelis van Dorsser, Karel Terwel and Han Vrijling helped me to acquire more insight into the failure consequences of quay walls. Since I am not a financial expert, it was a pleasure to discuss the impact of discount rates and the outcomes of the net present value analysis with my colleague Wouter Nus and with my brother Frank Roubos. I really appreciate the feedback from Wim Courage and Ton Vrouwenvelder, who were always willing to provide me with detailed information about the application of correlations and model uncertainty in reliability theory. Ronald Brinkgreve, Anita Laera, Micha van der Sloot and others from Plaxis are gratefully acknowledged for their contributions to the development of the reliability interface. The interpretation of the *LQI* criterion and the Abdo-Rackwitz algorithm would not have been possible without the help of Katherina Fischer and Regis Lebrun. Furthermore, I am grateful to Geerhard Hannink, Pieter Heijndijk, Dirk-Jan Jaspers-Focks, Adriaan van Seters and Rodriaan Spruit, who helped me to interpret my findings from a geotechnical perspective. Thank you Henk Brassinga for reviewing the finite element models used. Without the help of Johan Plugge and Peter Jan Plooy it would have been much more difficult to properly interpret Blum’s method. The research into berthing velocities would not have been possible without the contributions of Marco Gaal, Christian Hein and Juan Ollero. In addition, the Dutch Pilotage, the boatmen of KRVE and Trelleborg Marine Systems are acknowledged for their support. I am grateful to Leon Groenewegen for sharing his knowledge and for his contribution in interpreting the berthing records. I would also like to thank Piet Jongbloed for sharing his knowledge of corrosion. During this research, I had some fairly detailed questions about the effect of ‘notching’ and the stress-strain curves of various coupon tests. When they arose, I usually called my dear friend and true steel specialist Tom Graafland, who was always willing to brainstorm.

I would like to thank the Graduate School for bringing me in contact with other PhD students and enabling me to further develop my research and transferable skills. During the course How to Write a Dissertation, I met Veronica Alonso. She helped me to structure the thesis and provided great feedback with regard to my writing skills. Furthermore, I am

deeply grateful to Meinou de Vries and Cees van Itern, who helped me with the infographics and designing the cover, respectively. Thank you to all my colleagues from AM, DI&T, DHMR, Finance and PD at the Port of Rotterdam, and in particular to Joost Bos, Erik Broos, Joppe Burgers and Robert van der Linden for proof-reading parts of this thesis. I am in debt to my friends Anton de Fockert, Tom Graafland and Ton van der Plas, who provided me with useful feedback with regard to the propositions attached to this thesis. In addition, Nena Vandebroek is gratefully acknowledged for helping me prepare for the public defence. Finally, I would like to express my gratitude to Angel Koopman, Diana Keijzer and Judith Schooneveld for organising meetings, arranging field excursions and booking conferences.

During this research, my son Art and later my daughter Ella were born. The first sleepless period was especially tough, and sometimes it was real challenge to maintain progress. I had almost no time for sports or maintaining our house. By reading literature in the gym, while using cross and home trainers, I was able to restore my balance, stay in shape and still spend time with my family. My deepest appreciation goes to my friends and family, who supported me without fail. They are always there for me, and remind me of what is truly important. Love and thanks to my parents Arie and Toos, parents-in-law Ad and Manja and brothers Frank, Mark and Ralph, as well as their families. Also, Sabrina and Jeroen and their family. Thank you mum for always showing interest in my study and for telling me so often how special this is for you. Furthermore, I really enjoyed debating with my father and brother Ralph about my mathematical derivations. I am very grateful that I could take Wednesday afternoons off to spend time with Art and Ella. Lastly, with gratitude and love I would like to thank my wife Elvira for her love, understanding, support and proof-reading of parts of this thesis.

Alfred Roubos,
Delft, May 2019



